



Effect of initial microstructural conditions and tempering parameters on the carbide characteristics and hardness of alloyed quenched and tempered steel

By

AIMEE LOUISE GOODALL

A thesis submitted to the University of Birmingham for the degree of
DOCTOR OF PHILOSOPHY

Word Count – 42,278

School of Metallurgy and Material Science
College of Engineering and Physical Science
University of Birmingham
March 2019

UNIVERSITY OF
BIRMINGHAM

University of Birmingham Research Archive

e-theses repository

This unpublished thesis/dissertation is copyright of the author and/or third parties. The intellectual property rights of the author or third parties in respect of this work are as defined by The Copyright Designs and Patents Act 1988 or as modified by any successor legislation.

Any use made of information contained in this thesis/dissertation must be in accordance with that legislation and must be properly acknowledged. Further distribution or reproduction in any format is prohibited without the permission of the copyright holder.

Abstract

Commercial production of high strength steel plates by the quenching and tempering (Q&T) route requires control of alloy design and heat treatment parameters to achieve the desired strength and toughness through thickness. For thick plate the difference in cooling rate through thickness affects the as-quenched microstructure with martensite, auto-tempered martensite and lower and/or upper bainite being present. The different as-quenched microstructures can show a different response to tempering which affects the final strength and toughness.

The starting microstructure of a low alloy 0.17 wt. % C Q&T steel has been varied using isothermal heat treatment to create mixed martensite and lower bainite microstructures. The effects of tempering at 600 °C for times between 0.5 and 100 hours on the carbide precipitates and hardness of the mixed microstructures have been investigated and compared to the tempering response of single phase (martensite and lower bainite) microstructures. It has been found that the hardness decrease due to tempering is larger in the martensitic structure than the bainitic structure due to more rapid carbide coarsening. The as-quenched hardness of the mixed microstructures can be predicted by a rule of mixtures using the single-phase properties. The tempering response of the mixed microstructures is discussed.

Acknowledgements

I would like to express my thanks to Dr. Martin Strangwood and Professor Claire Davis for their experience and guidance throughout my PhD studies. Without their support and knowledge, I would not have had the opportunity to start this PhD and grow both professionally and personally. I owe a lot to their patience and wisdom.

I would like to thank the EPSRC for funding this project and TATA Steel Europe for material and an industrial perspective. Along with my industrial supervisors Heather Carey and Sally Parker.

The results would not have been possible without the support of Jas Singh, Avril Rodgers, Paul Stanley, Theresa Morris, Dave Price, Tim Doel, David Walker and Numan Aslam.

My life in Birmingham would have been very different without the support and encouragement of the 1B20 office and the friends who I have met along the way. Thank you!

A huge thank you to my family, partner David and friends who have supported me throughout my time at university and for always believing in me. Finally, a special thanks to my Mum who taught me to never give anything less than my best.

This PhD wouldn't have been written without my own motivation, determination and endless cups of tea.

This thesis is dedicated to Spike.

.

Contents

Acknowledgements	ii
List of Figures.....	viii
List of Tables.....	xii
Chapter 1: General Introduction	1
Chapter 2: Literature Review.....	3
2. 1: Tempering of steels	3
2.1.1: Continuous cooling Transformation (CCT) Diagrams.....	3
2.2: Martensite.....	5
2.2.1: Formation of martensite	5
2.2.2: Para-Equilibrium.....	5
2.2.3: Austenisation Temperature	7
2.2.4: Hardenability	9
2.2.5: Prior Austenite Grain Size	10
2.3: Carbon Content	11
2.4: Martensite Start Temperature.....	12
2. 5: Microstructure	14
2.5.1: Lath vs. Plate Martensite.....	14
2.5.2: Low carbon martensite lath-like structures:.....	16
2.5.3: Presence of Retained Austenite in Lath Martensite	18
2.6: Martensitic Tempering	21
2.6.1: Tempering of Martensite.....	21
2.6.2: Larson Miller Parameter	27
2.7: Alloying additions.....	29
2.7.1: Tempering an alloyed martensite	29
2.7.2: Chromium (Cr)	31
2.7.3: Molybdenum.....	32
2.7.4: Vanadium (V)	34
2.7.5: Molybdenum and Vanadium additions	36
2.7.6: Chromium and Molybdenum additions	38
2.7.7: Silicon (Si).....	43
2.8: Bainite	47
2.8.1: Introduction.....	47
2.8.2: Appearance	47
2.8.3: Role of Silicon	52
2.9: Bainite Transformation Temperatures.....	55
2.10: Tempering of Bainite	57
2.10.1: Cementite coarsening during tempering	61

2.10.2: Tempering of retained austenite.....	63
2.11: Secondary hardening of bainitic/ferritic steels with alloying additions	63
2.12: Differences between martensite and bainite.....	64
2.13: Strengthening mechanisms.....	64
2.13.1: Grain Size	64
2.13.2 Solid-solution-strengthening.....	69
2.13.3 Strain hardening.....	70
2.13.4: Precipitation Strengthening.....	72
2.13.5 Phase Balance –	73
2.14: Mixtures of martensite and lower bainite.....	74
2.14.1: Introduction.....	74
2.14.2: Strength of Mixed Microstructures	74
2.14.3: Rule of Mixtures – Ferrite Containing Microstructure	75
2.14.4: Rule of Mixtures – Upper Bainite and Martensite Microstructure.....	76
2.14.5: Rule of Mixtures – Lower Bainite and Martensite Microstructure	76
2.14.6: Refinement of martensite packet size in mixed microstructures.....	79
2.15: Tempering of mixed microstructures	82
2.16: Summary	87
Chapter 3: Aims and Objectives	89
Chapter 4: Experimental Method.....	90
4. 1: Materials.....	90
4.2: As received microstructure.....	91
4.2.1: Inclusions.....	91
4.2.2: Optical Microscopy.....	93
4.3: Sample Preparation:	95
4.4: Optical Microscopy/ SEM.....	95
4.5: Image Analysis.....	96
4.5.1: Phase Analysis	96
4.5.2 Carbide Analysis.....	98
4.5.3 Lath Size Analysis	98
4.6: Hardness Testing.....	99
4.7: Heat treatment	99
4.7.1: Furnace - Producing Martensitic Samples	99
4.7.2: Gleeble - Producing Bainitic/Mixed Microstructure samples.....	99
4.8: Dilatometry	103
4.8.1: Isothermal Holds.....	103
4.9: Gleeble Isothermal Hold	104
4.10: Predicted TTT Diagram	105

4.11: Continuous Cooling	105
4.12: Tempering	107
4.13: Modelling	107
4.13.1: Assumptions for cooling	108
4.13.2: Assumptions used for heating:	108
4.13.3: Details of Study in COMSOL for heating and cooling	109
4.13.4: Modelling: Cooling from 925 °C to room temperature	110
4.13.5: 2D Study	111
4.13.6: Modelling - Heating of steel from room temperature to 600 °C	111
4.13.7: XRD	112
Chapter 5: The Tempering of Martensitic Steel	113
5.1: Normalised and Quenched Microstructure (Martensite)	113
5.1.1: Auto-tempering - Quantification	120
5.1.2: Martensitic Start Temperature	122
5.1.3: Lattice Parameter	125
5.1.4: Grain Size	127
5.1.5: Laths	129
5.1.6: Alloying Elements	131
5.1.7: Initial Hardness	133
5.1.8: Summary of as-quenched martensitic samples	135
5.2: Tempering at 600 °C	136
5.2.1: Carbides	136
5.2.2: Laths	152
5.2.3: Lattice Parameter	156
5.2.4: Hardness	157
5.3: 100 Hours Temper	160
5.3.1: Hardness	160
5.3.2: SEM Images	161
5.3.3: Carbides	164
5.3.4: Hardness	166
5.4: Summary of martensitic tempering	168
5.5: Summary for Martensitic Microstructure	169
Chapter 6: Bainite	170
6.1: Bainite Production	170
6.1.1: Desired Microstructure	170
6.1.2: TTT Diagram	171
6.2: Microstructural Production	173
6.2.1: Oil Quenching	173

6.2.2: Furnace Cool.....	177
6.2.3: Air Cooling	179
6.2.4: Isothermal Holds.....	182
6.3: Isothermal Holds	184
6.3.1: Dilatometry Isothermal Holds.....	184
6.3.2: Dilatometry Isothermal Holds.....	190
6.4: Production of lower bainite - Summary	195
6.4.1: CCT Diagram.....	196
6.5: Analysis of lower bainitic microstructure	196
6.5.1: Bainitic Carbide Size	196
6.5.2: Bainitic Lath Size.....	197
6.6: Tempering	199
6.6.1: Microstructure.....	199
6.6.2: Hardness	200
6.6.3: Carbide Sizes on tempering	203
6.6.4: Lath Size	205
6.7: Summary	208
6.7.1: Bainite Production	208
6.7.2: Tempering	208
Chapter 7: Mixed Microstructure Results.....	209
7.1: As-quenched.....	209
7.1.1: Microstructure.....	210
7.1.2: Gleeble Stroke.....	213
7.1.3: Lath Size	215
7.1.4: Carbide Size.....	218
7.1.5: Hardness	222
7.2: Tempering 30 minutes to 16 hours.....	223
7.2.1: Vickers Hardness vs. Percentage of Lower Bainite	223
7.2.3: Tempering Carbide Analysis	230
7.2.4: Summary Tempering to 16 hours.....	241
7.3: Tempering 100 hours	242
7.3.1: Hardness	242
7.3.2: Micrographs	244
7.3.3: Lath Size	255
7.3.4: Carbide Size at 100 hours tempering	256
7.3.5: Compositions	262
7.3.6: Summary – 100 Hours	266
Chapter 8: Simulation of Heating and Cooling using COMSOL	267

8.1: Comparison to Experimental Data	267
8.2: Cooling Curve	268
8.3: Comparison of Parameters	269
8.3.1: Heat Capacity.....	269
8.3.2: Thermal Conductivity	270
8.3.3: Density	270
8.4: CCT Diagram.....	274
8.5: Heating of steel from room temperature to 600 °C	275
8.6: Comparison of Parameters	276
8.6.1: Comparison to Data	276
8.6.2: Surface Emissivity	278
8.6.3: Heat Transfer Coefficient	278
8.6.4: Heat Capacity at Constant Pressure	279
Chapter 9: Summary	281
9.1: Summary of Discussion	281
9.2: Conclusions.....	281
Chapter 10 Further Work.....	286
Bibliography:	287

List of Figures

Figure 1 Micrograph of S690 water quenched then tempered for 30 minutes at 600 °C (Driscoll, 2014).....	1
Figure 2 Comparison between core and surface cooling rates and resulting microstructure for a 0.3C, 2.0Mo (wt. %) oil quenched 95-mm diameter steel bar (H.K.D.H. Bhadeshia, 2001)	4
Figure 3 Atom probe cumulative plots for analyses across cementite/matrix interfaces in 2.25%Cr – 1%Mo – 0.15 wt. %C steel tempered for 5 min and 2 hr in a martensitic steel.	6
Figure 4 Effect of austenisation temperature on hardness and ultimate tensile strength for a 0.68 wt. %C, 3.15 wt. % Cr, 0.69 wt. % Mo steel, normalised for 30 minutes and quenched (Bakhsheshi-Rad et al., 2011)....	8
Figure 5 Solubility of carbide and nitrides in austenite as a function of temperature (Maalekian, 2007)	9
Figure 6 Hardness of as-quenched martensitic microstructures as a function of steel carbon content (G. Krauss, 1978).....	11
Figure 7 Variation in Vickers hardness of martensite with carbon content (Best fit from carbon content to the power half) (Samuel & Hussein, 1983).....	12
Figure 8 Effect of carbon content on Ms and Mf temperatures (Petty, 1970)	13
Figure 9 Lath martensite in 0.02 wt. %C Mn steel (Speich & Leslie, 1972).....	14
Figure 10 Structure of plate martensite in a 1.2 wt. % C steel (Speich & Leslie, 1972)	15
Figure 11 Schematic illustration of lath martensitic structure in low carbon steel - Adapted from (Morito, Huang, et al., 2006) by (Pham et al., 2013) and lath label added.....	17
Figure 12 Link between Lath width (nm) and C (wt%), data compiled by (Galindo-Nava & Rivera-Díaz-del- Castillo, 2015).....	18
Figure 13 Effect of carbon content on relative volume percent of lath martensite, Ms temperature, and volume percent of retained austenite in Fe-C alloys (Speich & Leslie, 1972).....	19
Figure 14 Effect of austenisation temperature on retained austenite content (Bakhsheshi-Rad et al., 2011)	20
Figure 15 Hardness of iron-carbon martensite tempered for 1 hour at 100 – 700 °C, with carbon contents from 0.39 – 0.026 wt. % C. Taken from (Speich, 1969).....	21
Figure 16 Variation of measured average cementite particle diameter in martensite with tempering time in a 0.45 wt. % C – 0.22 wt. % Si – 0.62 wt. % Mn – 0.004 wt. % P – 0.0038 wt. % S at 700 °C (W. J. Nam, 1999)	24
Figure 17 Total and high angle grain boundary area per unit volume as a function of the logarithm of the tempering time at 600 °C (Caron & Krauss, 1972)	24
Figure 18 Lath width distributions and their corresponding log normal fitting curves for long aged G11 samples (L1 - Ageing at 600 °C for 5,000h, L2- 600 °C for 10 000h, L3- 650 °C for 5000h, L4 – 650 °C for 10 000h (J. Liu et al., 2014).....	26
Figure 19 Fe-0.2 wt. %C alloy (Left Water-quenched, Right 6.05 × 10 ⁵ seconds at 690 °C) (Lindsley, 1998) ...	26
Figure 20 Effect of Mo on the tempering response of quenched 0.1wt. % C steels (Irvine & Pickering, 1960) found in (H.K.D.H. Bhadeshia, 2001)	28
Figure 21 Nucleation and dissolution sequence for precipitates in a Cr-1Mo steel (T22 HSLA steel – 2Cr, Mo, 0.5Si, 0.5Mn and 0.15C wt. %) (Kiattisaksri, 2011; S. Liu et al., 2009)	30
Figure 22 Effect of elements on the hardness of martensite tempered at 592 °C for 1 hour (Grange et al., 1977)	30
Figure 23 Effectiveness of Mo in reducing austenite grain size in a 0.13% carbon steel, held at 950 °C for varying time (hours)(Shorowordi & Ali Bepari, 2002).....	33
Figure 24 Effectiveness of vanadium additions on hardness in a 0.19C/0.3Mn steel compared to the V free steel adapted from (Grange et al., 1977)	34
Figure 25 Experimental time-temperature diagrams of carbide stability (Steel 1 - 0.02 wt. %V, 0.70 wt% Mo. Ratio 0.03:1) (Steel 2 - 0.12 wt. %V, 0.73 wt% Mo. Ratio 0.16:1) (Steel 3 - 0.32 wt. %V, 0.70 wt% Mo. Ratio 0.46:1) (Steel 4 - 0.34 wt. %V, 0.94 wt% Mo. Ratio 0.36:1) (Kroupa et al., 1998).....	37
Figure 26 Quenched and Tempered Hardness of low alloy Cr and Cr-Mo steel - C 0.41-0.44 wt. %- Cr 1.01-1.11 wt. % Mo 0.11 - 0.70 wt. % Data taken from (Gojic et al., 1998) As quenched hardness Cr – 661 HV /CrMo – 710 HV	40
Figure 27 Variations in hardness with aging temperature in Mo and Mo-Cr steel (2.10 Mo – 2.41 Cr – 0.2C) Data adapted from (Kwon, Lee et al. 1997).....	41
Figure 28 Isothermal diagram showing the sequence of carbide formation in a 2.25Cr-1Mo steel (Baker & Nutting, 1959).....	41
Figure 29 Calculations of multiple precipitation reactions for a) 3Cr1.5Mo and b) 2 ¼ Cr 1 Mo steels at 600 °C	

(Fujita, 2000)	42
Figure 30 Size distribution of secondary carbides; comparison between high silicon (Si - 0.92%) and low silicon (Si - 0.35%) grades. Austenisation at 980 °C for 1 hr – 550 °C 2 hours – 625 °C/ 623 °C for the HS/LS graded for 2 hours (Delagnes et al., 2005).....	44
Figure 31 Qualitative influence of silicon content on the secondary hardening peak (Delagnes et al., 2005)	45
Figure 32 Tempering curve for three Si-containing, C-0.4, Mn-0.35/36, Mo-1.3, V-0.40, 5% Cr martensite steels, tempered for 2 × 2 hr (Rafael Agnelli Mesquita & Kestenbach, 2012).	46
Figure 33 Split tempering curve of 2% Si alloy steel (Rafael Agnelli Mesquita & Kestenbach, 2012).....	46
Figure 34 Schematic representation of the transformation from austenite to lower bainite or upper bainite (H.K.D.H. Bhadeshia, 2001).....	48
Figure 35 Microhardness data from plain carbon steels transformed isothermally to a mixture of bainite and pearlite (Yasuya Ohmori et al., 1971) Taken from (H.K.D.H. Bhadeshia, 2001).....	50
Figure 36 Proximity histograms across the cementite particle in bainitic ferrite after transformation at 400 °C for 1800s in 0.3C - 0.25Si- 1.22Mn-0.14Cr-0.03Mo wt. % (Caballero et al., 2014).....	54
Figure 37 Transformation fractions during isothermal holding (Pinto da Silva et al., 2014)	55
Figure 38 The time scales associated with a variety of tempering phenomena for bainite (this is not for a specific type of steel – no composition details were given) - Taken from Bhadeshia (H.K.D.H. Bhadeshia, 2001)	57
Figure 39 Tempering of bainitic steels with carbon content of 0.06/0.14C wt. % (H.K.D.H. Bhadeshia, 2001)..	59
Figure 40 The variation of hardness (HV) with tempering at 973K (700°C) with time for martensite and bainite, 0.45% carbon steel, starting hardness martensite 667 HV – starting hardness bainite– 326 HV (W. J. Nam, 1999).....	60
Figure 41 Average particle diameter of cementite with tempering time for martensite (M) and bainite (B) in medium carbon steel (0.45%C) rods, tempered at 700 degrees C after quenching (W. J. Nam, 1999).....	62
Figure 42 50 hr temper at 973 K (700°C) (a) martensite (b) lower bainite taken from (W. J. Nam, 1999).....	62
Figure 43 Misorientation angle distribution of lath boundaries measured by TEM Kikuchi pattern analysis in 0.0049C, 3.14Mn (mass%) steel (Morito, Huang, et al., 2006)	66
Figure 44 Relationship between the prior austenite grain size and packet size in quenched martensite in the Fe-0.2C and Fe-0.2C-2Mn alloys (Morito, Yoshida, et al., 2006)	67
Figure 45 Relationship between the prior austenite grain size and the block width in quenched martensite in the Fe-0.2C and Fe-0.2C-2Mn alloys (Morito, Yoshida, et al., 2006).....	67
Figure 46 Comparison between Lath Width and Strengthening Contributions: Equation 2.9 from (Maropoulos & Ridley, 2005) has been used and values plotted for lath width between 0.1 and 1, with the strengthening contribution converted to Brinell hardness using Equation 2.8	68
Figure 47 Assumed variation in dislocation density of martensite or of bainite as a function of transformation start temperature (Young and Bhadeshia 1994).....	71
Figure 48 Variation in hardness (HV) with vol.% of lower bainite in LB-M steel, with 0.35% C. The prediction lines (eq. 7 mentioned on the figure) is the Rule of Mixtures for un-tempered and tempered at 473K (200 °C) for 10 minutes (Park & Kwon, 2001)	78
Figure 49 Effect of volume fraction of lower bainite on strength $\sigma_{0.2}$, σ_u and fracture ductility ϵ_f of (a) 0.2%C and (b) 0.4%C steel taken from (Y. Tomita, 1991).....	79
Figure 50 Schematic diagram of microstructural parameters of lower bainite (W_{lb} = width of lower bainite, L_{lb} =length of lower bainite, S_m =size of martensite (Y. Tomita, 1991)	80
Figure 51 Hardness of martensite, bainite and mixed martensite + bainite samples, taken from (Barranco 1992)	83
Figure 52 Hardness of martensite, bainite and mixed martensite + bainite samples that have been tempered from 260 °C to 704 °C for 1 hour, data taken from (Barranco, 1992) LB = lower bainite	84
Figure 53 Starting bainitic microstructure, α_b is bainite and α' is martensite – Intraplate carbides are not present – indicating upper bainite. Austenitised at 1050 °C for 15 minutes, 480 °C for 30 min, and then water quenched (Thomson & Bhadeshia, 1994a).....	85
Figure 54 Ferrite and upper bainite cementite. Cr enrichment Comparison of average Cr content in cementite in fully bainite and mixed microstructure specimen as a function of tempering time at 565 °C (Thomson and Bhadeshia 1994)	86
Figure 55 Inclusions in the three as-received plates through thickness, from left to right Base, BaseMoV, BaseSiCrMoV.....	92
Figure 56 Optical Images of martensitic start conditions (Base).....	93
Figure 57 Optical Images of martensitic start conditions (BaseMoV).....	94

Figure 58 Optical Images of martensitic start conditions (BaseSiCrMoV)	94
Figure 59 Example of mixed Martensitic and Lower Bainitic used for phase analysis with overlaid grid.....	96
Figure 60 Example of mixed Martensitic and Lower Bainitic used for phase analysis with overlaid grid - Magnified so grid can be easily observed.....	97
Figure 61 Lower Bainite.....	97
Figure 62 Martensite.....	97
Figure 63 Gleeble set up, showing location of sample, copper grips, thermocouples and quench head	100
Figure 64 Dilatometry transformation of BaseMoV, with isothermal hold at 430 °C for 1 hour.	101
Figure 65 Gleeble heating/cooling schedule (thermocouple measurements) for re-austenisation, cooling to isothermal hold temperature for formation of lower bainite followed by forced air cool to form martensite.	102
Figure 66 Isothermal hold at 430 °C showing martensitic start temperature	104
Figure 67 CCT diagram for BaseMoV	106
Figure 68 Showing the graph used for cooling.....	111
Figure 69 Example of how lattice parameter is determined	112
Figure 70 SEM of as-quenched Base steel showing a lath martensite structure with auto-tempered (intra-lath) carbides, ×4,000 magnification. (457.9 ± 29.8 HV)	114
Figure 71 SEM of as-quenched Base steel showing a lath martensite structure with auto-tempered (intra-lath) carbides. (Higher magnification – ×12,000) (457.9 ± 29.8 HV).....	115
Figure 72 SEM of as-quenched BaseMoV steel showing a lath martensite structure with auto-tempered (intra- lath) carbides, ×4,000 Magnification. (453.7 ± 26.9 HV).....	116
Figure 73 SEM of as-quenched BaseMoV steel showing a lath martensite structure with auto-tempered (intra- lath) carbides. (Higher magnification - ×12,000) (453.7 ± 26.9 HV)	117
Figure 74 SEM of as-quenched BaseSiCrMoV steel showing a lath martensite structure with auto-tempered (intra-lath) carbides. (470.6 ± 30.7 HV)	118
Figure 75 SEM of as-quenched BaseSiCrMoV steel showing a lath martensite structure with auto-tempered (intra-lath) carbides. (Higher magnification) (470.6 ± 30.7 HV).....	119
Figure 76 Point count analysis of microstructural features of as-quenched lath martensite	121
Figure 77 BaseMoV - Example micrograph showing difference features identified.....	122
Figure 78 Lath widths in as-quenched condition	130
Figure 79 Comparison between Vickers and Brinell hardness values	132
Figure 80 Base tempered for 2 hours at 600 °C, comparison between carbides on the boundary and within the matrix (263.4 ± 7.6 HV)	139
Figure 81 Contribution to hardness from the carbides.....	144
Figure 82 SEM micrograph showing carbides in the Base steel after 2 hours tempering at 600 °C (263.4 ± 7.6 HV)	146
Figure 83 SEM micrograph showing carbides in the Base steel after 2 hours tempering at 600 °C (higher magnification) (263.4 ± 7.6 HV)	146
Figure 84 SEM micrograph showing carbides in the Base steel after 16 hours tempering at 600 °C (221 ± 7.6 HV)	147
Figure 85 SEM micrograph showing carbides in the Base steel after 16 hours tempering at 600 °C (higher magnification) (221 ± 7.6 HV)	147
Figure 86 SEM micrograph showing carbides in the BaseMoV steel after 2 hours tempering at 600 °C (360.1 ± 12.2 HV)	148
Figure 87 SEM micrograph showing carbides in the BaseMoV steel after 2 hours tempering at 600 °C (higher magnification) (360.1 ± 12.2 HV)	148
Figure 88 SEM micrograph showing carbides in the BaseMoV steel after 16 hours tempering at 600 °C (321.3 ± 8.0 HV)	149
Figure 89 SEM micrograph showing carbides in the BaseMoV steel after 16 hours tempering at 600 °C (higher magnification) (321.3 ± 8.0 HV)	149
Figure 90 SEM micrograph showing carbides in the BaseSiCrMoV steel after 2 hours tempering at 600 °C (336.0 ± 10.5 HV).....	150
Figure 91 SEM micrograph showing carbides in the BaseSiCrMoV steel after 2 hours tempering at 600 °C (higher magnification) (336.0 ± 10.5 HV).....	150
Figure 92 SEM micrograph showing carbides in the BaseSiCrMoV steel after 16 hours tempering at 600 °C (320.0 ± 10.4 HV).....	151

Figure 93 SEM micrograph showing carbides in the BaseSiCrMoV steel after 16 hours tempering at 600 °C (higher magnification) (320.0 ± 10.4 HV).....	151
Figure 94 Changes in Lath Size Distribution with Tempering at 600 °C for Base.....	153
Figure 95 Changes in Lath Size Distribution with Tempering at 600 °C – For 2 Hours.....	154
Figure 96 Changes in Lath Size Distribution with Tempering at 600 °C – 16 hours temper.....	155
Figure 97 Change in hardness on tempering up to 16 hours (Base-BaseMoV-BaseSiCrMoV) – Grey region indicates the expected secondary hardening region based on literature reports (Baker & Nutting, 1959; Fujita, 2000; Grange et al., 1977; Kwon et al., 1997; Won Jong Nam et al., 2003; Tekin; & Kelly, 1965) Compositions C wt. % Min -0.15, Max – 0.19. Mo wt. % Min – 0.00, Max – 3.07. Cr wt. % Min – 0.00, Max – 2.25, V wt. % Min – 0.00, Max – 0.2. See section 2.7 for more details.	159
Figure 98 Hardness values after 100 hours tempering for Base, BaseMoV and BaseSiCrMoV martensitic steels.....	160
Figure 99 Base after 100 hours tempering (185.2 ± 14.5 HV).....	161
Figure 100 BaseMoV after 100 hours tempering (189.7 ± 7.3 HV).....	162
Figure 101 BaseSiCrMoV after 100 hours tempering (262.8 ± 7.3 HV).....	163
Figure 102 TTT curve predicted using Bhadeshia and Babu program for Base (H. K. D. H. Bhadeshia & Babu, 2015).....	171
Figure 103 TTT curve predicted using Bhadeshia and Babu program for BaseMoV (H. K. D. H. Bhadeshia & Babu, 2015).....	172
Figure 104 TTT/CCT curve predicted using Bhadeshia and Babu program for Base SiCrMoV (H. K. D. H. Bhadeshia & Babu, 2015).....	172
Figure 105 Phase analysis of oil quenched alloys - including hardness.....	173
Figure 106 Base Oil Quenched (407.4 ± 32.5 HV).....	174
Figure 107 BaseMoV Oil quenched (453.5 ± 16.4 HV).....	175
Figure 108 BaseSiCrMoV oil quenched (459.9 ± 16.0 HV).....	176
Figure 109 Phase Analysis of furnace cooled BaseSiCrMoV- including hardness.....	177
Figure 110 BaseSiCrMoV Furnace Cooled (306.3 ± 16.1 HV).....	178
Figure 111 Phase Analysis of Air Cooled Alloys - Including Hardness.....	179
Figure 112 Base Air Cooled (180.2 ± 4.2 HV).....	180
Figure 113 BaseMoV Air Cooled (288.1 ± 11.6 HV).....	181
Figure 114 BaseSiCrMoV Air Cool (359.1 ± 15.2 HV).....	182
Figure 115 Dilatometry transformation of BaseMoV, with isothermal hold at 430 °C for 1 hour.....	185
Figure 116 BaseMoV held at 430 °C for 5 minutes (351.5 ± 4.0 HV).....	187
Figure 117 300 (5 minute) second isothermal hold of BaseMoV at 430 °C.....	187
Figure 118 (111) – FCC peak and (110) – BCC peak in a 0.35 wt. % C low alloy bainitic steel (Talebi, Jahazi et al. 2018).....	188
Figure 119 XRD pattern of BaseMoV held for 430 °C for 5 minutes.....	189
Figure 120 XRD pattern of BaseMoV held for 430 °C for 5 minutes.....	189
Figure 121 BaseSiCrMoV held at 441 °C for 15 minutes (268.0 ± 9.0 HV).....	191
Figure 122 BaseSiCrMoV held at 441 °C for 60 minutes (368.4 ± 16.0 HV).....	191
Figure 123 XRD pattern of BaseSiCrMoV held at 441 °C for 15 minutes (Angle 28-128).....	193
Figure 124 XRD pattern of BaseSiCrMoV held at 441 °C for 15 minutes (Angle 48-58).....	193
Figure 125 Bainitic Carbide Size - After Isothermal Hold.....	196
Figure 126 BaseMoV isothermal hold for 5 minutes, showing carbide size and orientation.....	197
Figure 127 Comparison between the lath size of as-quenched martensite and bainite with an isothermal hold of 5 minutes.....	198
Figure 128 BaseMoV Bainite - 2 hours at 600 °C (312.6 ± 10.0 HV).....	199
Figure 129 BaseMoV Bainite - 16 hours at 600 °C (292.7 ± 10.0 HV).....	200
Figure 130 Tempering of martensite and bainite.....	202
Figure 131 Bainite - 2 hours vs. 16 hours.....	204
Figure 132 Bainitic lath size.....	205
Figure 133 Comparison of martensitic and bainitic lath sizes at 16 hours temper.....	207
Figure 134 BaseMoV 8 Second Isothermal Hold (Blue – Lower Bainite, Red – Martensite) (425.1 ± 4.0 HV).....	210
Figure 135 BaseMoV 13 second isothermal hold (Blue – Lower Bainite, Red – Martensite) (411.6 ± 6.2 HV).....	211
Figure 136 BaseMoV 20 second hold (Blue – Lower Bainite, Red – Martensite) (380.7 ± 4.2 HV).....	212
Figure 137 Change in Gleeble stroke measurement during isothermal hold at 430 °C between 0 and 300 seconds.....	

.....	215
Figure 138 Comparison of lath Size of Water Quenched Martensite and 13 second ITH Martensite	217
Figure 139 BaseMoV Isothermal Hold at 430 °C for 8 seconds showing elongation in bainitic carbides	218
Figure 140 BaseMoV Isothermal Hold at 430 °C for 20 seconds showing elongation in bainitic carbides	219
Figure 141 Bainitic Carbide Size in nm (Equivalent Circle Diameter) after Isothermal Hold	221
Figure 142 Vickers Hardness after isothermal hold (bainite/mixtures) and water quenching (martensite)	222
Figure 143 Comparison between Vickers Hardness and Predicted Lower Bainite Percentage	226
Figure 144 Comparison between Vickers Hardness and Tempering Time at 600 °C	229
Figure 145 Schematic representing the maximum and minimum dimensions of the carbides	230
Figure 146 2 hours - 100% Martensite vs. 56 % Martensite (Min Size/Max Size/Aspect Ratio)	237
Figure 147 16 Hours - 100% Martensite vs. 56 % Martensite (Min Size/Max Size/Aspect Ratio)	238
Figure 148 2 Hours 100% Bainite vs. 44% Bainite (Min Size/Max Size/Aspect Ratio)	239
Figure 149 16 Hours 44% Bainite vs. 100% Bainite (Min Size/Max Size/Aspect Ratio)	240
Figure 150 Hardness on tempering up to 100 hours (Hardness (HV) vs. Time (log) Hours)	243
Figure 151 Tempering up to 100 Hours (Hardness vs. Percentage of Lower Bainite)	244
Figure 152 Martensite- Comparison between 16 and 100 Hours Temper (16 Hours) – ×5,000 Magnification (321.3 ± 4.0 HV)	245
Figure 153 BaseMoV - Martensite - 100 Hours ×2,500 Magnification (189.7 ± 6.0 HV)	246
Figure 154 Martensite- Comparison between 16 and 100 Hours Temper (100 Hours) ×5,000 Magnification (189.7 ± 6.0 HV)	246
Figure 155 Bainite - Comparison Between 16 and 100 Hours Temper (16 hours) ×5,000 Magnification (292.7 ± 10.0 HV)	247
Figure 156 BaseMoV - Bainite - 100 hours ×2,500 Magnification (264.3 ± 10.0 HV)	248
Figure 157 Bainite - Comparison Between 16 and 100 Hours Temper (100 hours) ×5,000 Magnification (264.3 ± 10.0 HV)	248
Figure 158 Mixed Microstructure - Comparison Between 16 and 100 Hours Temper (16 hours) ×5,000 Magnification (297.0 ± 10.0 HV)	250
Figure 159 Mixed Microstructure - Comparison Between 16 and 100 Hours Temper (100 hours) ×5,000 Magnification (203.5 ± 10.0 HV)	251
Figure 160 BaseMoV - Mixed Microstructure - 100 Hours ×2,500 Magnification (203.5 ± 10.0 HV)	252
Figure 161 Bainite vs. Mixed Microstructure Lath Size - 100 Hours Temper	256
Figure 162 Min Mode of Carbides on tempering at 2, 16 and 100 hours	259
Figure 163 Max Mode of Carbides on tempering at 2, 16 and 100 hours	260
Figure 164 Carbide Size for 100 hours temper (Min - Width)	260
Figure 165 Carbide Size for 100 Hours Temper (Max - Length)	261
Figure 166 Carbide Size for 100 Hours Temper (Aspect Ratio)	261
Figure 167 Cooling of steel plates, figure provided by TATA Steel, looking at core cooling rates	267
Figure 168 Cooling Curve from COMSOL, using parameters in Table 16	268
Figure 169 Heat Capacity comparison	271
Figure 170 Thermal Conductivity Comparisons	272
Figure 171 Density Data Comparison	273
Figure 172 Real Time Data - Heating of 5 cm diameter cylindrical steel piece	275
Figure 173 Comparison between COMSOL and heating data	277
Figure 174 Surface emissivity on heating (Range 0 - 1)	280
Figure 175 Heat Transfer Coefficient Comparison	280

List of Tables

Table 1 Typical composition of S690 steel, all wt. %(McFarlane, 2018)	1
Table 2 Summary of reported martensitic structures for steels with different C contents	16
Table 3 Compositions of steels and carbides after tempering at 600 °C for 10 hours	37
Table 4 Difference between upper and lower bainite in ultra/low carbon steel (H. Bhadeshia, 1997; George Krauss & Thompson, 1995)	50
Table 5 Data taken from (H.K.D.H. Bhadeshia, 2001)- Showing the minimum and maximum compositions in which epsilon carbide was found in lower bainite	52
Table 6 Ratio of Fe to element in cementite and ferrite using data taken from Figure 35 and analysed by Image J	

taking the average atomic %, which is then divided by the iron concentration of ferrite and cementite, 99% and 75% respectively.	53
Table 7 The strengthening coefficients of each element (Llewellyn, 2013).....	69
Table 8 Predicted and measured strength values for martensite steels reported by Maropoulos and Ridley 2005). Values are taken from paper and converted to Brinell hardness	73
Table 9 Composition of steel used by Y. Tomita, 1991	76
Table 10 Summary of alloying elements covered in literature	88
Table 11 Composition wt. % and thickness of steels examined	90
Table 12 Comparison of hardness and microstructure of as-rolled steels.....	91
Table 13 Dilatometry Isothermal Temperatures and Holding Times	103
Table 14 Details of holding times and microstructures obtained.....	104
Table 15 Cooling rates, hardness and microstructure of BaseMoV.....	105
Table 16 Parameters used in COMSOL for cooling from 925 °C to room temperature	110
Table 17 Parameters used for heating of room temperature to 600 °C	111
Table 18 Predicted Ms temperatures for the three steels studied (predicted from Totten and Howes equation (Equation 2.2)(Totten & Howes, 1997)).....	122
Table 19 Percentage of cementite and epsilon carbide in the as-quenched condition for the three steels studied (Ju, 2018)	124
Table 20 Lattice parameter estimated and predicted carbon contents of the three steels.....	126
Table 21 Predicted strain in the three steels.....	127
Table 22 Grain Size	128
Table 23 Predicted precipitates present at 925°C, including volume fraction. Predicted using Thermo-Calc....	128
Table 24 Comparison between carbon in solid solution and expected lath size	131
Table 25 Table showing contribution to hardness from alloying elements	132
Table 26 Hardness of compositions compared to literature.....	133
Table 27 Equilibrium alloy carbides for Base-BaseMoV-BaseSiCrMoV, along with carbon in solid solution at 600 °C, predicted using Thermo-Calc	137
Table 28 Volume fraction of fine carbides in BaseMoV and BaseSiCrMoV	141
Table 29 Carbide sizes.....	145
Table 30 Change in average lath size on tempering at 600 °C for the three compositions	152
Table 31 Lattice parameter and predicted carbon content	156
Table 32 Summary of change in strengthening mechanism on tempering	157
Table 33 Summary of carbide for 100 hours temper	167
Table 34 Hardness of Base/BaseMoV/BaseSiCrMoV after normalisation for 1 hour at 925 °C, then moved to a 500 °C furnace for 5 minutes finished with a water quench	182
Table 35 Comparison between BaseSiCrMoV – 15 minutes at 441 °C followed by air cool and air cooled with subsequent liquid nitrogen quench.....	194
Table 36 Details of holding times and microstructures obtained.....	209
Table 37 Isothermal hold time comparing microstructural analysis and percentage change in stroke	214
Table 38 Larson Miller Tempering Parameters	225
Table 39 Ranking the mixed microstructure hardness on tempering.....	228
Table 40 Mode Min, Max and Aspect Ratio of the carbides in martensite and bainite microstructures, along with carbide density	231
Table 41 Comparison of microstructural features at 100 hours temper	254
Table 42 Mode Min, Max, Aspect Ratio of carbides in martensitic, bainitic and mixed microstructure at 100 hours tempering, including carbide density	257
Table 43 Alloying containing carbides of bainite, martensite and mixed microstructure.....	262
Table 44 Comparison between experimental data and COMSOL cooling rates from 800-600 °C.....	269

Chapter 1: General Introduction

Rolled Quenched and Tempered (RQT) steels are low alloy content materials that have excellent strength and toughness achieved through a desired tempered martensitic structure, a typical example is S690 steel ([Table 1](#) for composition and [Figure 1](#) for typical microstructure). Uses for the steel include quarrying and mining equipment, along with bridges, cranes and forklifts.

Table 1 Typical composition of S690 steel, all wt. % (McFarlane, 2018)

C	Si	Mn	S	P	Cr
0.20	0.50	1.60	0.010	0.025	1.00
Mo	Nb	V	Ni	Cu	B
0.70	0.060	0.08	1.50	0.40	0.004

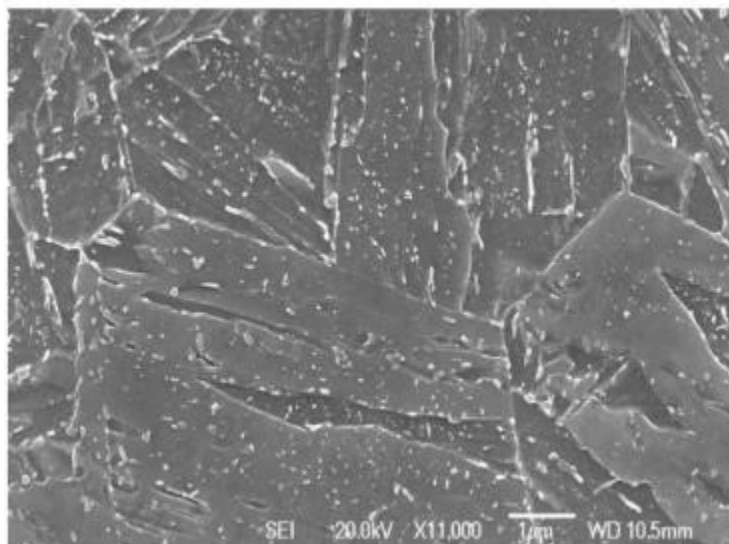


Figure 1 Micrograph of S690 water quenched then tempered for 30 minutes at 600 °C (Driscoll, 2014)

Rolled quenched and tempered (RQT) steel plate is produced from slabs of steel which are hot rolled to the desired thickness, then reheated and roller pressure cooled to room temperature, in a process called quenching. A range of thickness plates, for example from 8 to 130 mm (McFarlane, 2018), can be produced depending on the application, with thicker plates cooling more slowly than thinner plates during the quench process. The slower cooling rate in the centre of thick plates means that either the desired martensitic structure is not obtained, with different microstructure forming (see [Figure 2](#)) or higher alloy content is required to provide the greater hardenability necessary to achieve martensite.

After quenching the plates are tempered to improve the toughness. For thick plates the time at temperature during tempering to achieve the optimum structure will be different for the surface and centre of the plate due to the requirement to reach temperature in the furnace. In addition, if a mixed microstructure (martensite and/or bainite) is formed then differences in tempering response can be seen. In the literature there has been little consideration of the tempering response of lower bainitic and martensitic mixed microstructures in low carbon, low alloy steels. This work will look at the tempering response of a range of microstructures, including 100% martensite, 100% bainite and mixed martensite + bainite microstructures to determine the effect of initial microstructure and how they temper with varying tempering times. In addition, the effects of alloying elements (Cr, Si, Mo and V) on the tempering response will be considered. To link with industrial needs/objectives a focus on the tempering of plates will be considered, with prediction of what microstructure will form on cooling through thickness (hardenability) and how they will respond to tempering.

Chapter 2: Literature Review

2. 1: Tempering of steels

Tempering is a process of heating a material and holding it at a defined temperature, it is used to improve toughness and ductility in quenched martensitic steel. This is achieved through a reduction in internal stresses by a process of carbide precipitation, which removes carbon from solid solution. Tempering can also result in a secondary hardening effect through the precipitation of alloy carbides resulting from longer times at temperature (H. K. D. H. Bhadeshia & Honeycombe, 2006; Llewellyn, 2013). During tempering of martensite its strength is reduced, whilst the toughness is increased. Un-tempered martensite is a phase which is super saturated with carbon, providing a strong driving force for carbide precipitation (H. K. D. H. Bhadeshia & Honeycombe, 2006). This is in contrast with bainite, in which there is a slower response to tempering, due to the phase being formed at higher temperatures (with carbide precipitation) than martensite, allowing a longer time for recovery to occur during cooling and more stable microstructures being formed (H.K.D.H. Bhadeshia, 2001).

2.1.1: Continuous cooling Transformation (CCT) Diagrams

CCT diagrams are used to determine the transformation expected from a series of cooling curves. Figure 2 shows that the cooling rate of a steel is important, as it is possible to have differences in microstructure generated by different cooling rates such as through the thickness of a cooled steel part. Martensite needs the quickest cooling rate for the microstructure to be formed.

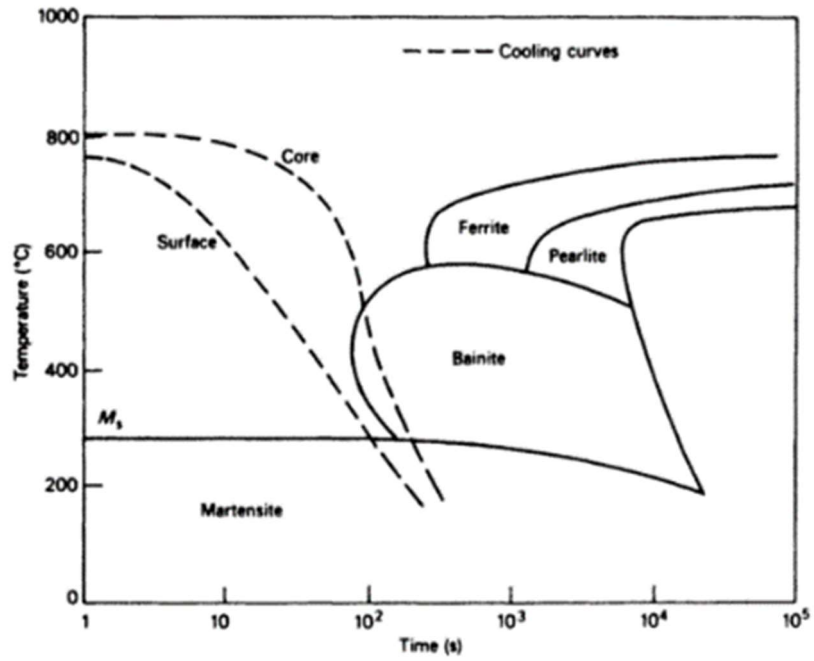


Figure 2 Comparison between core and surface cooling rates and resulting microstructure for a 0.3C, 2.0Mo (wt. %) oil quenched 95-mm diameter steel bar (H.K.D.H. Bhadeshia, 2001)

2.2: Martensite

2.2.1: Formation of martensite

As-quenched martensite is a brittle but strong phase, in comparison to the other microstructural phases shown in steels (bainite, ferrite, etc.). The cooling from the austenitic temperature region needs to be quick enough to avoid diffusional transformation phases forming. The rapid cooling from austenite traps carbon in solid solution, causing the crystal structure to distort, forming a body-centred-tetragonal structure. The carbon trapped in solid solution contributes to the martensitic strength (H. K. D. H. Bhadeshia & Honeycombe, 2007; Samuel & Hussein, 1982; Speich, 1969).

The martensitic transformation is diffusion-less and a critical temperature needs to be reached before transformation can begin (Campbell, 2008; Llewellyn, 2013). The amount of martensite does not depend on the time taken to cool within the martensitic region but is dependent on the amount of cooling below the martensite-start temperature with full transformation to martensite obtained if cooling is carried out below the martensitic finish (M_f) temperature (discussed in section 2.4).

2.2.2: Para-Equilibrium

Thomson and Miller found para-equilibrium in 0.15 wt. % C martensitic steel, with processing conditions which included holding at 350 °C for 5 minutes and holding another sample for 2 hours using atom probe techniques, as shown [Figure 3](#) (Thomson & Miller, 1998). [Figure 3](#) shows a cumulative ion composition plot across a carbide-matrix interface, showing a linear increase in the Cr, Mo, Mn and Si compared to a plateau in the C content, indicating that there is the same composition of alloying elements in the martensitic matrix and cementite particle. There is little change in profile in the cumulative curves between 5 minutes and 2 hours indicating that the cementite is not becoming enriched with the alloying elements at this tempering temperature and time.

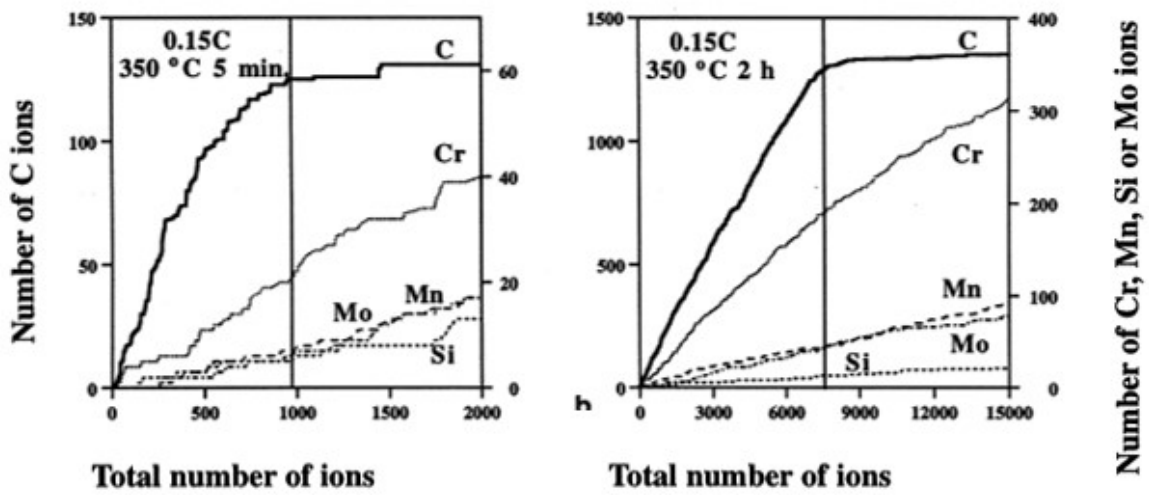


Figure 3 Atom probe cumulative plots for analyses across cementite/matrix interfaces in 2.25%Cr – 1%Mo – 0.15 wt. %C steel tempered for 5 min and 2 hr in a martensitic steel (Thomson & Miller, 1998)

2.2.3: Austenisation Temperature

To produce a fully austenitic microstructure the austenisation/normalising temperature needs to be approximately 100 °C above the Ac₃ temperature. The sample is then cooled to produce the different steel phases (H. K. D. H. Bhadeshia & Honeycombe, 2006). The temperature of austenisation influences the mechanical properties; Figure 4 demonstrates the optimum temperature range for a 0.68 wt. %C - 3.15 wt. % Cr - 0.69 wt. % Mo steel, normalised for 30 minutes and then quenched. Austenitising below 880 °C the austenite means that alloy carbides are not dissolved resulting in a low amount of carbon alloying elements in solution, which causes the hardness to reduce in the as-quenched martensite. As the temperature increases there are more alloying element carbides dissolved, releasing both alloying elements and carbon to increase the strength in the as-quenched martensite from trapped carbon and solid solution strengthening. Above 950 °C the hardness decrease is reported to be due to the sharp increase of alloying elements and carbon which were dissolved in high temperature austenite, decreasing the M_f temperature below room temperature and resulting in retained austenite. Therefore, the austenisation temperature chosen can have a large effect on the subsequent mechanical properties, particularly in higher alloyed steels where the M_f temperature might be reduced to below room temperature.

The increasing austenite temperature from 950 °C to 1100 °C showed an increase in austenite grain size from 32-35 to 60-70 μm and packet and lath width of the martensite increased.

This indicates that the temperature of austenisation is important and can affect the properties of the steel (Bakhsheshi-Rad et al., 2011).

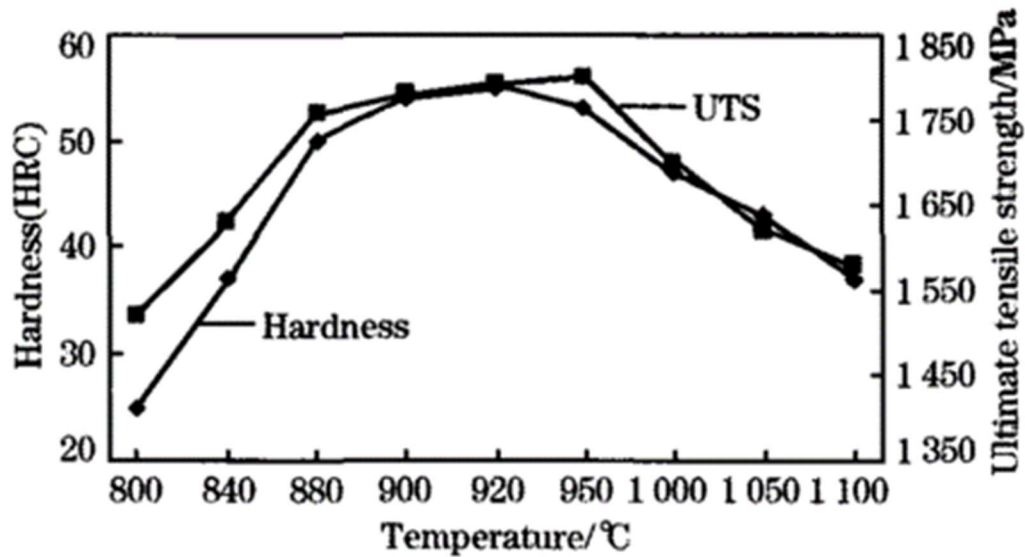


Figure 4 Effect of austenitisation temperature on hardness and ultimate tensile strength for a 0.68 wt. % C, 3.15 wt. % Cr, 0.69 wt. % Mo steel, normalised for 30 minutes and quenched (Bakhsheshi-Rad et al., 2011)

Figure 5 shows that with increased austenitisation temperatures there is more solution of microalloyed elements (Maalekian, 2007). This agrees with Bakhsheshi-Rad's work which states that there is a difference in hardness due to increased precipitation dissolution at higher temperatures. It is also important to note that the carbides and nitrides present during austenitisation can pin grain boundaries, resulting in slow grain growth and a lower hardenability, this is discussed next in section 2.2.4.

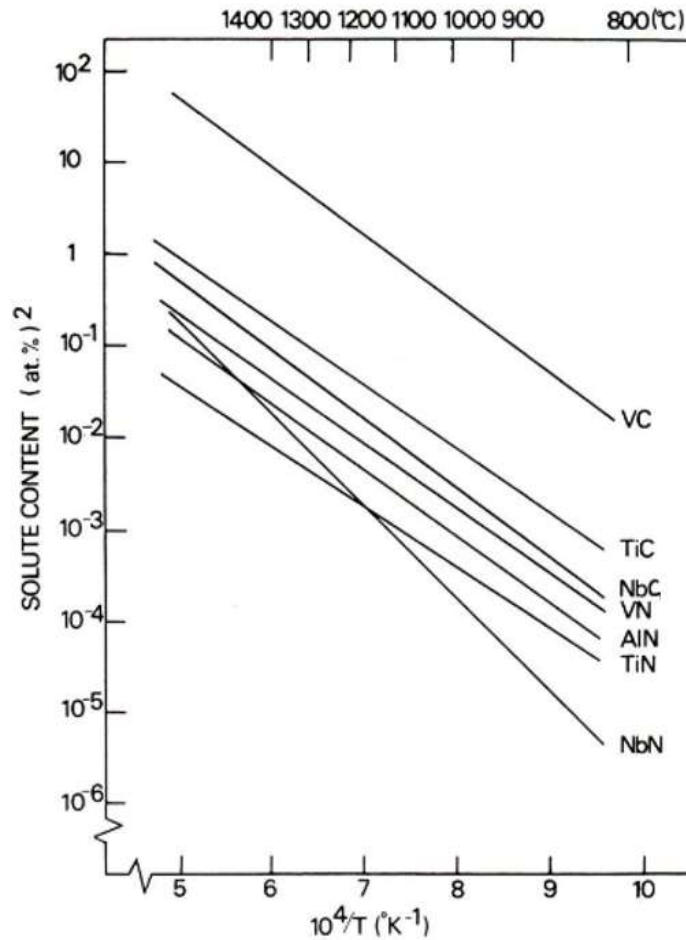


Figure 5 Solubility of carbide and nitrides in austenite as a function of temperature (Maalekian, 2007)

2.2.4: Hardenability

The ability of a steel to form martensite at a given cooling rate is related to its hardenability (H. K. D. H. Bhadeshia & Honeycombe, 2006) and is therefore extremely useful in determining the rate at which a steel should be cooled (e.g. air cooled or quenched) to achieve martensite (Wadhwa & Dhaliwal, 2008). If steel has a high hardenability, a slower cooling rate (such as air cooling) may be enough to produce a martensitic microstructure.

Hardenability is influenced by a number of different factors, such as the alloying elements present and austenite grain size (H. K. D. H. Bhadeshia & Honeycombe, 2006; Llewellyn, 2013). The carbon content has a strong effect on hardenability and controls the hardness level

in as-quenched martensite. Small additions of certain alloying elements slow diffusional and displacive-diffusional transformations of pearlite, ferrite and bainite, having the effect of increasing hardenability and ability to form martensite. This means slower cooling rates can be used and therefore thicker plate gauges, which cool slower, can be produced with a martensitic structure. Alloying elements such as Mo, Cr and Mn are added for increased hardenability (Llewellyn, 2013).

2.2.5: Prior Austenite Grain Size

The prior austenite grain size influences factors such as M_s temperature, martensite lath/plate size and amount of retained austenite. With an increased grain size there is a decrease in M_s temperature, as the area of grain boundary decreases; this results in a decrease of nucleation sites and martensitic transformation is suppressed to lower temperatures. This will therefore mean that the chance of retained austenite is increased as the M_f temperature may be reduced below room temperature. With increased grain size there is an increase in hardenability. This is because the grain boundaries acts as nucleation site. With increased grain size there are fewer nucleation sites for phase transformation and it is easier for martensite to form without other phases present (H. K. D. H. Bhadeshia & Honeycombe, 2006). The size of laths and plates are also affected by the prior austenite grain size, as this is related to the packet size (discussed in more detail in section 2.13.1) (Morito, Yoshida, et al., 2006).

2.3: Carbon Content

2.3.1: Hardness

The greatest contribution to strength of as-quenched martensite is the amount of carbon present (Hutchinson et al., 2011).

There is a positive linear relationship between carbon content and hardness, demonstrated by [Figure 6](#) and [Figure 7](#) for a range of carbon contents. Krauss shows deviation from an upwards linear trend noticeable above 0.5 wt. % C. The deviation from the trendline is reported to be due to the presence of retained austenite (associated with higher carbon contents), which does not provide significant strengthening (Hutchinson et al., 2011; G. Krauss, 1978; Samuel & Hussein, 1983).

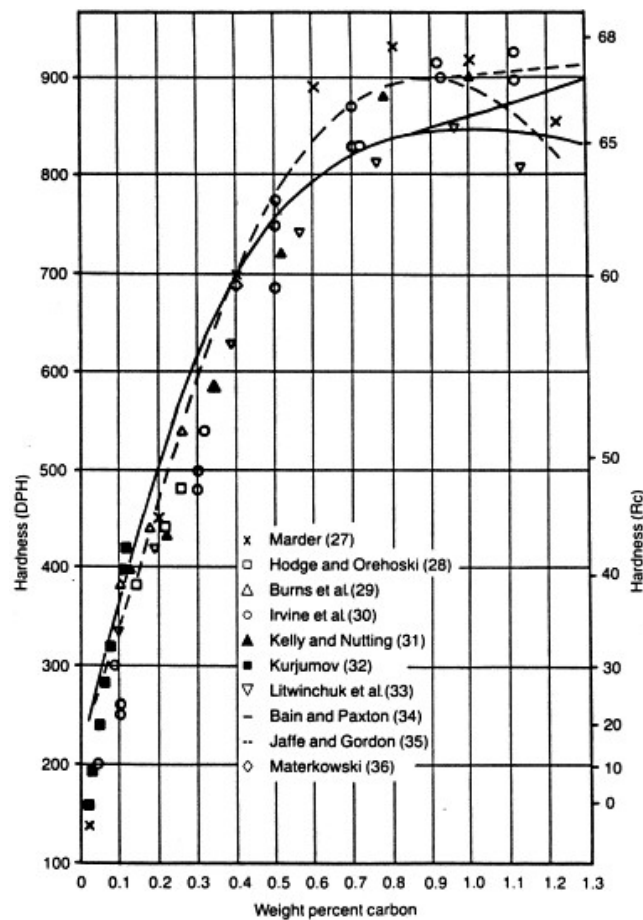


Figure 6 Hardness of as-quenched martensitic microstructures as a function of steel carbon content (G. Krauss, 1978)

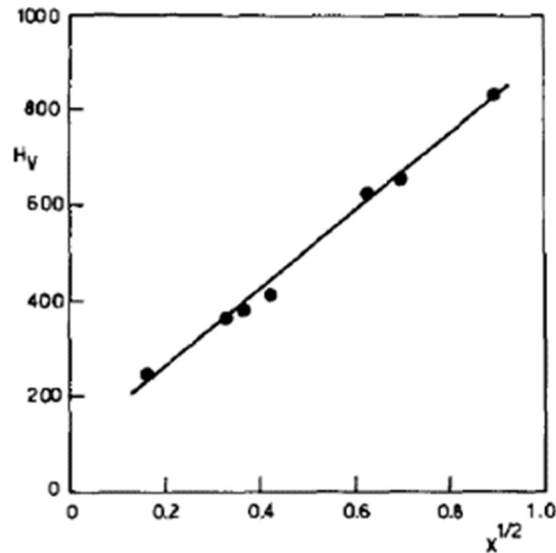


Figure 7 Variation in Vickers hardness of martensite with carbon content (Best fit from carbon content to the power half) (Samuel & Hussein, 1983)

2.4: Martensite Start Temperature

The martensite start temperature (M_s) determines the temperature at which martensite is formed. One such equation which can be used to determine the M_s is Andrews equation (Equation 2.1), which Van Bohemen discussed as being valid for steels with 0.1 – 0.6 wt. %C (Andrews, 1965; Van Bohemen, 2012). Van Bohemen mentions that this equation is valid if all the alloying elements are dissolved in solid solution. Capdevila looked at different M_s temperature predictions and found Andrews equation to have excellent agreement between experimental and predicted M_s temperatures (Capdevila et al., 2002).

Andrews Equation

$$M_s (^{\circ}C) = 539.0 - 423.0 (\text{wt } \% C) - 30.4 (\text{wt } \% Mn) - 12.1 (\text{wt } \% Cr) - 17.7 (\text{wt } \% Ni) - 7.5 (\text{wt } \% Mo) + 10.0 (\text{wt } \% Co) - 7.5 (\text{wt } \% Si)$$

Equation 2.1

Another equation is the Totten and Howes (Equation 2.2) M_s equation, which is suitable for steel with carbon contents between 0.2 -0.8 wt. % C, also having a good agreement with experimental data. It is noted that the equation can give inaccurate results from multi – alloyed steels, this means the results should be treated with caution, but can give an approximate M_s temperature (Totten & Howes, 1997). Both the Andrews and Totten and

Howes equations can be suitable for S690 steel, and this is dependent on the alloying elements present, for example if there is no Co present then it is plausible to use the Totten and Howes equation.

$$M_s(oC) = 520 - 320(wt\%C) - 50(wt\%Mn) - 30(wt\%Cr) - 20[wt\%(Ni + Mo)] - 5[wt\%(Cu + Si)]$$

Equation 2.2

The Ms temperature may be altered with the addition of certain elements, such as those present in the equation. The martensite finish (Mf) temperature is normally around 200 °C lower than the Ms temperature and is when the martensitic transformation is completed (Llewellyn, 2013); this should be taken into account when designing alloy compositions as an Mf temperature lower than room temperature will mean that not all austenite present will transform to martensite if there is no sub-zero freeze included in the heat treatment schedule, leaving retained austenite. Figure 8 shows that with increasing carbon content the Ms and Mf temperatures decrease, at around 0.7 wt. % C the Mf temperature is lower than room temperature for a plain carbon steel, this does not consider alloying elements.

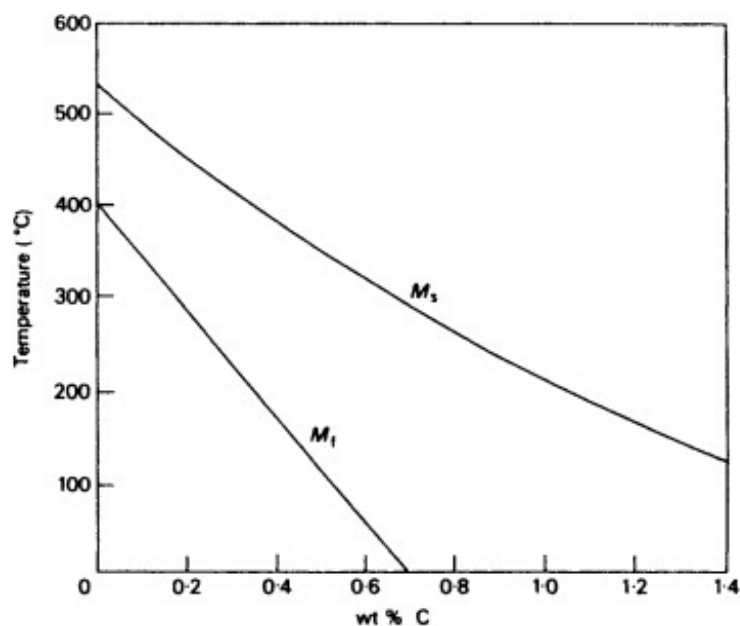


Figure 8 Effect of carbon content on Ms and Mf temperatures (Petty, 1970)

2. 5: Microstructure

2.5.1: Lath vs. Plate Martensite

Figure 9 and Figure 10 shows lath and plate structures for Fe-C steels (Speich & Leslie, 1972). Grange et al. also observed martensite with a lath structure in 0.12 wt. % C steel and plate structures in a steel with 0.42 wt. % C. This indicates that between 0.12 and 0.42 wt. % C a change in microstructure occurs as it changes from lath to plate martensite (Grange et al., 1977).

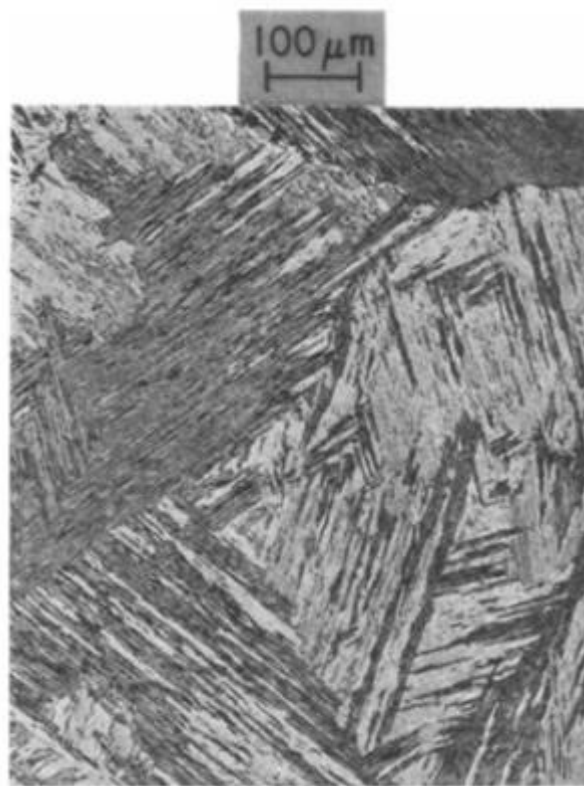


Figure 9 Lath martensite in 0.02 wt. %C Mn steel (Speich & Leslie, 1972)



Figure 10 Structure of plate martensite in a 1.2 wt. % C steel (Speich & Leslie, 1972)

Samuel found that as-quenched microstructures of plain-carbon steels with carbon contents between 0.11-0.18 wt. % were formed of dislocated laths. Steels with a carbon content between 0.4 and 0.5 wt. % was found to have micro twins in the interior of laths. There were slight differences with austenisation temperature, with the lower carbon contents having a higher austenisation temperature (0.01 wt. % C = 1100 °C/0.80 wt. % C = 900 °C), which may result in a difference in austenite grain size and M_f temperature, as discussed in section 2.4. (Samuel & Hussein, 1983). In agreement with this work, Man found twin structures, as a substructure within the laths, at carbon contents as low as 0.2 wt. % C (Man et al., 2018), this is in stark contrast with Lindsley, who found lath martensite at 0.2 and 0.6 wt. % C, mixtures of plate and lath in 0.8 – 1.0 wt. % C martensite and plate in 1.2 – 1.4 wt. % C martensitic steel (Lindsley, 1998). The 0.6 wt. % C value is significantly higher than the wt. % C of the other compositions which contain laths. As the 0.2 and 0.6 wt. % C has such vast differences in austenisation temperature, 1050 °C and 850 °C respectively, this not thought to be

comparable, as it differs so vastly from the literature, therefore the 0.6 wt. % C has not been included in the summarised results. Table 2 summaries the microstructures found by different authors.

Table 2 Summary of reported martensitic structures for steels with different C contents

Author	Lath wt. %C	Mixed wt. %C	Plate wt. % C
Lindsley (Lindsley, 1998)	0.2	0.8, 1.0	1.2, 1.4
Man (Man et al., 2018)		0.2	
Samuel (Samuel & Hussein, 1983)	0.11, 0.18	0.4, 0.5	0.8
Grange (Grange et al., 1977)	0.12		0.42, 0.97
Speich (Speich & Leslie, 1972)	0.2	0.2 +	1.0 +
Summary	0.11 – 0.2	0.2 – 1.0	0.42 – 1.4

2.5.2: Low carbon martensite lath-like structures:

Low carbon martensite has a lath structure with the laths typically being 0.5 μm wide and much longer in length (H. K. D. H. Bhadeshia & Honeycombe, 2007). Laths are within blocks, which are in turn within packets, all within a grain. Figure 11 shows a schematic diagram showing the relationship between laths, blocks, packets and grains (Morito, Huang, et al., 2006).

There are two types of grain boundaries which shall be referred to in this literature review; low grain boundary and high grain boundary. These refer to the angle between two structures within the steel, a high angle grain boundary has a mis-orientation that is typically higher than 15° , (an example are blocks and larger structures within the martensite) and require more energy for dislocations to travel across (Gottstein, 2004). Laths have low angle grain boundaries typically have a mis-orientation angle less than 3° (Morito, Huang, et al., 2006).

The block size is an important structural feature when it comes to analysing the strength in relation to structure of lath martensite in low carbon steel. Morito found that the high angle

boundaries within the structure are dominated by the block boundaries, which in turn are dependent on the austenite grain size. The work also found that the substructure strengthening within the blocks are independent of the grain size, meaning substructure strengthening is not determined by size of the grain (Morito, Yoshida, et al., 2006). This indicates that the low angle boundaries, which are found within the substructure, are not dependent on the grain size, but other strengthening factors. The strengthening mechanisms/hardness of microstructures is commented in greater detail later in section 2.13. For example, the sizes of laths have a relationship to carbon content that is close to a rectangular hyperbolic, shown in [Figure 12](#), which helps strengthen support that lath dimensions are also dependent on other factors. (Galindo-Nava & Rivera-Díaz-del-Castillo, 2015).

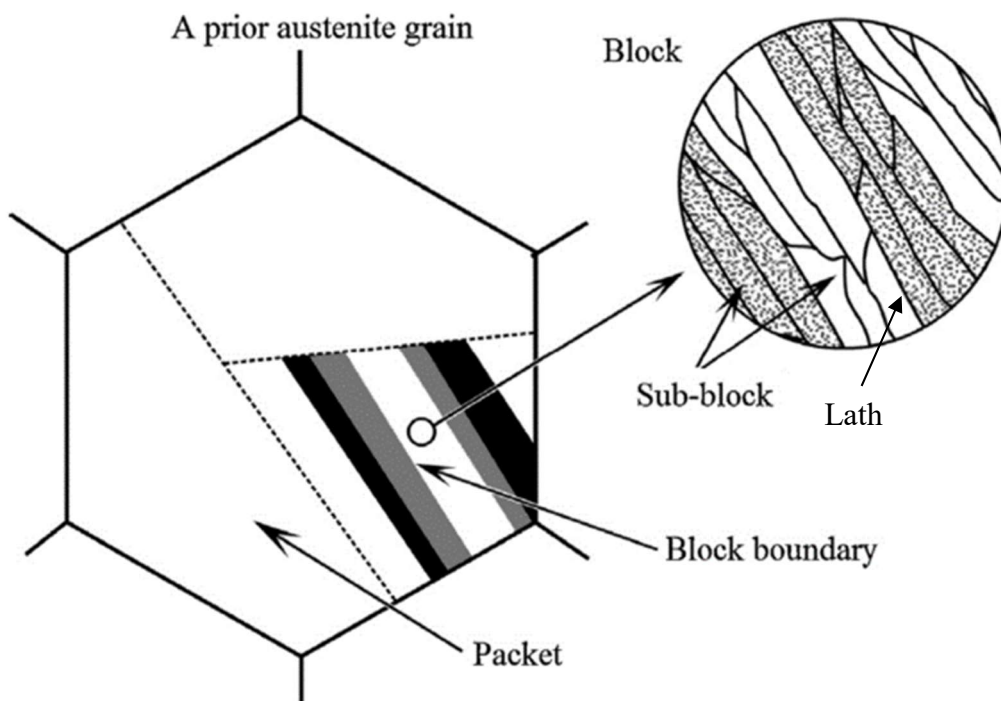


Figure 11 Schematic illustration of lath martensitic structure in low carbon steel - Adapted from (Morito, Huang, et al., 2006) by (Pham et al., 2013) and lath label added

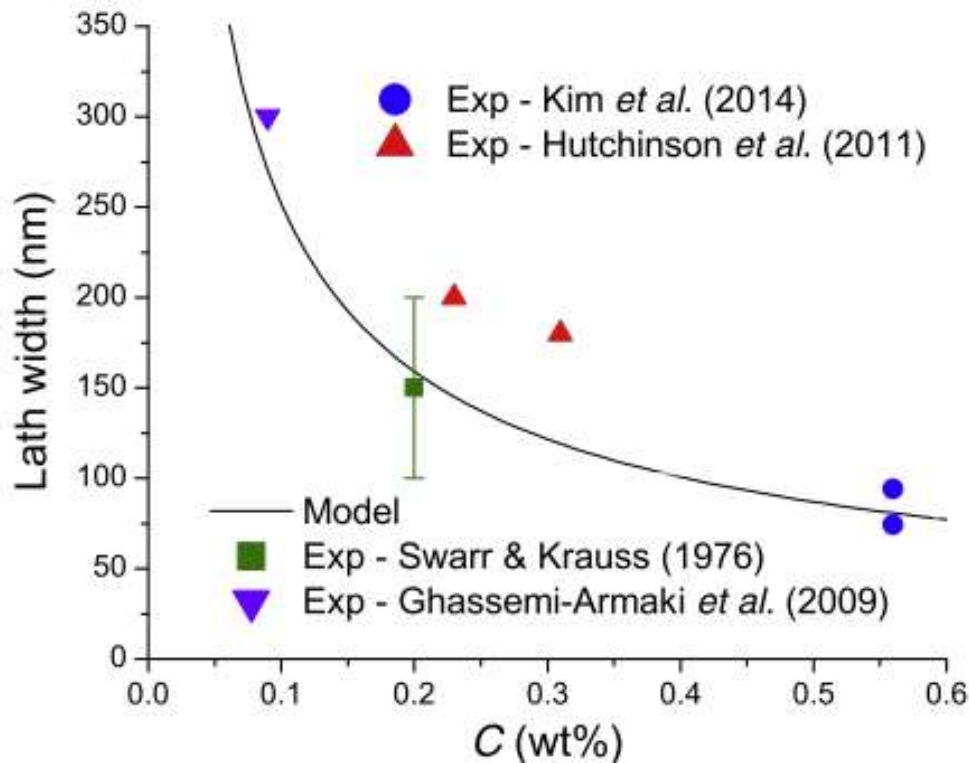


Figure 12 Link between Lath width (nm) and C (wt%), data compiled by (Galindo-Nava & Rivera-Díaz-del-Castillo, 2015)

2.5.3: Presence of Retained Austenite in Lath Martensite

Speich shows that as the carbon content increases the amount of lath martensite decreases and the amount of retained austenite increase. Retained austenite is reported by Speich and Leslie, 1972, with carbon contents higher than 0.4 wt. %, with a higher percentage of retained austenite found when the carbon content increases, see [Figure 13](#) (Speich and Leslie 1972), this does not take into account factors such as austenite grain size and alloy content. [Figure 13](#) shows a noticeable trend of hardness being affected by retained austenite after 0.4 wt. % C, high carbon, indicating C amount affects the percentage of retained austenite. It is also important to note that the microstructure present is 100% lath martensite in carbon contents less than 0.2 wt. % (G. Krauss, 1978). The figure shows a 0.2 wt. % C to have an Ms temperature of 500 °C, when compared with other data this is accurate.

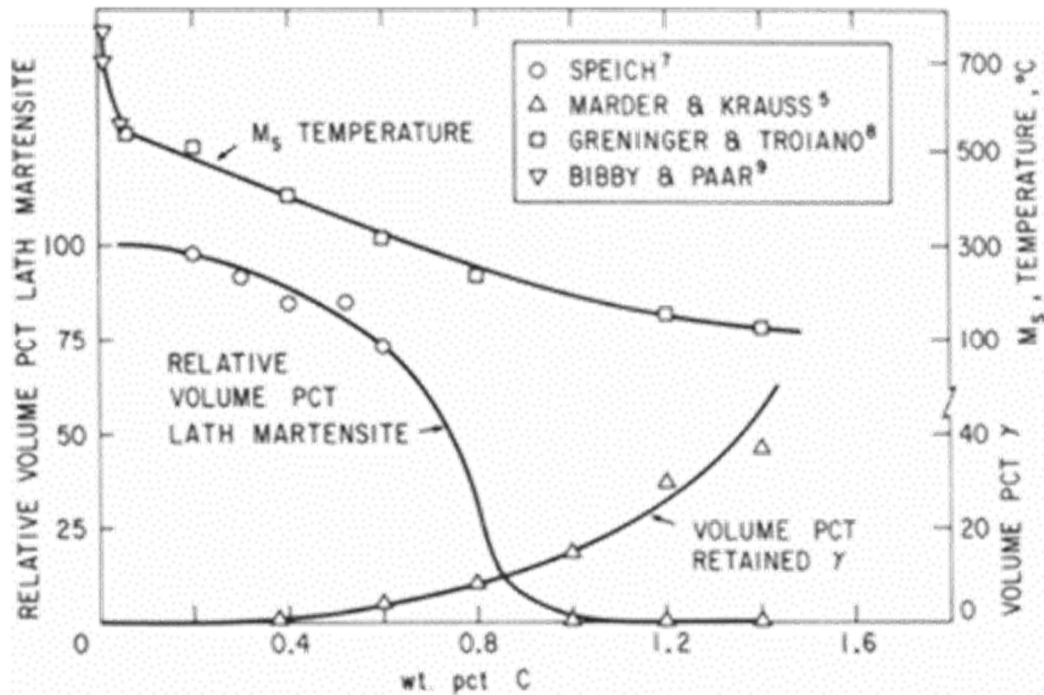


Figure 13 Effect of carbon content on relative volume percent of lath martensite, Ms temperature, and volume percent of retained austenite in Fe-C alloys (Speich & Leslie, 1972)

Vieira reports the presence of retained austenite (amounts not specified) in a 0.17 wt. %C, 1.23 wt. % Mn, 0.29 wt. % Si steel, which shows that retained austenite may be seen in steel with less than 0.4 wt. % C (Vieira, 2017). The retained austenite could be due to a higher austenisation temperature, which may increase the austenite grain size, increasing the amount of retained austenite (997 °C for 10 minutes).

Figure 14 shows the measured retained austenite content against austenisation temperature for 0.68 wt. % C, 0.31 wt. % Si, 3.15 wt. % Cr, 0.77 wt. % Mn steel and indicates that the amounts of retained austenite is dependent on more than carbon content, as indicated in Figure 13. This trend is reported to be due to more alloying element (Si, Cr, Mn) and carbon being in solid solution at the higher austenisation temperatures, decreasing the Mf temperature below room temperature. It is also reported that the coarser austenite grain at higher temperature (above 920 °C) means there is more retained austenite than for the finer austenite grains at lower reheating temperatures (Bakhsheshi-Rad et al., 2011). This means

that retained austenite may be seen in lower carbon steels.

Retained austenite can also result from strain accumulation in the matrix, which prevents any further shear induced transformation (Yi et al., 2011).

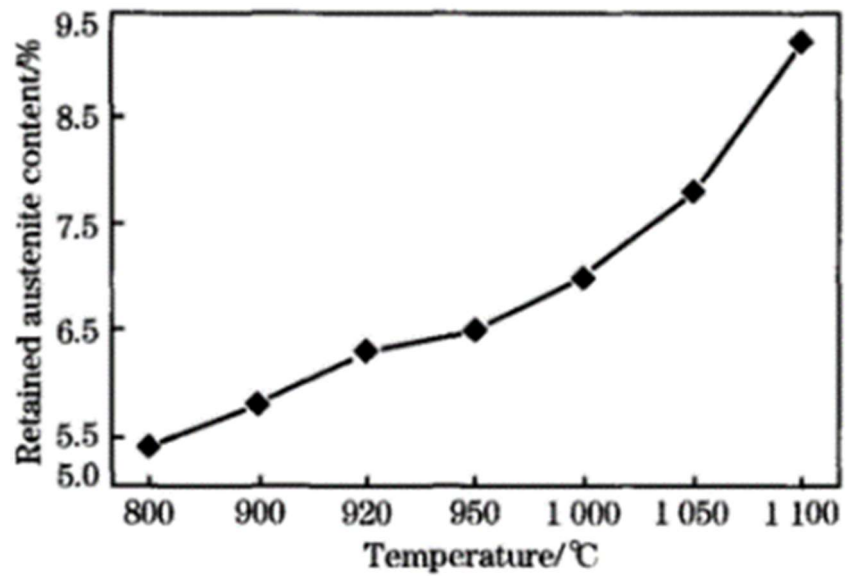


Figure 14 Effect of austenisation temperature on retained austenite content (Bakhsheshi-Rad et al., 2011)

2.6: Martensitic Tempering

2.6.1: Tempering of Martensite

Figure 15 shows a typical tempering response for Fe-C martensitic steel, when comparing hardness against tempering temperature.

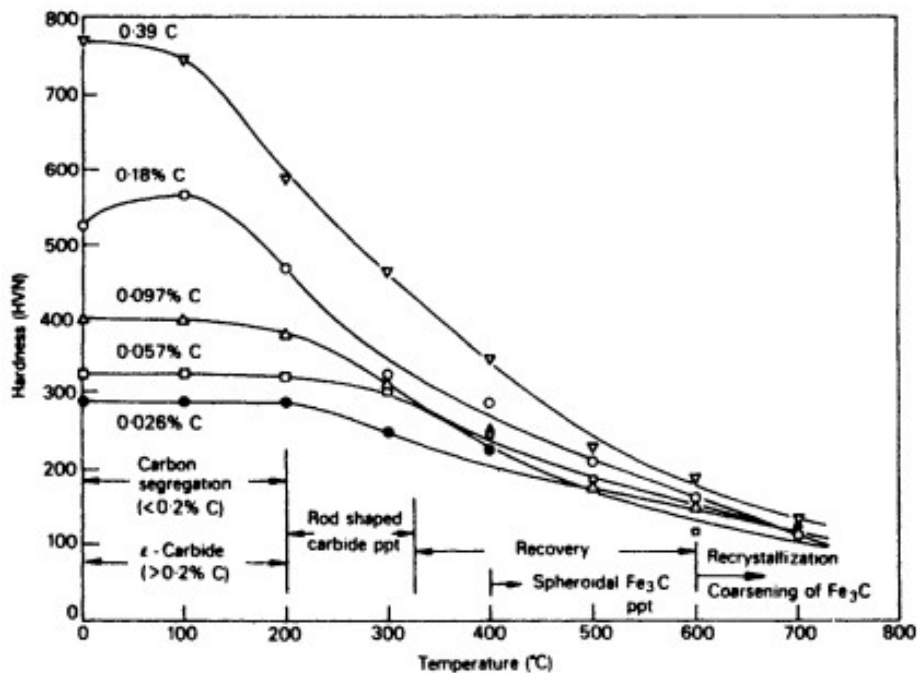


Figure 15 Hardness of iron-carbon martensite tempered for 1 hour at 100 – 700 °C, with carbon contents from 0.39 – 0.026 wt. % C. Taken from (Speich, 1969)

There are several stages associated with the tempering of martensite, which are discussed below: these stages are not distinct and may overlap. Tempering can occur during cooling after martensite has formed (auto-tempering) or during a separate heat treatment stage (tempering). Auto-tempering occurs during quenching when there is a relatively high M_s temperature for the steel (Thomson & Miller, 1996), for example Driscoll reported auto-tempered martensite showing the presence of carbides after ice quenching in S690 steel (Driscoll, 2014). Auto-tempering occurs when there is differential cooling of the core compared to the surface. In practical terms auto-tempering is caused by the heat of the core coming out of the plate, resulting in elevated surface temperatures.

Tempering stages:

1. Carbon segregation
2. Eta / ϵ carbide formation and transition to cementite
3. Recovery of dislocations
4. Cementite spheroidisation and coarsening
5. Secondary hardening (only possible in alloyed steel)
6. Lath coarsening/ grain growth

It is appropriate to mention here that lath martensite is formed in low carbon steel, less than approx. 0.2 wt. % C. This is most relevant to S690 with a 0.17 wt. % C content. Therefore, the discussion on tempering will be focused on lath martensite only.

2.6.1.1: Carbon Segregation

Carbon is initially trapped in solid solution then segregates to dislocation sites and lath boundaries, forming carbides during the first stage of tempering and is associated with the most softening during tempering.

2.6.1.2: Eta / ϵ -carbide formation and transition to cementite

There are carbides associated with lath martensite Fe-C steel. The most prominent in low carbon alloyed steel is cementite (Fe_3C) and there are also the transition carbide epsilon or eta ($\text{Fe}_{2.4}\text{C}$), which is formed first.

ϵ -carbide is not typically found for lower carbon contents, this is reported to be due to a lower driving force for precipitation of epsilon carbide than cementite, however it has been reported in low carbon steels with M_s temperatures of 400 °C and above (Deng et al., 2016; Ooi et al., 2013; Speich, 1969). Barton also find epsilon carbide in a 0.2 wt. % carbon, internally twinned martensite, commenting that the morphology of martensite can determine the tempering response and carbide orientation, not just the carbon content (Barton, 1969). This

would mean that epsilon carbide can form in different martensite microstructures; in this instance there is an associated orientation relationship (OR) which forms stable carbides. Reported to be the Jack OR for ϵ -carbides and Bagaryatski OR and Isaichev OR for cementite and the tempered martensite matrix (H. K. D. H. Bhadeshia, 2018; H. K. D. H. Bhadeshia & Honeycombe, 2007).

Cementite (Fe_3C) is able to form on dislocation sites, normally within the martensitic laths; if the transition carbide epsilon-carbide ($\text{Fe}_{2.4}\text{C}$) is present then this transitions to cementite (B.-N. Kim et al., 2012; Speich, 1969). Cementite is reported to form from 200 °C upwards (Caron & Krauss, 1972; Speich, 1969; Vieira, 2017). It is reported that with increasing carbon content the size of cementite increases, but the number density remains similar for the same tempering time and temperature. The author also notes that the mean distance between particles remains similar, therefore hardness changes relatively little (Grange et al., 1977).

Kozeschnik, 2008, suggests that the cementite precipitation (number density) is limited by the rate in which defects and dislocations can be eliminated within a BCT (Body-centred-tetragonal) structure, cementite is then available to form on these sites (Kozeschnik & Bhadeshia, 2008). Bhadeshia discusses that the carbides show lattice coherency in the early stages of precipitation, this means that the carbides lie in a predetermined orientation relationship; ϵ -carbides which first form have a Jack relationship in martensite and results in carbides which are in three orientations (H.K.D.H. Bhadeshia, 2001).

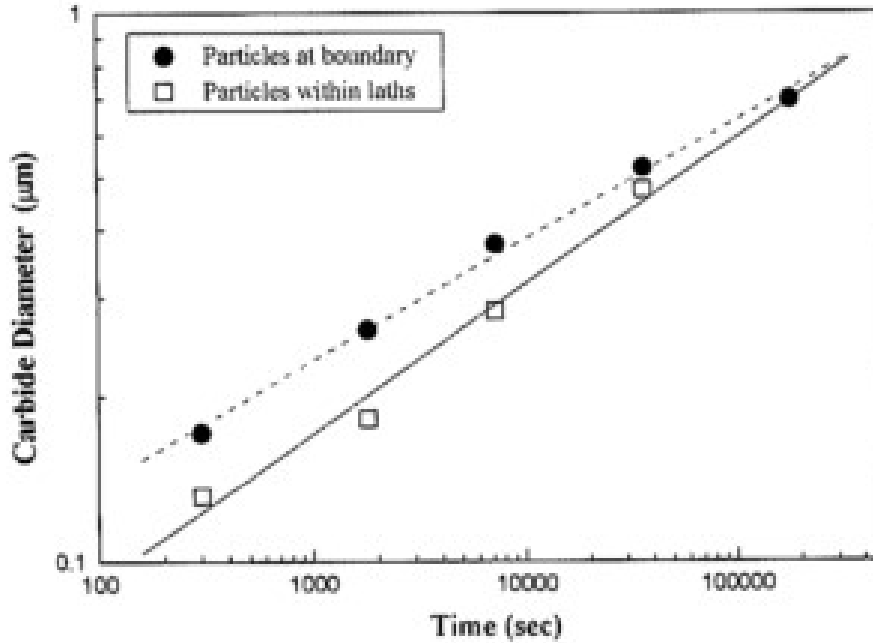


Figure 16 Variation of measured average cementite particle diameter in martensite with tempering time in a 0.45 wt. % C – 0.22 wt. % Si – 0.62 wt. % Mn – 0.004 wt. % P – 0.0038 wt. % S at 700 °C (W. J. Nam, 1999)

2.6.1.3: Recovery of dislocations

On tempering recovery of dislocation occurs within laths, and there are less low angle boundaries with increasing time. Figure 17 from Caron and Krauss shows that the high angle boundaries are stable in comparison to other boundaries, which show a drop in boundary area during the initial stages of tempering (Caron & Krauss, 1972).

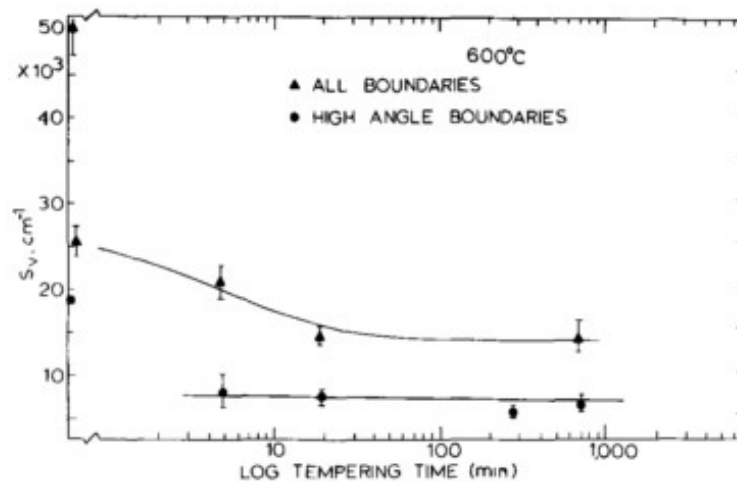


Figure 17 Total and high angle grain boundary area per unit volume as a function of the logarithm of the tempering time at 600 °C (Caron & Krauss, 1972)

2.6.1.4: Cementite spheroidisation and coarsening

Bhadeshia states that for cementite particles there is an Ostwald ripening process with increased tempering time, where smaller carbides are dissolved, providing carbon for larger carbide growth (H. K. D. H. Bhadeshia & Honeycombe, 2007). Figure 16 shows the changes in carbide size during tempering, with the carbides within the laths and on the boundary becoming larger with increasing tempering time. It is reported that there are no particles in the laths at the longest tempering time, as these have dissolved; there is a lath free equiaxed structure (W. J. Nam, 1999). This further backs up that Ostwald ripening is occurring as the smaller carbides within the laths have been dissolved.

Work by Nam found that the carbides on the boundaries coarsen via boundary diffusion and diffusion along dislocations, while carbides within laths coarsen via boundary and matrix diffusion. This agrees with Lindsley's discussions that the coarsening kinetics are controlled by carbon diffusion along grain boundaries and dislocations (Lindsley, 1998; W. J. Nam, 1999).

2.6.1.5: Change in Lath Size

Grain size is one of the key factors which affect strength (section 2.1.4.1). Packets and blocks are substructures within the martensitic grains (previously shown in Figure 11) add to strength by acting as sub grains, with high angle boundaries, these will have a greater strengthening contribution compared to the laths. During the coarsening stage of tempering laths are replaced by more equi-axed ferrite, the hardness of martensite drops as sub-structural strengthening mechanisms are removed (Speich, 1969). As the coarsening of lath width occurs it is reported that the length remains stable (G. Krauss & Marder, 1971).

Lath size is known to increase on tempering (Caron & Krauss, 1972; Galindo-Nava & Rivera-Díaz-del-Castillo, 2015; Ghassemi-Armaki et al., 2009; G. Krauss & Marder, 1971; J. Liu et al., 2014). Figure 18 shows the change in lath size for a range of tempering treatments,

in a 0.11 wt. %C – 0.39 wt. %Mn – 8.8 wt. %Cr – 0.91 wt. %Mo – 0.21 wt. %V steel. It is expected that laths will coarsen in a plain C-Mn martensitic steel at shorter tempering times than the very long ageing times reported for the alloyed power generation steel in [Figure 18](#).

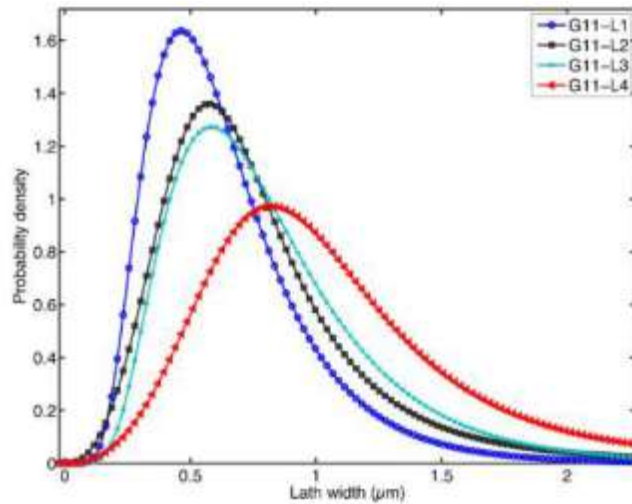


Figure 18 Lath width distributions and their corresponding log normal fitting curves for long aged G11 samples (L1 - Ageing at 600 °C for 5,000h, L2- 600 °C for 10 000h, L3- 650 °C for 5000h, L4 – 650 °C for 10 000h (J. Liu et al., 2014)

[Figure 19](#) shows that with increased tempering times (close to 70 hours) there is a loss of lath structure, there are also no carbides within laths at longer tempering times, this is not quantified but indicates that these strengthening mechanisms reduce over longer tempering times. Carbides are shown on the grain boundaries (Lindsley, 1998).

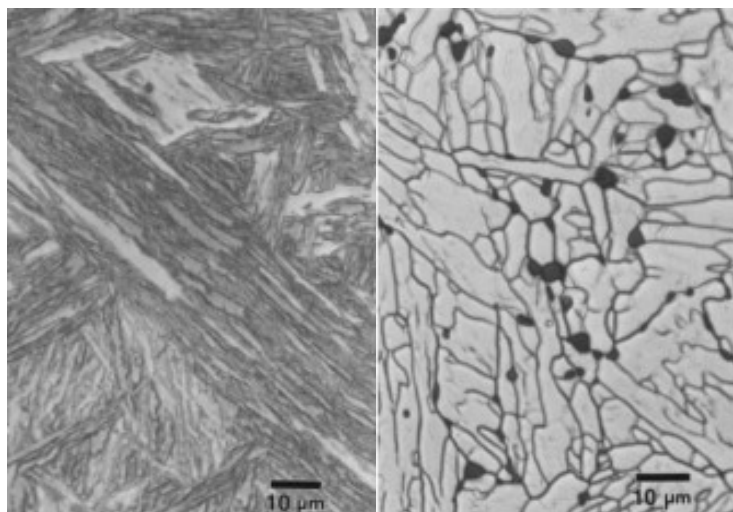


Figure 19 Fe-0.2 wt. %C alloy (Left Water-quenched, Right 6.05×10^5 seconds at 690 °C) (Lindsley, 1998)

2.6.2: Larson Miller Parameter

The Larson Miller Parameter can be used to interpret data regarding time and temperatures on tempering (Furillo et al., 1977). This is useful for comparing heat treatments which have different tempering times and/or temperature and how these relate to hardness.

The Larson Miller Parameter (LMP) is reported to be used for low carbon steels and build on the Hollaman-Jaffe equation which is well established and looks at the effect of time and temperature on hardness; the Hollaman-Jaffe equation can be seen equation 2.3 (Canale et al., 2008).

$$H = f \left[t e^{-\frac{Q}{RT}} \right]$$

Equation 2.3

Where

H = Hardness

t = Time at tempering temperature (hours)

T – The tempering temperature (absolute)

R = The ideal gas constant

Q = The activation energy for the structural changes involved in the tempering process of the steel

F = An appropriately selection function, such as hardness

The Holloman-Jaffe equation was derived based on data for 6 steels with carbon contents between 0.31- 1.51 wt. %, that do not exhibit secondary hardening. The equation has a stronger relation to the temperature the steel is held at than what time it is held for. The equation is empirically based and was not been experimentally verified developed, however it has been used by authors. On the other hand, the Larson Miller Parameter was experimentally justified when developed and is therefore determined to be more suitable (Canale et al., 2008). Another advantage of the LMP is that it avoids calculating materials properties at specific temperatures, meaning that it can be used to compare different tempering temperatures. An example where the LMP has been used is [Figure 20](#) which has been used to

compare the tempering of a low carbon, Mo containing steel.

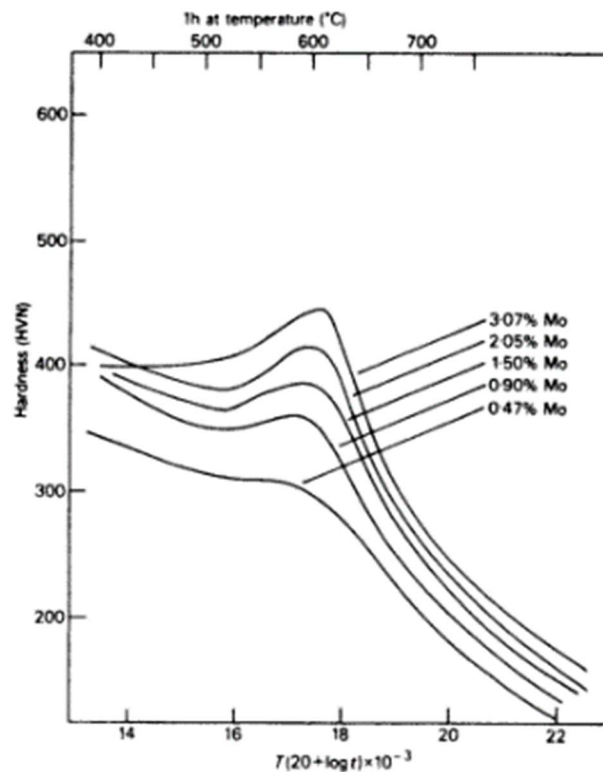


Figure 20 Effect of Mo on the tempering response of quenched 0.1wt. % C steels (Irvine & Pickering, 1960) found in (H.K.D.H. Bhadeshia, 2001)

The LMP can be used to help compare steels which have had different tempering treatments, for example 8 hours at 610 °C had an LMP of 18.02 and 16 hours at 600 °C has an LMP of 18.08. The tempering times and temperatures are different, so the LMP helps determine comparable tempering.

The LMP is given by;

$$\text{Larson Miller Parameter} = T [C + \log t]$$

Equation 2.4

C = Materials specific constant (18) Recommended for all carbon and low alloy steels (Grange & Baughman, 1956)

t = Time

T = Temperature in Kelvin

2.7: Alloying additions

2.7.1: Tempering an alloyed martensite

Alloying elements influence all stages of quench and tempering of steels, these are discussed fully in the following section which is separated by alloying element.

The final stage of tempering can produce alloying carbides, the carbide formation and coarsening rate is dependent on the initial alloying content. Alloying elements are used to influence the structure and properties of the steel (H. K. D. H. Bhadeshia & Honeycombe, 2006). Alloying elements have effects on tempering such as retardation of the softening by increasing the martensitic stability (with stable carbides resulting in stable laths), along with carbide formation (G. Krauss, 2012). Maalekian covers the carbides which can be formed in alloyed steels, these include M_3C , $M_{23}C_6$, M_7C_3 , M_6C , MC and M_2C (Maalekian, 2007).

Figure 21 shows that there are a variety of different carbides which can form. These are dependent on the alloying contents, for example Mo_2C and Cr_7C_3 would not be able to form if the alloying element is not present in the steel. This could provide an opportunity for $M_{23}C_6$ and M_6C to form earlier. The alloying elements and amounts that have an effect of what the carbides form, the stability and amount of occurrence. The enthalpy of formation of different carbides, such as Fe_3C and Mo_3C_2 are different, therefore there is a range of carbides which can be formed for each element.

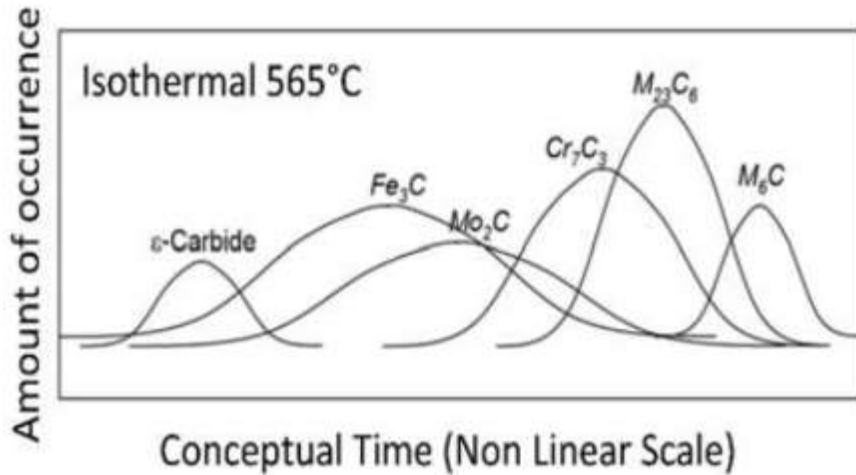


Figure 21 Nucleation and dissolution sequence for precipitates in a Cr-1Mo steel (T22 HSLA steel – 2Cr, Mo, 0.5Si, 0.5Mn and 0.15C wt. %) (Kiattisaksri, 2011; S. Liu et al., 2009)

Figure 22 gives a visualisation of how different amounts of alloying element have different contributions to hardness for a martensite tempered at 592 °C for 1 hour, with V being the most potent. This is discussed below as different alloying elements work with different mechanisms but gives an insight that the different alloying elements have different overall effects.

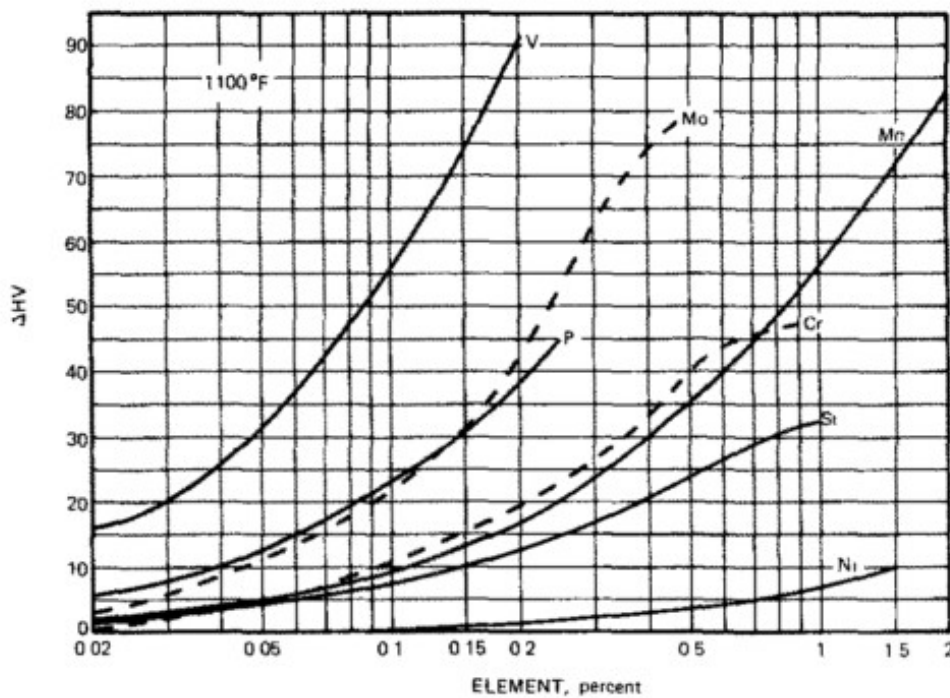


Figure 22 Effect of elements on the hardness of martensite tempered at 592 °C for 1 hour (Grange et al., 1977)

2.7.2: Chromium (Cr)

It is well established that Cr is a strong carbide former, as well as increases the hardenability of steels and inhibits the decomposition of martensite during tempering (Gingell et al., 1997; Kwon et al., 1997; Maalekian, 2007).

Cr can partition into cementite $(\text{FeCr})_3\text{C}$ on formation of martensite (as mentioned in section 2.2.2) Cr can also form carbides, these include M_7C_3 , M_3C and M_{23}C_6 , reported to form in this order. Maalekian notes that Cr is not as strong a carbide former as Mo and V, and M_{23}C_6 is not present unless other carbide formers are absent. (Maalekian, 2007; Thomson & Miller, 1998).

Korablev and Baker found that increased chromium content slows the precipitation of M_7C_3 , with it forming after 2.5 hours at 600 °C in a 4.6 wt. % Cr, compared to 45 minutes in a 0.67 wt. % Cr steel. However, the higher Cr content had no M_3C after 3.5 hours, while the lower Cr content steel retained both M_3C and M_7C_3 until 5 hours (no data reported for tempering times after this). With chromium in solid solution, it was found that chromium carbides were formed more readily than when compared to other alloy containing carbides (Korablev et al., 1975; Kwon et al., 1997; Smith & Nutting, 1957).

Kaneko found that M_{23}C_6 Cr rich carbides precipitate quicker on prior austenite grain boundaries (PAGB) in comparison to on martensitic lath boundaries (Kaneko et al., 2004).

Grange also found that chromium retards the tempering of martensite in a 0.19C – 0.3 wt. %Mn steel. The temperature range of effectiveness is most potent at 427 °C for 1 hour, with 1 wt. % Cr inducing a 60 Vickers hardness increase, at 592 °C for 1 hour, for 1 wt. %Cr there is a 47 Vickers hardness increase, compared to a 0.2 wt. %C – 0.5 wt. %Mn steel without Cr.

The author attributes the retardation of tempering to the higher Cr steel having smaller and more numerous carbides, along with a finer structure of packets. It is discussed that the Cr substitutes for the Fe in the cementite particles, and retards the coalescence of carbides.

(Grange et al., 1977).

2.7.3: Molybdenum

Mo is another ferrite stabilising, strong carbide former, which gives: an increase in hardness, increased hardenability and resistance to tempering. The increased resistance to tempering is due to Mo being a substitutional alloy within carbides slowing their coarsening process due to its low diffusivity (Maalekian, 2007; Mohrbacher, 2010).

Irving and Pickering found that a secondary hardening peak occurred around 600 °C for a 0.1 wt. %C quenched steel on tempering with varying levels of Mo (0.47 - 3.07 wt. %), resulting from secondary carbide precipitation, the carbide sequence was $Fe_3C \rightarrow Mo_2C \rightarrow M_{23}C_6$. The higher levels of Mo addition (0.90 – 3.07 wt. %) also exhibited carbides of M_aC_b , M_bC , over the same time period, where the values of a and b was not determined. The level of hardening increased with the amount of Mo additions, there is also a delayed secondary hardening effect with greater additions, shown in Figure 20 (Irvine & Pickering, 1960). Irani, in 4% Mo – 0.2% C steel found that Mo_2C carbide can be detected when secondary hardening occurred (Irani, 1965).

Work by Shorowordi and Ali Bepari, 2002 has found the Mo is useful in the refinement of austenite grain size.

Figure 23 shows the difference in grain size for a 0.13 wt. % C and 0.13 wt. % C/0.47 wt. % Mo steel, with a 1 – 4 hours hold at 950 °C. Mo and C form Mo_2C carbide, useful in pinning the prior austenite grain boundaries at high temperature restricting grain growth, these carbides must have formed before the re-austenisation process. The work also demonstrated that the finer the Mo_2C carbide the more effective the pinning. It is important to note that these carbides do not influence the secondary hardening as they form before tempering occurs but are important for microstructural features such as grain size.

In summary Mo produces alloy carbides, the extent of the formation and secondary hardening is dependent on the amount of the alloy present. It also slows the rate of decomposition

during tempering due to it being a substitutional alloy within carbides. The addition of Mo can also decrease austenite grain size resulting in an increased hardness and temper resistance.

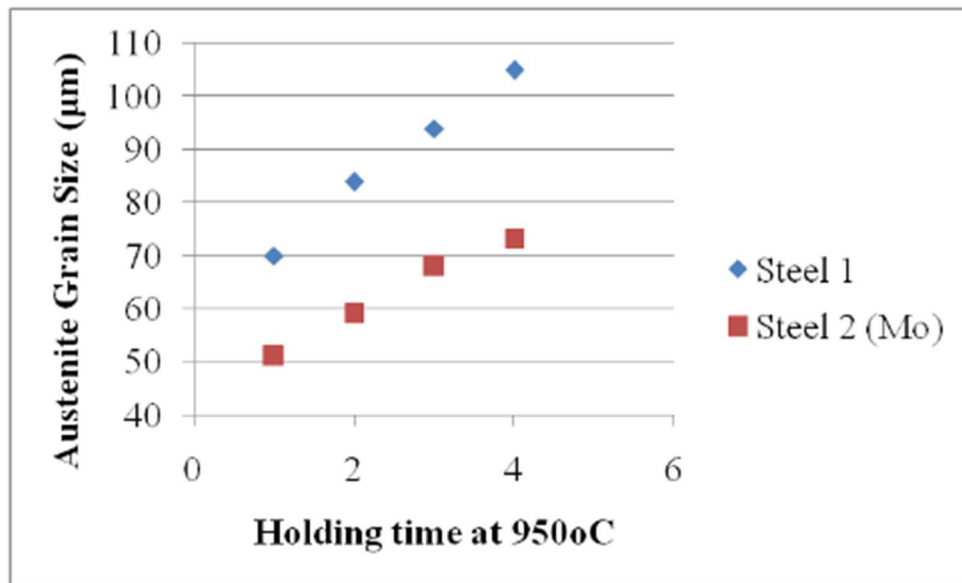


Figure 23 Effectiveness of Mo in reducing austenite grain size in a 0.13% carbon steel, held at 950 °C for varying time (hours)(Shorowordi & Ali Bepari, 2002)

2.7.4: Vanadium (V)

Vanadium is a carbide former, with some common secondary carbides being $V_{23}C_6$, V_4C_3 and VC adding to precipitation strengthening (Grange et al., 1977; Maalekian, 2007; Peng et al., 2018). Early work by Grange found the hardness of a tempered martensite with vanadium additions (592 °C for 1 hour) was higher than that of a comparable Fe-C plain steel, and a Fe-C steel with a range of individual alloying elements. Figure 22 shows that for additions of 0.2 wt. % V there as an additional 90 HV after 1 hour at 592 °C. This was thought to be due to the high carbide forming potency of vanadium, with V_4C_3 or VC forming and replacing cementite.

The effectiveness of V was looked at over a range of temperatures and increases up to 649 °C in 0.19 wt. % C/0.3 wt. % Mn steel; this can be seen in Figure 24. The difference in hardness was proposed to be due to the formation of alloying carbides V_4C_3 or VC which replace cementite at higher tempering temperatures and remain stable. Therefore, these alloying carbides not expected to form at lower temperatures, resulting in a less potent effect on the hardness at lower temperatures (Grange et al., 1977).

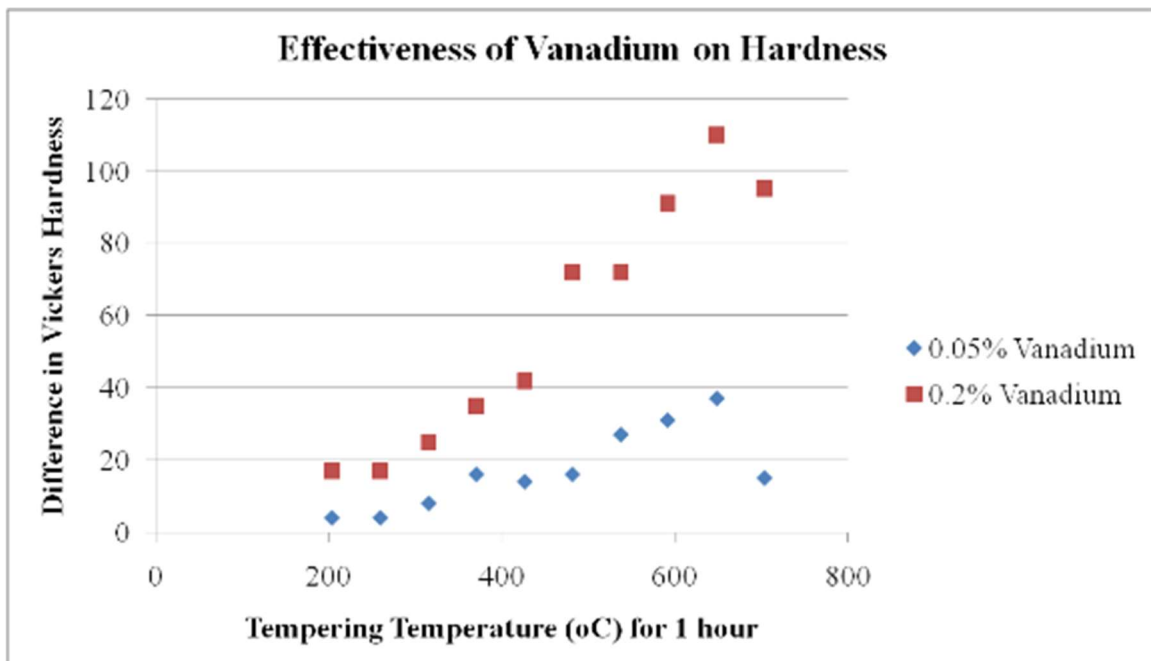


Figure 24 Effectiveness of vanadium additions on hardness in a 0.19C/0.3Mn steel compared to the V free steel adapted from (Grange et al., 1977)

Tekin, found for steels with 0.1/0.2 wt. % C 0.5/0.1 wt. % V that the Fe-C steel tempers in a similar manner to the Fe-C-V steel below 300 °C, cementite is found on laths up to 500/550 °C. It was found that the precipitation of V_4C_3 on dislocations delays recovery and recrystallization during tempering, this was found to happen at temperatures above 600 °C (Tekin; & Kelly, 1965). This agrees with Grange's work, which finds there is little effect of V additions until tempering at higher temperatures.

Overall the addition of vanadium can be seen to increase resistance to tempering, mainly by the formation of alloy carbides, and the rate at which tempering can occur at a given temperature.

2.7.5: Molybdenum and Vanadium additions

When Mo and V are used together for alloying additions, the ratio of the two elements is important, as it determines which carbides precipitate and when. Carbides which can precipitate include M_3C , M_7C_3 , M_2C , MC and M_6C . A higher level of Mo compared to V can cause a shift in the M_6C dissolution temperature, indicative that Mo is responsible for the stability of M_6C carbide (Kroupa et al., 1998). Figure 25 shows 4 steels with the following alloying elements and ratio of V to Mo, shown in Table 3. It indicates that a higher ratio of V to Mo shifts the area of $M_{23}C_6$ formations downwards (steel 3). The ratio can also alter what carbides form, after 10 hours at 600 °C (873K) the 4 steels have different types of carbides predicted, see Table 3. Higher levels of vanadium to molybdenum lower the probability of M_2C carbide precipitating and M_6C was found to precipitate earlier. Another trend, which was observed in this work, is that the MC was not shown in the Steel 1 but was shown in the other 3 steels. It is discussed in section 2.7.4 that V promotes MC, while in section 2.7.3 Mo it is not found to promote MC. In Kroupa's work a mixed composition with a lower amount of V compared to Mo does not form MC, thought to be due to the Mo suppressing the MC formation. The carbon contents vary from 0.09 – 0.12 wt. % (Janovec et al., 2005; Kroupa et al., 1998).

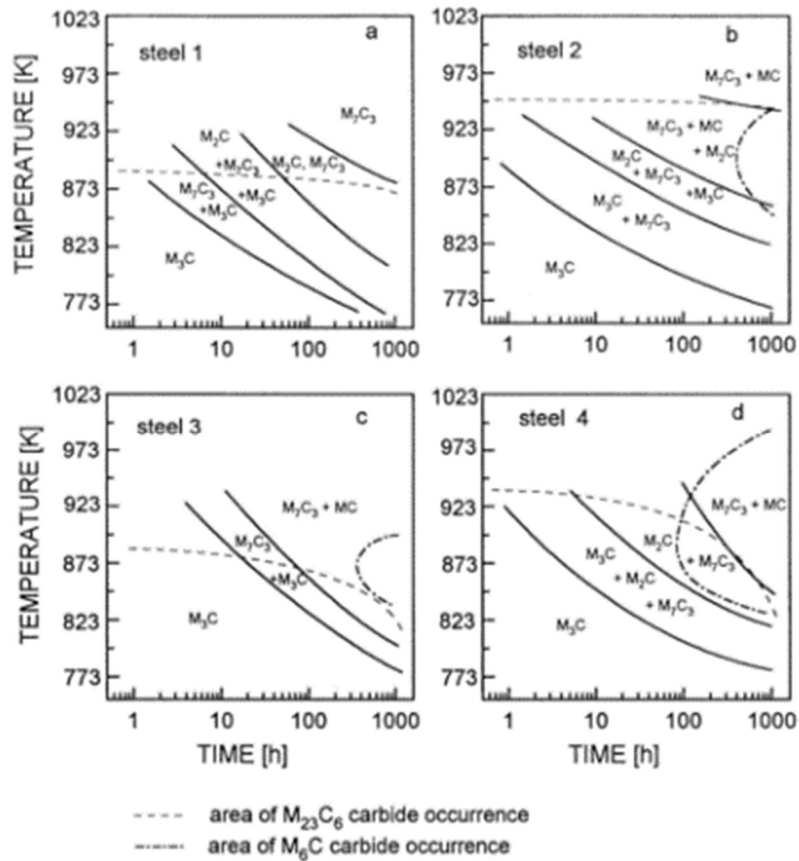


Figure 25 Experimental time-temperature diagrams of carbide stability (Steel 1 - 0.02 wt. %V, 0.70 wt% Mo. Ratio 0.03:1) (Steel 2 - 0.12 wt. %V, 0.73 wt% Mo. Ratio 0.16:1) (Steel 3 - 0.32 wt. %V, 0.70 wt% Mo. Ratio 0.46:1) (Steel 4 - 0.34 wt. %V, 0.94 wt% Mo. Ratio 0.36:1) (Kroupa et al., 1998)

Table 3 Compositions of steels and carbides after tempering at 600 °C for 10 hours

	Ratio V to M	Carbide at 600 °C for 10 hours
Steel 1 0.02 wt. %V, 0.70 wt. % Mo	0.03:1	$M_2C + M_7C_3 + M_3C$
Steel 2 0.12 wt. %V, 0.73 wt. % Mo	0.16:1	$M_3C + M_7C_3$
Steel 3 0.32 wt. %V, 0.70 wt. % Mo	0.46:1	M_3C
Steel 4 0.34 wt. %V, 0.94 wt. % Mo	0.36:1	$M_3C + M_2C + M_7C_3$

2.7.6: Chromium and Molybdenum additions

Additions of Cr and Mo are beneficial in alloy steels individually, as discussed above. There is an increased benefit when used simultaneously. Cr and Mo have an effect on the resistance of martensite to the loss of tetragonality on tempering (Hussein et al., 2016). Although the reason is not reported this is thought to be due to the slowing of the tempering process. As the solid-solution-strengthening effect is reduced when the element is within carbides, which results in precipitation strengthening. These take longer than a plain Fe-C carbide when it comes to dissolution and therefore strength is increased for prolonged periods. Any additions are also found to have effects on properties such as hardness and carbide precipitation. With both elements in addition it resulted in stabilisation of carbides to higher temperatures, and in some instances reduced the effect of secondary hardening (discussed in greater detail below) (Gojic et al., 1998; Kwon et al., 1997; Maalekian, 2007; Won Jong Nam et al., 2003).

Kitattisaksri provided a nucleation and dissolution sequence for Cr-1Mo steel, see [Figure 21](#), this is for a 2Cr, 1 Mo, 0.5Si, 0.5Mn and 0.15C wt. % HSLA steel. The samples were isothermally held between 565 °C and 750 °C, for different times. The higher temperature was to imitate the longer tempering times which could not be experimentally achieved. These were then compared using the heat treatments Larson-Miller Parameter. [Figure 21](#) shows that cementite and epsilon carbides were some of the first carbides to precipitate, with epsilon carbide reaching a peak occurrence before cementite, where it then transitions to cementite. Although not implicit in the work the Mo_2C has a lower occurrence than the Cr_7C_3 , which forms once the ϵ -carbide is not in solid solution and a Fe_3C starts to decline in occurrence. The Cr_7C_3 does appear to be sensitive to the transition carbides, suggesting that Cr affects the carbide transitions, and consequently the time for the full occurrence of Mo_2C to occur; this is expected to have a smaller occurrence as there is less Mo alloy in the steel composition available to form carbides. (Kiattisaksri, 2011; S. Liu et al., 2009).

Nam, Kim et al, 2013 found that in a C0.19/0.21 wt. % – Cr0.98/1.08 wt. % steel that additions of 0.19 wt. % Mo would delay the precipitation of cementite particles to temperatures higher than 400 °C for 40 seconds by induction heating (Won Jong Nam et al., 2003).

Gojic also found benefits of adding Cr along with Mo (Cr – C-0.44%, Cr-1.11%, Mo-0.11%) (Cr-Mo – C-0.41%, Cr-1.01%, Mo-0.70%). At tempering temperatures of 700 °C for 2400 seconds (40 minutes) the Cr steel contains only orthorhombic cementite. When Cr-Mo was added, cementite and hexagonal Mo₂C particles were found, which provides additional hardening. Figure 26 shows with higher tempering temperatures there is a larger difference in hardness between the two compositions, once tempering has started. This is due to carbide precipitation and also benefits from Mo₂C pinning the prior austenite grain boundary (PAGB), reducing growth during austenisation. This is due to the addition of the Mo to the Fe-C-Cr steel, it is not discussed how the Mo would affect an Fe-C steel, as it is only compared to a Fe-C-Cr in terms of solid solution strengthening. However, section 2.7.3 discusses how Mo provides resistance to tempering along with a secondary hardening effect, it is plausible it is providing this effect in these steels. When it is a Fe-C-Cr steel the prior austenite grain boundary is 14µm, this reduces to 7µm when it a Fe-C-Cr-Mo steel. The effect is shown during normalisation, but the lower PAGB will increase the overall temper resistance (Gojic et al., 1998).

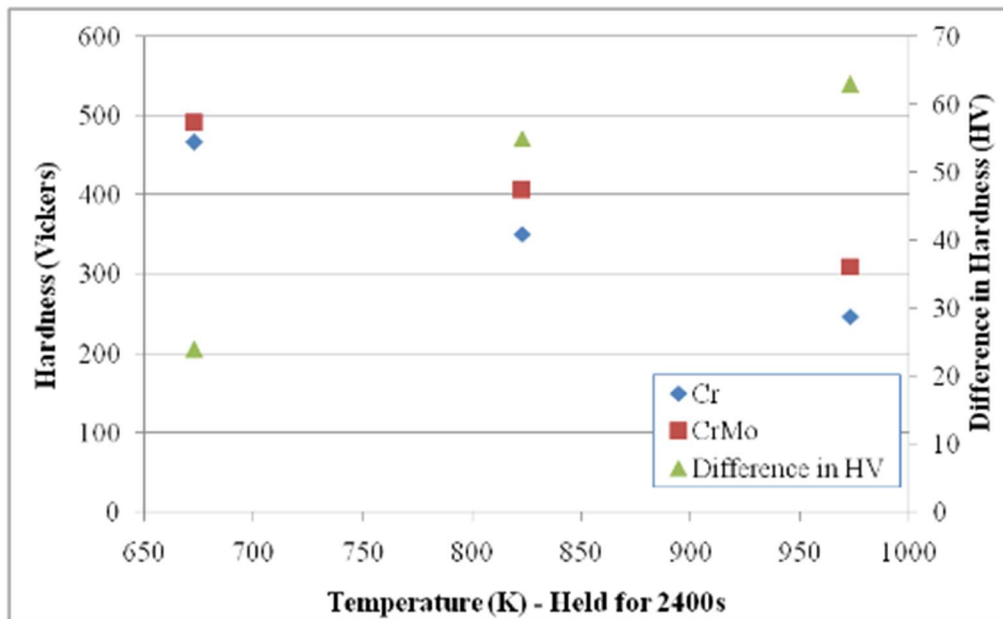


Figure 26 Quenched and Tempered Hardness of low alloy Cr and Cr-Mo steel - C 0.41-0.44 wt. %- Cr 1.01-1.11 wt. % Mo 0.11 - 0.70 wt. % Data taken from (Gojic et al., 1998) As quenched hardness Cr – 661 HV /CrMo – 710 HV

Kwon looked at a Mo and Mo-Cr steel: in the 4 wt. %Mo steel (0.2C) for 1 hour at 600 °C there was a dense precipitation of M_2C carbides, along with a near complete dissolution of cementite. When Cr was added (2.10 wt. %Mo – 2.41 wt. %Cr – 0.2 wt. %C) the Cr stabilized the cementite at 600 °C, inhibiting the fine dispersion of M_2C carbides below 600 °C, resulting in a drop of hardness on tempering. This is thought to be a consequence of low availability of carbon, as cementite dissolution hasn't occurred; therefore, little carbon is available for M_2C carbides. It is important to also note that if there is a decrease in Mo content, less secondary hardening would be expected, see [Figure 27](#). [Figure 27](#) also shows that there is a reduction in hardness after 600 °C for the Cr-Mo steel, while the Mo steel shows an increase in secondary hardening, followed by a reduction. After secondary hardening the hardness of the Mo steel remains higher than Mo-Cr steel. There were no Cr carbides formed, the alloying elements main role was in stabilising the cementite (Kwon et al., 1997).

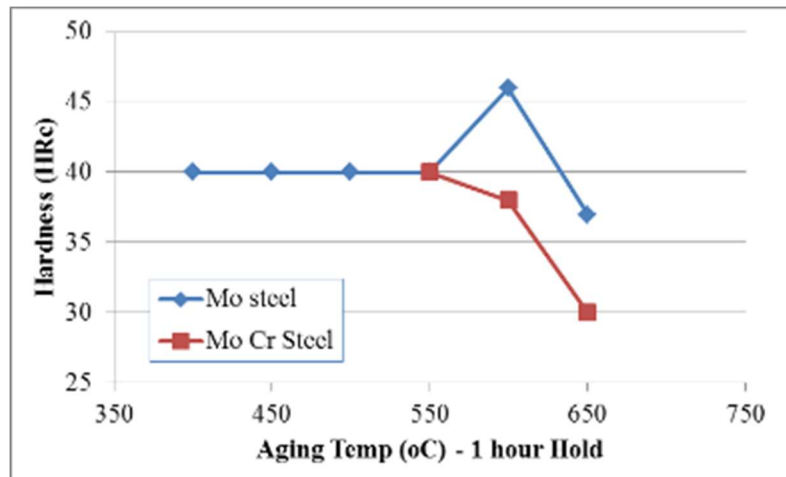


Figure 27 Variations in hardness with aging temperature in Mo and Mo-Cr steel (2.10 Mo – 2.41 Cr – 0.2C) Data adapted from (Kwon, Lee et al. 1997)

Baker and Nutting looked at 2.25Cr-1Mo- 0.15% C steel; [Figure 28](#) is an isothermal diagram showing the sequence of carbide formation; it was found that after 5 hours at 600 °C Mo₂C carbides had precipitated, shown using carbon extraction replica techniques. Cr-Mo steel had a hardness of 419 HV after quenching, and a peak hardness was found at 600 °C, which is linked to the precipitation of Mo₂C carbides. The number density and size was not determined (Baker & Nutting, 1959).

Gojic looked at whether Mo₂C formed in 1.1Cr-0.7Mo steel and found similar results to Baker and Nutting, for 40 minutes at 700 °C, finding cementite and Mo₂C carbides, as predicted in [Figure 28](#).

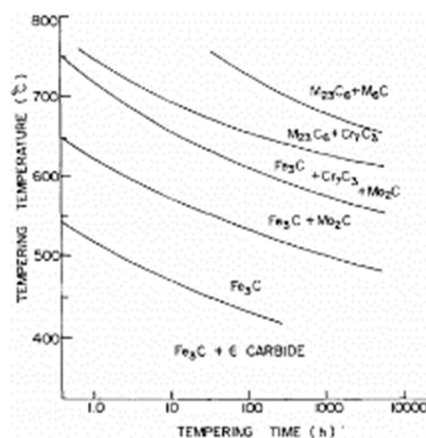


Figure 28 Isothermal diagram showing the sequence of carbide formation in a 2.25Cr-1Mo steel (Baker & Nutting, 1959)

Fujita, shows the evolution of carbides in a 3Cr1.5Mo and a 2.25Cr1Mo steel at 600 °C where there is a difference in what carbides are expected and the tempering times associated with their formation, shown in Figure 29 (Fujita, 2000). When there is less Cr the M_2C carbides precipitate before M_7C_3 , this demonstrates that the ratio of Cr and Mo is important. This difference is discussed to be based on the different diffusion rates in the system. This work focuses on different amounts of Cr compared to Mo and shows that the additional Cr changes the sequence of alloying carbides, showing that the addition of the two alloys can control the presence of carbides.

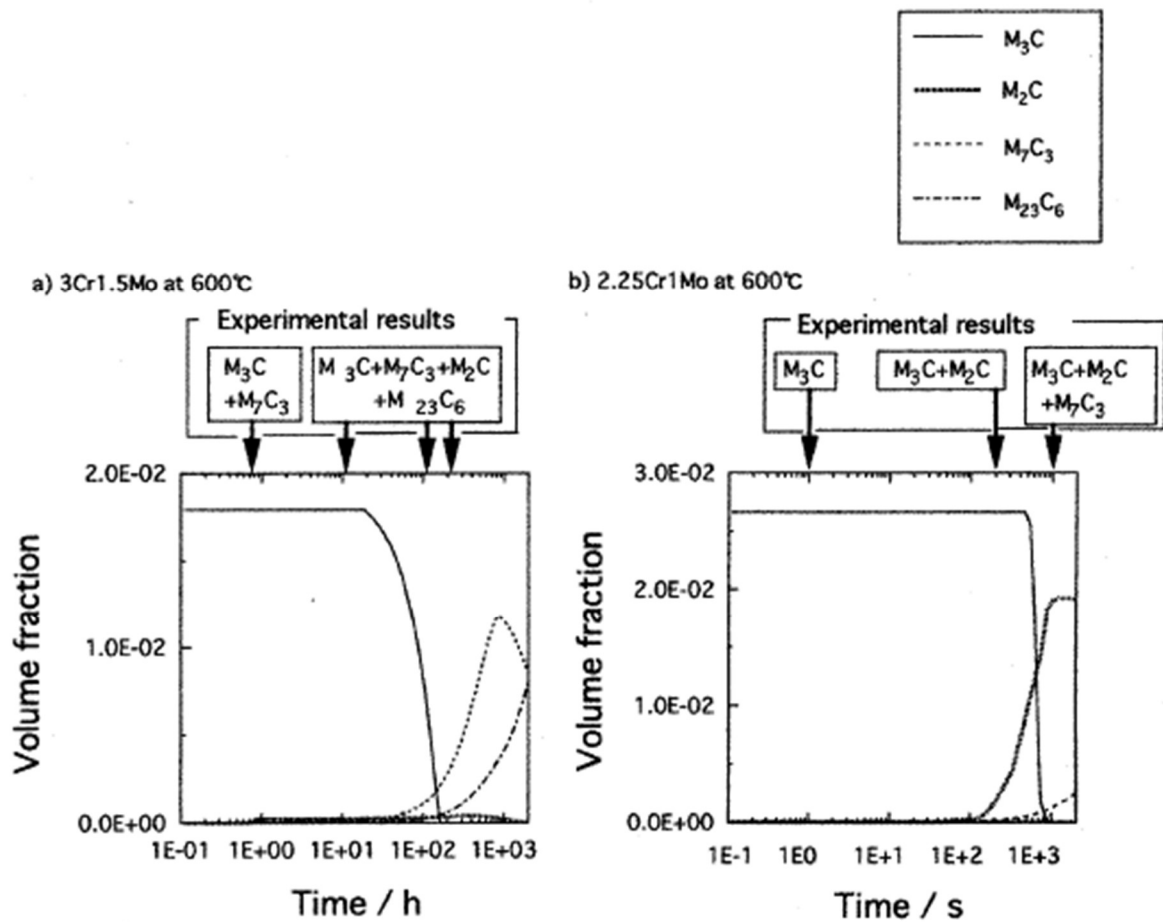


Figure 29 Calculations of multiple precipitation reactions for a) 3Cr1.5Mo and b) 2 ¼ Cr 1 Mo steels at 600 °C (Fujita, 2000)

2.7.7: Silicon (Si)

Silicon increases solid solution strengthening and affects carbides on tempering (Rafael Agnelli Mesquita & Kestenbach, 2012). A low addition of silicon is considered as less than 1 wt. %, whilst higher additions are 1 wt. % and above, with a typical limit of 2 wt. % in most steels (Delagnes et al., 2005; Rafael Agnelli Mesquita & Kestenbach, 2012; Ollilainen et al., 2003; Padmanabhan & Wood, 1984; Pavlina et al., 2015; Mathew J. Peet et al., 2017).

It has been extensively reported in the literature that Si retards the formation of cementite (H. K. D. H. Bhadeshia & Edmonds; Chang, 1984; Delagnes et al., 2005; R. A. Mesquita et al., 2011). This results in slower coarsening rates and slower recovery of martensite during tempering, as the carbides are still stable and the next stage of tempering is delayed (B. Kim et al., 2014). There is some experimental evidence from Jang, Kim et al. 2010, which finds that silicon can increase the formation rate of epsilon-carbide (Jang et al., 2010). Chang, 1984 found that in a martensitic steel with 0.75 wt. % C and 1.4 wt. % Si that silicon retards the formation of cementite. A 1-2nm layer with high Si content (12wt. %Si) was found around cementite particles after 1-hour tempering at 380 °C. The high Si layer reduces the mobility of carbon and therefore delays coarsening of the cementite (Chang, 1984). The diffusion coefficient of silicon in iron is $1.1 \times 10^{-7} \text{cm}^2/\text{sec}$ (Bradshaw et al., 1953), whereas it is $1.8 \times 10^{-6} \text{cm}^2/\text{sec}$ for carbon (H. K. D. H. Bhadeshia & Honeycombe, 2007); resulting in silicon not being able to diffuse away from the region readily leading to the build-up of the Si rich layer around cementite.

The addition of silicon shifts the times of secondary hardening peaks in martensitic alloyed steels to shorter times / lower temperatures. When the formation of cementite is less favoured there is carbon readily available to form alloy carbides at lower temperatures, as compared to lower Si steel which will typically have a secondary hardening peak at higher temperatures (Delagnes et al., 2005; R. A. Mesquita et al., 2011).

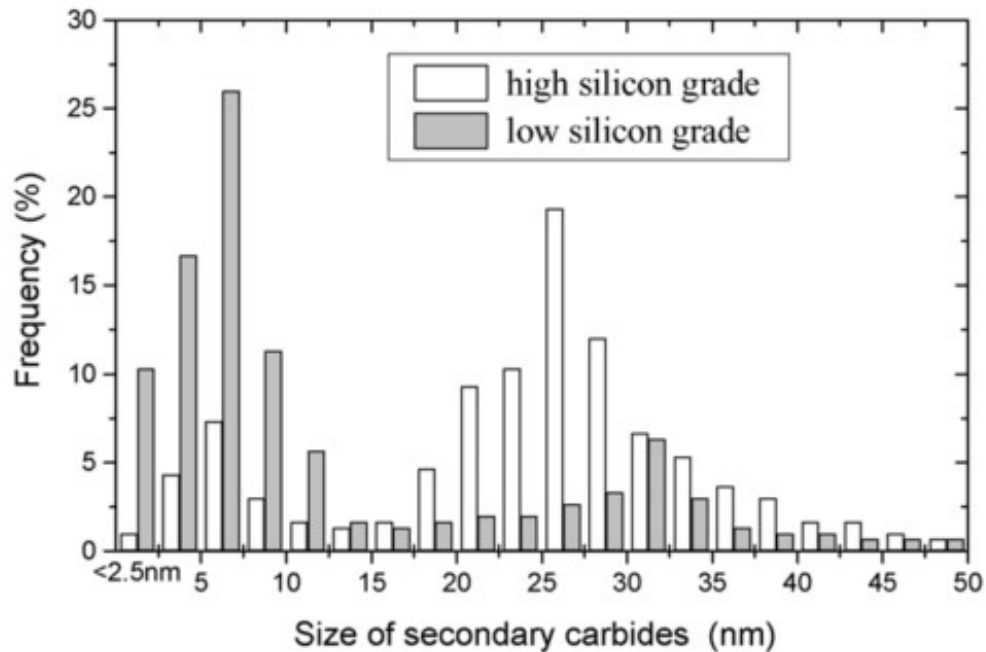


Figure 30 Size distribution of secondary carbides; comparison between high silicon (Si - 0.92%) and low silicon (Si - 0.35%) grades. Austenisation at 980 °C for 1 hr – 550 °C 2 hours – 625 °C/ 623 °C for the HS/LS graded for 2 hours (Delagnes et al., 2005)

Delagnes, 2005 found that in tempered martensite that for high silicon additions there were carbides with two population distributions, with average sizes of 6.1 and 28.8nm whereas for the low silicon additions this was 6.6 and 33.1nm respectively, using TEM analysis.

Although the average size of the two populations sets are similar, [Figure 30](#) shows that the higher Si steel shows a greater frequency for the second (larger) population of carbides.

There is no detail of which size population corresponds to which carbide types, however M_7C_3 – $M_{23}C_6$ – M_3C and MC are found in both compositions with no significant difference.

There is indication that VC carbides are within the smaller size population. Carbon is available to form secondary carbides, whilst inhibiting cementite growth, and promoting its dissolution, with the higher Si level therefore being associated with a larger number of secondary hardening precipitates as evidenced with the lower frequency of smaller carbides compared to the frequency of larger carbides (Delagnes et al., 2005). It has also been found that silicon in a martensitic steel (0.36 – 0.4wt. %C; 0.35 – 0.92 wt. % Si; 5 wt. % Cr; 1.25wt. % Mo; 0.47-0.49 wt. % V) has the effect of inhibiting the coarsening of cementite and

promoting dissolution of these particles. [Figure 31](#) shows how there is expected to be a shift in secondary hardening peak temperature, with the higher Si steel showing secondary hardening happening sooner (Delagnes et al., 2005). [Figure 32](#) shows experimental data for three steels with different Si levels: there is a higher base hardness with increased silicon content (due to solid solution strengthening), it is not possible to see if the secondary hardening happens at different times as limited tempering times were investigated. At tempering temperatures higher than 600 °C there is a convergence in hardness, indicating that the solid solution strengthening effects are reduced after longer tempering times. This may be due to the Si having a prominent effect on cementite, inhibiting coarsening and promoting dissolution of these particles, it means that there is less effect of the Si once secondary carbides form and strengthening mechanism of solid solution strengthening is less dominant. [Figure 33](#) shows a splitting of tempering response for 2% Si steel, showing that there is a greater contribution to strength from the carbon. Precipitation strengthening is greater than solid solution strengthening, until 650 °C for 2 × 2 hr, where the hardness converges.

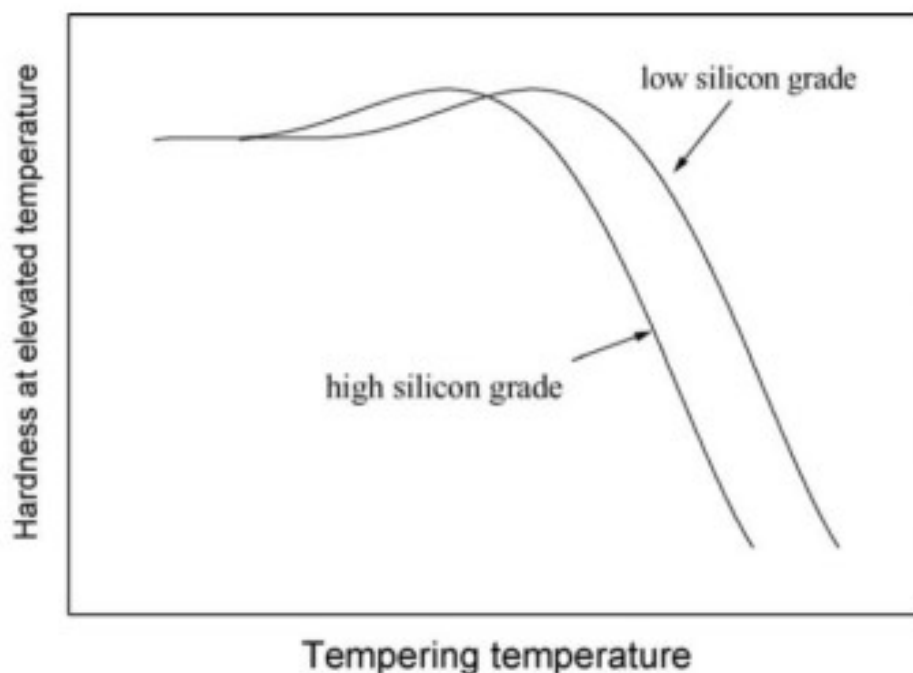


Figure 31 Qualitative influence of silicon content on the secondary hardening peak (Delagnes et al., 2005)

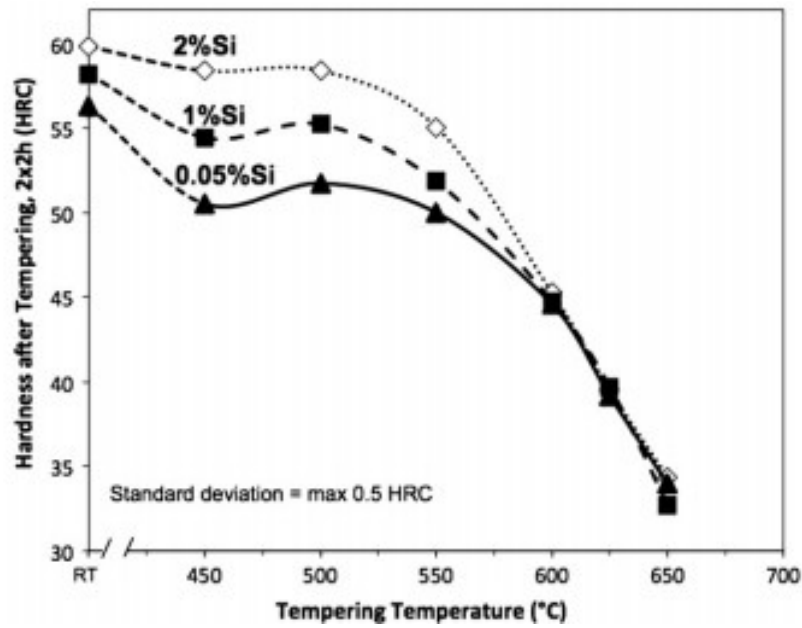


Figure 32 Tempering curve for three Si-containing, C-0.4, Mn-0.35/36, Mo-1.3, V-0.40, 5% Cr martensite steels, tempered for 2 × 2 hr (Rafael Agnelli Mesquita & Kestenbach, 2012)

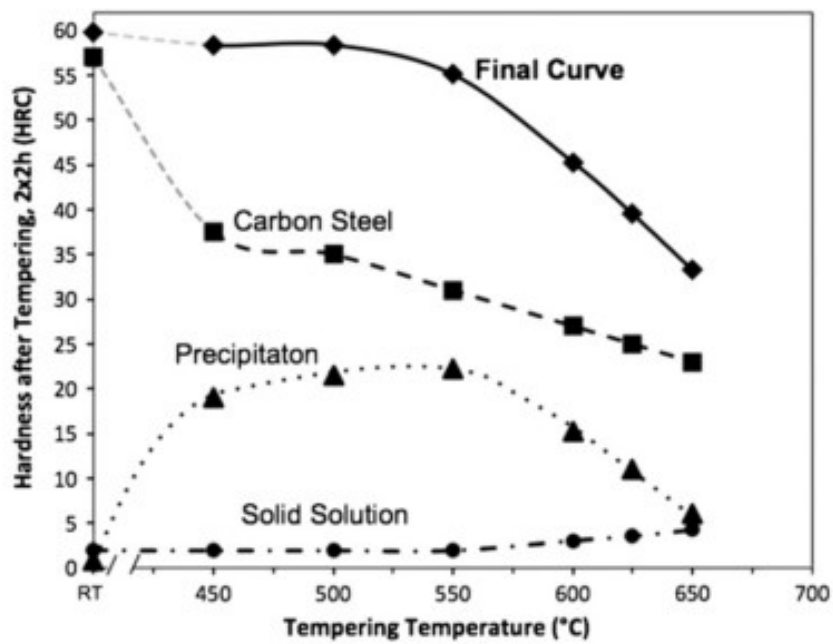


Figure 33 Split tempering curve of 2% Si alloy steel (Rafael Agnelli Mesquita & Kestenbach, 2012)

2.8: Bainite

2.8.1: Introduction

In thick RQT steel plates there can be mixtures of martensite and lower bainite through thickness due to the varying cooling rate experienced, therefore to understand the tempering of these mixed phases, it is first important to understand how lower bainite forms; its appearance and response to tempering as a singular phase.

2.8.2: Appearance

Bainite is a microstructure consisting of ferritic plates and carbides (H. Bhadeshia, 1997).

There are two types of bainite which shall be discussed (upper bainite and lower bainite), these can be distinguished by considering the location of carbide precipitation and transformation temperatures (George Krauss & Thompson, 1995). Temperatures of transformation are typically 550-400 °C for upper bainite and 400-250 °C for lower bainite, however this is dependent on the alloying content (H. K. D. H. Bhadeshia & Honeycombe, 2007). Figure 34 shows a schematic diagram of the transformation from austenite to upper bainite or lower bainite, along with details of carbide locations. With upper bainite carbides shown between plates and lower bainitic carbides are found between, and within, plates.

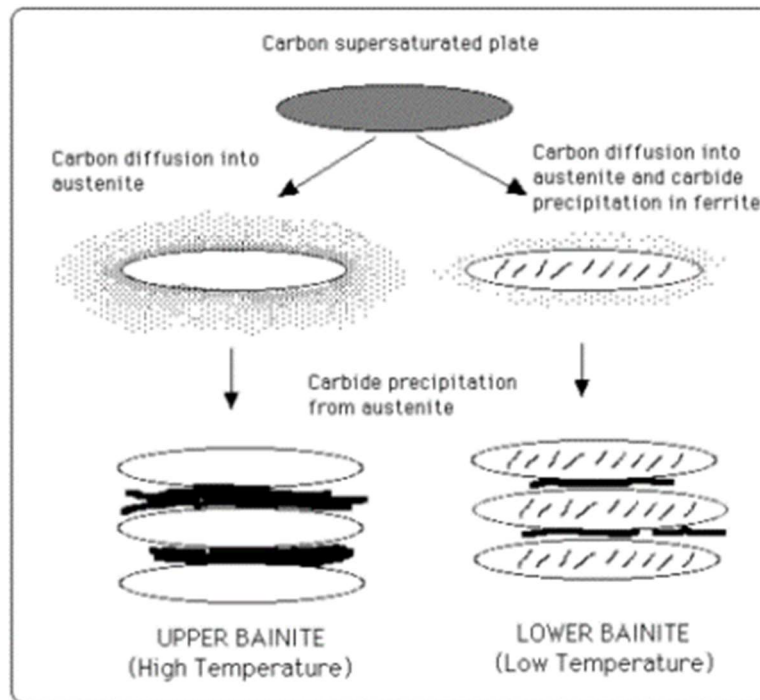


Figure 34 Schematic representation of the transformation from austenite to lower bainite or upper bainite (H.K.D.H. Bhadeshia, 2001)

2.8.2.1: Lower bainite

Lower bainitic cementite carbides form in the Bagaryatski orientation relationship resulting in intra-plate lenticular carbides laying in the same orientation, around 60° to the ferritic plate (H.K.D.H. Bhadeshia, 2001; Tu et al., 2008). This helps to relax stresses associated with transformation (Hehemann et al., 1972). The lower transformation temperature of lower bainite compared to upper bainite means the partitioning of carbon is slower. There are carbides between the plates, but they are smaller in comparison to upper bainite (H. Bhadeshia, 1997). Lower bainite has refined intra-lath carbides, which are found to contribute to strengthening (Edmonds & Cochrane, 1990).

2.8.2.2: Upper bainite

Upper bainite is carbide free within the plates, but has relatively large cementite carbides between the plates, with the cementite particles having a Pitsch orientation relationship with the ferrite. In upper bainite, carbon is readily partitioned into the austenite surrounding the ferritic plate (H. Bhadeshia, 1997). This results in carbide precipitation along the edge of the plates during transformation.

The upper bainitic carbides distribution has less effect on hardness than carbides in the plates as they form along the edge of plates, in between laths. Upper bainite also has retained austenite present between the plates.

The differences in upper and lower bainite are summarised in [Table 4](#), this is for ultra-low and low carbon steels. It is also important to consider that bainite has the following strengthening mechanisms, summarised by Edmonds as; a) packet and lath size strengthening, b) dislocation substructure, c) solid solution hardening, d) dispersion hardening effects, from carbides. This leads to a difference in mechanical properties between the two forms of bainite (Edmonds & Cochrane, 1990). [Figure 35](#) gives a visual representation of change in hardness with transformation temperature, which is associated with upper and lower bainite. It is known that in a plain carbon steel that the lower the transformation temperature the more likely the lower bainite will be formed. The figure is for high carbon steel, but it clearly shows that the lower the transformation temperature the higher hardness, indicating that there is a difference in hardness between upper and lower bainite.

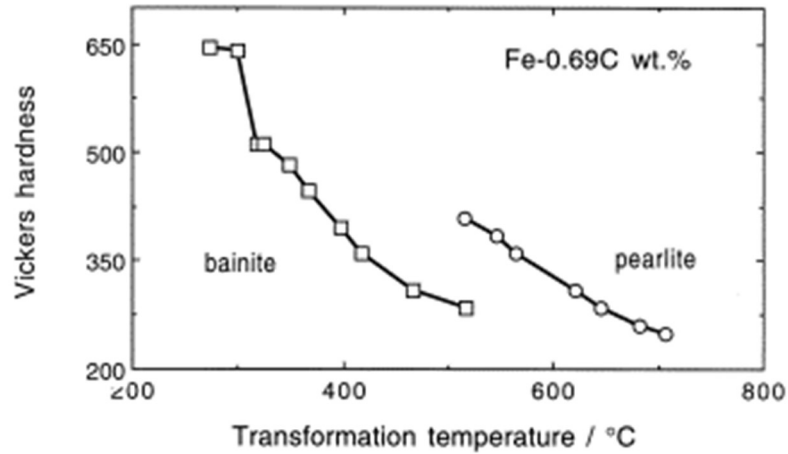


Figure 35 Microhardness data from plain carbon steels transformed isothermally to a mixture of bainite and pearlite (Yasuya Ohmori et al., 1971) Taken from (H.K.D.H. Bhadeshia, 2001)

Table 4 Difference between upper and lower bainite in ultra/low carbon steel (H. Bhadeshia, 1997; George Krauss & Thompson, 1995)

Structure	Carbide Location within laths	Carbide Distribution	Transformation Temperature (°C)
Upper Bainite	Carbide-free Retained austenite or carbides between laths	Along the lath interface	550 – 400
Lower Bainite	Lath – like, with lenticular carbides present at ~60° to the long axis of the ferrite laths	Within laths and lath interface	400 – 250

2.8.2.3: Carbides in bainite

Matas and Hehemann 1961 proposed a sequence of carbide formation, for upper and lower bainite. In steel with 0.58C-0.35Si-0.78Mn-3.90Cr-0.13Mo and a Ms temperature of 193 °C, only cementite was found for transformation at 260 °C, associated with upper bainite. This is an alloyed steel; therefore, the alloys will change the Bs and Ms temperatures, resulting in a different Bs temperature. Only epsilon carbide was found during isothermal transformations at 185 °C (this is slightly below the Ms temperature; therefore 10% martensite was found on cooling), associated with lower bainite. A mixture of the two carbides was found at 237 °C in the microstructure that was predicted to be lower bainite. This was suggested to indicate that epsilon carbide forms first, and then evolves into cementite during isothermal holding if there is sufficient time (holds carried out to 19 hours) (Matas, 1961).

Bhadeshia, 2001 looked at a range of authors work (See [Table 5](#)) and found that there are cases in which epsilon carbide was found in lower bainite in alloyed steels (H.K.D.H. Bhadeshia, 2001) suggesting that composition has a significant effect on the microstructure evolution. From [Table 5](#) it is evident that no low carbon steels are found to have epsilon carbide in the lower bainitic structure. Based on observations in Fe 0.55C- 2.2Si wt. % C martensitic steel that epsilon carbide transforms to cementite at 400 °C within 1800 seconds (B.-N. Kim et al., 2012) it is plausible that the higher transformation temperatures typically associated with bainite in low carbon steels results in the transformation of any epsilon carbide that forms to cementite at low hold times.

Table 5 Data taken from (H.K.D.H. Bhadeshia, 2001)- Showing the minimum and maximum compositions in which epsilon carbide was found in lower bainite

Element	Min	Max
C	0.40	1.3
Si	0	3.09
Mn	0	0.86
Ni	0	4.15
Cr	0	3.90
Mo	0	0.45
V	0	0.90

2.8.3: Role of Silicon

High additions of silicon can retard the formation of cementite, in martensite and bainite (R. A. Mesquita et al., 2011). It is mentioned in section 2.7.7 that higher levels of silicon are 1 wt. % and more. In bainitic steels, the retardation of cementite results in an incomplete formation of bainite, due to the lack of cementite carbides. An additional consequence of carbon not forming cementite is that it stabilises retained austenite to room temperature, which can result in a carbide free bainite with inter lath retained austenite. Lower additions of silicon (<1 wt. % Si) are not regarded as having this effect.

2.8.4.1: Para-equilibrium

In the literature it is generally agreed that martensite and lower bainite form via a para-equilibrium transformation (Caballero et al., 2007; Ghosh & Olson, 2002; Miyamoto et al., 2007; Thomson & Miller, 1998). This means that the concentration of alloying element is the same in both the ferrite and cementite on transformation. However Caballero et al. showed contrary results for a lower bainitic carbide, shown in [Figure 36](#) (Caballero et al., 2014) with the ratio of Fe to each element in [Table 6](#) determined using data taken from [Figure 36](#). The analysis of this data shows that Si and Mn appear to follow a para-equilibrium trend, showing similar ratio for the ferrite and cementite. The ratio of Cr to Fe, however, appears to be high

within the cementite, indicating that it does not follow a para-equilibrium transformation. The composition profile in the cementite is flat with Cr, Mn and C, which indicates that there is no elemental enrichment from the matrix at the carbide interface. The Si shows partitioning with a higher concentration at the interface, however Si is known to affect the formation and coarsening of cementite. Therefore, bainite is only showing a partial-para-equilibrium transformation, with Cr, as a strong carbide former showing some segregation into the cementite.

Table 6 Ratio of Fe to element in cementite and ferrite using data taken from Figure 36 and analysed by Image J taking the average atomic %, which is then divided by the iron concentration of ferrite and cementite, 99% and 75% respectively

<u>Element (x)</u>	<u>Ferrite</u> <u>Ratio Fe to x (at. % / 99)</u>	<u>Cementite</u> <u>Ratio Fe to x (at. %/75)</u>	<u>Comment</u>
<u>C</u>	0.6/99 = 0.006	22.8/75=0.304	C enriched in cementite
<u>Si</u>	0.11/99=0.001	0.12/75=0.001	No difference
<u>Cr</u>	0.31/99=0.003	0.46/75=0.006	Cr enriched in cementite
<u>Mn</u>	0.90/99=0.009	0.66/75=0.009	No difference

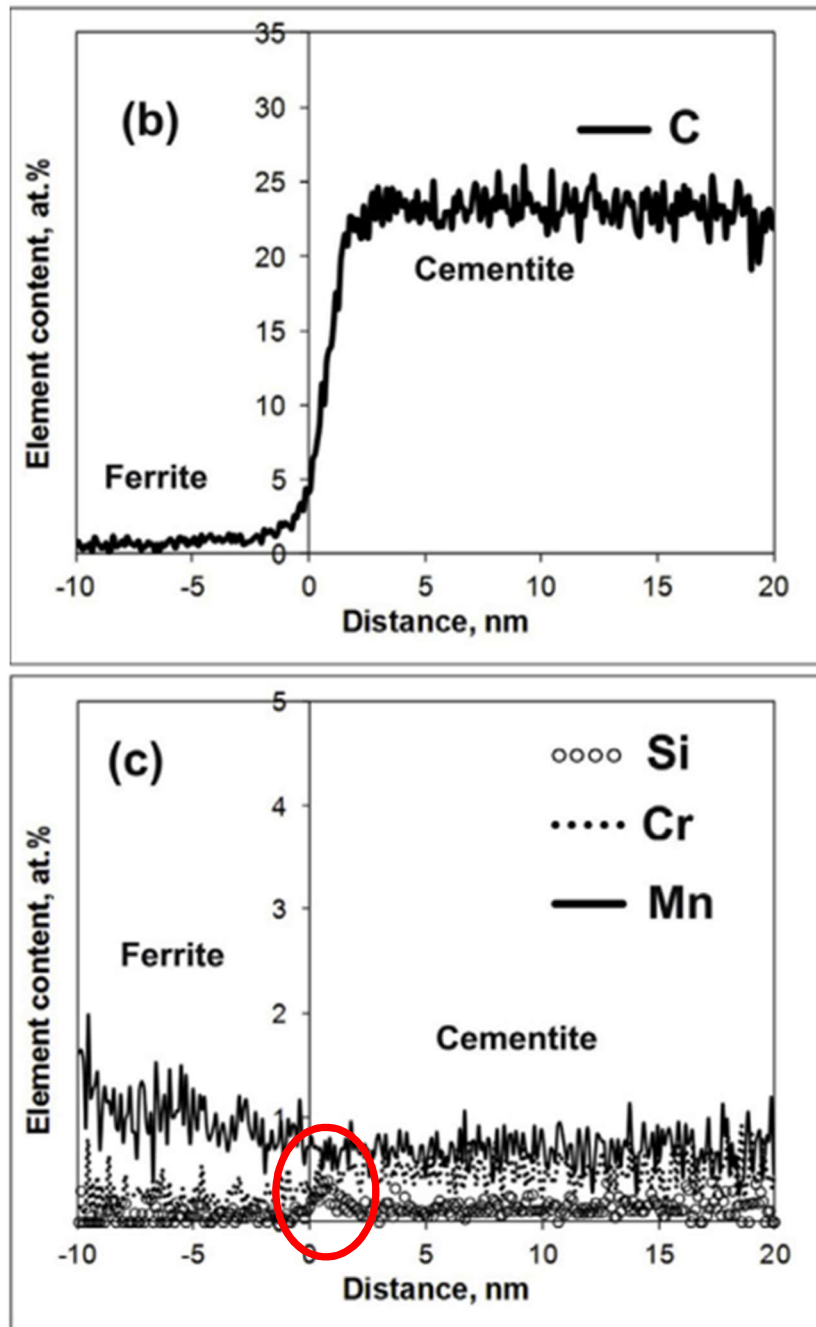


Figure 36 Proximity histograms across the cementite particle in bainitic ferrite after transformation at 400 °C for 1800s in 0.3C - 0.25Si- 1.22Mn-0.14Cr-0.03Mo wt. % (Caballero et al., 2014)

2.9: Bainite Transformation Temperatures

Steven and Haynes have predicted the isothermal upper bainitic start temperature using equation 2.5, determined for low alloy, low carbon steels(Steven, 1959).

$$B_{s\pm 25}[^{\circ}C] = 830 - 270[\text{wt. pct. C}] - 90[\text{wt. pct. Mn}] - 37[\text{wt. pct. Ni}] - 70[\text{wt. pct. Cr}] - 83[\text{wt. pct. Mo}]$$

Equation 2.5

Bainite forms via a different transformation mechanism to martensite. There is debate on the exact mechanism; one school of thought regards plates and carbides to form simultaneously via a shear process. The opposing view determines the two events as being distinct, with a shear and diffusional process respectively (Yang & Fang, 2005). Dilatometry data shows that length change associated with phase change occurs over a longer time scale than when compared to the almost instantaneous martensitic transformation. The amount of change in length is associated with the volume of bainite using the following equation (Podder, 2011).

$$(\Delta L/L_o = \Delta V/3V_o)$$

Equation 2.6

$\Delta L/ \Delta V = \text{Change in length/volume}$
 $L_o/ V_o = \text{Original length/volume}$

Pinto da Silva, 2014 showed that with increasing holding time (up to 10 seconds) at different bainite transformation temperatures there is an increased amount of bainite produced, [Figure 37](#) (Pinto da Silva et al., 2014).

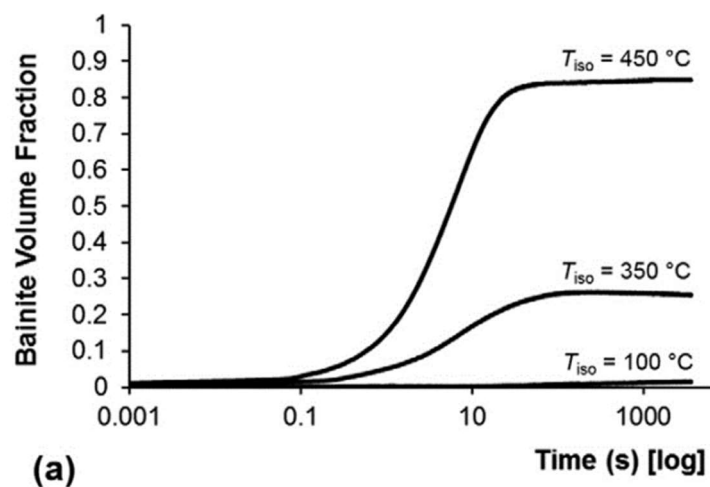


Figure 37 Transformation fractions during isothermal holding (Pinto da Silva et al., 2014)

The growth rate of bainite is dependent on the transformation temperature and composition, with authors reporting this time to take between minutes to hours. In some instances, there was not completion of transformation due to insufficient driving force (for bainite or martensite), resulting in retained austenite. An example of this is reported by Matas on the transformation to bainite, finding that at a low transformation temperature of 265° C holding for 10^5 seconds resulted in complete transformation to lower bainite, which was slower than the higher temperature transformation of 400 °C, where 10^3 seconds resulted in 75% transformation, with no increase at 10^4 (Matas, 1961).

Work by Bhadeshia found that the presence of Si alters the formation of cementite a crucial process in bainite formation and therefore slowing the formation of the bainite (H. K. D. H. Bhadeshia & Edmonds, 1979).

Bainite transformed at a lower temperature has a higher hardness in comparison to an identical composition transformed at a higher temperature. This is partially explained by Bhadeshia; bainite formed at lower temperatures (lower bainite) should have a finer plate size and larger dislocation density. There are also small carbides orientated within the laths for the lower bainite (H.K.D.H. Bhadeshia, 2001).

2.10: Tempering of Bainite

Bhadeshia produced a figure describing the tempering of bainite, shown in [Figure 38](#), (H.K.D.H. Bhadeshia, 2001). No compositions are given, but it is assumed to be alloyed due to the stage “alloy carbide precipitation”. Other works show this stage over a shorter time period. [Figure 38](#) is a good example of the stages which occur, but the timescale cannot be relied on.

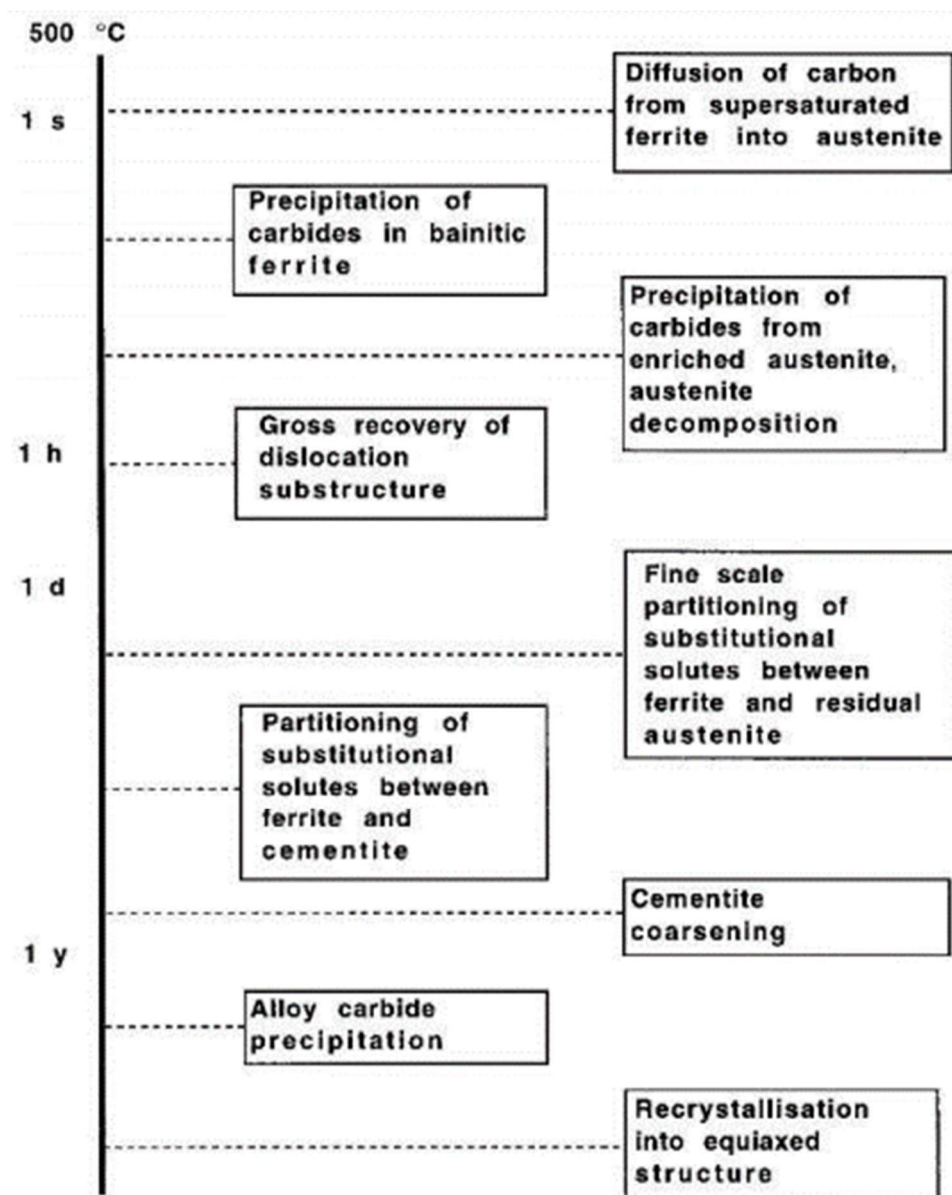


Figure 38 The time scales associated with a variety of tempering phenomena for bainite (this is not for a specific type of steel – no composition details were given) - Taken from Bhadeshia (H.K.D.H. Bhadeshia, 2001)

Bainite forms at higher temperatures than martensite, which allows carbide formation during quenching (H.K.D.H. Bhadeshia, 2001). Due to carbon coming out of solid solution to form the carbides associated with bainite, there is less strength in bainite when compared to martensite. Tempering lower bainite has less effect compared to tempering martensite, as there is a lower reduction in hardness due to the carbon already being out of solid solution (Irvine et al., 1957; Vieira, 2017).

Figure 39 shows the tempering response of two bainitic compositions (the type of bainite is not specified), with different carbon contents; the tempering response is similar for the two compositions. The similar hardness at the start of tempering is reported to be because although carbon is a potent solid solution strengthener as bainite has already formed carbides, and has little carbon in solid solution there is no difference in strengthening between the two carbon contents. This may suggest that the bainitic carbides are similar in number but larger in the higher carbon steel, assuming the same type of bainite. The significant hardness decrease in the tempering curve is due to the loss of fine effective grain size. Irvine and Pickering also discuss how the strength of bainite is dependent on the fine grain size, from laths and plates, with reinforcing carbides. Once these are lost and ferritic grain growth occurs then there is a steep decline in hardness, which is seen for tempering conditions (temperature and time) that give a Larson Miller Parameter greater than 18 (H.K.D.H. Bhadeshia, 2001; Irvine et al., 1957).

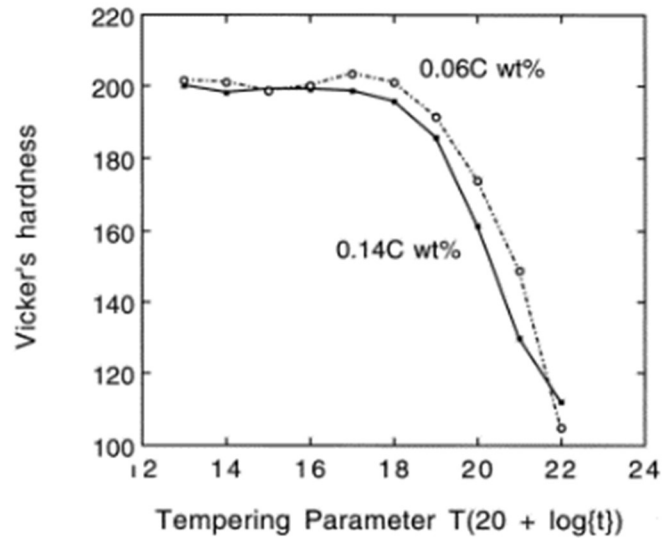


Figure 39 Tempering of bainitic steels with carbon content of 0.06/0.14C wt. % (H.K.D.H. Bhadeshia, 2001)

Nam, 1999 looked at the effect tempering has on carbides in bainite. They noted that bainitic carbides are more stable than martensitic carbides to changes in size with tempering (W. J. Nam, 1999). They investigated 0.45%C – 0.22%Si-0.62%Mn-0.004%P – 0.0038% S steel rods (10 mm diameter rods), austenised at 900 °C for 30 minutes, followed by a water quench (to produce martensite) or a salt bath treatment with temperatures of 653 K (380°C) for 1 hour (to produce lower bainite). The rods were then tempered at 973K (700 °C) for times between 5 minutes and 50 hours. The starting hardness of martensite was 667 HV dropping to 267 HV after 5 minutes tempering. The bainitic hardness went from 326 HV to 226 HV over the same time, see [Figure 40](#). On tempering for 50 hours the bainite ended up with a higher hardness than martensite, this was found to be because the bainitic carbides are less sensitive to coarsening when compared to martensitic carbides. The reasons stated for this are the cementite in bainite has a higher thermal stability than in martensite, as there is less C in solution and therefore less driving force for dissolution and coarsening, which is also affected by the uniform size distribution of the bainitic cementite particles. Changes in features such as lath size were not discussed (W. J. Nam, 1999).

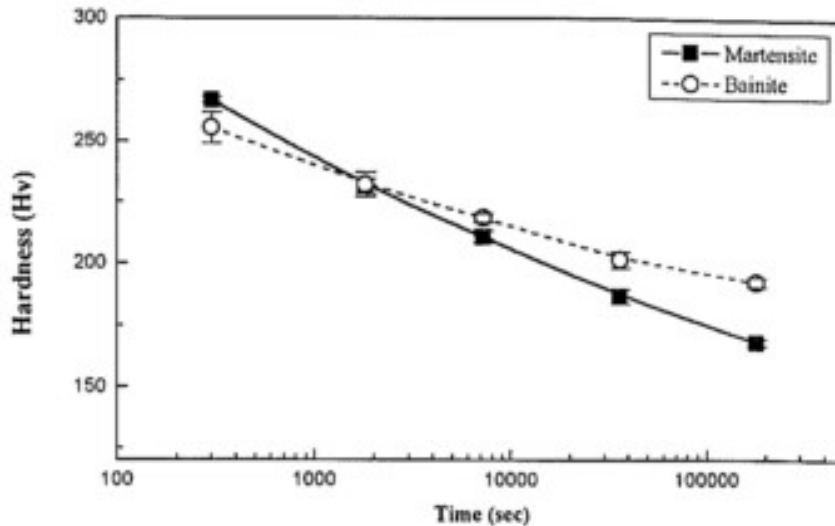


Figure 40 The variation of hardness (HV) with tempering at 973K (700°C) with time for martensite and bainite, 0.45% carbon steel, starting hardness martensite 667 HV – starting hardness bainite– 326 HV (W. J. Nam, 1999)

Ohmori, 1974 found that the cementite within bainite did not exhibit significant changes after tempering for 1 hour at 550 °C; in contrast they found in tempered martensite that the auto-tempered cementite laths within the matrix grew for the same tempering treatment. The PAGB also starts to exhibit evidence of being decorated with cementite. This is thought to be due to carbon, which is in solid solution in the martensitic matrix, being able to form carbides that will then grow (Y. Ohmori et al., 1974). Vieira, 2017 also found that in a 0.17 wt. % carbon steel – 1.23 Mn - 0.29 Si that martensite had a higher sensitivity to tempering than when compared to the fully bainitic steel, with martensite showing a greater instability on tempering in comparison to bainite. The reasons for this are reported to be due to carbon in solid solution (Vieira, 2017). It is also reported to be due to the presence of retained austenite, however when SEM images produced by the author are examined they do not show the presence of retained austenite, and the steel is not significantly alloyed meaning that very little retained austenite might be expected and therefore it is not thought to contribute significantly to the reported tempering behaviour.

2.10.1: Cementite coarsening during tempering

Nam 1999 investigated the tempering of martensite and lower bainite and how the cementite carbides coarsen. Figure 41 shows that the carbide size of the martensitic (on lath boundary) and bainitic carbides (on lath boundary and inside of laths) are similar in diameter after 5 minutes (300 seconds) temper, there is no discussion about any change in the volume fraction. Martensite does have a smaller carbide size in the inside of the laths after 5 minutes, indicating that they start off smaller. Bainite and martensite carbides all increase on tempering up to 50 hours, shown in Figure 41. Bainitic carbides are slower to increase in size and after 50 hours are smaller than the martensitic carbides (for both intra- and inter-lath types). All carbides show an increase in growth rate between 10 and 50 hours (36,000 and 180,000 seconds respectively). Nam suggests that martensite and bainite carbides can coarsen at different rates because of differences in the relative contribution of spheroidisation compared to coarsening, with the hypothesis that there is more spheroidisation in the earlier stages of tempering for the bainitic carbides than the martensitic ones, however the paper does not give details in terms of aspect ratio to determine exactly how the carbide shape changes. The paper reports that the difference in coarsening between the two microstructures is due to; the thermal stability of cementite, with smaller amounts of carbon in solution, and less driving force for carbon diffusion due to the uniform size distribution of cementite in bainite.

It was found that the difference in hardness between tempered bainite and martensite is not large once martensitic dislocations are removed during the initial stage of tempering, Figure 40, but it does show that over longer tempering times that bainitic carbides are more stable, remaining smaller, Figure 41. It is possible to observe that at 50 hours martensitic carbides have a lower number density than when compared to the bainite structure, which has had the same tempering treatment. This would agree with the Ostwald ripening mechanism, with smaller martensite carbides dissolving to give larger carbides, see Figure 42.

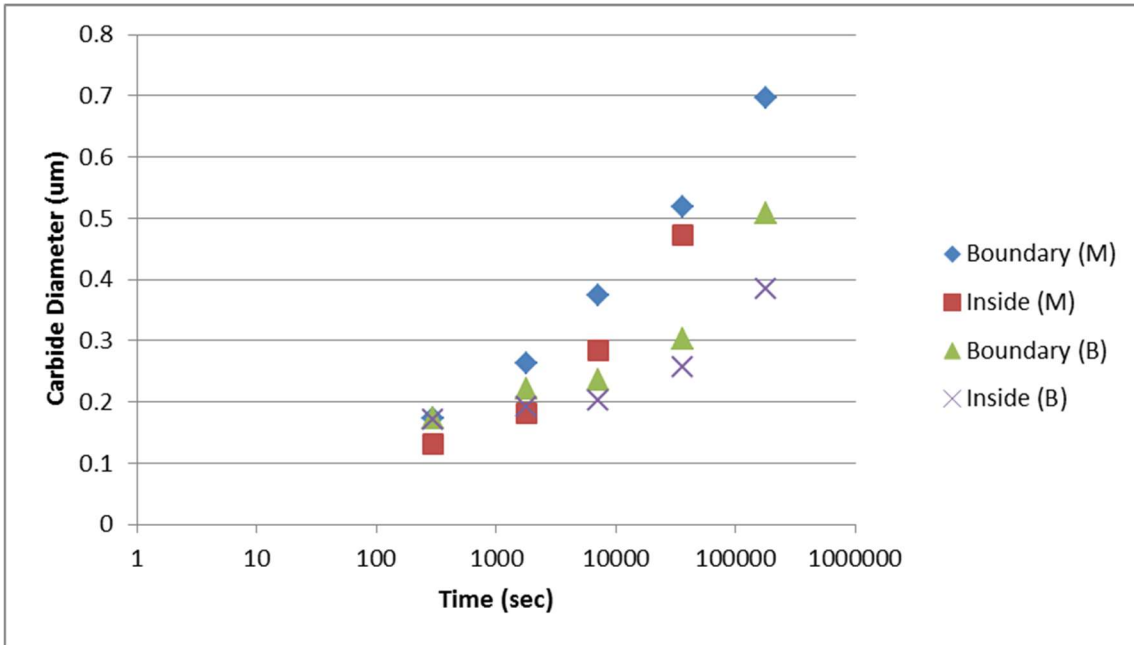


Figure 41 Average particle diameter of cementite with tempering time for martensite (M) and bainite (B) in medium carbon steel (0.45%C) rods, tempered at 700 degrees C after quenching (W. J. Nam, 1999)

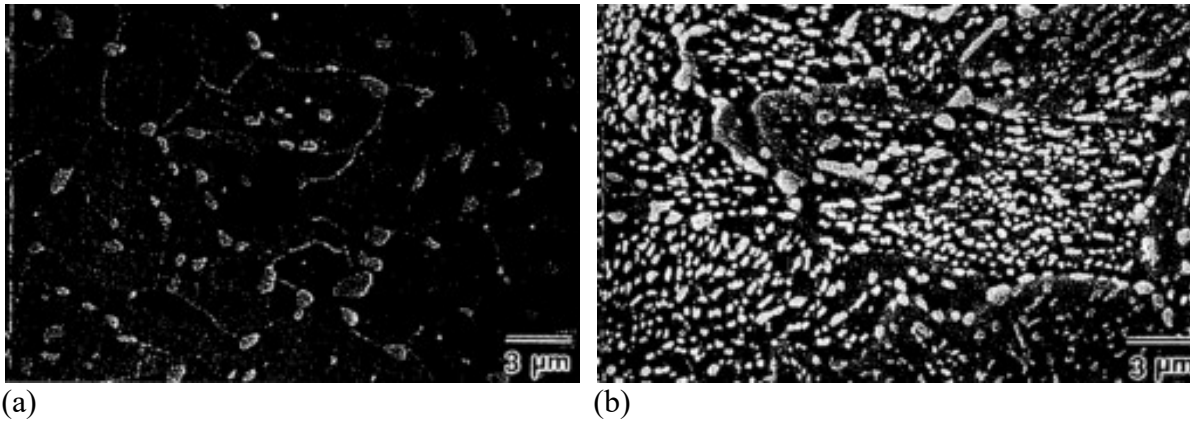


Figure 42 50 hr temper at 973 K (700°C) (a) martensite (b) lower bainite taken from (W. J. Nam, 1999)

2.10.2: Tempering of retained austenite

During tempering of a bainitic microstructure the carbon which is in any retained austenite is able to diffuse and form cementite as the equilibrium phase, which will form on any defects in the microstructure, such as dislocations or lath / grain boundaries. If carbides have not formed on cooling from the austenitic temperature when the microstructure was produced, then the cooling after tempering can result in the formation of martensite from the austenite destabilised on tempering (Molkeri et al., 2016). Additional partitioning may occur in the cooling period after tempering, as the solubility of carbon reduces. This would alter the microstructural phases present and change the overall properties observed in the bainite.

2.11: Secondary hardening of bainitic/ferritic steels with alloying additions

The work carried out by Baker and Nutting, determined that for a 2.25 wt. %Cr – 1 wt. %Mo steel that slight secondary hardening occurred in the bainite, whilst ferrite was found to not be affected by secondary hardening and the mean hardness did not differ from 145 HV over the whole period of tempering (1000 hours)(Baker & Nutting, 1959).

Work carried out by Bhadeshia, 2001 on bainite found that there is no reason why secondary hardening should not occur in bainite when there is occurrence in a comparable martensite, but adds that as cementite particles are coarser in bainite then dissolution is expected to take longer than in a comparable martensite, therefore secondary hardening in a bainite structure is expected to occur later, these observations are not verified experimentally and are theoretical (H.K.D.H. Bhadeshia, 2001). Bhadeshia, 2001 mentioned the work of Irvine et al. finding that Mo containing steel cementite transformed to $(Fe,Mo)_{23}C_6$ in bainite, while in martensite it transformed to Mo_2C . Little explanation is given, but it is worth mentioning as it means that the type of alloy carbide shown in bainite may alter from the alloy carbides shown in martensite (H.K.D.H. Bhadeshia, 2001; Irvine et al., 1957).

2.12: Differences between martensite and bainite

As mentioned previously, and summarised here, the main difference between martensite and lower bainite are as follows;

- Temperature of formation
- Alignment and size of carbides
- Stability on tempering (bainite being more stable)
- Martensite is harder than bainite on formation

2.13: Strengthening mechanisms

There are a number of mechanisms which contribute to the strength of steels, these are well established within the literature, and are summarised below with reference to martensite and bainite structures.

The relationship between strength, MPa, and hardness, Brinell hardness, is reported by Dieter, as the following (Dieter & Bacon, 1988). This is useful in converting MPa to hardness within the following section;

$$\text{Brinell Hardness} = \text{MPa} / 3.4$$

Equation 2.7

2.13.1: Grain Size

Often described by the Hall-Petch equation (H. K. D. H. Bhadeshia & Honeycombe, 2007) where the larger the grain size, the lower the strength.

$$\sigma_0 = \sigma_i + kD^{-1/2}$$

Equation 2.8

σ_0 = the yield strength

σ_i = the “friction stress” representing the overall resistance of the crystal lattice to dislocation movement

k = the “locking parameter” which measures the relative hardening contribution of the grain boundaries

D = grain diameter

The Hall Petch equation was developed for ferritic steels where high angle boundaries separate the ferritic grains. In the case of bainitic and martensitic steels the microstructure is comprised of smaller sub structures, such as blocks, packets and laths (see [Figure 11](#) and [Figure 34](#)). Low angle boundaries separate the laths whilst high angle boundaries ($>15^\circ$ mis-orientation) are found between blocks and packets (Ohmura et al., 2004). Morito, 2006 (Morito, Huang, et al., 2006) shows in [Figure 43](#) the highest frequency of lath orientation angles to be less than 5° , whilst Zhu et al found laths to be within $2-7^\circ$ (Zhu et al., 2010). This means that strengthening contribution from substructures within the bainite or martensite grain need to be known to determine overall strength.

Laths are associated with low-angle boundaries. Ohurma, 2004, found dislocations to pile up against the boundary when a stress was applied, once a critical (undetermined) stress was reached then the dislocations were able to move past the lath into the rest of the structure. The higher the mis-orientation angle the more difficult it is for dislocations to pass, and this provides greater strength.

Work by Ghassemi-Armaki, looked at static recovery of lath martensite in a 9-12 wt. % Cr steel with a carbon content of 0.093 – 0.098 wt. % C. Ageing was carried out between 1000-2000 seconds at 650°C . Lath widths were between $0.3 - 0.5\ \mu\text{m}$ for the range of compositions, and width increased in size as the spacing between the carbides increased. The stability of the laths is controlled by the thermal stability of particles; static recovery is caused by the loss of particle stability (Ghassemi-Armaki et al., 2009). In relation to strength this means that the material will lose the lath structure, and associated strength contribution, if there are no carbides to stabilise the laths.

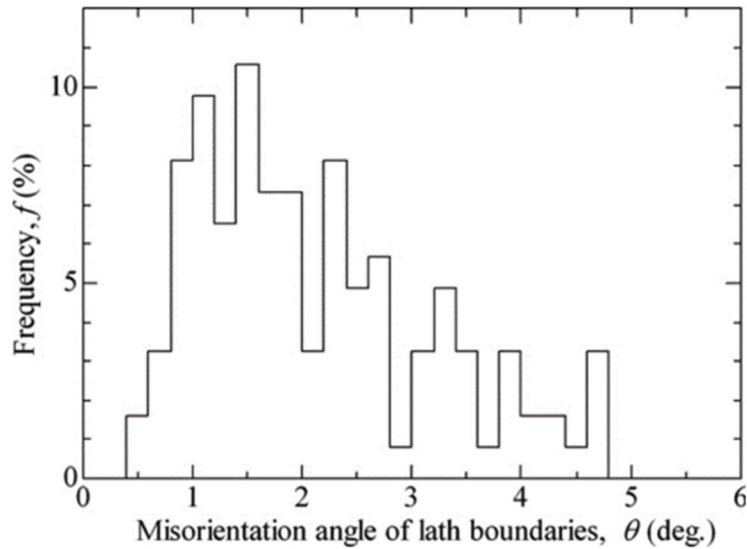


Figure 43 Misorientation angle distribution of lath boundaries measured by TEM Kikuchi pattern analysis in 0.0049C, 3.14Mn (mass%) steel (Morito, Huang, et al., 2006)

When it comes to predicting strength from grain size it is important to know how the sub-microstructures relate, for example whether the lath size can be related to grain size. The relationship between packet size and PAGES was reported by Morito in 2006, [Figure 44](#), as having a linear relationship. However, there is not as clear a relationship between PAGES and block width, with Mn additions found to enhance subdivision of packets into blocks, [Figure 45](#). The work concludes that substructure hardening is not dependent on the PAGES (Morito, Huang, et al., 2006). This means that when determining strength in martensite and bainite then the grain size should not be the only microstructure feature observed and features like block and lath size should also be included.

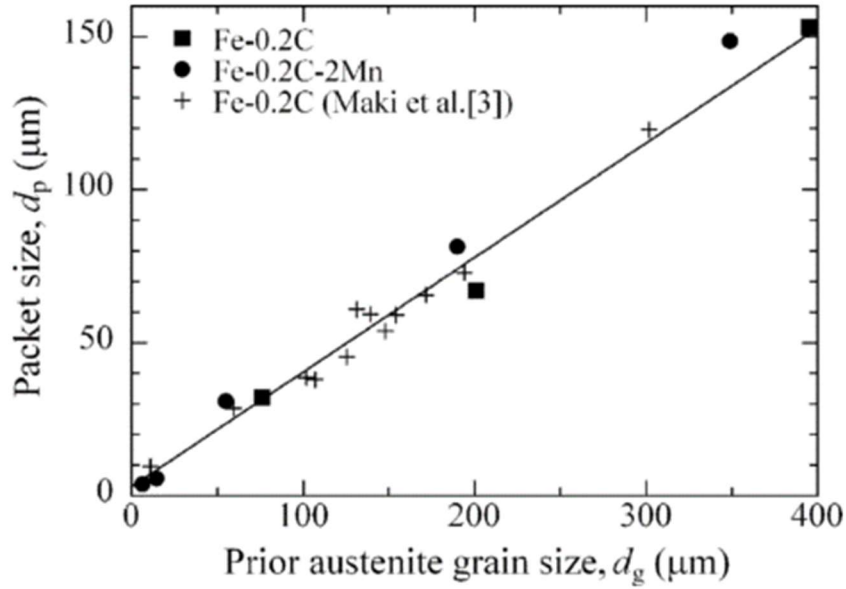


Figure 44 Relationship between the prior austenite grain size and packet size in quenched martensite in the Fe-0.2C and Fe-0.2C-2Mn alloys (Morito, Yoshida, et al., 2006)

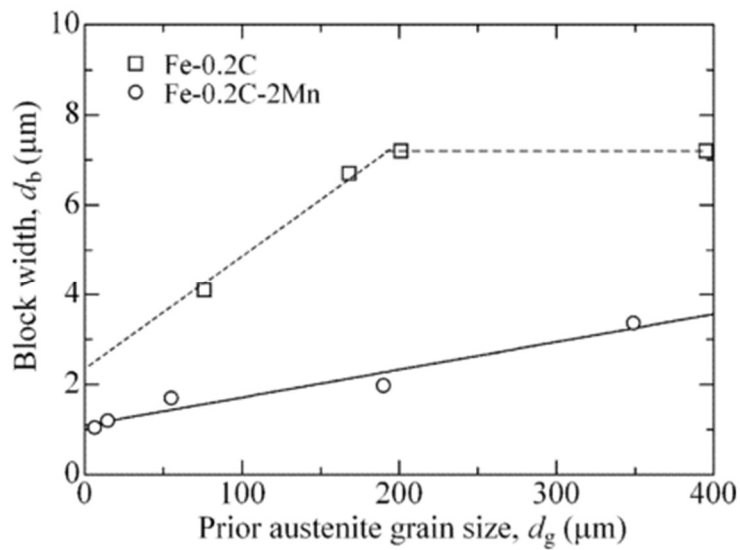


Figure 45 Relationship between the prior austenite grain size and the block width in quenched martensite in the Fe-0.2C and Fe-0.2C-2Mn alloys (Morito, Yoshida, et al., 2006)

A relationship between strength and lath width has been reported, equation 2.9 (Maropoulos & Ridley, 2005), Figure 46, and shows a decreasing contribution to strength as lath size increases. This will be additional to grain size strengthening.

$$\sigma_{lb}(MPa) = 8.62 \times 10^{-2} w^{-1}$$

Equation 2.9

w = lath width in millimetres

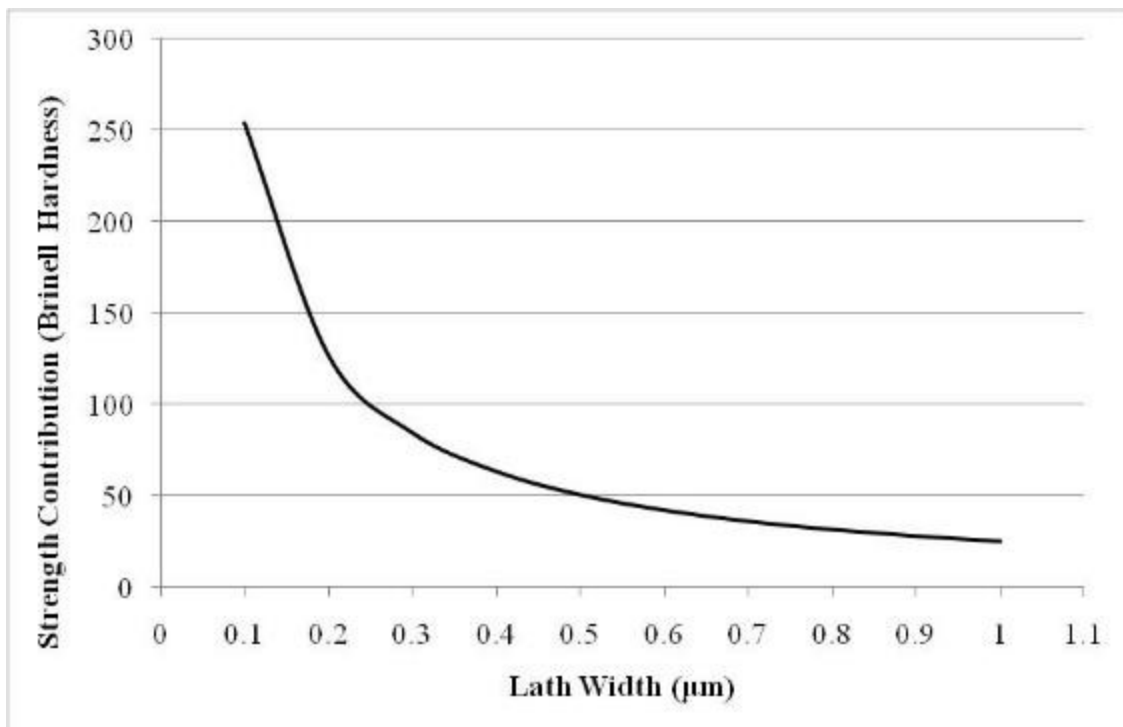


Figure 46 Comparison between Lath Width and Strengthening Contributions: Equation 2.9 from (Maropoulos & Ridley, 2005) has been used and values plotted for lath width between 0.1 and 1, with the strengthening contribution converted to Brinell hardness using Equation 2.8

2.13.2 Solid-solution-strengthening

It is known that adding additional elements to a metallic matrix can change strength. Work by Pickering and Gladman detailed the effects of alloying elements in a ferrite-pearlite steel, up to 0.25 wt. %C and 1.5 wt. % Mn: [Table 7](#) details the strengthening coefficients of each element (Llewellyn, 2013). As auto-tempered martensite and bainite have a BCC structure then the solid-solution strengthening effect is expected to be similar. The effect of carbon in solution in martensite is discussed in more detail in section 2.3, which found a strong correlation between carbon content and strength. It is important to note that Hutchinson finds that the carbon redistributes during quenching of martensite. Carbon redistributes from solid solution in the metastable BCT to lower energy sites such as defects or forms clusters, resulting in a BCT to stable BCC transformation. This segregated carbon is expected to have the same or more strengthening effect as the interstitial carbon in [Table 7](#) (Hutchinson et al., 2011).

Table 7 The strengthening coefficients of each element (Llewellyn, 2013)

Element	N/mm ² per 1 Wt. %
C and N	5544
P	678
Si	83
Cu	39
Mn	32
Mo	11
Ni	~ 0
Cr	-31

2.13.3 Strain hardening

Dieter, 1988 discusses strain hardening, also known as work hardening, as being caused by dislocations interacting with each other and barriers, impeding further motion through the crystal lattice (Dieter & Bacon, 1988). This could result from applied strain, or from dislocations generated due to transformation. Martensite for example has a BCT crystal structure on transformation, due to carbon being trapped in solid solution, which results in the formation of dislocations to accommodate the strain of the transformation (H. K. D. H. Bhadeshia & Honeycombe, 2007). The greater the carbon content in the as-quenched martensite the larger the strain and hence the higher the number density of dislocations produced, and the greater the contribution of strain hardening.

Young predicted the dislocation density generated relative to the transformation temperature for martensite and bainite, see [Figure 47](#) (Young & Bhadeshia, 1994). The dislocation density and subsequent strengthening are based on the transformation temperature, with a reduction in dislocation density / strengthening being shown at higher temperatures which is linked to recovery. The dislocation density can be calculated by equation 2.10, which can be used between the temperatures of 570 – 920K (~300 – 890 °C) and is applicable for most low alloy steels (Young & Bhadeshia, 1994). As martensite typically forms at a lower temperature than bainite it is expected to have a higher dislocation density.

$$\log\{p_D\} = 9.2840 + \frac{6880.73}{T} - \frac{1\ 780\ 360}{T^2}$$

Equation 2.10

Where

T = Transformation temperature (K)

P_D = Dislocation density (m^{-2})

Young then goes on to determine the strengthening contribution of the steel based on the dislocation density.

$$\sigma_p(MPa) = 0.38\mu b\rho_D^{1/2} \approx 7.34 \times 10^{-6}\rho_D^{1/2}$$

Equation 2.11

Where

μ = Shear modulus

b = the magnitude of the Burgers vector.

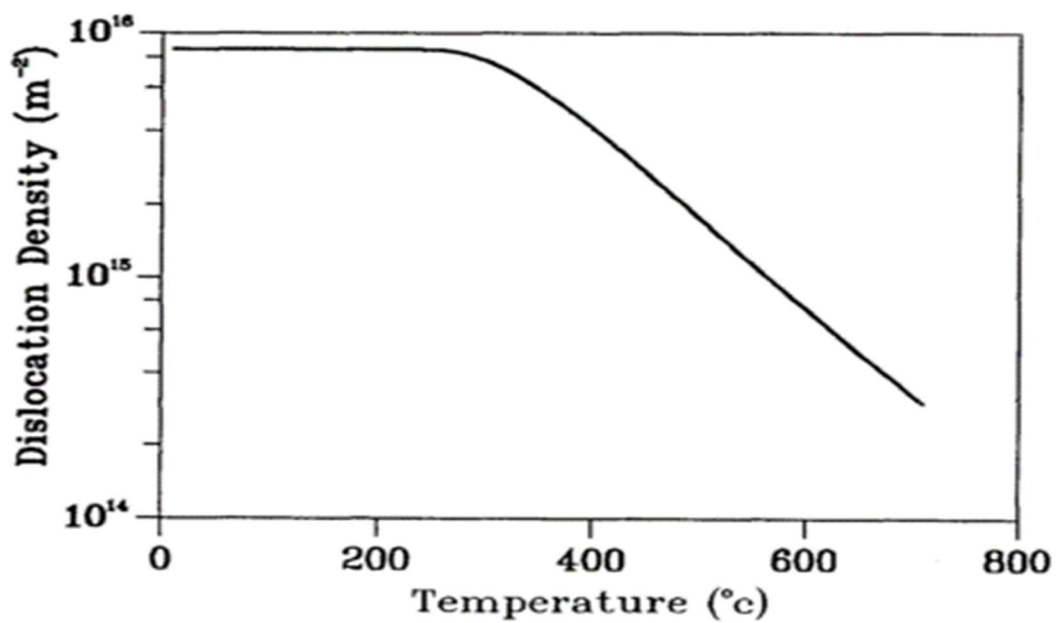


Figure 47 Assumed variation in dislocation density of martensite or of bainite as a function of transformation start temperature (Young and Bhadeshia 1994)

2.13.4: Precipitation Strengthening – Orowan was first to describe the relationship between particle size and number density with the strength, this equation can be seen below (Martin & Doherty, 1976).

$$\Delta\tau = 2T_1/\lambda b$$

Equation 2.12

$\Delta\tau$ = Change in shear stress
 T_1 = Bowing of dislocations
 λ = Inter-particle spacing
 b = Burgers vector

Other forms of this equation have been produced, such as the equation produced by Hirsch and Humphreys in Argon's book (Argon & J. Bikerman, 1971; Maropoulos & Ridley, 2005).

$$\sigma_p (MPa) = \frac{6.26}{\lambda} \ln \frac{D}{2.48 \times 10^{-4}}$$

Equation 2.13

D = Mean planar intercept diameter of a precipitate (μm)
 λ = The surface to surface precipitate spacing (μm)

As it is expected that the carbides on the laths and in the boundaries will coarsen differently, the strengthening contribution from each should be determined separately.

As mentioned previously, auto-tempered martensite typically has smaller more numerous carbides in comparison to bainite on formation, indicating there would be more strengthening from precipitation strengthening, if there is the same volume fraction of cementite observed. (Maropoulos & Ridley, 2005) used a range of equations, such as equation 2.9 and 2.13 to determine the different aspects of the strength (work hardening strengthening, substitutional strengthening, packet size strengthening, lath boundary strengthening, precipitation hardening and dislocation density strengthening) and the maximum difference was found to be about 4% between the actual strength and predicted strength for the martensitic quenched and

tempered steel, this is summarised in Table 8. The studied steels had carbon contents between 0.29 – 0.35 wt. % C, where the cementite had fully precipitated. The work did not look at different carbide distributions and focused on the average carbide spacing. The work shows that the precipitation hardening is predicted to be around 15 – 20% of the total hardness.

Table 8 Predicted and measured strength values for martensite steels reported by Maropoulos and Ridley 2005). Values are taken from paper and converted to Brinell hardness

Alloying Content (wt. %)	Observed MPa (Converted Brinell Hardness)	Predicted MPa (Converted Brinell Hardness)	Predicted MPa from Precipitation(Converted Brinell Hardness)
0.35 C, 0.88 Cr, 3.26 Ni, 0.66 Mo, 0.22 V, 0.18 Si	1068 (314)	1085 (319)	173 (51)
0.29 C, 0.77 Cr, 3.10 Ni, 0.57 Mo, 0.14 V, 0.15 Si	875 (257)	845 (249)	141 (41)
0.29 C, 0.80 Cr, 3.09 Ni, 0.57 Mo, 0.16 V, 0.12 Si	864 (254)	850 (250)	166 (49)

2.13.5 Phase Balance – The amount of each microstructure present will have a contribution towards the hardness. The main method of calculating this is the Rule of Mixtures and is discussed in section 2.14.2.

2.14: Mixtures of martensite and lower bainite

2.14.1: Introduction

The cooling time for thick plate RQT steels during quenching, along with its hardenability i.e. extent of alloying, affects the microstructures present through thickness, such that regions of martensite, bainite and mixed martensite + bainite can form. These steels are subsequently tempered and therefore there is a need to understand how mixed bainite + martensite microstructures temper.

2.14.2: Strength of Mixed Microstructures

The Rule of Mixtures is commonly used where strength (hardness) contributions from two materials added together are used to calculate an overall material strength (hardness). The Rule of Mixtures for microstructures is as follows, adapted from Alibeyki, 2017 (Alibeyki et al., 2017);

$$P_{MB} = V_M P_M + (1 - V_M) P_B$$

Equation 2.14

P = Hardness, yield strength or ultimate tensile strength of material

V = Volume fraction of phase

M = Martensite

B = Bainite

2.14.3: Rule of Mixtures – Ferrite Containing Microstructure

The Rule of Mixtures applies to any mixed microstructure and has been considered here in the content of mixed microstructures with martensite or bainite present. Saeidi, 2009 looked at mixtures of martensite and ferrite and another mixture set with bainite and ferrite, each with 34% ferrite, in a 0.4 wt. % C steel. They found that the ferrite in the martensitic mixture was harder than compared to the ferrite in bainite, due to the higher levels of strain from the martensite transformation compared to bainite transformation imposed on the softer phase (Saeidi & Ekrami, 2009). This indicates that individual phase hardness may not be the only factor which needs to be considered when predicting hardness using the Rule of Mixtures. Other authors have discussed dual phase (ferrite and martensite) steels and how they don't necessarily follow the Rule of Mixtures (Bergstrom, 2010; Fereiduni & Ghasemi Banadkouki, 2013; Gau, 1981; Y. Koo et al., 1980). The volume fraction of the softer ferrite phase is found to have an effect; for example the formation of ferrite causes partitioning of carbon into the austenite, resulting in martensite with a higher carbon content and strength than suggested for the overall carbon content, therefore a modified strength of martensite to be used (Fereiduni & Ghasemi Banadkouki, 2013).

Bergstrom has also found that plastic deformation is not homogenous between the two phases, with martensite not taking the strain load during application. The consequence of this is that the dual phase steel has a hardness more comparable to the softer ferrite than martensite, when there is more martensite than ferrite (Bergstrom, 2010).

2.14.4: Rule of Mixtures – Upper Bainite and Martensite Microstructure

Khan and Bhadeshia, 1990, looked at a Si - 0.67 wt. %, medium carbon 0.44 wt. % steel and found that in bainite transformed at higher temperatures (upper bainite) that the M_s temperature of the martensite in the mixture was lower, due to carbon being partitioned from the bainite to give more carbon in the austenite on transformation to martensite (Khan & Bhadeshia, 1990). The effect of increased carbon in the austenite as martensite forms is a difference in the M_s temperature, with martensite stabilised to lower temperature (Speich & Leslie, 1972), and consequently auto-tempering and lath size are affected. This means that the carbon content should be considered as it may alter the transformation temperature, and factors which are pertinent to strength.

2.14.5: Rule of Mixtures – Lower Bainite and Martensite Microstructure

Work has been carried out looking at the mixtures of martensite and lower bainite (Park & Kwon, 2001; Y. Tomita, 1991; Yoshiyuki Tomita & Okabayashi, 1985; Young & Bhadeshia, 1994). Much of this work has considered steels with medium/high levels of carbon, and it has been found that there is little comparison to the singular phases, i.e. the hardness of a bainite in a mixed microstructure is not compared to a fully bainitic microstructure. Tomita 1991 has looked at 0.2 wt. %C steel in comparison to a 0.4 wt. %C steel and found there is a peak in hardness at 20% lower bainite fraction for the higher carbon steel but no peak for the lower carbon steel, full compositions are in [Table 9](#).

Table 9 Composition of steel used by Y. Tomita, 1991

Element wt. %	Composition 1	Composition 2
C	0.20	0.40
Si	0.30	0.25
Mn	0.53	0.71
Cr	0.50	0.87
Mo	0.24	0.25

The martensite in the 0.2 wt. % C steel produces a reduced plastic constraint effect on bainite, as the transformation strain is less, compared to the 0.4 wt. % C steel, and the effect is not sufficient to increase the overall hardness, i.e. the lower carbon steel shows no brazing effect (Y. Tomita, 1991). The 0.2 wt. % carbon steel therefore follows the Rule of Mixtures for the mixed bainite + martensite microstructures. This effect has also been reported by Park et al in 0.35-0.4 wt. % C steel (Park and Kwon 2001), [Figure 48](#) and [Figure 49](#). Equation 7 (a fitting factor 0.15% was used), within [Figure 48](#), refers to the Rule of Mixtures for mixed lower bainite-martensite steel using experimental data for the bainite and martensite properties. This equation is fully shown in equation 2.15 the authors have taken into consideration grain size refinement of martensite packets from the bainite formation and assumed that the carbon content of the martensitic matrix increases linearly in proportion to the volume percentage of bainite formed, as carbon content in the untransformed austenite during lower bainite transformation and subsequent increase in martensite hardness. The carbon partition was not verified and assumed based on another author's work, it was noted that any retained austenite would decrease strength. There was a liquid nitrogen quench which would have removed any austenite and subsequent softening. Park does not contribute the peak as a brazing effect, as they comment that the constraint effect may cause a counter effect that may soften surrounding martensite matrix. This is not commented on further, but [Figure 48](#) and [Figure 49](#) both show a peak for high carbon steel (Park & Kwon, 2001).

$$\begin{aligned}\sigma_{LB-} &= \sigma_M(1 - V_{LB}) + \sigma_{LB}V_{LB} \\ &= (\sigma_{n=0}^M + \Delta\sigma_1 + \Delta\sigma_2) \left(1 - \left(\frac{ndl}{l}\right)\right) + \sigma_{LB} \frac{ndl}{l}\end{aligned}$$

Equation 2.15

Where

σ = Micro hardness

σ_1 = Refinement of austenite grain size

σ_2 = Strength increase of martensite from partitioned carbon from lower bainite

α = Assumed to be 0.15%

V = Volume

l = Grain size

dl = Width of LB

n = Number of LB plates

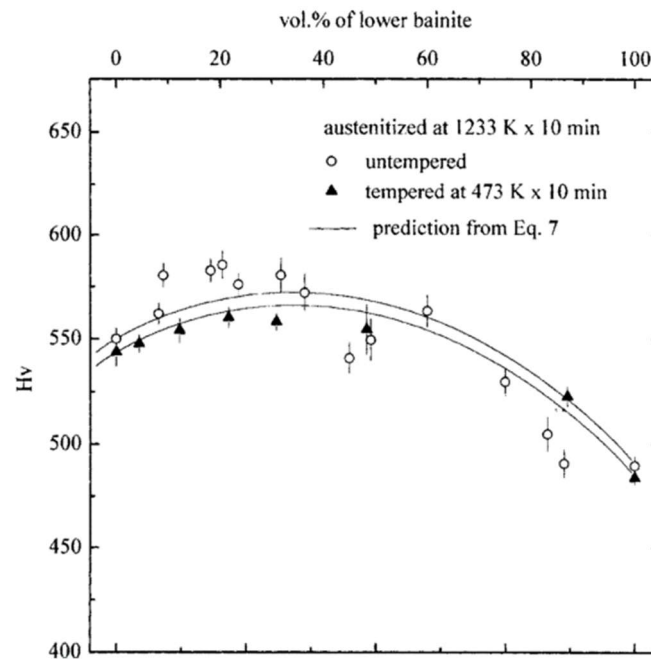


Figure 48 Variation in hardness (HV) with vol.% of lower bainite in LB-M steel, with 0.35% C. The prediction lines (eq. 7 mentioned on the figure) is the Rule of Mixtures for un-tempered and tempered at 473K (200 °C) for 10 minutes (Park & Kwon, 2001)

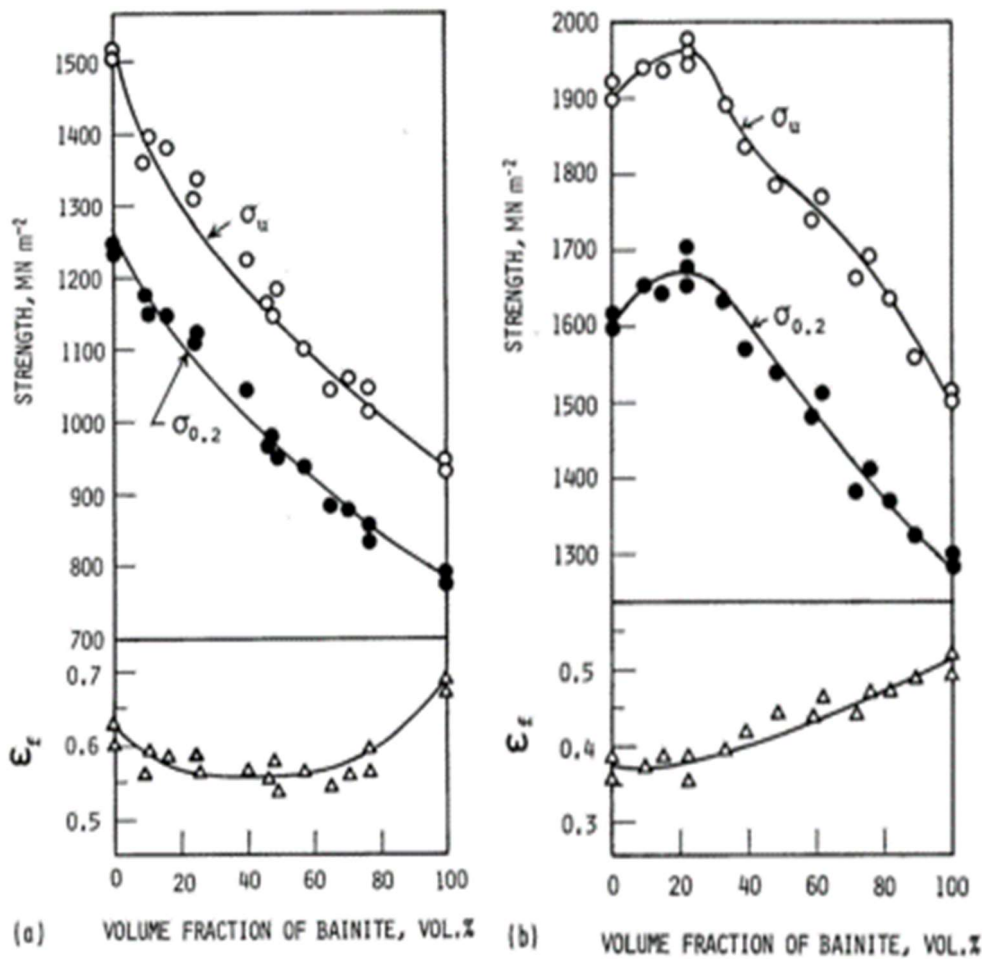


Figure 49 Effect of volume fraction of lower bainite on strength $\sigma_{0.2}$, σ_u and fracture ductility ϵ_x of (a) 0.2% C and (b) 0.4% C steel taken from (Y. Tomita, 1991)

2.14.6: Refinement of martensite packet size in mixed microstructures

Figure 50 shows the way in which bainite formation is thought to affect the martensite packet size in a mixed microstructure, reducing the resulting martensitic packet size and lath width (Y. Tomita, 1991). As mentioned in the strengthening mechanisms for martensite discussion (section 2.13), there is a strengthening contribution from the substructure, i.e. lath, block and packet boundaries, therefore any increase in the number of boundaries should increase the strength.

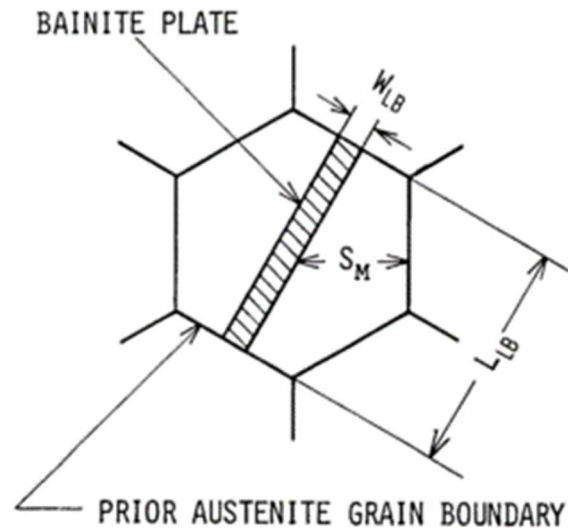


Figure 50 Schematic diagram of microstructural parameters of lower bainite (W_{lb} = width of lower bainite, L_{lb} =length of lower bainite, S_m =size of martensite (Y. Tomita, 1991)

Work by Park and Kwon determined that the presence of bainite does not alter the way in which martensite is transformed in a 0.35 wt. % C, and hence the packet size, in the lower carbon steels, while the higher carbon steels (0.4 wt. % in the Tomita work) does show a refinement (Park & Kwon, 2001; Y. Tomita, 1991). Therefore, in low carbon steels a mixed martensite + bainite microstructure will have martensite with a similar structure to that which would form in a fully martensitic sample.

2.14.6.1 Summary

There have been a number of reasons discussed why mixed martensite + bainite microstructures do not necessarily follow a standard Rule of Mixtures to predict strength, as summarised by Park and Kwon, and Young and Bhadeshia and given below. These reasons are typically only shown for high carbon steels (0.4 wt. %) and is not exhibited in lower carbon steels (0.2 wt. %).

- 1) Refinement of martensitic substructure by bainite, acting in a similar manner as grain size refinement.
- 2) Carbon partitioning from the bainitic ferrite into remaining austenite, altering the amount of carbon in solution affecting the martensite transformation, such as altering M_s Temperature, changing auto-tempering extent and lath size, as well as affecting the amount of C in solution/dislocation density and inherent strength.
- 3) High carbon martensite causes a plastic constraint effect (“brazing effect”, when there are relatively low fractions (~20%) of lower bainite, providing bainite additional strength.

2.15: Tempering of mixed microstructures

Barranco, 1992, tempered 100% martensite, 100% lower bainite and mixtures of martensite with 66% bainite and 22% bainite, produced in a steel with composition of Cr1.02 – Mo 0.48 – V 0.10 wt. % (Barranco, 1992). There was an undisclosed C wt. % in the steel, however, considering the overall composition it might be expected to be 0.3 – 0.4% wt. %C as the martensitic start temperature was given as 286 °C (determined using the equation 2.2). This carbon level is consistent with the reported presence of twinned martensite for the 100% martensitic un-tempered steel. An issue with this work is that there is no error or standard deviations given for this work, so results should be questioned, as it unknown how much of an effect this will have on the given hardness after quenching and tempering.

Figure 51 shows that at room temperature the material follows the Rule of Mixtures for the prediction of hardness, suggesting that brazing effect does not occur in this steel as there is no increase in hardness for the 22% bainite sample compared to the Rule of Mixtures prediction. This is likely because the carbon content is not high enough to give significant constraint to the bainite i.e. as it is assumed to be lower than 0.4 wt. % C, which was found to be significant in 2.14.

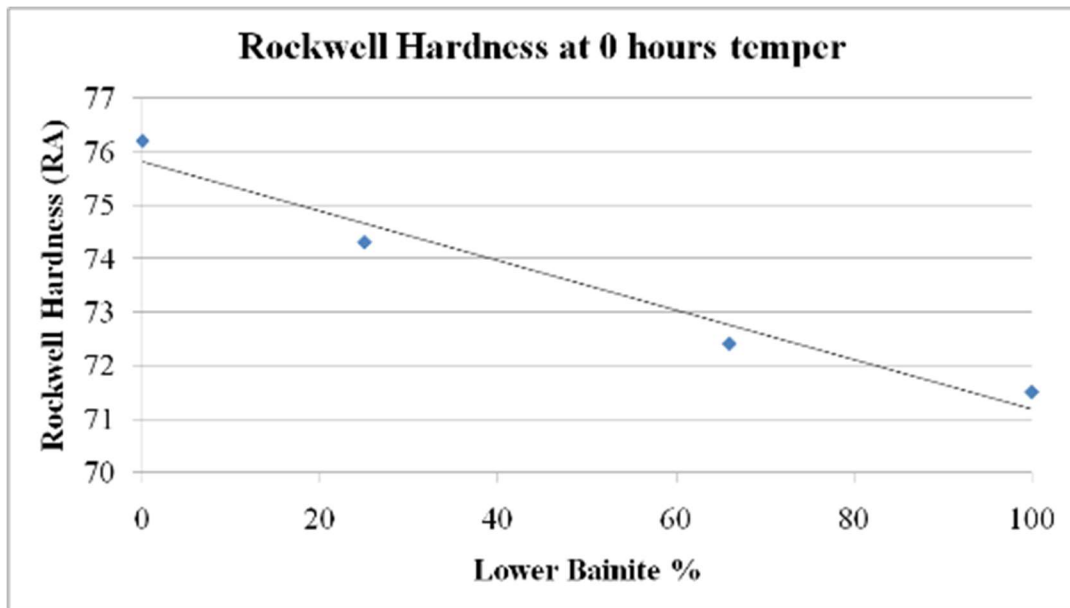


Figure 51 Hardness of martensite, bainite and mixed martensite + bainite samples, taken from (Barranco 1992)

After 1-hour tempering all the microstructures show a decrease in hardness. The higher the tempering temperature, the more severe the decrease in hardness. At 593 °C the hardness values have started to converge on a hardness at around 68 – 70 Rockwell hardness. The 100% martensite and 66% bainite + martensite microstructures have overlapping hardness values and the 100% bainite and 25% bainite + martensite microstructures have overlapping values at 593 °C for 1 hour. At 704 °C for 1 hour the hardness values of the 25% bainite + martensite is harder than the 100% martensite, shown in [Figure 52](#). It is again important to note that there are no associated errors/standard deviation, therefore robustness and statistically significant cannot be commented on.

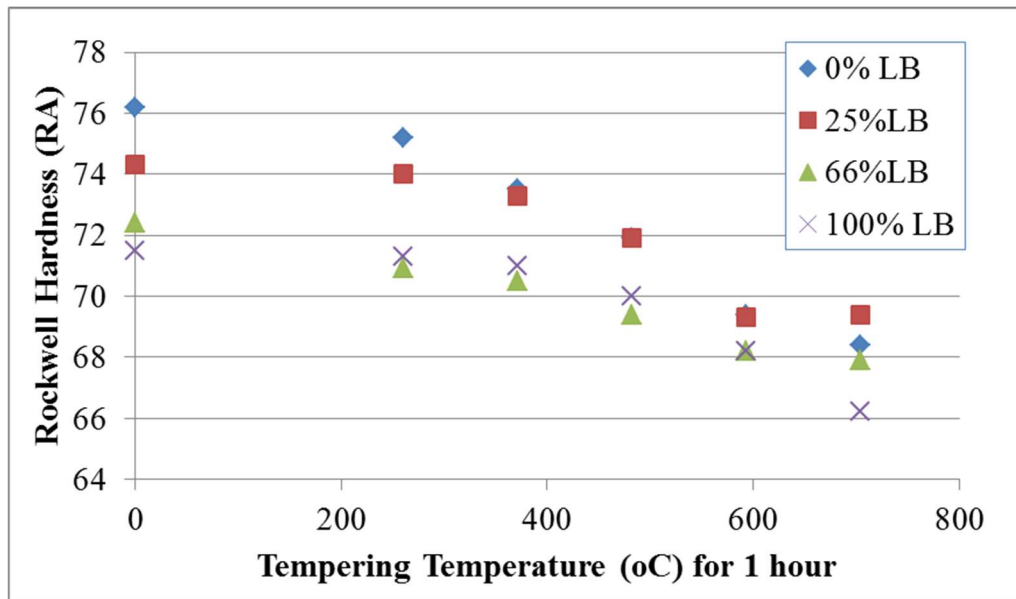


Figure 52 Hardness of martensite, bainite and mixed martensite + bainite samples that have been tempered from 260 °C to 704 °C for 1 hour, data taken from (Barranco, 1992) LB = lower bainite

There are no associated errors with the work; this means that changes in hardness cannot be completely relied on. The 704 °C temper was said to exhibiting the early stages of spheroidisation, this matches the drop-in strength. There is discussion around the change in microstructure within the paper, where it is commented on that there is no a marked change in the microstructure with increased tempering times in the 66% bainitic samples. Although there is no clear indication of associated errors, it appears that any difference in hardness between martensite, bainite and martensite + bainite decreases at higher tempering temperatures, up to 593 °C. There is no explanation why the 25% bainite is harder, however it appears to be softening at 593 °C temper. The 66% lower bainite is at times softer and harder than the 100% bainite, when the lack of error is considered this may not be significant, expect for the higher tempering temperatures. The same issue is associated with the 25% lower bainite which is harder than the 100% martensite at 704 °C. It is important to note that this paper is the only one discussing hardness in a low carbon mixed martensite and lower bainite microstructure on tempering. This work is limited and does not provide errors; therefore, it does not provide a clear explanation of the changes which occur on tempering.

2.15.1: Changes to Carbides in Mixed Microstructures on tempering

Thomson, 1994 looked at upper bainitic microstructures (with a small amount of martensite - the amount was not stated but it was small enough to be disregarded by the author in any analysis) and compared this to mixtures of upper bainite and ferrite (50%), in a C-0.15/Mn-0.49/Cr-2.20/Mo-0.96 steel. The bainite did not have any intra-plate carbide precipitation prior to tempering, indicating an upper bainitic microstructure, [Figure 53](#). As ferrite forms first, carbon is partitioned into the austenite, so that in the mixed bainite and ferrite microstructure the bainite will have a higher carbon content in comparison with the fully bainitic structure (Thomson & Bhadeshia, 1994a, 1994b).

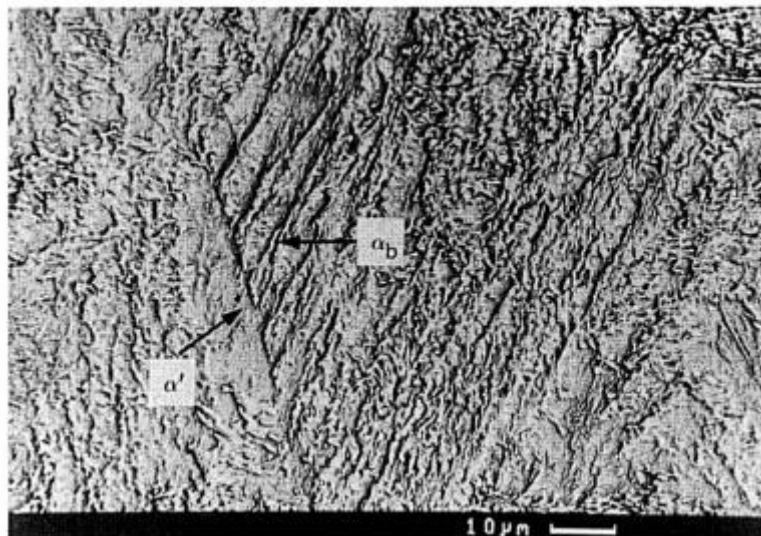


Figure 53 Starting bainitic microstructure, α_b is bainite and α' is martensite – Intraplate carbides are not present – indicating upper bainite. Austenitised at 1050 °C for 15 minutes, 480 °C for 30 min, and then water quenched (Thomson & Bhadeshia, 1994a)

It was found that the cementite enrichment with Cr was slower in the bainitic regions of the mixed microstructures compared to fully bainitic structures, at 565 °C for times between 1 and 128 hours, see [Figure 54](#). This is reported to be due to the increased concentration of carbon in the bainitic regions of the mixed microstructure preventing Cr enrichment, thought to be due to the carbon enriching the carbides easier (Thomson & Bhadeshia, 1994a). It should also be noted that in the mixed microstructure the Cr content of the mixed and bainite

associated cementite starts to converge around 180 hours at around 24 wt. % Cr, this is thought to there being more carbon in the mixed microstructure for initial carbide precipitation), but it does demonstrate that cementite within different microstructural regions of the same steel composition responds differently to tempering, reaching an equilibrium amount at different rates.

Cementite particles in the bainite region of the bainite-ferrite sample had a higher number density compared to the cementite particles in the fully bainitic sample on tempering. This is postulated to be due to increased carbon content in the bainite (0.277%), than the ferrite (0.0228%) as ferrite forms and carbon is rejected into the remaining austenite that then transforms to bainite (Thomson & Bhadeshia, 1994b).

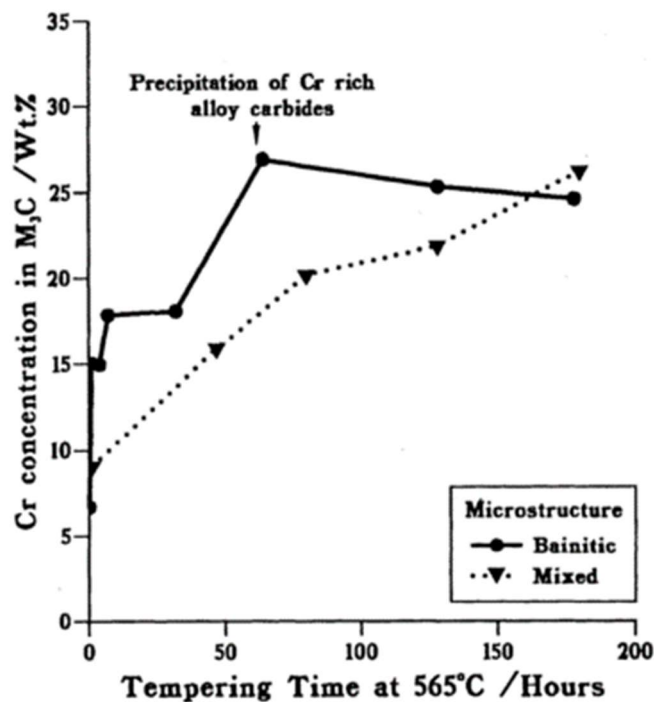


Figure 54 Ferrite and upper bainite cementite. Cr enrichment Comparison of average Cr content in cementite in fully bainite and mixed microstructure specimen as a function of tempering time at 565 °C (Thomson and Bhadeshia 1994)

2.16: Summary

This literature review has summarised the current state of knowledge on the tempering of martensite, lower bainite and mixtures of these two phases. There are several areas that are not fully understood for low carbon low alloy quenched and tempered steels.

The difference in microstructure (martensite/bainite) affects the precipitation behaviour of alloy carbides. It is well documented that martensite softens over time with tempering, in the presence of alloying elements (CrMnSi) giving a reduction in softening rate and, in the case of Mo and V, contributing to a secondary hardening effect if present. Bainite is less extensively studied in terms of tempering, partially due to the fact that bainite does not need to be tempered as this does not typically improve its mechanical properties, unlike with martensite. It is observed however that both phases show a reduction in hardness during tempering (unless secondary hardening from alloy carbides occurs). The addition of alloying elements (CrMoV) on tempering has been studied for a range of compositions; see [Table 10](#); however, there is very little reported looking at micro additions (SiCrMoV), i.e. 1wt. % or less, in martensitic steels and even less studies for a mixture of bainite and martensite.

Currently the literature extensively discusses the tempering of martensite and bainitic separately and this is well understood. Whilst there have been reports on the strength / hardness of bainite, martensite and bainite + martensite microstructures in the initial and tempered conditions much of the work for mixed microstructures has been for steels with carbon contents >0.2 wt. %. There have been different findings on whether a mixed bainite + martensite microstructure has strength / hardness that can be predicted by the Rule of Mixtures (i.e. bainite and martensite acting independently) or shows deviation from this, for example due to carbon partitioning from bainite into austenite to give higher carbon martensite, or due to residual stress, and constraint factors, from the volume expansion on transformation to martensite, on bainite. These latter effects have been shown to be less

significant for lower carbon steels, but it is not reported what the effect might be in low alloy RQT steels.

Table 10 Summary of alloying elements covered in literature

Element	Brief Summary
C	Adds strength from solid solution strengthening. Alters what microstructure type may be present in martensitic steels
Cr	Carbide former and causes an increase in hardenability. Inhibits martensite decomposition. 1 wt. % Cr steel after 1 hours at 592 °C found an increase in hardness of 40 HV, compared to Cr free composition, with 0.2 wt. % C. Cr is incorporated into the cementite and promotes transition to Cr rich alloy carbides.
Mo	Carbide former and causes an increase in hardenability, forms separate secondary hardening precipitates (compared to Cr and V). Retards PAGB size increase during austenitic holds (by ~20µm per hour). 1 hour at 600 °C shows secondary hardening (0.90-3.06Mo %) – Up to 150 HV increase in hardness.
V	Carbide former, forming separate secondary hardening precipitates than Cr and Mo containing steels. Vanadium additions decrease the austenite grain size (Han et al., 1995). Increased hardness for 0.2 wt. % V after 1 hour at 592 °C (90 HV increase) – compared to V free composition, with 0.2wt. % C.
Si	Adds strength by solid solution strengthening. Retards cementite formation (may form carbide free bainite/ retained austenite). At 600 °C for 2 × 2 hr temper there is no difference in hardness between 0.05 – 2% Si. Indicating that the SSS effects are reduced after longer tempering times.
Mo + V	A higher level of V to Mo changes the carbides which form. This reduces the amount of M ₂ C carbide precipitating and M ₆ C was found to precipitate earlier. With a lower V to Mo ratio then MC is not promoted.
Cr + Mo	Mo + Cr increases stability of martensite to tempering, with a 10 Rockwell hardness difference after 1 hour at 600 °C, compared to Mo only containing steel.

Chapter 3: Aims and Objectives

The aim of the project was to understand the effect of tempering on martensitic, bainitic and mixed martensite + bainite microstructures and hardness values in a low carbon, low alloy steel (based on S690) along with the role of alloying content (Mo, Cr, V, Si). The specific objectives of the work are:

- Produce fully martensitic microstructure in the Base steel and compositions with mixtures of alloying elements (BaseMoV/BaseSiCrMoV).
- Produce fully lower bainitic microstructure in the three steels.
- Produce systematic mixed microstructures of martensite and lower bainite, from 0 – 100% of lower bainite.
- Determine hardness and microstructure characteristics of initial microstructures and consider Rule of Mixtures prediction.
- Temper for varying times (30 minutes to 100 hours) for martensite, lower bainite and martensite + lower bainite and assess the microstructure and hardness changes.
- Investigate effects of tempering on carbide size and distribution and lath size.
- Determine through thickness microstructure and hardness for a thick plate for a given composition on quenching using a predicted cooling rate (from a CCT curve). Predict the tempering response through thickness, using COMSOL modelling.

Chapter 4: Experimental Method

4. 1: Materials

Three plates, measuring approximately 25cm in length with a 16 cm width, of Q&T steel were provided by TATA Steel UK; compositions and thicknesses given in Table 11. The lab cast plates were processed in the TATA Steel STC pilot casting and rolling facilities, thicknesses before rolling is not available. Samples were rolled with a finishing rolling temperature of approximately 900 °C, then reheated to 925 °C for one hour and water quenched.

Table 11 Composition wt. % and thickness of steels examined

Name	C	Si	Mn	P	S	Cr	Mo	Al	N	Nb	Ti	V	B	Plate Thickness
Base	0.17	0.29	1.2	0.015	0.002			0.03	0.004	0.03	0.024		0.0025	40 mm
Base-Mo-V	0.17	0.28	1.2	0.015	0.002		<u>0.5</u>	0.03	0.004	0.03	0.026	<u>0.05</u>	0.0025	36 mm
Base-Si-Cr-Mo-V	0.17	<u>1.24</u>	1.2	0.016	0.002	<u>0.8</u>	<u>0.5</u>	0.04	0.006	0.03	0.027	<u>0.05</u>	0.0025	32 mm

4.2: As received microstructure

The initial lab cast samples had differences in hardenability this led to differences in microstructure and hardness for the received samples, these were investigated, and results shown in [Table 12](#).

Table 12 Comparison of hardness and microstructure of as-rolled steels

Composition	Average HV	Microstructure
Base	212 ± 4	Ferrite/Pearlite
Base Mo V	335 ± 5	Mixed Bainite
Base Si Cr Mo V	386 ± 6	Bainite/Martensite

4.2.1: Inclusions

The as-received samples were characterised for inclusion content: there was no noticeable variation in inclusion distribution between the three steels ([Figure 55](#)) and no evidence of any centreline segregation, which, if present, would be expected to give a higher concentration of inclusions at that location.

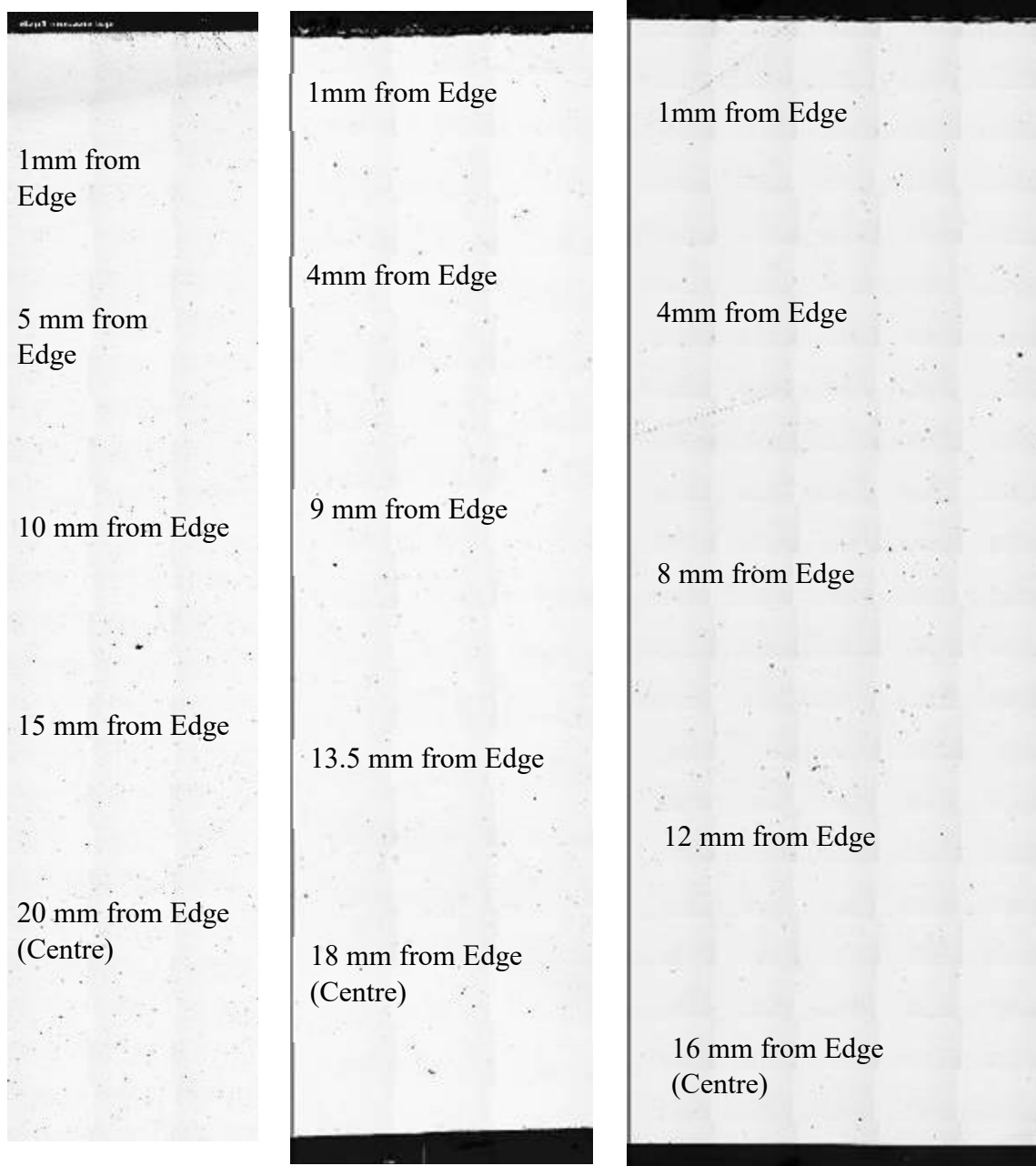


Figure 55 Inclusions in the three as-received plates through thickness, from left to right Base, BaseMoV, BaseSiCrMoV

4.2.2: Optical Microscopy

Optical images show that there is little difference between the quenched conditions with a martensitic structure. There is no evidence of some localised segregation in the samples from the etching response, for example in BaseSiCrMoV ([Figure 58](#)).

There are even distributions of inclusions across the three microstructures. There is no evidence of segregation which is having a significant effect on what phases transformed i.e. the three steels produce lath martensite.

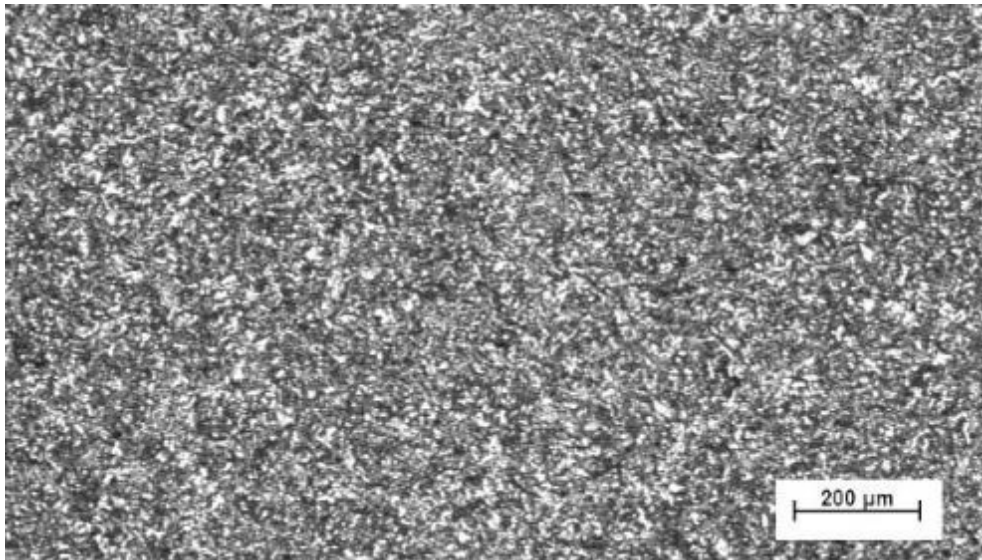


Figure 56 Optical Images of martensitic start conditions (Base)

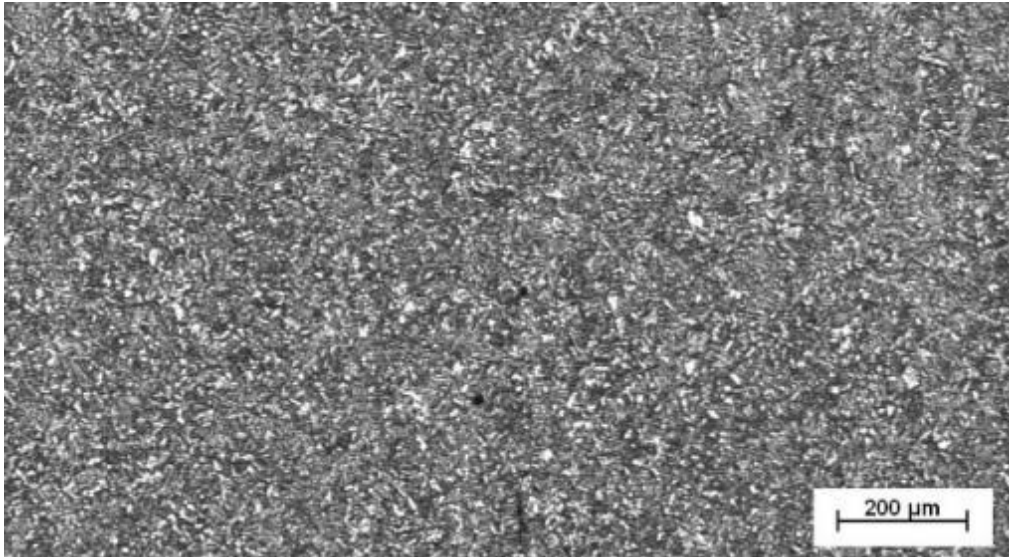


Figure 57 Optical Images of martensitic start conditions (BaseMoV)

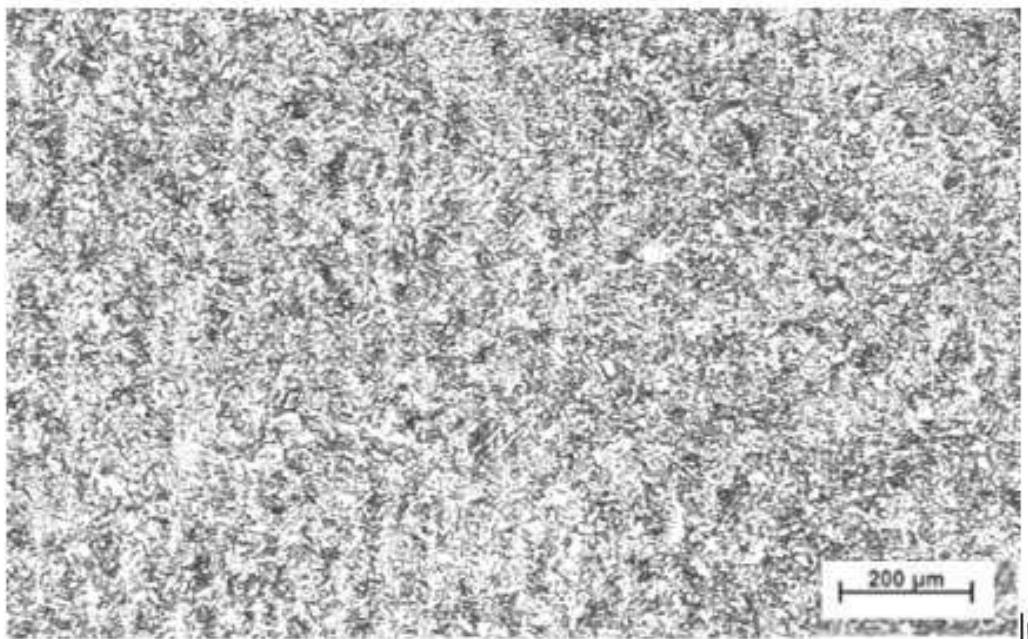


Figure 58 Optical Images of martensitic start conditions (BaseSiCrMoV)

4.3: Sample Preparation:

Samples for furnace heat treatment, measuring $15 \times 20 \times 20$ mm (15 mm through thickness), were cut from the steel plates provided with 3 mm machined from the plate surface to remove any influence of surface scale or decarburisation. Samples for Gleeble heat treatment, measuring $10 \times 10 \times 60$ or 77 mm, were machined (band saw or EDM) from the plates. Dilatometry samples were machined (EDM) as cylinders of 5 mm diameter with 10mm length. After the heat treatments were carried out the samples were cut, using a diamond edged disc, through the mid position, then mounted in conducting Bakelite for optical and SEM analysis.

The mounted samples were ground and polished using Metlog Method E (Bjerregaard et al., 2000). An additional $3 \mu\text{m}$ step using a MD-Dac disc was also introduced. Prior to etching a final OPS polish was carried out for one minute, followed by etching in 2% nital, to reveal the microstructure present.

4.4: Optical Microscopy/ SEM

Optical microscopy (Akioskop 2 microscope) was used to examine the etched samples. A JEOL 7000 SEM with standard operating conditions of 20.0 kV, aperture of 3 and working distance of 10 mm was used to examine the microstructures at higher resolution.

SEM images, with a range of magnifications were used.

4.5: Image Analysis

4.5.1: Phase Analysis– Phase analysis was carried out to determine the microstructures present. The point counting method was used in accordance with ASTM Standards for the Standard Test Method for Determining Volume Fraction by Systematic Manual Point Count (International, 2016). A grid of 88 points was overlaid onto SEM images, which had magnifications ranging from $\times 2,000$ to $\times 5,000$, depending on the sample. Carbide orientation was used to distinguish between lower bainite and martensite, which was done manually; example images of lower bainite and martensite are shown in [Figure 59](#) where single direction aligned carbides can be observed in lower bainite whilst multiple carbide orientations can be observed in the auto-tempered and tempered martensite.

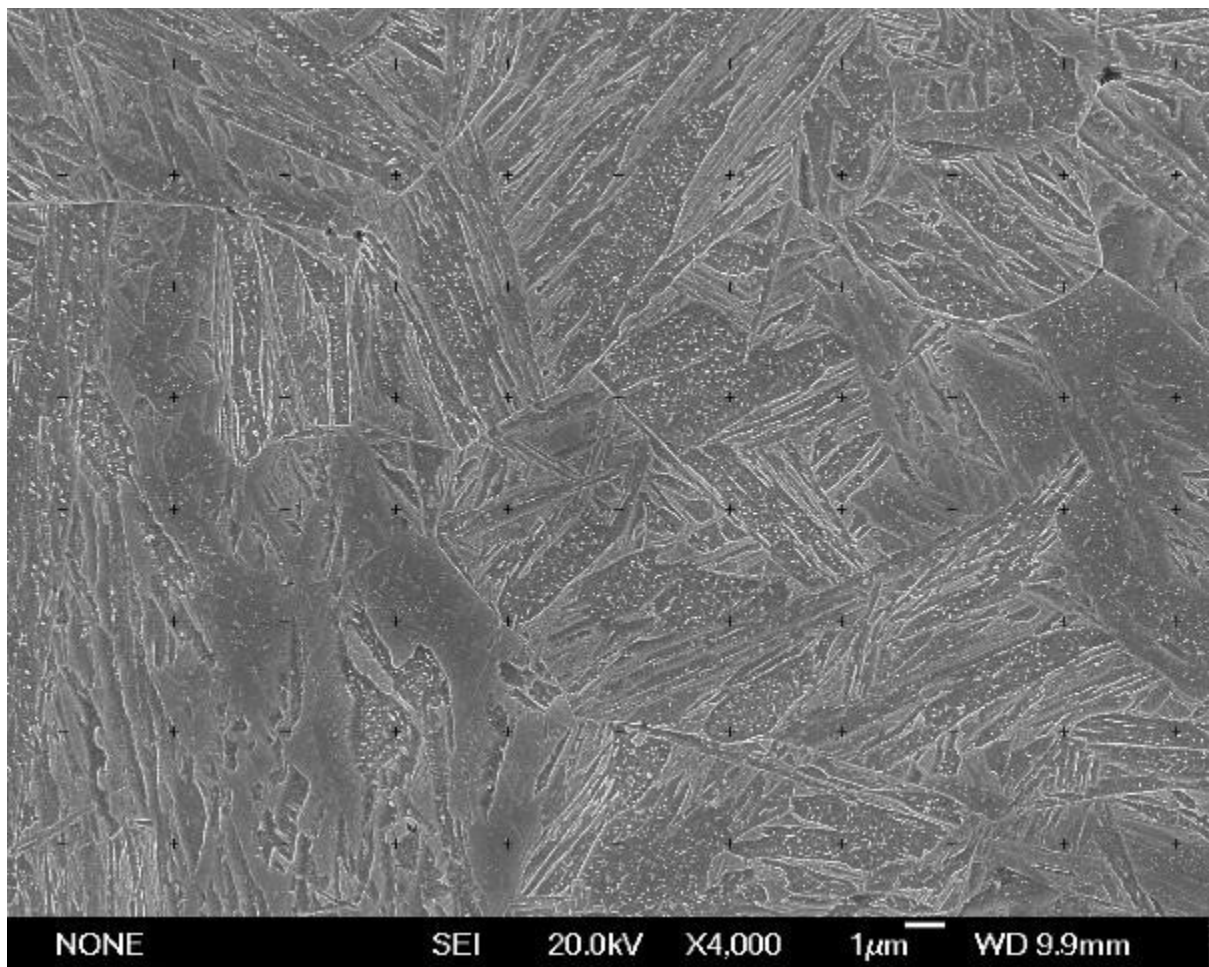


Figure 59 Example of mixed Martensitic and Lower Bainitic used for phase analysis with overlaid grid

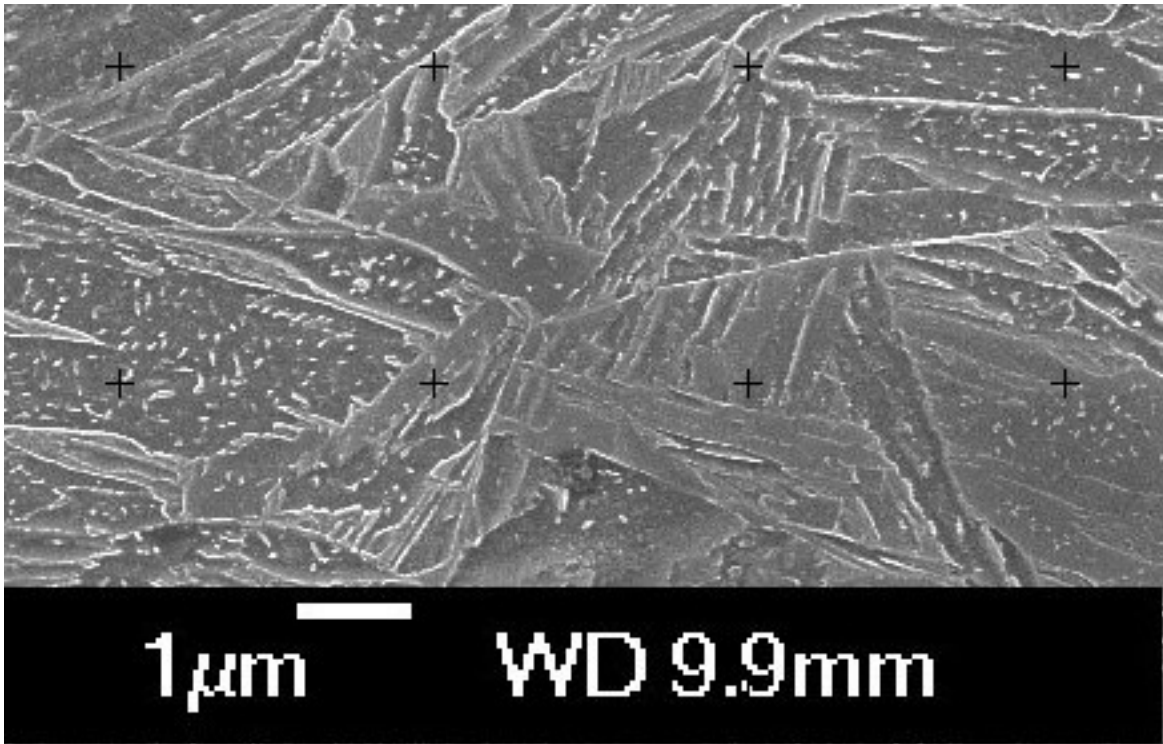


Figure 60 Example of mixed Martensitic and Lower Bainitic used for phase analysis with overlaid grid - Magnified so grid can be easily observed

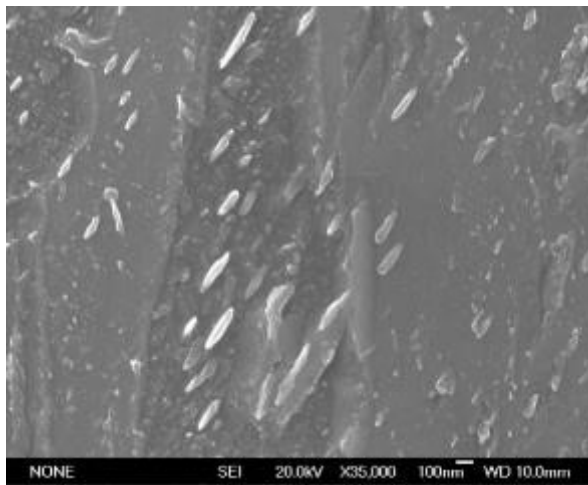


Figure 61 Lower Bainite

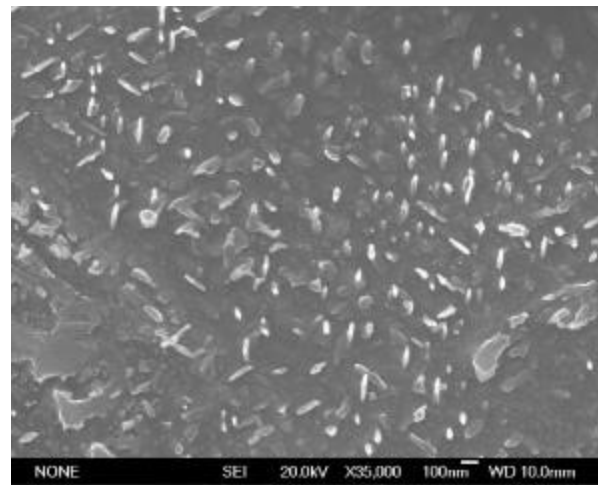


Figure 62 Martensite

4.5.2 Carbide Analysis– Carbide size was analysed using an AxioSkop 2 microscope fitted with AxioVision 4.6.3 image analysis software. Efforts were made to ensure that the brightness and contrast was sufficient when SEM images were taken to allow all carbides to be resolved. Where necessary optimisation was carried out using the AxioVision Programme Wizard; focusing on contrast and brightness.

Most of the carbides were automatically selected using the software, but carbides which were not detected were manually added. This was due to a number of reasons; carbides being too close together to be distinguished separately, less than optimum contrast or small carbides. At least 1000 carbides were measured using the software. Carbides under 10nm in size were then disregarded, as this is close to the resolution limit, then the feret min, feret max and aspect ratio were calculated. The resolution limit of the JEOL 7000 is 1.2nm @30kV in optimum use.

4.5.3 Lath Size Analysis–SEM images at $\times 5,000$ magnification were taken using the JEOL 7000. Image areas were analysed with ImageJ software. Images represented an area of around $24 \times 20 \mu\text{m}$. Lines were imposed on the image normal to the lath length and the intercepts and line length measured.

Some laths were measured more than once, to ensure accuracy the imposed lines were at least $0.7 \mu\text{m}$ apart. When averaged, more than 800 lath width measurements were taken per sample.

4.6: Hardness Testing

Vickers macro hardness (20kg load) was used to determine sample hardness. Indents were taken 3 mm away from the edge to avoid any decarburisation from the heat treatments. The number of indents was dependent on the size of the sample. 20 × 20 mm samples had 25 indents taken, while 10 × 10 mm samples had 9 indents. This was to ensure that the work hardened areas around the indents did not interact.

2 indents per dilatometry sample were used.

Errors were calculated for hardness values. An average human eye resolution of 0.1mm was used and multiplied by the × 2.5 objective lens.

4.7: Heat treatment

4.7.1: Furnace - Producing Martensitic Samples

Samples were re-austenised using an Elite Thermal Systems Limited furnace at 925 °C for one hour and quenched using water at room temperature. Previous work by Driscoll (Driscoll, 2014) suggested that room temperature water quenching is sufficient to generate martensite in these steels for the same sample dimensions used in this work and that auto-tempering occurs, both for room temperature water quenching and ice water quenching (Driscoll, 2014).

4.7.2: Gleeble - Producing Bainitic/Mixed Microstructure samples

A Gleeble 3500 thermo-mechanical simulator was used to heat treat samples with different isothermal holds (temperatures and times) following re-austenisation. Copper grips (27 mm apart to allow for the quench head) were used to hold samples (10×10×60 or 77 mm) in place; the Gleeble set up is shown in [Figure 63](#). K type thermocouples were spot welded to the midpoint of the sample (30 or 38.5 mm), and no more than 2 mm apart, this was the area later analysed.

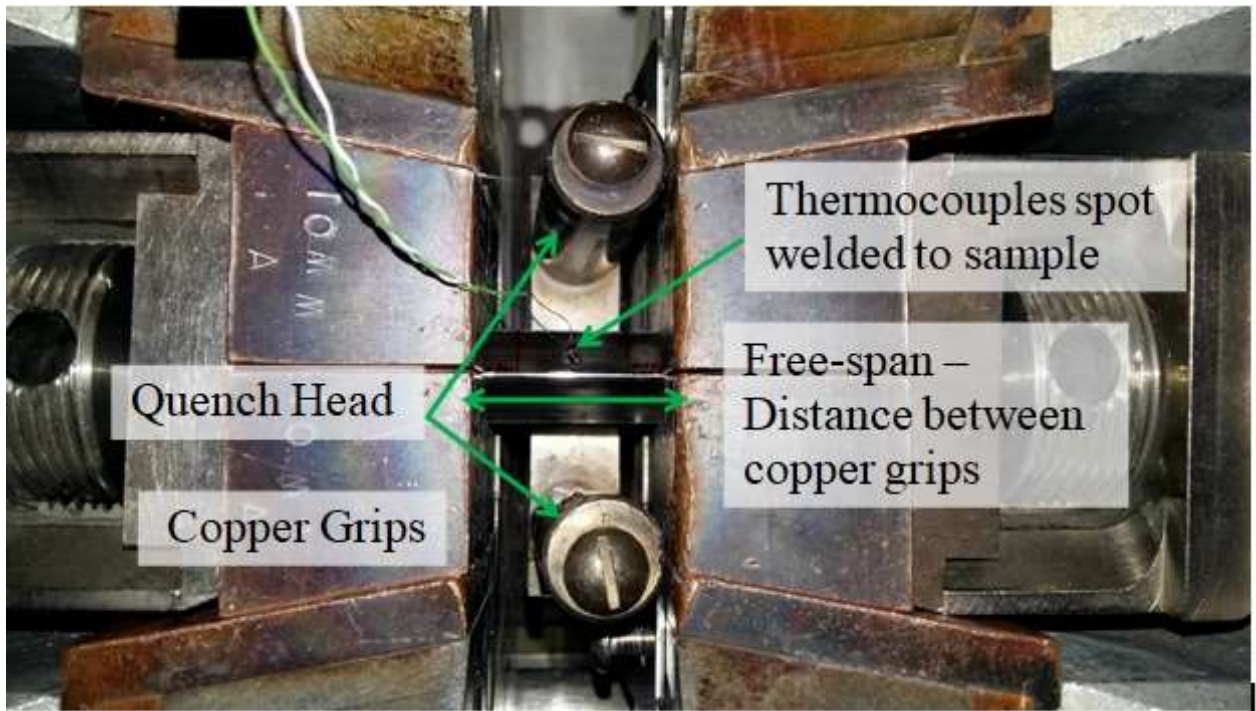


Figure 63 Gleeble set up, showing location of sample, copper grips, thermocouples and quench head

An example of a heating/cooling schedule is displayed in [Figure 65](#). Samples were heated to 925 °C and held for 1 minute, for austenisation. They were then cooled to 430 °C, at around 30 °C/s, this was sufficiently fast enough to avoid ferrite transformation. The sample was then held for a range of times (8, 13, 20 and 300 seconds) to form different fractions of lower bainite, with the aim of 25%, 50%, 75% and 100%. Dilatometry transformation curves provided by Tata Steel were used to determine time needed for the transformation completion. [Figure 64](#) shows the transformation of BaseMoV at 430 °C for 1 hour.



Figure 64 Dilatometry transformation of BaseMoV, with isothermal hold at 430 °C for 1 hour

These curves were then used to determine the time required for 25%, 50% and 75% lower bainite. Trials were carried out on the Gleeble and the final holding times adjusted according based on the determined microstructure and hardness of the sample. After the isothermal holding time the samples were cooled to room temperature, using an air quench to ensure the remaining untransformed austenite formed martensite.

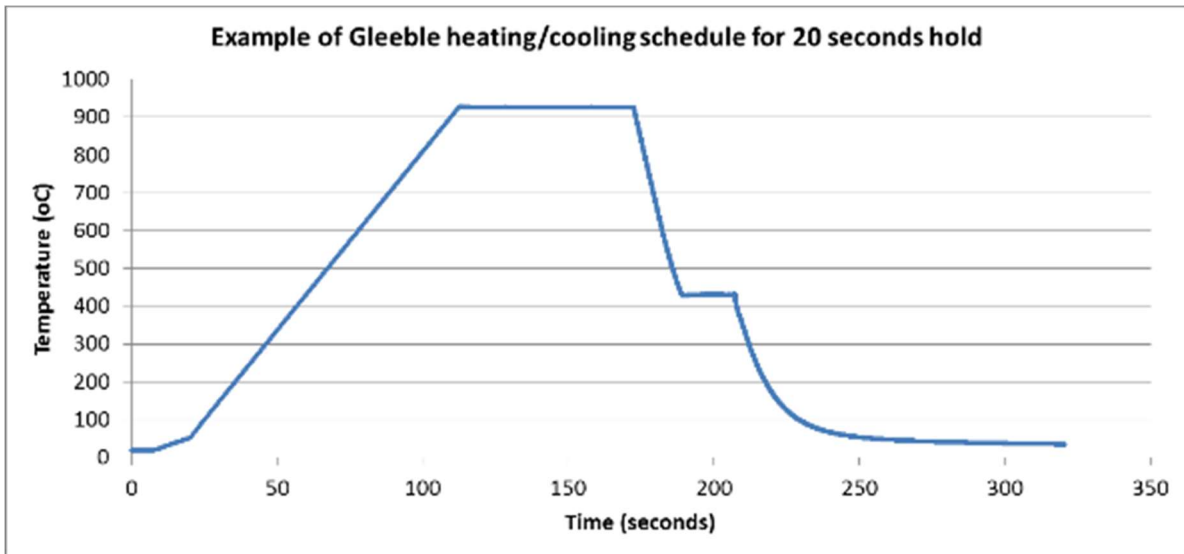


Figure 65 Gleeble heating/cooling schedule (thermocouple measurements) for re-austenisation, cooling to isothermal hold temperature for formation of lower bainite followed by forced air cool to form martensite

4.8: Dilatometry

4.8.1: Isothermal Holds

Samples were sent to Tata Steel STC for dilatometry testing on a Bahr Thermo Analyse instrument. Six tests were carried out, with samples heated to 925 °C in 1 minute 30 seconds followed by cooling to the specified holding temperature at the quickest rate possible (120 °C/s) to ensure that no ferritic phase would form, see [Table 13](#). The sample was held for the time stated before being cooled to room temperature.

Table 13 Dilatometry Isothermal Temperatures and Holding Times

Sample	Isothermal Holding Temperature	Holding Time	Predicted Martensitic Start Temperature (°C)
Base	430 °C	1 hour	422
Base	525 °C	1 hour	422
BaseMoV	430 °C	1 hour	420
BaseMoV	525 °C	1 hour	420
BaseSiCrMoV	430 °C	2 hours	405
BaseSiCrMoV	525 °C	1 hour	405

The temperatures chosen were based on being higher than the predicted martensitic start temperature (predicted using equation 2.2). This was then verified using Gleeble Tests, as disruption of isothermal holds produced a kink around 400 °C indicative of a martensitic temperature. Shorter isothermal holds produced a longer plateau indicative of more martensite being formed, see [Figure 66](#).

4.9: Gleeble Isothermal Hold

Lower bainitic microstructures were obtained from an isothermal hold, with martensite forming afterwards, during the quench to room temperature. Details of the hold time and microstructures obtained are detailed in [Table 14](#).

Dilatometry attachments have not been used on the Gleeble, due to the air quench and copper grips not allowing enough space for the dilatometry attachment.

Table 14 Details of holding times and microstructures obtained

Isothermal Hold Time (Seconds)	Martensite (%)	Lower Bainite (%)	Sample Identifier
8	70	30	70%Martensite: 30% Bainite
13	56	44	56% Martensite: 44%Bainite
20	30	70	30% Martensite: 70: Lower Bainite

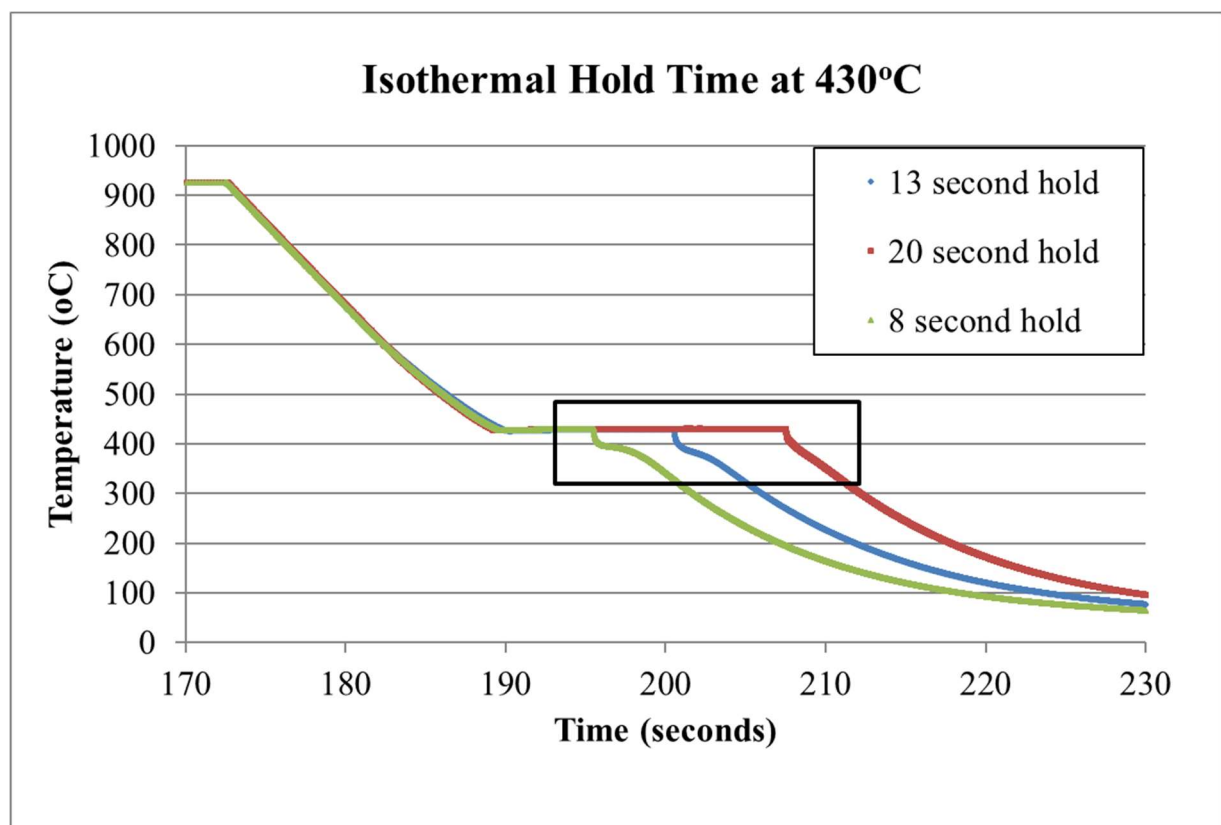


Figure 66 Isothermal hold at 430 °C showing martensitic start temperature

4.10: Predicted TTT Diagram

TTT curves predicted using Bhadeshia and Babu software (H. K. D. H. Bhadeshia & Babu) to predict an approximate Ms temperature and cooling times needed to avoid ferrite transformation on cooling, these are shown in section 6.1.2.

Holding temperatures related to upper and lower bainitic transformation temperatures were chosen so that different transformation rates could be determined. Holding times of 1 or 2 hours were used for the isothermal hold to ensure completion of the transformation based on the literature TTT curves.

4.11: Continuous Cooling

The same piece of equipment used for the isothermal holds was used to produce a continuous cooling curve for BaseMoV, shown in [Figure 67](#). The following cooling rates produced the hardness and microstructure present, [Table 15](#). The dilatometry instrument used to produce the CCT diagram had limited availability, therefore only one steel composition could be tested. The CCT diagram was constructed using transformation temperatures associated with change in gradient of the cooling curve, identified using dilatometry data.

Table 15 Cooling rates, hardness and microstructure of BaseMoV

Cooling Rate °C/s (800°C – 500 °C)	BaseMoV Vickers Hardness (20kgf)	BaseMoV - Microstructure
125	421.1	Martensite
71	420.8	Martensite
37	428.9	Martensite
21	419.9	Martensite
12	387.7	Martensite and Small Percentage of Bainite
6	347.5	Bainite and Small Percentage of Martensite
3.3	336.9	Bainite
1.6	303.8	Bainite and Small Percentage of Pearlite
0.8	282.6	Bainite and Small Percentage of Pearlite
0.4	263.2	Bainite, Pearlite and Ferrite
0.2	257.1	Bainite, Pearlite and Ferrite

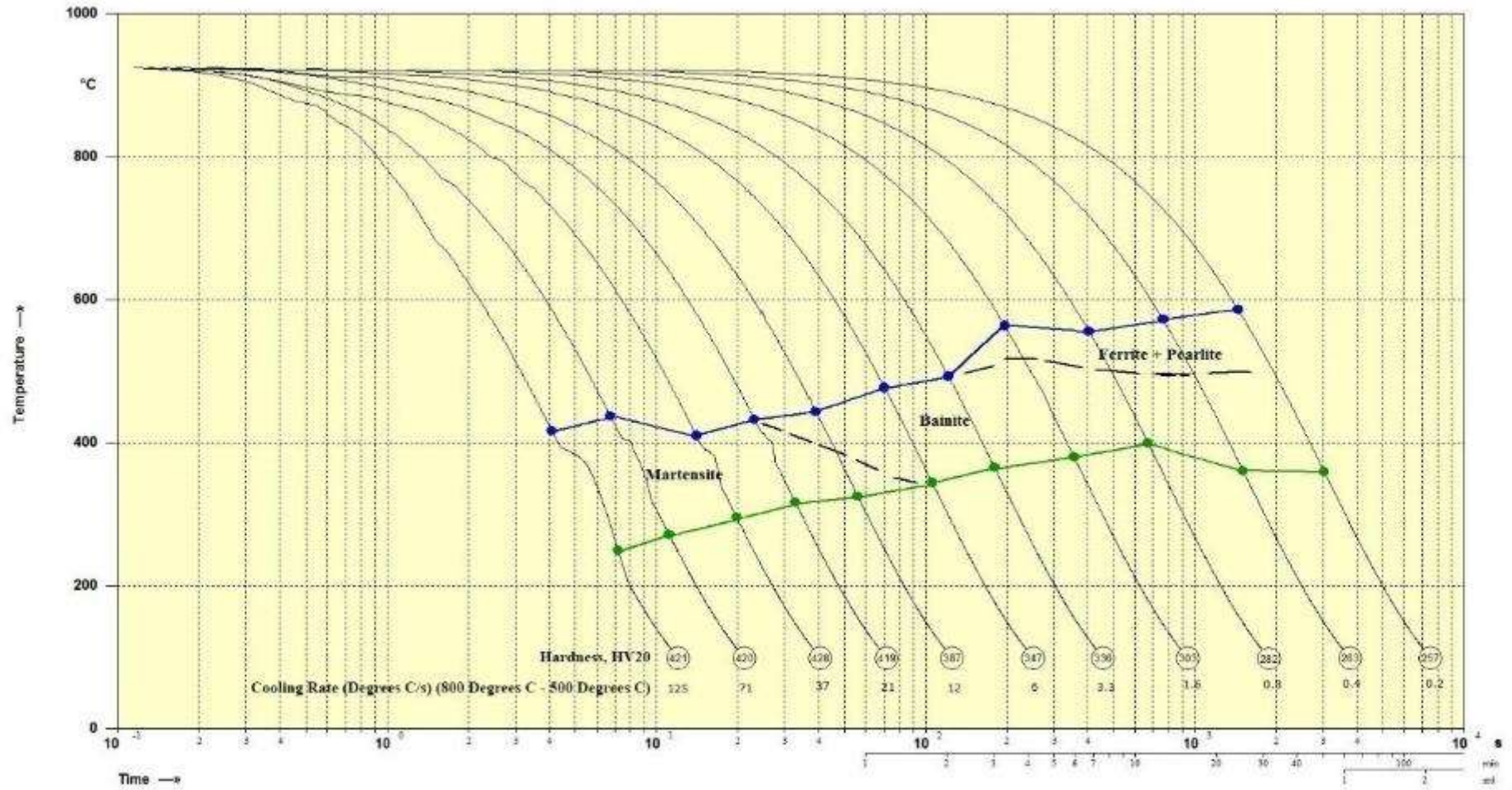


Figure 67 CCT diagram for BaseMoV

4.12: Tempering

Samples were tempered in Elite Thermal Systems Limited furnaces at 600 °C for a range of times varying between 30 minutes and 16 hours. 15 × 20 × 20 mm samples were heated for an additional 8 minutes, to allow the sample centre to reach the required temperature before the tempering time commenced, this time as determined using a thermocouple threaded into the sample at 925 °C. 10 × 10 × 66/77 mm samples were not given an extra heating time as the time needed to heat up was thought to be lower due to their smaller cross-sectional area. Once tempering was completed samples were water quenched.

4.13: Modelling

Thermal modelling was carried out to determine the effect of plate thickness on the cooling rate, and therefore the variation in as-quenched microstructure through thickness (for a given composition based on the material TTT curve). Thermo-Calc 4.0 was used to determine the material properties using the TCFE7: TCS Steels/Fe-alloys database, v7.

Averages from these were then used to in COMSOL 5. A 1D steel plate was modelled, looking at through thickness. Heat-transfer modules were used.

COMSOL is being FE-based software that provides numerical solutions to multi-physics problems, there are different modules which can be used depending on the situation, in this instant the heat transfer module has been used.

Data points were produced every 0.1 seconds for the cooling. Intervals of 5 seconds were used for the heating, due to the heating taking significantly more time than cooling.

4.13.1: Assumptions for cooling

- 1D=2D. Heating properties are uniform in 1D and 2D direction.
- No phase changes.
- Convection dominated boundaries (See [Figure 68](#)) – The material loses heat through the boundaries and the method of heat loss is convection from the steel.
- No inflow heat flux – The material only loses heat on cooling.
- Using Heat Transfer in Solids module in COMSOL
- Heat loss equal at both surfaces of the plate

4.13.2: Assumptions used for heating:

- 1D=2D
- No phase changes.
- Convection dominated boundaries (See [Figure 68](#)) – The material gains heat through the boundaries and the method of heat gain is convection through the samples.
- No outwards heat flux – This means that the sample does not lose heat during heating
- Using Heat Transfer in Solids module in COMSOL
- Equations are based on solution being time dependent

4.13.3: Details of Study in COMSOL for heating and cooling

The following COMSOL modules were used.

- Heat Transfer in Solid Used
 - Solid - This is where the thermal conductivity, density and heat capacity values are defined.
 - Initial Values – The initial temperature of the steel is input here
 - Thermal Insulation – Overridden, so no values needed to be input
 - Diffuse Surface – This is where the ambient temperature of the steel and surface emissivity are defined
 - Heat Flux - Convection Heat Flux (Material type non-solid) is defined here.
Heat transfer coefficient and external temperature are also defined.
- Mesh – Finer Size
- Study – The study is a Time Dependent Solver. The tolerance is Physic controlled.
- Average/Min/Max temperatures are plotted

4.13.4: Modelling: Cooling from 925 °C to room temperature

The following COMSOL parameters were chosen, see [Table 16](#), these are used to produce modelling graphs, showing the cooling of the plate, indicating the edge, centre and average temperatures on cooling. The figures shown in the thesis are for a 50 mm thick plate.

Sensitivity analysis was not carried out, as the parameters were based on Thermo-Calc, literature and experimental fit. This is something which could be improved in further work.

Table 16 Parameters used in COMSOL for cooling from 925 °C to room temperature

Parameter	Value
Ambient Temp	293.15 K
Thermal Conductivity◇(Metals, 1985; M. J. Peet et al., 2011; ToolBox, 2003)	43 W/ (m.K)
Density●	7750 kg/m ³
Heat Capacity at constant pressure *	925 J/ (kg. K)
Temperature of material (starting temp)	1198K
Surface Emissivity◇(ToolBox, 2003)	0.79
Heat Transfer Coefficient*	10,000 W/ (m ² . K)
External Temperature	293.15K

● Calculated from Thermo-Calc

◇ Value from literature

* Determining factor, fitted to match experimental data

4.13.5: 2D Study

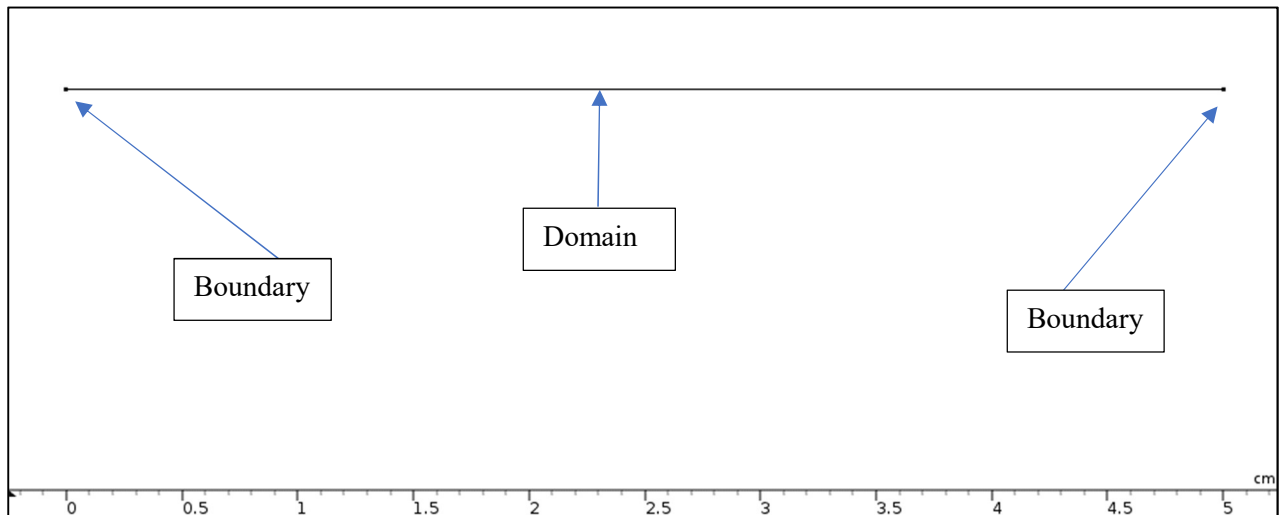


Figure 68 Showing the graph used for cooling

4.13.6: Modelling - Heating of steel from room temperature to 600 °C

Table 17 shows the parameters used by COMSOL for the heating of steel from room temperature to 600 °C. As the conditions of the simulation change to heating to 600 °C, the parameters involved are expected to change slightly. For instant the ambient temperature is now 873K (600 °C). The steps taken to obtain the parameters are outlined in Chapter 8.

Table 17 Parameters used for heating of room temperature to 600 °C

Parameter	Value
Ambient Temp	873 K
Thermal Conductivity●	43 W/ (m.K)
Density●	7750 kg/m ³
Heat Capacity at constant pressure◇	925 J/ (kg. K)
Temperature of material (starting temp)	273 K
Surface Emissivity◇	0.79
Heat Transfer Coefficient*	400(m ² . K)

4.13.7: XRD

XRD to determine retained austenite fraction was carried out at Warwick University using a PANalytical Empyrean XRD instrument. A cobalt target was used with a wavelength of 1.78901 Å, scan step size of 0.1313 degrees two theta, and a Gonio scan axis. Solid-state PiXcel detector with an active length of $\sim 3.2^\circ 2\theta$ is used. The lattice parameter (Å) of the martensite was determined by running a scan for 30 minutes between 28 - 128 θ , with a time per step of 58 seconds. As the martensite was determined to be auto-tempered the ferritic lattice parameter was expected. XRD peaks $(001)_\alpha$, $(002)_\alpha$, $(211)_\alpha$, and $(022)_\alpha$ were used to find $\cos^2\theta$ and the lattice parameter was extrapolated from the Y intercept, see [Figure 69](#).

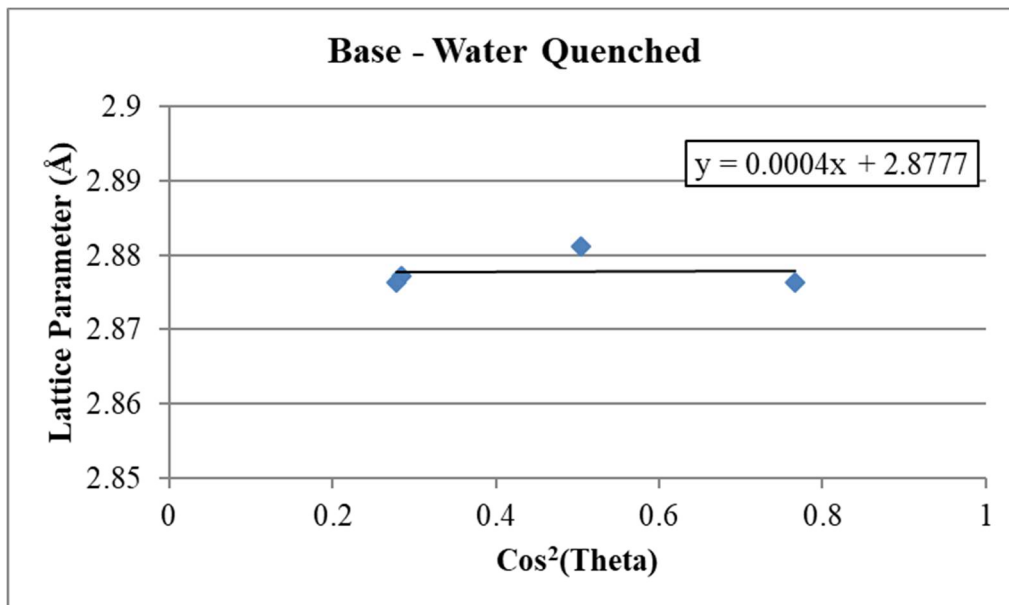


Figure 69 Example of how lattice parameter is determined

To determine if austenite is present in the samples a high-resolution scan was carried out over the angular range of 45-60 θ for 1 hour 15 minutes, with time deviation of 798 second per θ step.

Chapter 5: The Tempering of Martensitic Steel

This Chapter discusses the formation of martensite microstructures and the subsequent tempering between 30 minutes and 16 hours at 600 °C. A longer tempering time of 100 hours is also examined. Three compositions are studied, Base, BaseMoV and BaseSiCrMoV, full compositions are detailed in Chapter 4. Martensitic microstructures were developed by normalising at 925 °C for 1 hour, followed by water quenching. Sample sizes were 15 × 20 × 20 mm.

5.1: Normalised and Quenched Microstructure (Martensite)

The microstructures of the three as-quenched and tempered steels have been investigated to rationalise the variation in hardness during tempering. The as-quenched microstructures for the three different steels are shown in [Figure 70](#)- [Figure 75](#). Auto-tempering is evident in all three steel compositions studied, as fine scale carbides are found in the martensitic laths; these are distinguished more readily in the higher magnification images. Lath martensite is expected in a 0.17 wt. % carbon content steel, based on previous reports for plain carbon steels (Speich and Leslie 1972) (Grange et al., 1977).

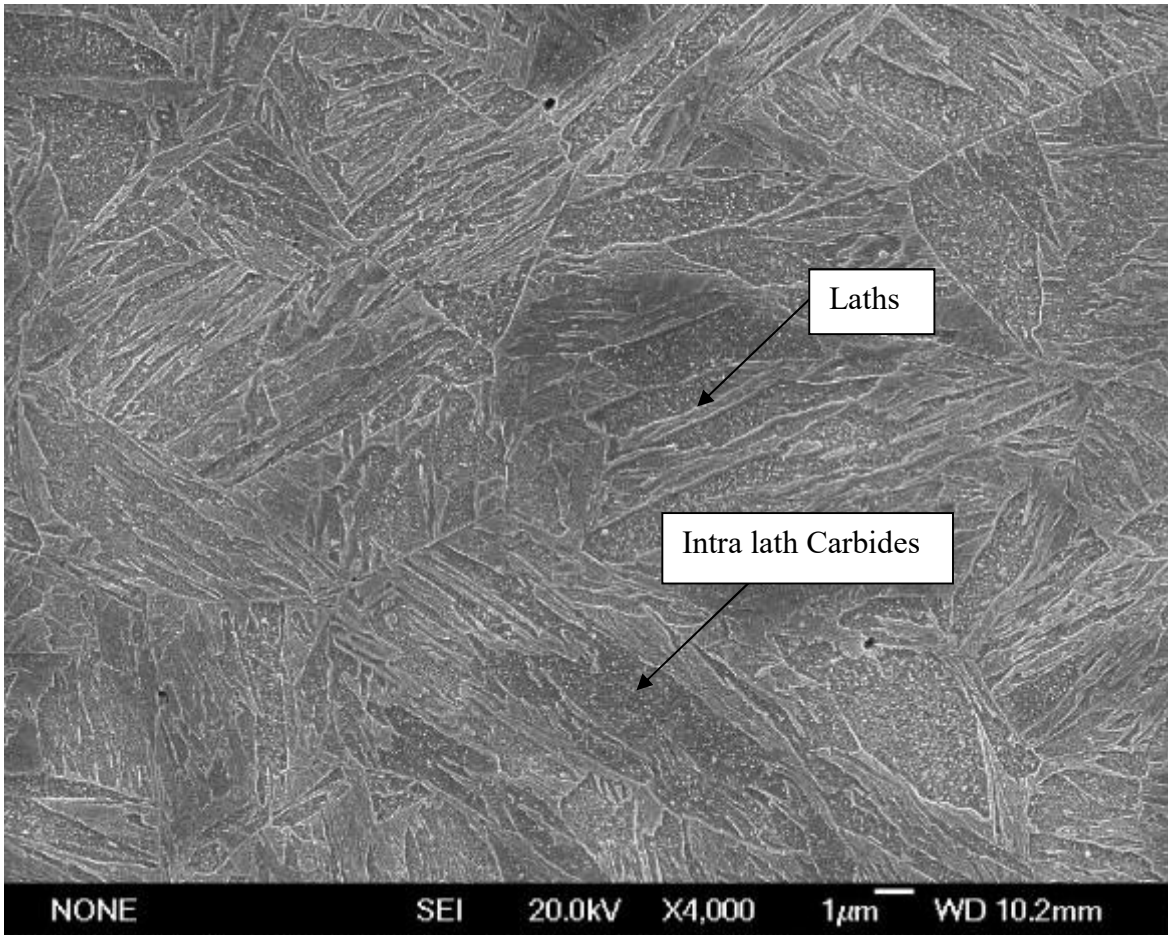


Figure 70 SEM of as-quenched Base steel showing a lath martensite structure with auto-tempered (intra-lath) carbides, ×4,000 magnification. (457.9 ± 29.8 HV)

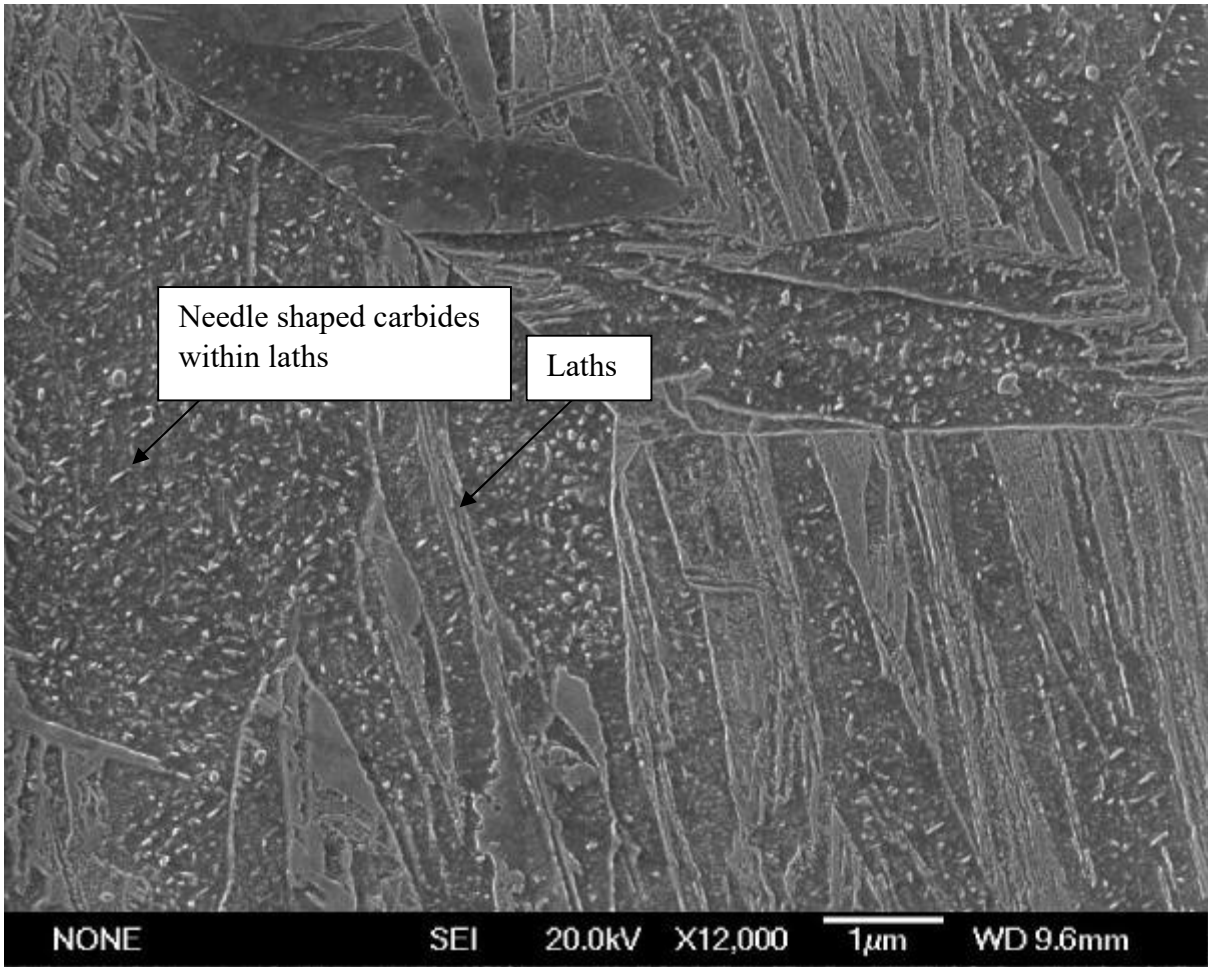


Figure 71 SEM of as-quenched Base steel showing a lath martensite structure with auto-tempered (intra-lath) carbides. (Higher magnification – $\times 12,000$) (457.9 ± 29.8 HV)

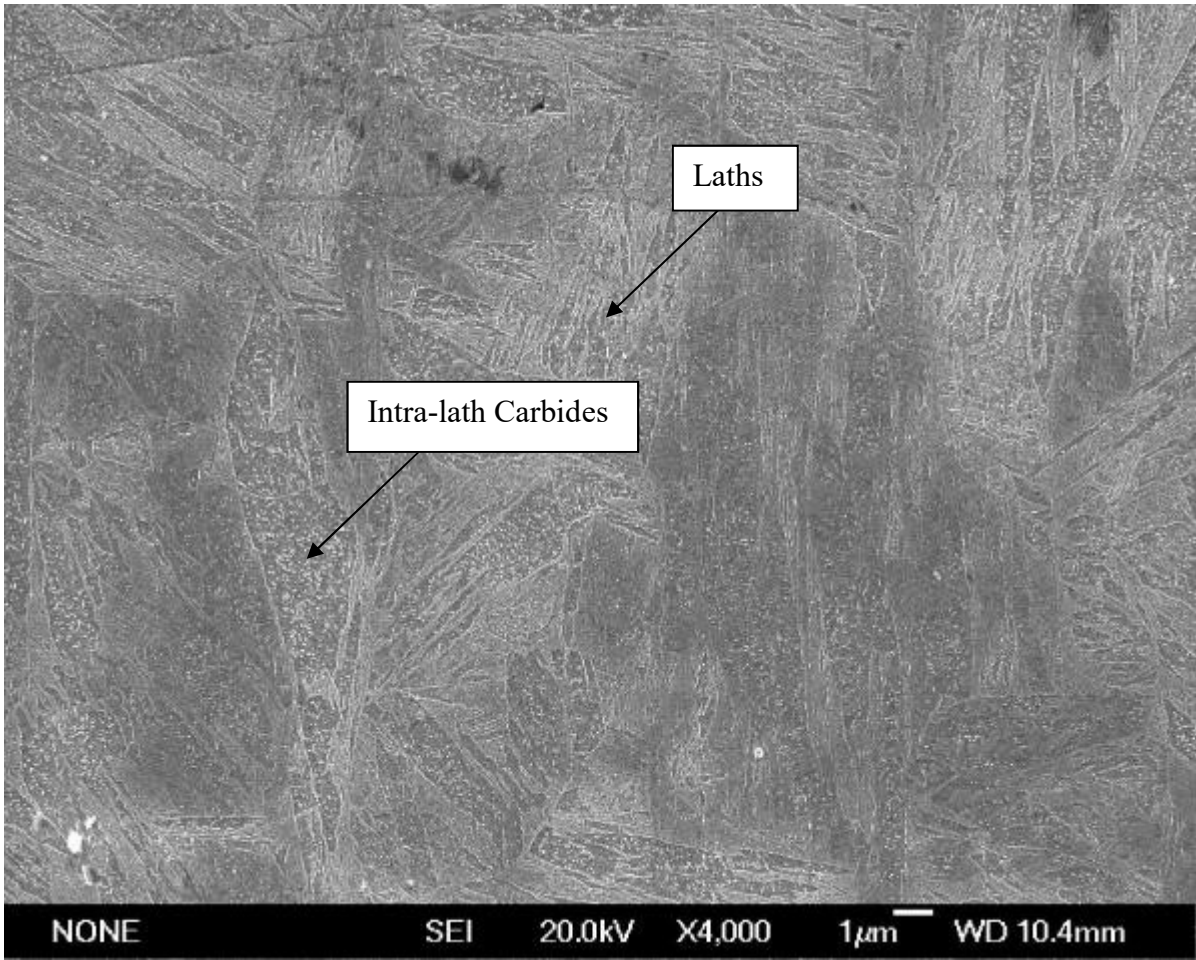


Figure 72 SEM of as-quenched BaseMoV steel showing a lath martensite structure with auto-tempered (intra-lath) carbides, ×4,000 Magnification. (453.7 ± 26.9 HV)

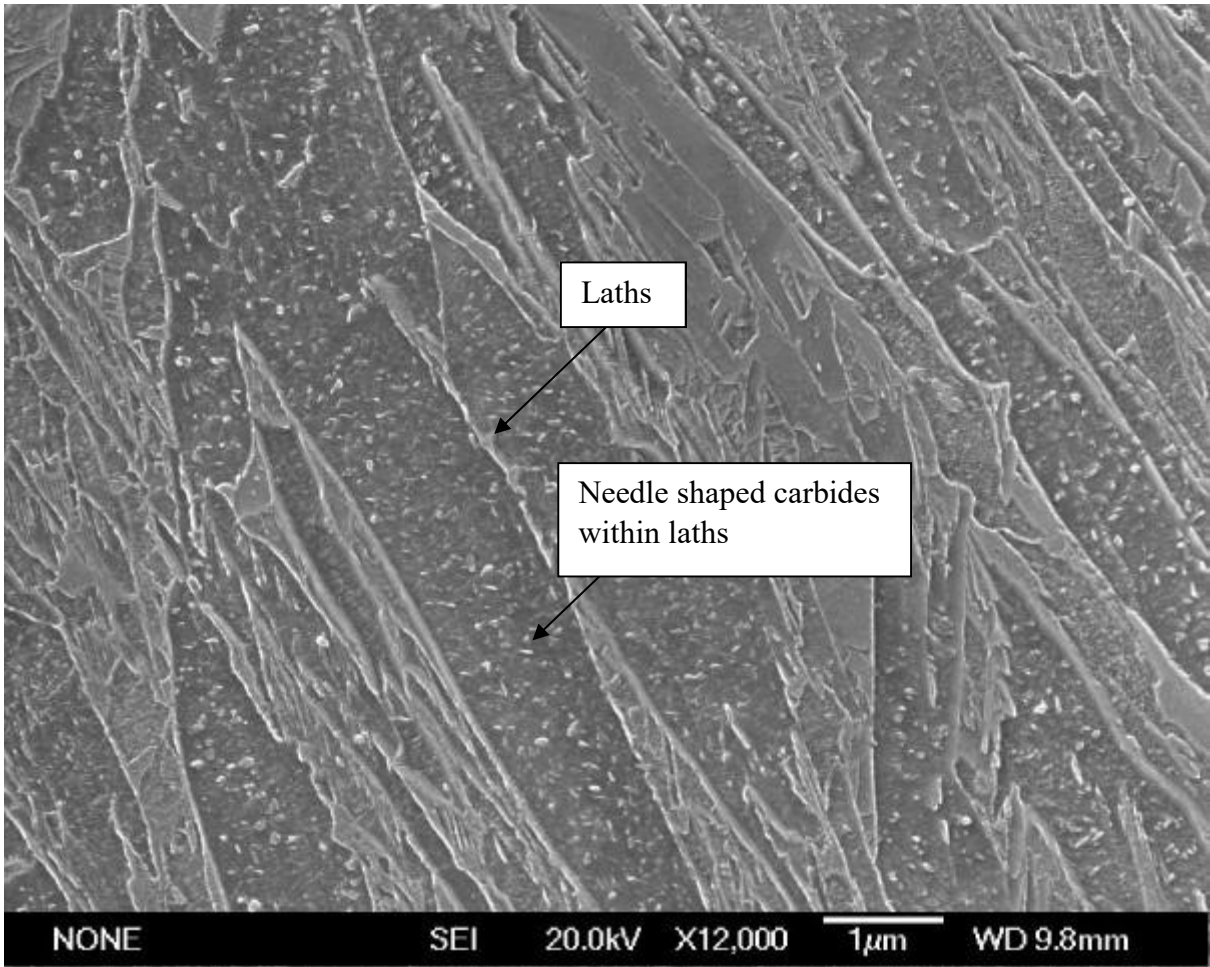


Figure 73 SEM of as-quenched BaseMoV steel showing a lath martensite structure with auto-tempered (intra-lath) carbides. (Higher magnification - $\times 12,000$) (453.7 ± 26.9 HV)

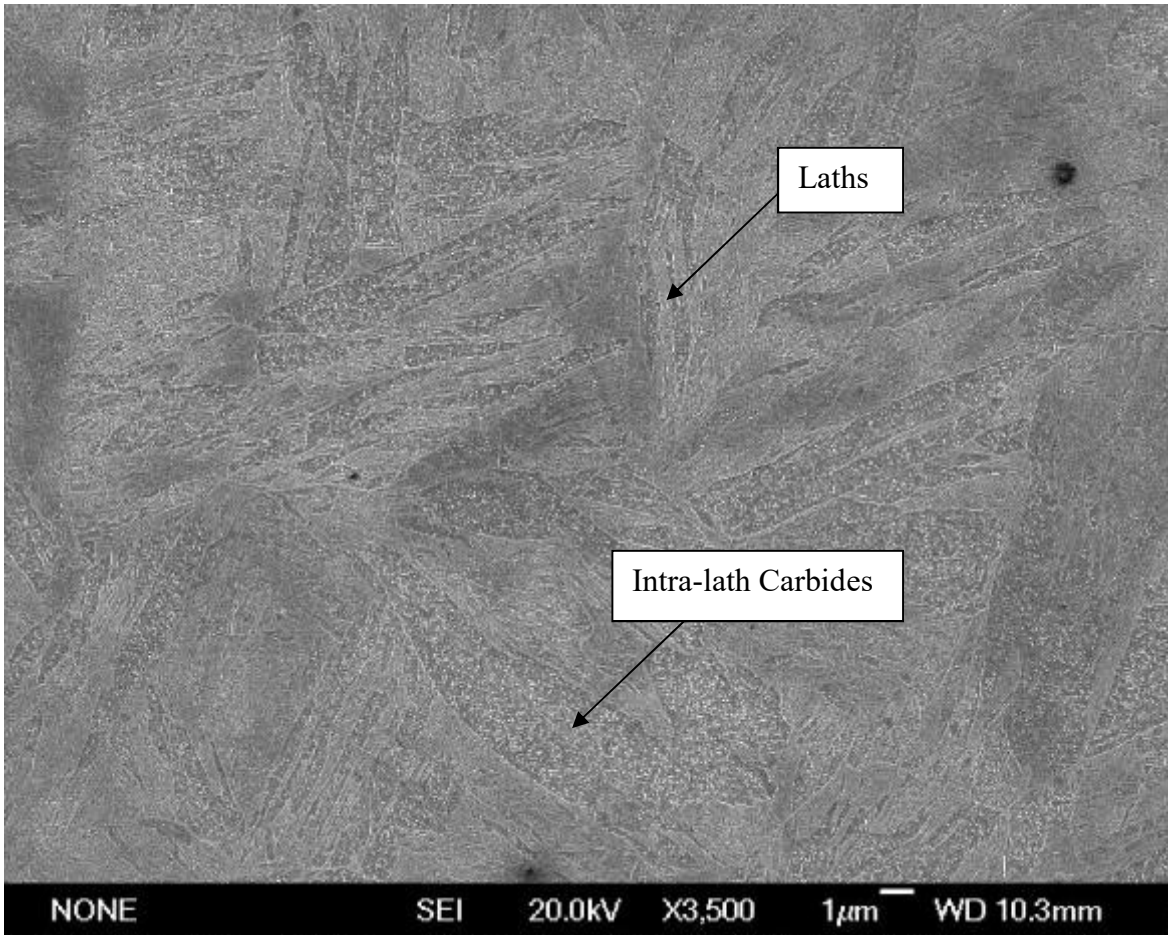


Figure 74 SEM of as-quenched BaseSiCrMoV steel showing a lath martensite structure with auto-tempered (intra-lath) carbides. (470.6 ± 30.7 HV)

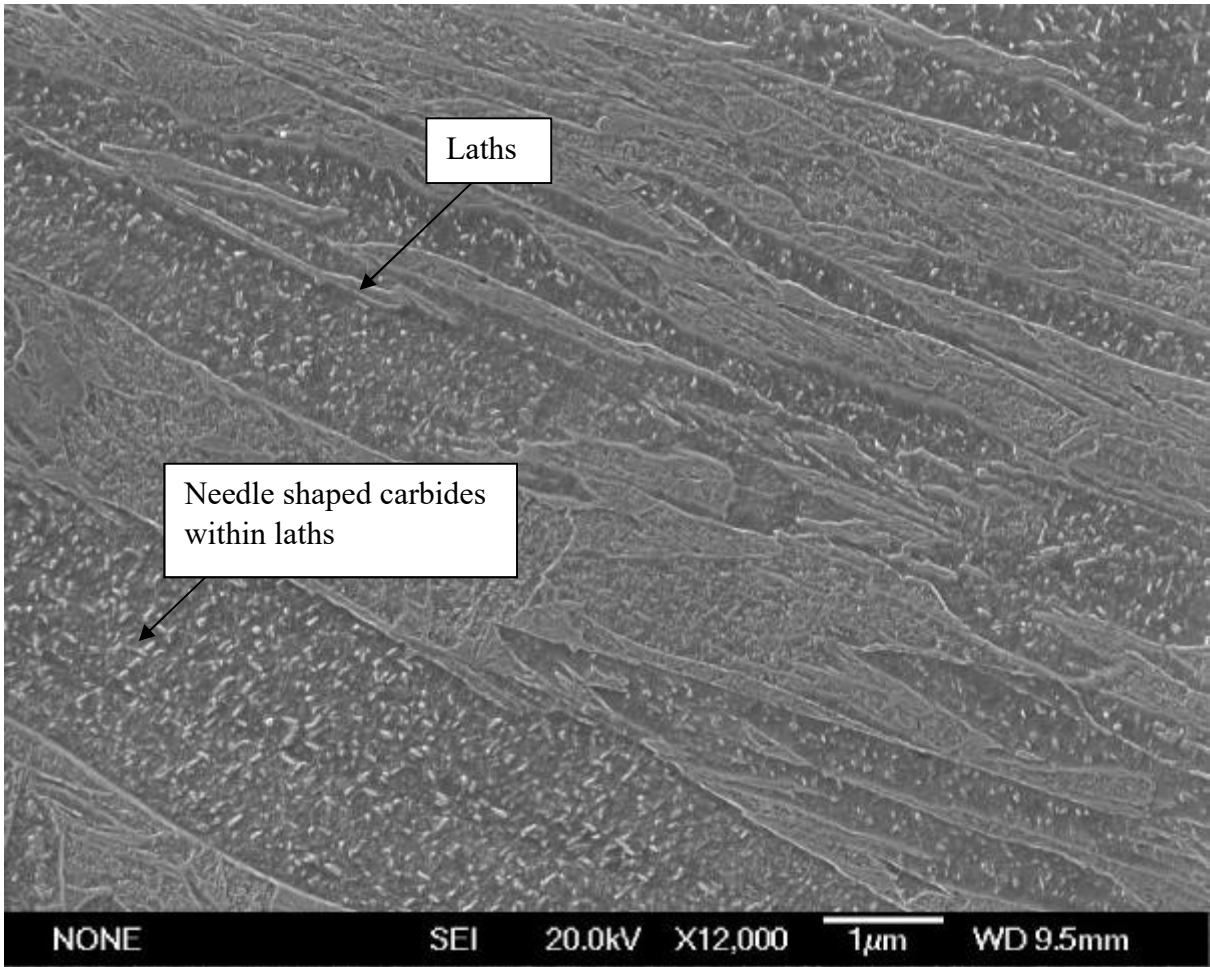


Figure 75 SEM of as-quenched BaseSiCrMoV steel showing a lath martensite structure with auto-tempered (intra-lath) carbides. (Higher magnification) (470.6 ± 30.7 HV)

5.1.1: Auto-tempering - Quantification

The amount of auto-tempering has been quantified, using point counting, section 4.5, image analysis and the results summarised in [Figure 76](#). The lath areas have been compared with representative individual microstructural features distinguished and labelled in [Figure 77](#). Point counting methods have been used to quantify regions that are (i) laths containing carbides in multiple orientations (taken to be auto-tempered martensite), (ii) laths with carbides in a single orientation (which may be lower bainite), and (iii) laths with no resolvable carbides (which may indicate that auto-tempering has not taken place).

To enhance the contrast of the carbides with the martensitic background, etching in 2 % nital has been applied, which has resulted in broadening of lath boundaries so that a number of points fall on boundaries. These points have not been used in quantification of auto-tempering. Of all the points measured, less than 10% of them contained carbides in the same orientation within a lath; this is for all the compositions, which are expected to be martensite, due to the rapid quenching, but there is the potential that there is a small percentage of lower bainite in this steel, however it shall be referred to as fully martensitic. Another reason for the single orientation carbides is that some lath orientations would not readily show multiple carbide orientations, along with the potential for carbides being lost on etching. For the remaining laths, the ratio of those exhibiting multiple-oriented carbides to those that are apparently carbide-free is about 50:50 for the BaseSiCrMoV steel and 60:40 to 67:33 for the other two steels. Martensite laths form over a range of temperatures between M_s and M_f . This results in differing amounts of auto tempering; the increasing narrowness of laths formed at the lower formation temperatures would make carbide identification with SEM more difficult. It is expected that the degree of auto-tempering would follow trends in M_s and M_f temperatures.

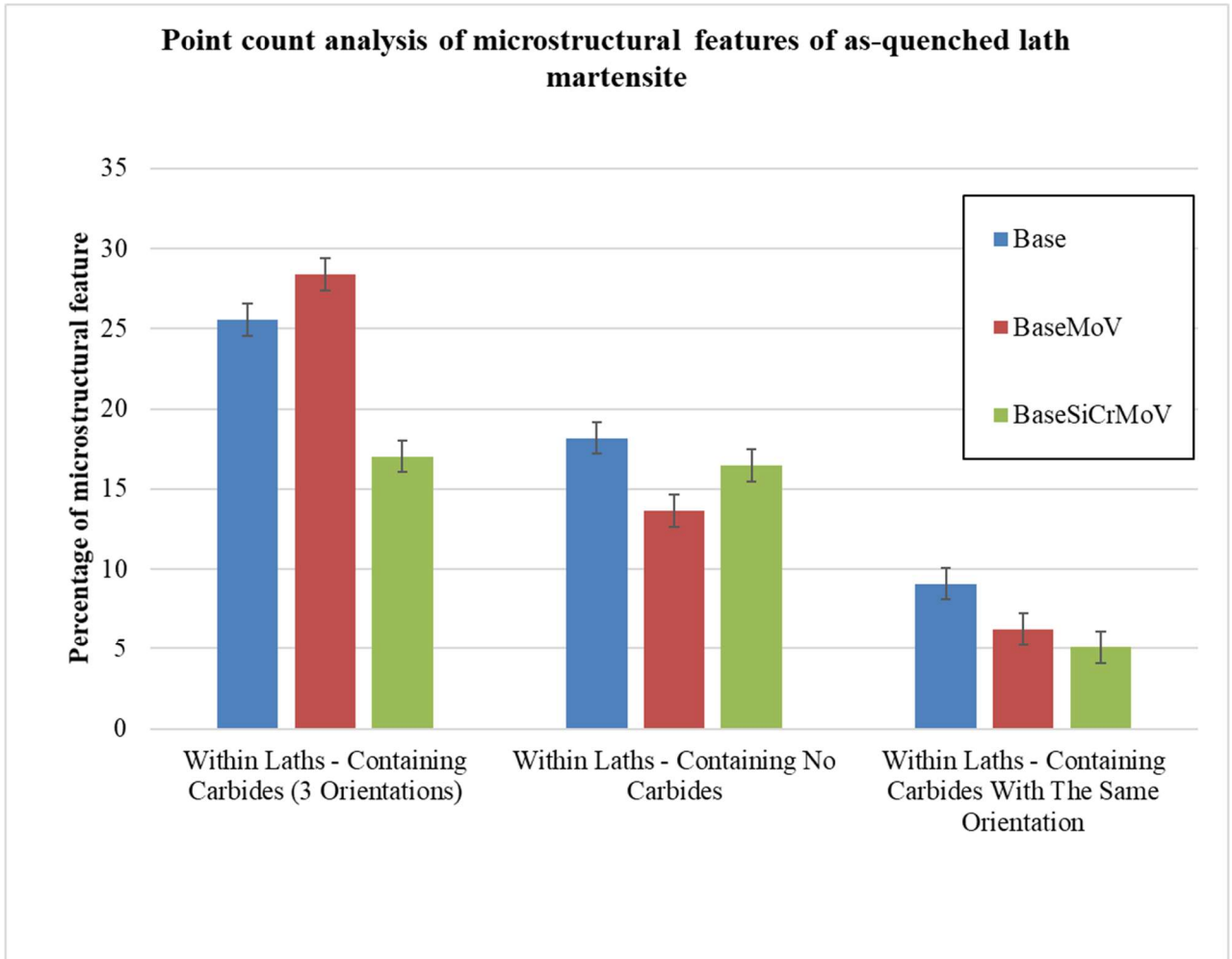


Figure 76 Point count analysis of microstructural features of as-quenched lath martensite

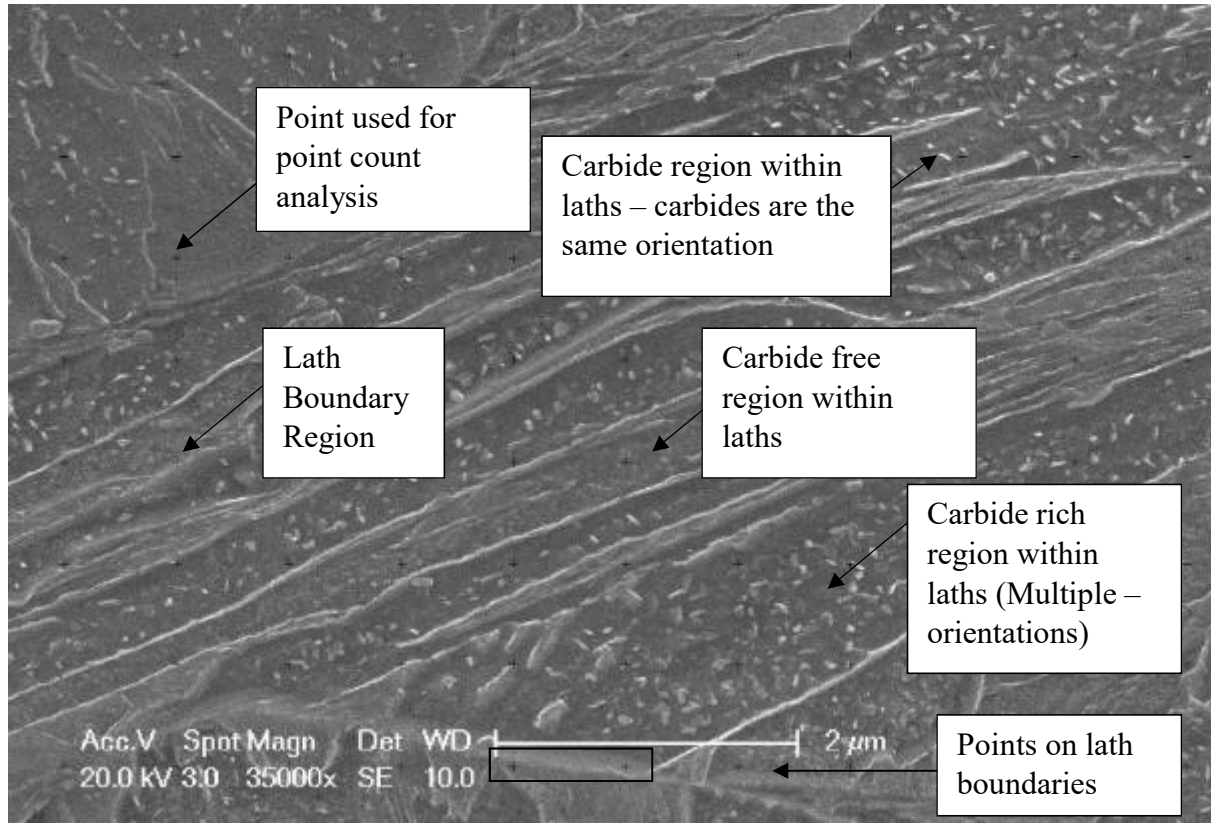


Figure 77 BaseMoV - Example micrograph showing difference features identified

5.1.2: Martensitic Start Temperature

Using the Totten and Howes equation, equation 2.2 (Totten & Howes, 1997), martensite start temperatures for these steels are predicted to be in the range 406 – 427 °C, Table 18. M_f is predicted to be 200 °C below M_s , and therefore austenite is expected to be fully transformed to martensite at room temperature.

Table 18 Predicted M_s temperatures for the three steels studied (predicted from Totten and Howes equation (Equation 2.2)(Totten & Howes, 1997))

Composition	Predicted M_s Temp
Base	427 °C
BaseMoV	423 °C
BaseSiCrMoV	406 °C

The Ms temperature which is predicted is relatively high, this means that auto-tempering would be expected during quenching, at least for the initially-formed laths. The composition of BaseMoV is very similar to that of the steel in previous work, identified in the as-quenched condition as auto-tempered martensite (Driscoll, 2014). BaseSiCrMoV is expected to start martensite formation at a lower temperature than the other two compositions (406 °C compared to 423 °C and 427 °C) and therefore marginally less auto-tempering is expected, consistent with [Figure 76](#), where BaseSiCrMoV has a lower fraction of laths with carbides present. Work by Ju, 2018 has found that the as-quenched carbide types for all three compositions are cementite and epsilon carbide. As-quenched Base and BaseMoV steels can be seen to have similar amounts of epsilon carbide and cementite, while BaseSiCrMoV has significantly more epsilon carbide and less cementite, [Table 19](#). This indicates that there is less auto-tempering for BaseSiCrMoV, consistent with its lower Ms that gives less time for C diffusion during quenching. The difference in carbide types may contribute to an apparently reduced auto-tempering extent in BaseSiCrMoV, as the smaller epsilon carbides would be less readily identified using SEM. Sizes have not been accurately determined in this study as they are less than 100 nm when imaged using TEM (Ju, 2018). However, the reduced auto-tempering response in BaseSiCrMoV is further evidenced by complementary XRD studies, discussed later in this section, where the amount of carbon left in solid solution in BaseSiCrMoV is ~15% more than Base and BaseMoV amounts, this matches with results in [Figure 76](#), which finds ~10% fewer laths containing carbides.

Table 19 Percentage of cementite and epsilon carbide in the as-quenched condition for the three steels studied (Ju, 2018)

	Epsilon Carbide (%)	Cementite (%)
Base	10±5	90±5
BaseMoV	15±5	85±5
BaseSiCrMoV	65±5	35±5

Literature reports (H. K. D. H. Bhadeshia & Edmonds, 1979; Chang, 1984; Delagnes et al., 2005; R. A. Mesquita et al., 2011) indicate that silicon in solution retards the formation and coarsening of cementite; it is therefore expected to slow down auto-tempering processes involving the formation of cementite. Chang discusses how a layer of Si enrichment in the iron, rejected from a cementite particle, forms at the interface which slows down diffusion of carbon, through the silicon rich iron compared to an iron matrix. There is experimental evidence that silicon can increase the formation rate of epsilon-carbide (Jang et al., 2010). This is not shown in this work because it would reduce the amount of carbon in solid solution for BaseSiCrMoV. However, as silicon reduces the transformation rate from epsilon carbide to cementite, it helps explain why there is more epsilon carbide in BaseSiCrMoV compared to the other two conditions. The difference ratio of epsilon carbide to cementite may be due to the much higher Si content in BaseSiCrMoV (1.24 wt. %) compared with Base (0.29 wt. %) and BaseMoV (0.28 wt. %).

5.1.3: Lattice Parameter

The lattice parameters of the three steels, determined from X-ray diffraction data, are given in Table 20, from the results there is little difference (0.001 Å) between the values. The XRD data used for this have a step size between readings of 0.01 θ and a resolution of 0.026°, resulting in a conservative error of ± 0.001 Å. This also agrees with user repeatability errors when XRD peak identification is carried out to determine the lattice parameter. The XRD data were used to estimate the C concentration still in solid solution. The equation was determined at room temperature using discs of solid material, not powders. This equation solely considers alloying elements. (H. K. D. H. Bhadeshia et al., 1991);

$$a_{BCC} = 0.28664 + (3a_{Fe}^2)^{-1} \times [(a_{Fe} - 0.0279x_C^\alpha)^2(a_{Fe} + 0.249x_C^\alpha) - a_{Fe}^3] - 0.003x_{Si}^\alpha \\ + 0.006x_{Mn}^\alpha + 0.007x_{Ni}^\alpha + 0.031x_{Mo}^\alpha + 0.005x_{Cr}^\alpha + 0.0096x_V^\alpha \dots$$

Equation 5.1

a_{BCC} is the measured lattice parameters.

a_{Fe} is the lattice parameters of pure ferrite (0.28664nm) (Bureau, 1955)

x_i^α represents the mole fraction of the species i in the matrix

a_{BCC} is in nm.

The resulting values are summarised in Table 20, which also includes the Thermo-Calc predicted equilibrium carbon content for BCC and cementite. This indicates that BaseSiCrMoV has retained more C in solution in the as-quenched state (compared to Base and BaseMoV), in agreement with quantification of the degree of auto-tempering from SEM images, Figure 76 and Figure 77.

Table 20 Lattice parameter estimated and predicted carbon contents of the three steels

Sample	Lattice Parameter (Å) *	Retained carbon content in matrix (%)	Predicted C in BCC phases. Thermo-Calc only allowing BCC + Cementite **	Predicted C in Cementite phases. Thermo-Calc only allowing BCC + Cementite**
Base	2.8702	0.108	0.0187	0.1631
BaseMoV	2.8712	0.109	0.0197	0.1614
BaseSiCrMoV	2.8717	0.130	0.0171	0.1651

* ± 0.001 Å – Based on experimental uncertainty

**Mass Fraction \times Volume Fraction

Lattice parameter data were also used in conjunction with change in volume, to determine the amount of plastic strain induced by the martensitic transformation, [Table 21](#). As discussed in section 2.2.1 of the literature review, the formation of martensite involves a phase change from FCC to BCT, due to super saturated carbon in solid solution distorting the crystal structure, contributing to martensitic strength.

The strain was calculated using the $\Delta L/L_0$ values from the Gleeble data. The thermal expansion coefficient for BaseMoV was found to be $14.13 \mu\text{m}/^\circ\text{C}/\text{m}$, between room temperature and 600°C , using the Gleeble thermal expansion data. The Gleeble stroke has been used to calculate the change in length. This has then been converted to volume, using equation 2.6 in section 2.9. The thermal expansion coefficient was used along with the martensitic start temperature to calculate the expansion associated with the martensite transformation and any associated strain. It is these values that are summarised in [Table 21](#).

The similarity of the strain in all three steels indicates that there will be a similar contribution to strengthening from any transformation-induced strain (excess dislocation density for this displacive transformation) for the as-quenched condition. The accuracy of the change in volume and associated strain is not to be relied on completely. The trend it shows is useful, as it finds there is no significant difference in strain.

Table 21 Predicted strain in the three steels

Sample	L_0 – Original Volume (μm^3)	ΔL – Change in Volume (μm^3)	Strain $\Delta L/L_0$
Base	23.640	0.331	0.014
BaseMoV	23.665	0.333	0.014
BaseSiCrMoV	23.665	0.333	0.014

5.1.4: Grain Size

The grain size has been examined for all three steel compositions, results summarised in [Table 22](#). Optical images were taken, and grains identified using ImageJ software. There is no significant difference in the average prior austenite grain sizes (PAGSs) between the three steels, as expected as they were all processed to the same conditions. The similar prior austenite grain size will therefore not affect the martensite start temperature or be expected to contribute to any difference in hardness, which will be controlled by other microstructural features (lath size, carbide size / number density, solid solution strengthening, etc). Literature reports (section 2.7.3.) indicate that Mo can have a refining effect on prior austenite grain size, due to small Mo_2C carbides pinning the grain boundaries, and that similar additions of Mo (0.47 wt. % in the literature compared to 0.5 wt. % in BaseMoV and BaseSiCrMoV) can alter the grain size by 20 μm for similar heat treatments (reducing from 70 to 50 μm diameter); 1 hour at 950 °C in the literature compared to 1 hour at 925 °C used in this study (Shorowordi & Ali Bepari, 2002). The literature values are for larger grain sizes than those shown in this steel; this may explain why a larger grain refinement was found in the literature but is not evident in this steel with a finer grain size; or pinning particles may not be present. Thermo-Calc simulations do not predict the presence of M_2C carbides at 925 °C, therefore the similarity of PAGS is logical for Base and alloyed steels. [Table 23](#) shows that all three compositions are expected to have cementite at 925 °C. Cementite should form (as seen in oil quenched and air cooled samples). Water quenching will give martensite when epsilon

carbide forms. Ti and Nb precipitates are predicted, with Base and BaseMoV having the same precipitates predicted (i.e. Ti(CN) and Nb(CTi)) along with BaseSiCrMoV predicting TiN and NbC. The volume fractions of the Base and BaseMoV precipitates are similar, while BaseSiCrMoV is predicted to have more NbC precipitates and more TiN precipitates. BaseMoV and BaseSiCrMoV should have some alloy carbides at equilibrium, but are not kinetically favoured. All of the PAGB will experience pinning, however as the same PAGB has been determined the difference is not significant after normalisation. The Ti-rich carbonitrides will not provide much pinning so that the PAG size will be fixed by the re-austenitising temperature, not by the composition.

Table 22 Grain Size

Composition	Equivalent Circle Diameter (μm) \pm Standard Deviation
Base	16 \pm 4.3
BaseMoV	17 \pm 3.2
BaseSiCrMoV	18 \pm 4.3

Table 23 Predicted precipitates present at 925 °C, including volume fraction. Predicted using Thermo-Calc

	Precipitates present at 925 °C (Volume Fraction)
Base	Cementite (2.8285E-04), Nb(CTi) (4.0921E-04), Ti(CN) (3.6633E-04).
BaseMoV	Cementite (2.8095E-04), Nb(CTi) (4.3819E-04), Ti(CN) (3.8683E-04).
BaseSiCrMoV	Cementite (3.0554E-04), NbC (3.8247E-04), TiN (4.6807E-04).

5.1.5: Laths

Lath widths in all three as-water quenched steel samples were measured to determine if there were any significant differences, which could influence hardness. The size distributions are shown in [Figure 77](#) and the average lath width values are $0.31\text{-}0.40 \pm 0.3 \mu\text{m}$ for the Base and BaseMoV steels and $0.41 - 0.50 \pm 0.3 \mu\text{m}$ for the BaseSiCrMoV steel. Base has a lath width distribution between $0.11 - 0.80 \mu\text{m}$, and BaseMoV between $0.11 - 0.60 \mu\text{m}$ compared to BaseSiCrMoV $0.11 - 1.30\mu\text{m}$. The differences in average values are not significant, however the BaseSiCrMoV steel does show a wider range of lath widths (shown in [Table 24](#)). There is not expected to be any difference between the lath sizes, the three steels have the same carbon composition in the bulk, and are therefore expected to have the same initial lath sizes (Galindo-Nava & Rivera-Díaz-del-Castillo, 2015). The three compositions studied undergo auto-tempering, after the laths have formed. Base undergoes the most auto-tempering and BaseSiCrMoV the least due to the higher and lower Ms temperatures respectively. This means that laths have the most opportunity to coarsen. Based on this it would be expected that Base and BaseMoV would have a wider lath size than BaseSiCrMoV. BaseSiCrMoV has Si which retards the formation of cementite which results in smaller carbides within the matrix. This may not act as an effective pinning of laths, compared to Base and BaseMoV and would result in a wider lath distribution for BaseSiCrMoV in the as quenched condition.

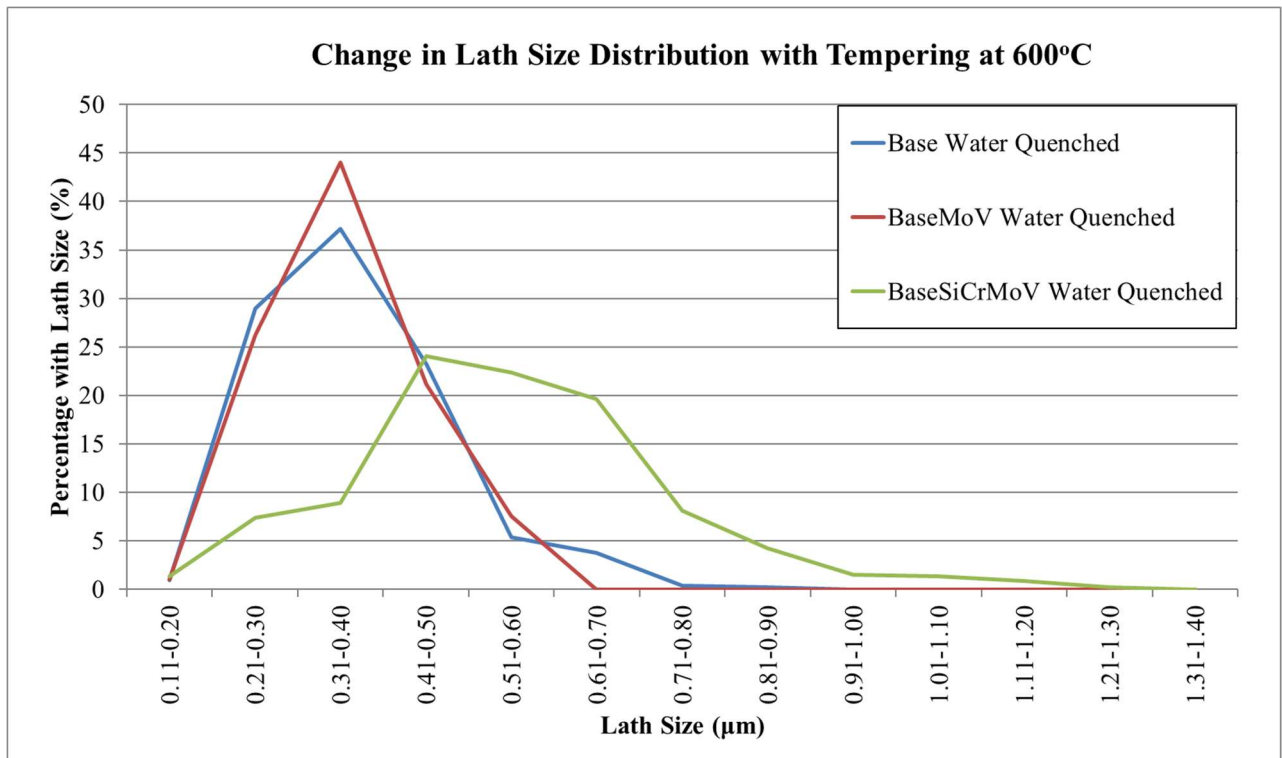


Figure 78 Lath widths in as-quenched condition

Galindo-Nava, 2015, reported that lath width is proportional to carbon concentration, with a higher carbon content in the martensite producing smaller laths, section 2.5.2 (Galindo-Nava & Rivera-Díaz-del-Castillo, 2015). The carbon contents reported in the compositions is compared to the expected and actual lath sizes in [Table 24](#); using the relationship found by Galindo-Nava, 2015 (Galindo-Nava & Rivera-Díaz-del-Castillo, 2015). With the level of accuracy used in this study there is not expected to be any distinguishable difference between the three steels and the reported lath widths, any differences found in the BaseSiCrMoV mean may be accounted for by the large associated errors. However, the shape of the distribution may indicate that there is a larger range of BaseSiCrMoV lath widths. Another distraction in this work is that SEM measurements are used instead of TEM measurements, this may result will be less accurate than TEM, however as in excess of 1,000 measurements were taken for lath size this is thought to be sufficient in giving trends in lath sizes on tempering.

Table 24 Comparison between carbon in solid solution and expected lath size

Composition	Carbon Content	Expected Lath Size (nm)	Actual Lath Size (nm)
Base	0.17	175	310 - 400 ± 300
BaseMoV	0.17	175	310 - 400 ± 300
BaseSiCrMoV	0.17	175	410 – 500 ± 300

5.1.6: Alloying Elements

5.1.6.1: Strengthening

The amount that alloying elements in solid solution contribute to martensite hardness has been summarised by Llewellyn, 2013, Table 25, this is used to predict any additional strength from alloying elements in terms of solid solution strengthening (values from Table 7, section 2.13.2).

The relationship between ultimate tensile strength in MPa and Brinell hardness is reported by Dieter, as the following (Dieter & Bacon, 1988);

$$\text{Brinell Hardness} = \text{MPa} / 3.4$$

Equation 5.2

Brinell Hardness is not the same as Vickers Hardness, the two have been used interchangeably due to the close values. The following values show how similar the results are, especially at lower hardness values, a relationship has been derived of $y = 0.942x + 1.246$, where x Vickers hardness and y is the Brinell Hardness (See Figure 79) (Metals, 1985).

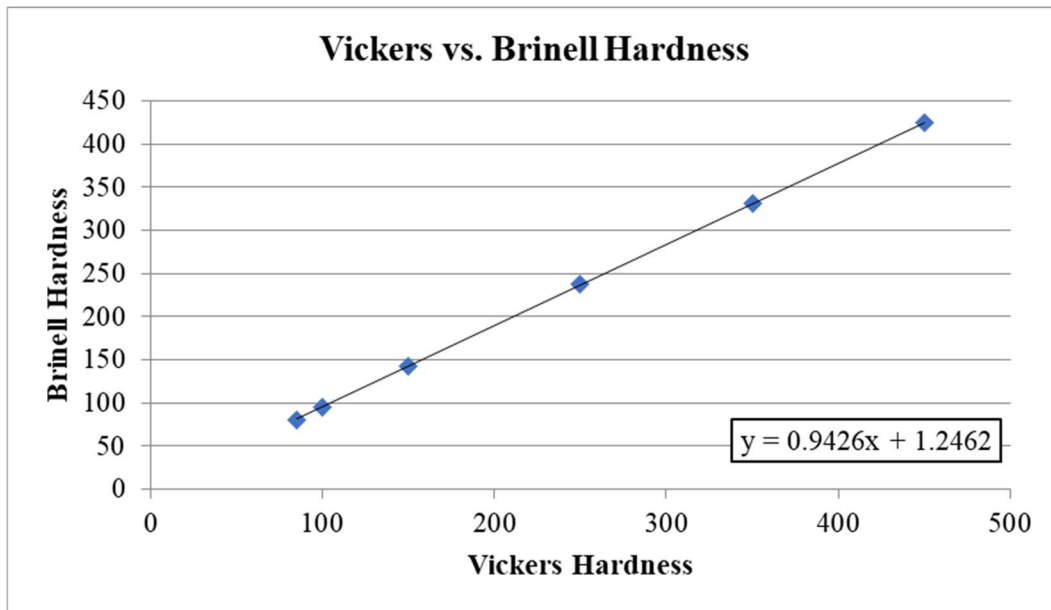


Figure 79 Comparison between Vickers and Brinell hardness values

Table 25 Table showing contribution to hardness from alloying elements

Strengthening N/mm ² per wt. %	Base	BaseMoV	Base SiCrMoV
P: +678	0	0	0
Si: +83	24.9	24.9	107.9
Cu: +39	0	0	0
Mn: +32	40	40	40
Mo: +11	0	5.5	5.5
Ni: +0	0	0	0
Cr: -31	0	0	-24.8
Sum of rows	64.9	70.4	128.6
Converted to Brinell Hardness	19	21	38

5.1.7: Initial Hardness

The carbon content of the steels can be used to predict as-quenched hardness, as this contributes to solid solution strengthening; tetragonality of martensite and the type of martensite present (laths or blocks). It is important to note that this is most appropriate when there is no auto-tempering. However, in this study there is carbon which is still in solid solution, which can contribute to the strength, so this has been determined an appropriate method to gain an understanding of what hardness can be expected.

Work by Krauss, 1978, shown in section 2.3.1, found that martensite with a carbon percentage of 0.17 wt. % is expected to give a hardness of 450 HV in the as-quenched condition; this is shown in [Figure 12](#) with data relevant to this work in [Table 26](#). Speich, 1969 reported a 0.18 wt.% C martensitic steel to have a hardness of 510 HV on quenching, where little auto-tempering was observed.

Table 26 Hardness of compositions compared to literature

Composition	Predicted Carbon content in solid solution %	Expected HV contribution from C (Krauss)	Expect HV from alloying elements	Overall HV Expected	Actual Hardness on quenching
Base	0.11	~400	19	~419	457±12
BaseMoV	0.11	~400	21	~421	453±11
BaseSiCrMoV	0.13	~425	38	~463	470±31

Hardness values have been predicted from Krauss's work using extrapolation, the hardness values of the as-quenched steels in this work are given in [Table 26](#), along with predicted values based on Krauss's data, which compares the wt. % C against the hardness (Vickers), Krauss's data cover a larger data set than other authors, and therefore give a better indication of the trends associated with carbon content and hardness. The amount of carbon in this work

is based on the carbon in solid solution calculated from XRD data. The contribution to hardness from the carbon in solid solution assumes that the calculation of carbon content is correct. The contribution to hardness from substitutional alloying elements in solid solution has been taken from Table 25 and the strengthening N/mm² per wt. % and is set at the amount of alloying element reported for this steel and converted to Brinell Hardness. The expected contribution to hardness from alloying elements and carbon is less than the actual hardness values, shown in Table 26. BaseSiCrMoV is expected to have a higher hardness than Base and BaseMoV, which matches experimental data.

In the as-quenched sample there is a 15 HV difference between Base/BaseMoV and BaseSiCrMoV, this is in line with what is predicted from solid solution strengthening. Carbon can be expected to give an additional 25 HV to BaseSiCrMoV, compared to Base and BaseMoV. This is based on predicted carbon content and expected HV contribution from C, therefore there is some uncertainty, however it is expected that BaseSiCrMoV will be harder.

Another consideration is that auto-tempering carbides may be fine and readily dispersed enough to provide strengthening and contribute to hardness. Base and BaseMoV would have the greatest contribution than BaseSiCrMoV, and this may account for some discrepancies between calculations and measured values.

This also indicates that the contributions to hardness from the other strengthening features (lath size, packet size, carbides, dislocation density) are similar overall and some of the discrepancies can be accounted for by auto-tempering carbides.

5.1.8: Summary of as-quenched martensitic samples

This work finds that the three steels are composed of lath martensite (with potentially a small amount of lower bainite) in the as-water quenched condition. BaseSiCrMoV is found to have a smaller proportion of laths containing carbides present within the laths; the carbide sizes have not been investigated, also BaseSiCrMoV has a lower ratio of cementite to epsilon carbides than the other compositions amongst those auto-tempered carbides that are present.

The main difference between the three steels being considered is the alloying elements present (Mo, Cr, Si and V), affecting the martensite start temperature and the amount of auto-tempering, which then affects the amount of carbon in solid solution. The BaseSiCrMoV shows an increase in carbon content in solution and less auto-tempering indicating that the Si and Cr additions affect the as-quenched microstructure whilst the Mo and V have no significant effect, as the Base and BaseMoV steels show the same carbon content in solution and degree of auto-tempering. This then affects the predicted and measured hardness levels with the BaseSiCrMoV steel showing a higher hardness than the other two steels, predominantly from solid solution strengthening from the Si and Cr content, along with predicted higher carbon content and lesser degree of auto-tempering.

There is no significant difference in the values of the prior austenite grain size between the three steels, the same is true of lath size. Although there is an indication from lath size data that BaseSiCrMoV has a wider distribution than the other two compositions. These are not shown to be significant enough to influence the hardness. It is also possible that it offsets some of the hardness due to the higher content of carbon predicted to be in solid solution.

5.2: Tempering at 600 °C

5.2.1: Carbides

5.2.1.1: Carbide Types

As mentioned above, in the as-quenched conditions there is a mixture of epsilon carbide and cementite. TEM analysis by Ju found only cementite to be present after 2 hours tempering at 600°C for all three steel compositions (Ju, 2018). This is consistent with previous literature reports (section 2.8.2.3) which find epsilon carbide to have been fully replaced by cementite after 5 minutes at 400 °C in a Fe-0.55C-2.2Si wt. % steel (literature with values closer to the studied composition is not available). Although the concentration of carbon is higher than that of the three compositions studied, it does indicate that the transformation to cementite can occur quickly and backs up experimental data showing no epsilon carbide present after 2 hours at 600 °C (B.-N. Kim et al., 2012).

Thermo-Calc has been used to predict the volume fraction of cementite (considering pseudo-equilibrium conditions when alloy carbides are suppressed), the volume fraction and type of all carbides (when alloy carbides are permitted in calculations) and the amount of carbon remaining in the solid solution. Thermo-Calc predications of the equilibrium carbide content in the three steels studied, shown in Table 27, indicate a change from cementite (Base) to mixed cementite and alloy carbides (BaseMoV) and finally just alloy carbides (BaseSiCrMoV). BCC and FCC phases have not been included in the table as they are not carbides.

Base does not contain any alloying elements to promote secondary carbide formation, unlike BaseMoV and BaseSiCrMoV; it is therefore expected to reach the next stage of tempering quicker.

The predicted amount of carbon in solid solution (BCC - all phases allowed) shows that there is almost double the amount of carbon in the Base and BaseMoV steels compared to the

BaseSiCrMoV steel. The predicted values are lower than experimental values; however, this still shows an expected difference between Base/BaseMoV and BaseSiCrMoV.

BaseSiCrMoV is also predicted to have a lower volume fraction of carbides (2.18×10^{-2}) compared to Base (2.5×10^{-2}) and BaseMoV (2.2×10^{-2}). As the steels have the same bulk carbon it is not expected that the BaseSiCrMoV would have a reduced carbon content, however, it is found to have a higher mass fraction of carbon in the carbides based on Thermo-Calc data, which finds less carbon in BCC compared to the Base and BaseMoV.

Table 27 Equilibrium alloy carbides for Base-BaseMoV-BaseSiCrMoV, along with carbon in solid solution at 600 °C, predicted using Thermo-Calc

	Base	BaseMoV	BaseSiCrMoV
Equilibrium Precipitates with Volume Fraction (All steel phases allowed)	Cementite (2.5×10^{-2})	Cementite (1.3×10^{-2}) M ₇ C ₃ (6.3×10^{-3}) MC (2.7×10^{-3})	M ₇ C ₃ (1.6×10^{-2}) M ₆ C (3.3×10^{-3}) MC (1.6×10^{-3}) M ₂₃ C ₆ (8.6×10^{-4})
Total Volume Fraction of Carbides (All steel phases)	2.5×10^{-2}	2.2×10^{-2}	2.18×10^{-2}
Mass fraction of carbon in carbides (cementite) (All steel phases)	0.065932	0.064610	-
Mass fraction of carbon in carbides (non-cementite) (All steel phases)	-	0.204923	0.2789459
Mass Fraction of all carbides/ Volume Fraction of carbides	2.636116*	12.16952	12.66628
Mass fraction of carbon in BCC (i.e. not in carbides) (All steel phases)	2.73E-05	2.66E-05	1.21E-05
Predicted Mass fraction Carbon in Solid Solution – For 2 hours (Only BCC + cementite allowed)	0.2549	0.2532	0.2494
Mass fraction Carbon in BCC– For equilibrium condition (Only BCC + Cementite allowed)	0.0027	0.0026	0.0014

* Lower value as there is less mass fraction of carbon in carbides.

5.2.1.2: Carbide Shape/Sizes

Figure 80 shows Base, tempered for 2 hours at 600 °C; the arrows indicate differences in carbide shapes, and a visual comparison can distinguish a difference in the size of carbides in the matrix and on the lath boundaries. The intra- and inter-lath carbides have been separated out during measurements due to their bimodal distribution in carbide size and spacing, along with their differences in coarsening behaviour on tempering. Although it may be argued that the spacing is the more important factor in hardness contribution, it was found to be simpler to measure the two carbide locations separately, ensuring that a representative sample of each carbide type was taken. The intra- and inter-lath carbides are also expected to coarsen at different rates based on the literature (discussed in 2.6.14) and is important in monitoring how the microstructures changes on tempering.

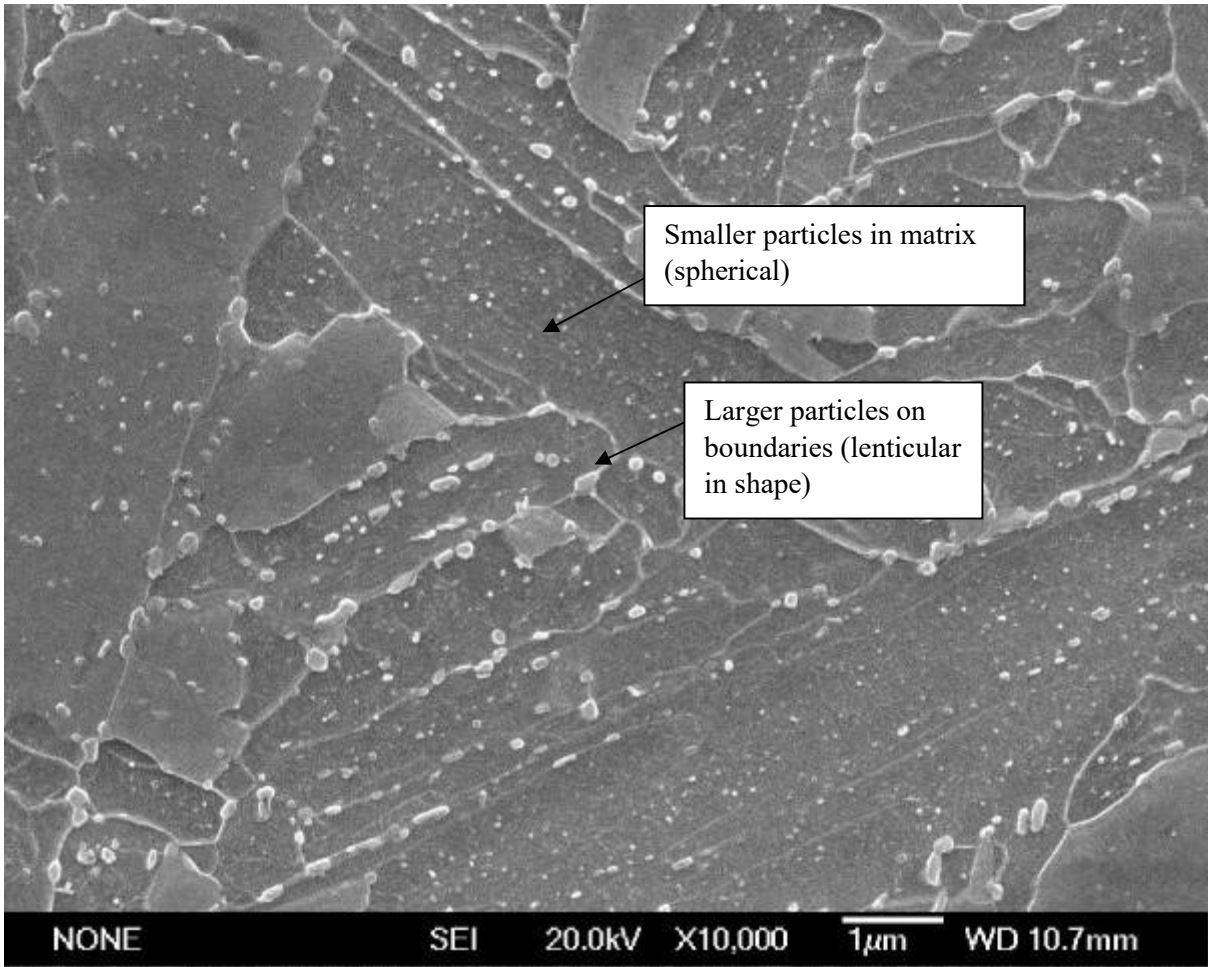


Figure 80 Base tempered for 2 hours at 600 °C, comparison between carbides on the boundary and within the matrix (263.4 ± 7.6 HV)

5.2.1.3: Carbide Strengthening

Using equation 5.3 the predicted carbide strengthening values can be determined for the three steels, tempered for 2 hours and 16 hours. These can then be converted to Brinell hardness.

Where D is the mean planer intercept diameter of a precipitate and λ is the surface to surface precipitate spacing, λ and D are in micrometres (Maropoulos & Ridley, 2005).

$$\sigma_p(MNm^{-2}) = \frac{6.26}{\lambda} \ln \frac{D}{2.48 \times 10^{-4}}$$

Equation 5.3

Assumptions which have been made include using the equivalent circle diameter (ECD) for carbide diameter, where, for the diameter of needle-shaped carbides, the carbide area has been measured and the equivalent circle diameter (ECD) calculated. There is also the assumption that intra-lath and inter-lath carbides act independently, and that the strengthening contributions are added to get the total contribution to strength. This assumption is made on the basis that inter-lath and intra-lath carbides have different distributions and carbide sizes and carbides will have different coarsening rates, shown in [Table 29](#). There is the potential for error to be introduced because carbides in this work are not all spherical, measuring slightly higher or lower strength, however as there are a large number of carbides measured this difference should be negligible. When (Maropoulos & Ridley, 2005) compared strengthening equation predictions with actual data (for steels with carbon contents between 0.29 – 0.35 wt. % C where the cementite had fully precipitated) there was a maximum 4% discrepancy, which should be considered when examining the results of this study.

Ju, 2018 reports that there are finer needle-shaped carbides present in BaseMoV and BaseSiCrMoV after 2 to 16 hours temper these are summarised in [Table 28](#), but these have not been added to the calculations, as the SEM images are used and the resolution limit is not sufficiently accurate to analyse the smaller carbides, and therefore associated errors would be

large and not representative of the actual hardness contribution (Ju, 2018). The results do show that there is a decrease in volume fraction from 0 to 2 hours, there is an increase in volume fraction of finer carbides at 4 hours. At 16 hours it appears that the BaseSiCrMoV is retaining the finer carbides more than BaseMoV.

There is an increase in volume fraction of carbides at 4 hours for the alloyed steel. This does not match the hardness, indicating it is not showing a significant effect on hardness. The increase is thought to due to the precipitation of secondary carbides. The decrease from 4 to 16 hours is due to the dissolution of cementite (Ju, 2018).

Table 28 Volume fraction of fine carbides in BaseMoV and BaseSiCrMoV

Volume Fraction of fine carbides / μm^{-3}	0 hours	2 hours	4 hours	16 hours
BaseMoV	475 ± 25	175 ± 25	300 ± 50	100 ± 25
BaseSiCrMoV	525 ± 25	225 ± 50	275 ± 50	200 ± 50

The fine needle-shaped carbides are expected to add to the additional 100 HV between Base and BaseMoV/BaseSiCrMoV, based on the differences from predicted and experimental hardness value determined, the volume fraction of these are unknown, however it would help start to explain the difference in strength between Base and BaseMoV/BaseSiCrMoV.

At 2 hours it is not expected that there is as significant solid solution strengthening from Base and BaseSiCrMoV, as the alloying elements are expected to be within carbides. It is not expected that there would be any differences in hardness between BaseMoV and BaseSiCrMoV, as contribution from the larger cementite carbides is similar for the three steels, and alloying elements are expected to be within carbide. Table 29, shows the carbide sizes and spacing on the lath boundaries and within the laths. Each carbide type increases in size while the number density decreases on continued tempering from 2 to 16 hours,

indicating that larger particles are growing at the expense of smaller particles (such as in Ostwald ripening).

Figure 82- Figure 92 show the differences in carbides between the three steels after 2 and 16 hours at 600 °C. Figure 84 shows more carbides on the lath boundaries in Base compared to BaseMoV and BaseSiCrMoV , while Figure 88 and Figure 92 show more numerous, smaller intra-lath carbides for BaseMoV and BaseSiCrMoV.

Inter-particle spacing increases for the Base carbides on the lath boundaries and in the laths. The inter-particle spacing of carbides on the lath boundaries increases from $0.34 \pm 0.02 \mu\text{m}$ at 2 hours to $0.63 \pm 0.03 \mu\text{m}$ at 16 hours. Coupling this with the increase in inter-lath carbide diameter ($95.8 \pm 24\text{nm}$ to $152.4 \pm 43\text{nm}$) it indicates that carbides are becoming larger in size and with an increased inter-particle spacing. This trend is also true of the carbides within the laths.

BaseMoV and BaseSiCrMoV show similar levels of inter-particle spacing on lath boundaries after 2 hours ($0.30 \pm 0.02 \mu\text{m}$ / $0.29 \pm 0.03 \mu\text{m}$). BaseMoV exhibits an increase in inter-particle spacing on the lath boundaries from 2 to 16 hours ($0.30 \pm 0.02 \mu\text{m} \rightarrow 0.44 \pm 0.03 \mu\text{m}$), whilst the BaseSiCrMoV lath carbide spacing remains stable during the same tempering time ($0.29 \pm 0.03 \mu\text{m} \rightarrow 0.27 \pm 0.02 \mu\text{m}$). This suggests that BaseMoV carbides are undergoing Ostwald ripening at a quicker rate than BaseSiCrMoV and that BaseSiCrMoV has an increased stability, this is verified by volume fraction results. However, as the hardness values are so similar it suggests that the Ostwald ripening is not significant.

Base shows an 85% increase in carbide size on lath boundaries from 2 to 16 hours, this is compared to 46% for BaseMoV; BaseSiCrMoV shows a slight in 43% same tempering time. For the carbides in the laths, Base carbide size shows an increase in size of 58%, after tempering from 2 to 16 hours. BaseMoV shows an increase in carbide size of 59% and

BaseSiCrMoV has a carbide size which does not increase significantly on tempering (20%). This indicates that the BaseMoV and BaseSiCrMoV are coarsening at a slower rate compared to Base, for both carbide positions.

After 2 hours tempering there is little difference in predicted carbide strengthening between the three compositions, with a difference of 7 HV between Base (66 HV) and BaseSiCrMoV (73 HV). The data have been summarised in Figure 81, where it is possible to observe that the contribution to hardness from the carbides is lower after 16 hours for all three compositions. The contribution to strength is similar for both the carbides within the laths and on the lath boundaries; this may be due to the lath boundaries being low angle boundaries (mis-orientation angle predicted to be around 2 degrees, section 2.13.1). This means that there is a small, but not significant barrier to dislocations, in terms of carbides between the matrix carbides and lath carbides. It should be noted that this strengthening mechanism is just looking at the carbide strengthening; lath width is considered in more detail below.

Between 2 to 16 hours there is a 36% decrease in expected hardness contribution from the carbides in Base and a 23 / 5% decrease in hardness contribution for BaseMoV/BaseSiCrMoV respectively. This indicates that there is more strengthening contribution from the smaller carbides, which are reported but not analysed. The difference in actual hardness values for Base and BaseMoV/BaseSiCrMoV is consistently 100 HV, indicating the softening gradient is consistent for the three steels, between 2 and 16 hours. The measurements indicate that carbide softening does not occur at the same rate in the three steels, therefore it is thought that the carbides do not produce a pronounced softening on tempering. If the carbides were the dominant strengthening mechanism, then it would be expected that the hardness decrease of BaseSiCrMoV should be a fifth of what BaseMoV has. This is not seen. It is plausible that the smaller carbides, which are not visible using SEM, are having a strengthening effect, resulting in BaseMoV and BaseSiCrMoV having the same

hardness.

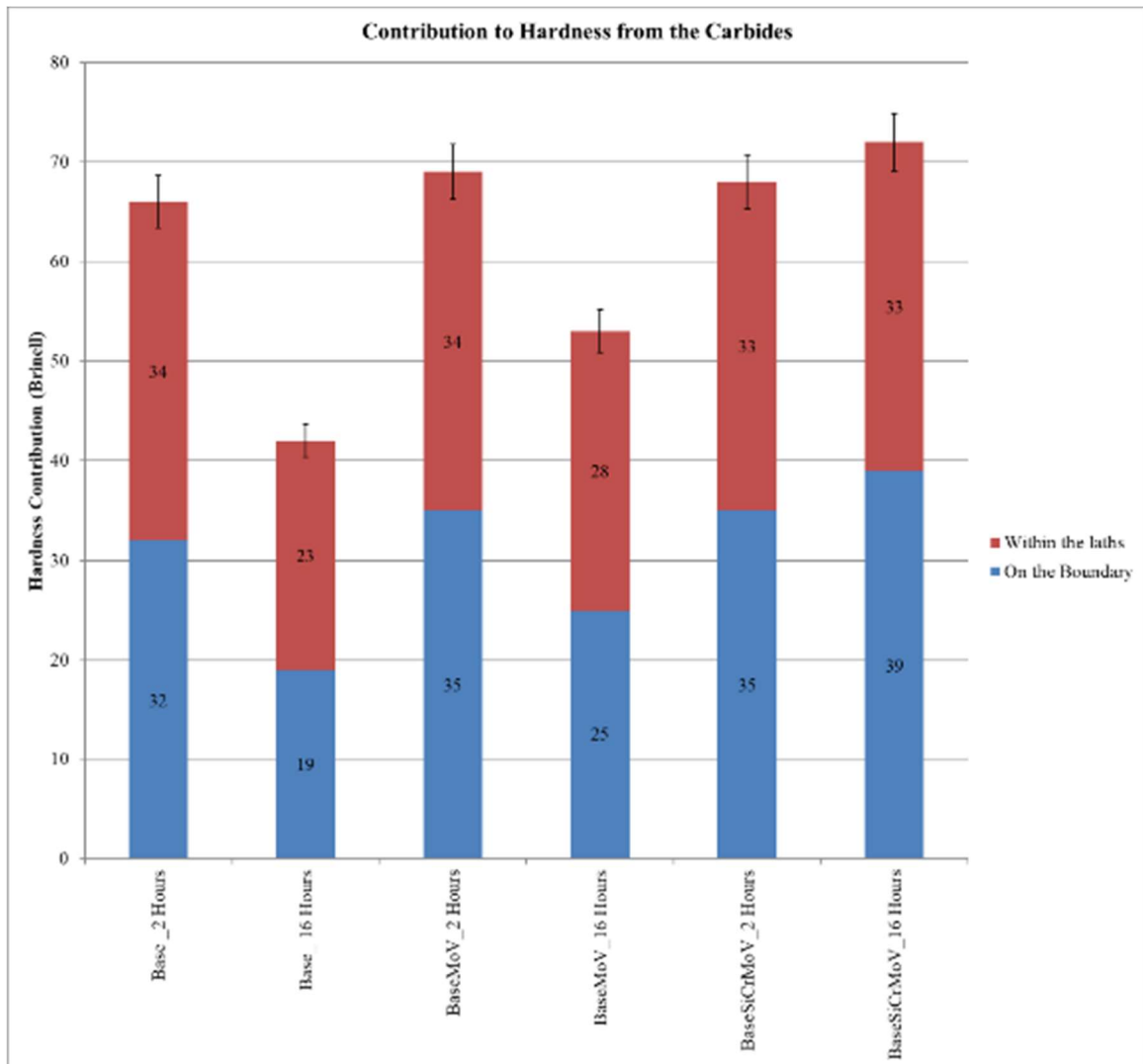


Figure 81 Contribution to hardness from the carbides

Table 29 Carbide sizes

Composition	Tempering time at 600 °C (Hours)	Carbide Location	Number Density $+/\mu\text{m}^{-2}$	Inter-Particle Spacing μm	Diameter -ECD (nm)*	MPa strengthening contribution ($\pm 4\%$)	Converted to Brinell Hardness	Volume Fraction (Number Density/Diameter)
Base	2	On lath boundaries	3.5	0.34 ± 0.02	95.8 ± 24	110	32	0.037
Base	2	In laths	1.0	0.29 ± 0.02	53.2 ± 8	115	34	0.019
Base	16	On lath boundaries	1.3	0.63 ± 0.03	152.4 ± 43	64	19	0.009
Base	16	In laths	0.3	0.46 ± 0.03	84.4 ± 14	79	23	0.004
BaseMoV	2	On lath boundaries	6.9	0.30 ± 0.02	68.6 ± 30	117	35	0.101
BaseMoV	2	In laths	1.4	0.28 ± 0.01	45.0 ± 7	116	34	0.031
BaseMoV	16	On lath boundaries	3.7	0.44 ± 0.03	94.6 ± 43	85	25	0.039
BaseMoV	16	In laths	1.0	0.36 ± 0.02	55.8 ± 8	94	28	0.018
BaseSiCrMoV	2	On lath boundaries	9.1	0.29 ± 0.03	61.2 ± 24	119	35	0.149
BaseSiCrMoV	2	In laths	2.4	0.28 ± 0.01	42.0 ± 8	113	33	0.034
BaseSiCrMoV	16	On lath boundaries	6.5	0.27 ± 0.02	70.6 ± 25	131	39	0.155
BaseSiCrMoV	16	In laths	2.2	0.29 ± 0.01	49.2 ± 8	113	33	0.045

* For conservative errors the largest standard deviation of the length and width measurement is used

+ Error quoted smaller than data points in graph from Ju, 2018.

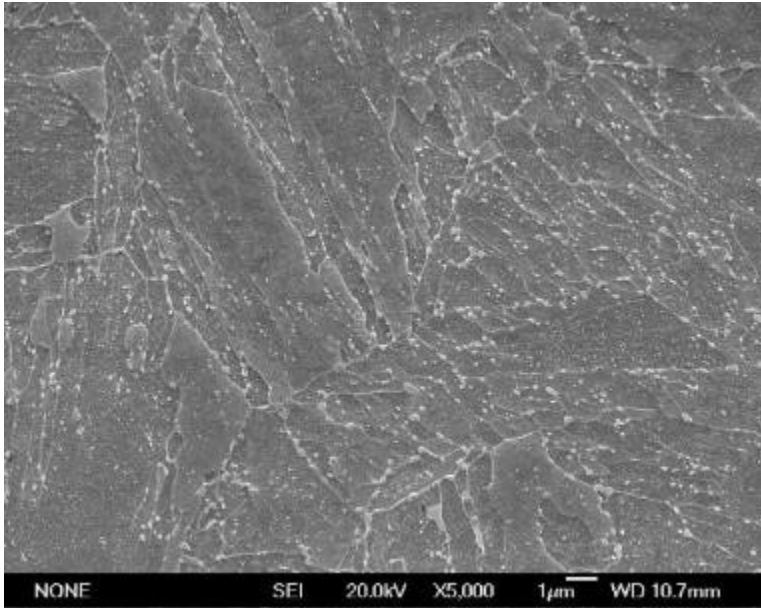


Figure 82 SEM micrograph showing carbides in the Base steel after 2 hours tempering at 600 °C (263.4 ± 7.6 HV)

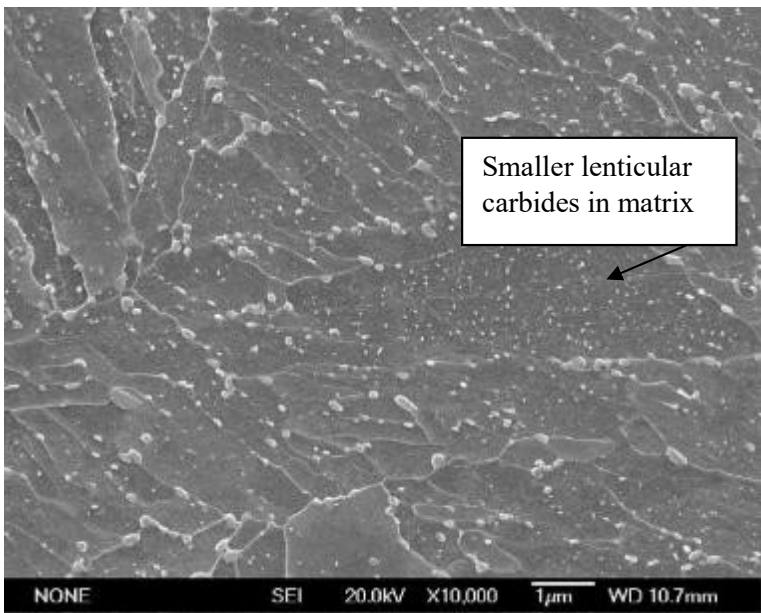


Figure 83 SEM micrograph showing carbides in the Base steel after 2 hours tempering at 600 °C (higher magnification) (263.4 ± 7.6 HV)

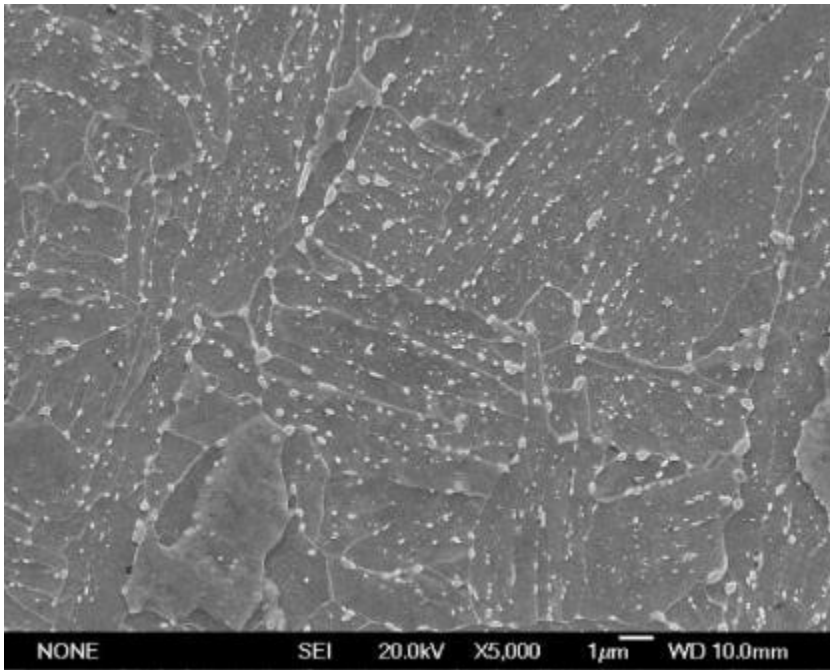


Figure 84 SEM micrograph showing carbides in the Base steel after 16 hours tempering at 600 °C (221 ± 7.6 HV)

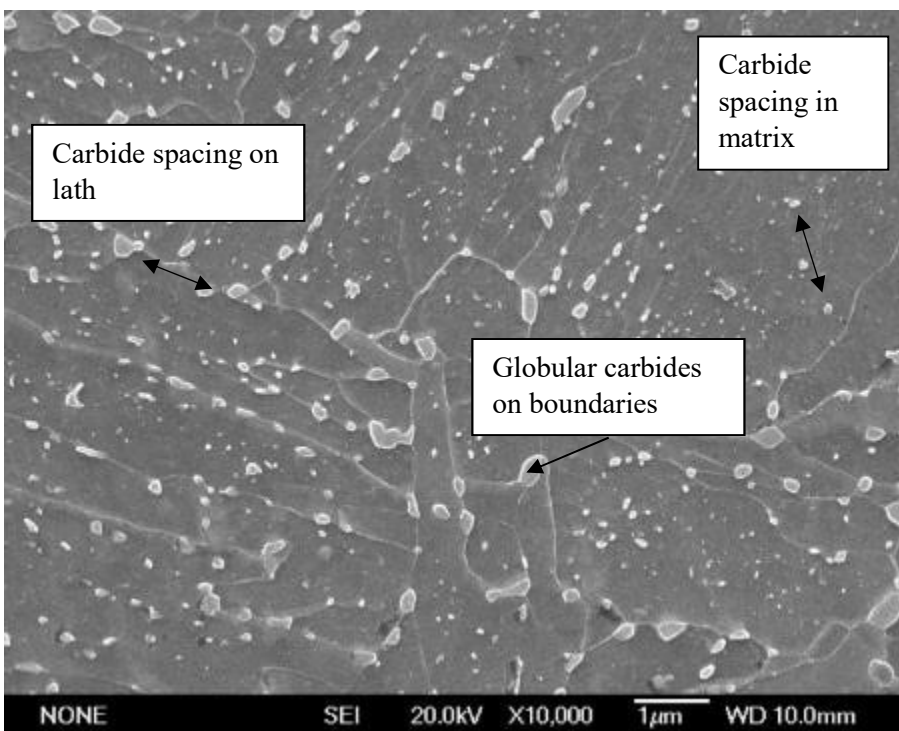


Figure 85 SEM micrograph showing carbides in the Base steel after 16 hours tempering at 600 °C (higher magnification) (221 ± 7.6 HV)

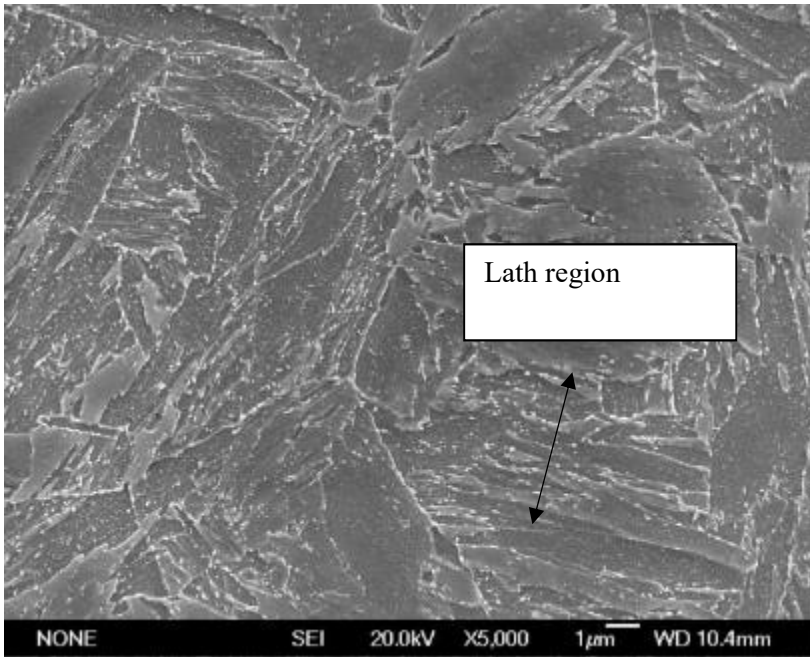


Figure 86 SEM micrograph showing carbides in the BaseMoV steel after 2 hours tempering at 600 °C (360.1 ± 12.2 HV)

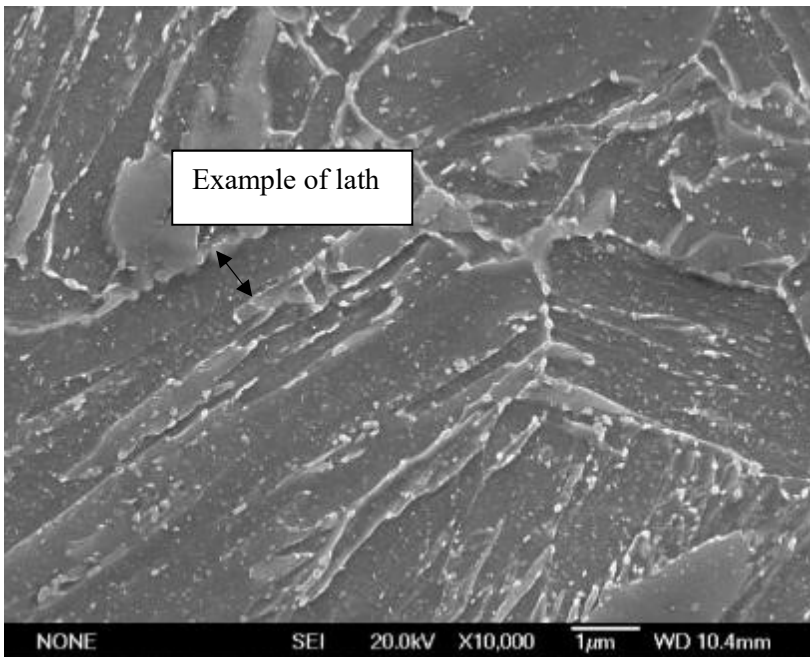


Figure 87 SEM micrograph showing carbides in the BaseMoV steel after 2 hours tempering at 600 °C (higher magnification) (360.1 ± 12.2 HV)

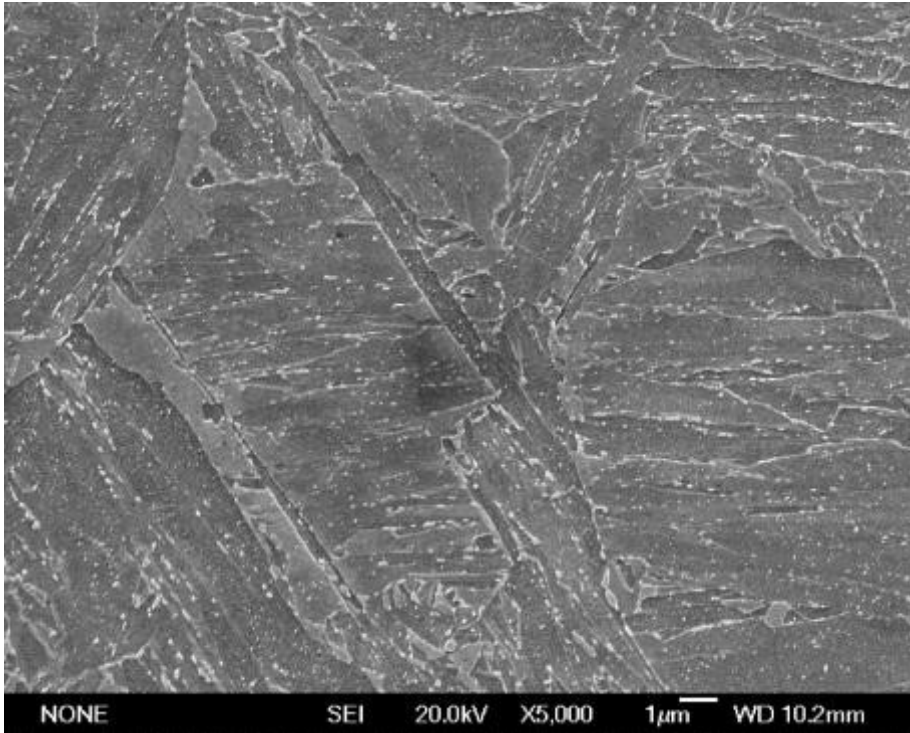


Figure 88 SEM micrograph showing carbides in the BaseMoV steel after 16 hours tempering at 600 °C (321.3 ± 8.0 HV)

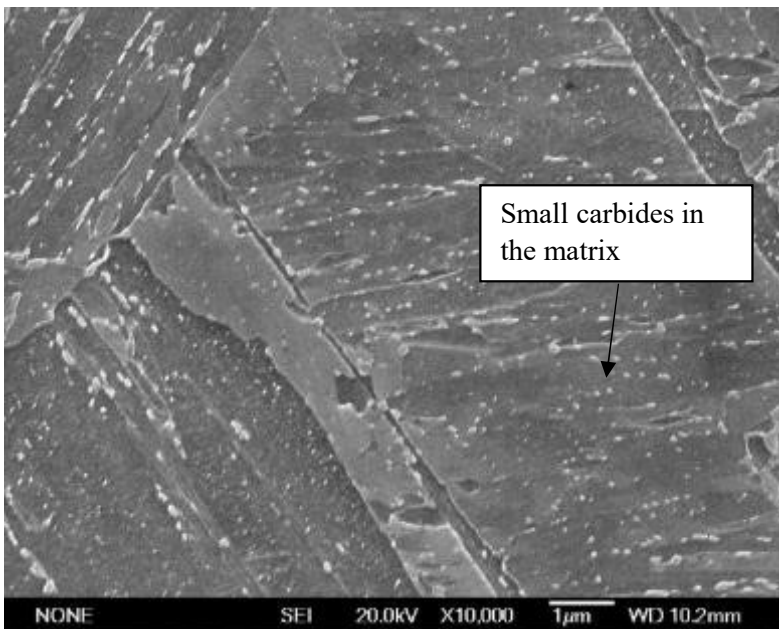


Figure 89 SEM micrograph showing carbides in the BaseMoV steel after 16 hours tempering at 600 °C (higher magnification) (321.3 ± 8.0 HV)

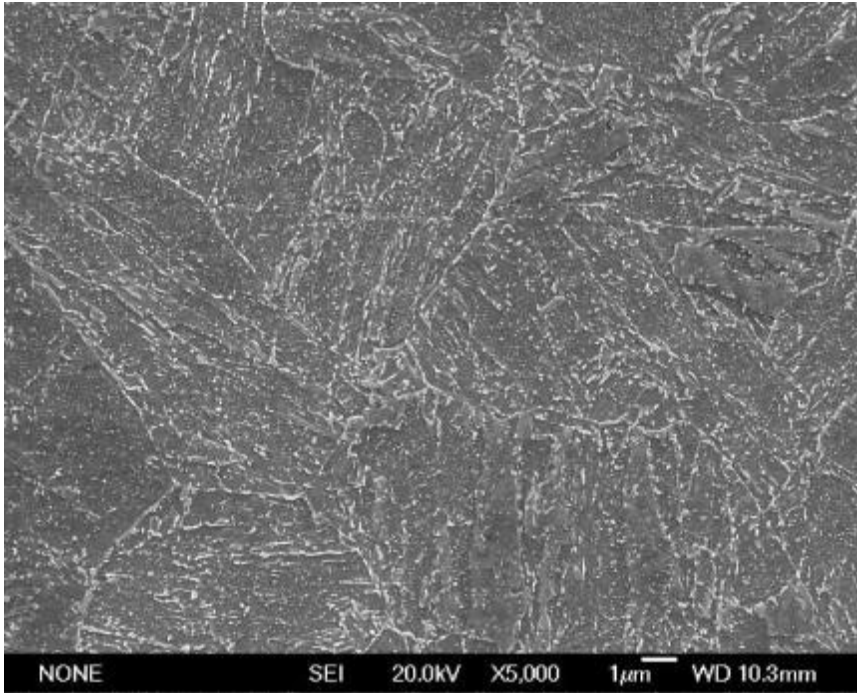


Figure 90 SEM micrograph showing carbides in the BaseSiCrMoV steel after 2 hours tempering at 600 °C (336.0 ± 10.5 HV)

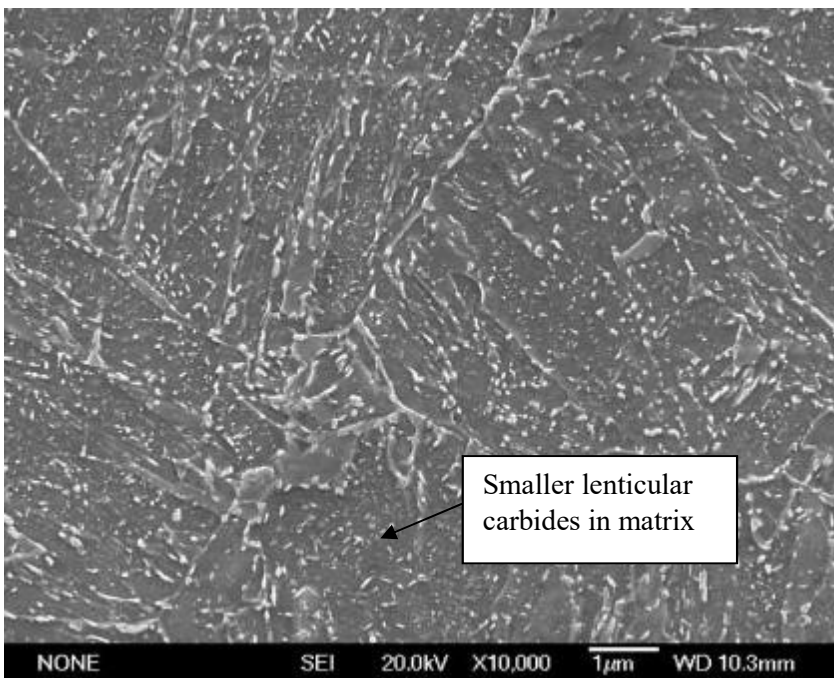


Figure 91 SEM micrograph showing carbides in the BaseSiCrMoV steel after 2 hours tempering at 600 °C (higher magnification) (336.0 ± 10.5 HV)

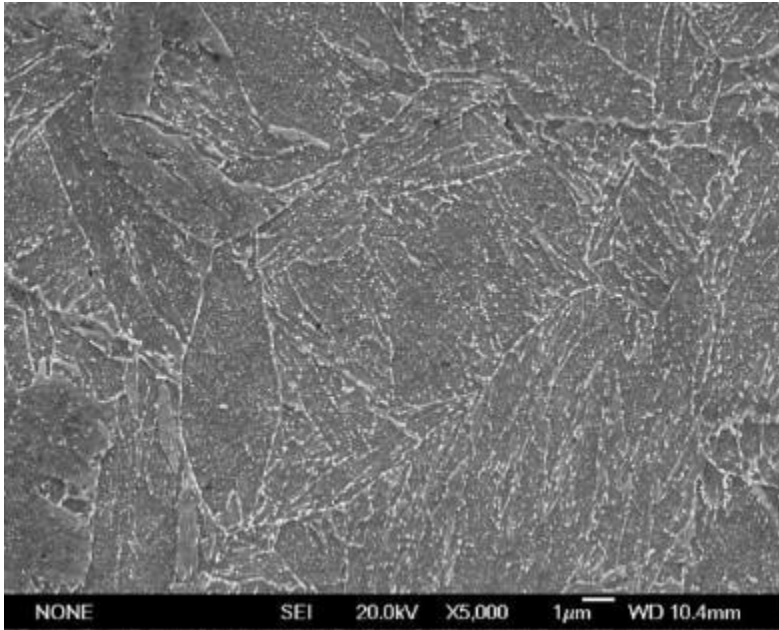


Figure 92 SEM micrograph showing carbides in the BaseSiCrMoV steel after 16 hours tempering at 600 °C (320.0 ± 10.4 HV)

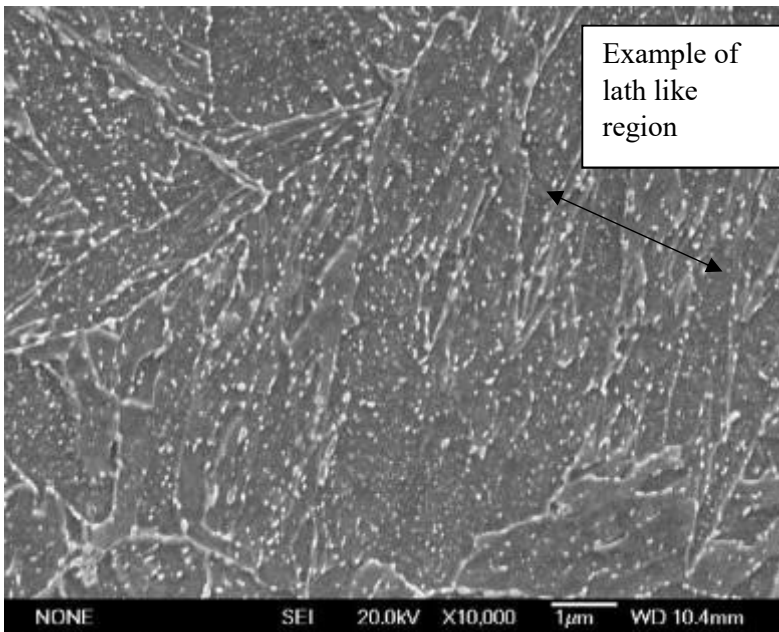


Figure 93 SEM micrograph showing carbides in the BaseSiCrMoV steel after 16 hours tempering at 600 °C (higher magnification) (320.0 ± 10.4 HV)

5.2.2: Laths

The change in lath size on tempering has been investigated. From the literature it is expected that the lath sizes will coarsen via boundary motion, with longer tempering times as removal of particles reduce pinning forces. However, this is also expected to be accompanied by a reduction in precipitation strengthening, as lath coarsening is easier when the carbides are larger with a lower number density (section 2.6.1.5).

Data from Maropoulos and Ridley (2005) have been used to produce Figure 46, section 2.13.1, showing the contribution lath width has to hardness. Brinell hardness has been used; this is comparable to Vickers hardness and gives a good indication of HV contribution from lath size. Figure 46 shows that there is an exponential decrease in hardness with an increase in lath width (Maropoulos & Ridley, 2005). The measured lath width distribution is shown in Table 30 for the Base steel composition in the as-quenched, tempered for 2 hours and tempered for 16 hours conditions; this is based on equation 2.9, where MPa has subsequently been converted to Brinell hardness, using equation 2.7.

Base shows a change in distribution, with a coarsening of the lath width as tempering time increases. The average size increases from 0.31 – 0.40 μm to 0.71 – 0.80 μm , shown in Table 30. There is no logical explanation of why BaseSiCrMoV is getting narrower on tempering from 2 to 16 hours, therefore this to be used as the basis of the error associated with these measurements. Associated errors are therefore $\pm 0.30\mu\text{m}$.

Table 30 Change in average lath size on tempering at 600 °C for the three compositions

Steel	After Quenching (μm)	2 Hours Temper (μm)	16 Hours Temper (μm)
Base	0.31 - 0.40	0.61 – 0.70	0.71 – 0.80
BaseMoV	0.31 – 0.40	0.61 – 0.70	0.51 - 0.60
BaseSiCrMoV	0.41 – 0.50	0.61 – 0.70	0.41 – 0.50

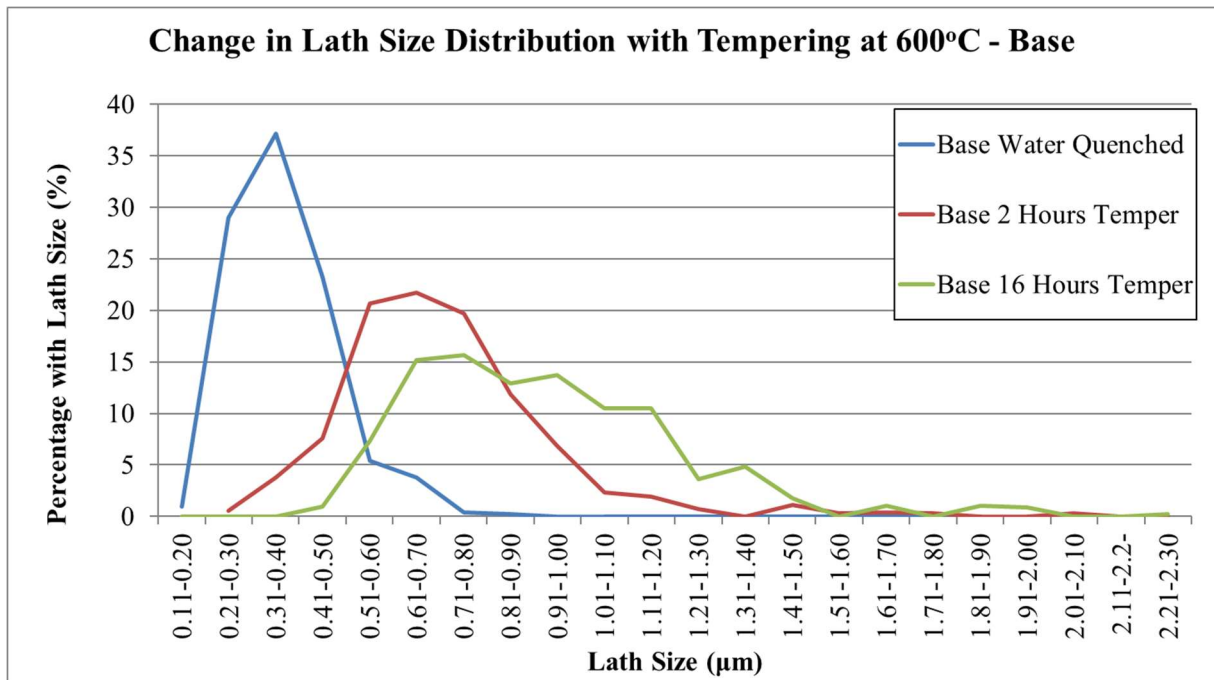


Figure 94 Changes in Lath Size Distribution with Tempering at 600 °C for Base

After water quenching all of the compositions have a similar average lath width (0.31-0.40/0.41-0.50µm). BaseSiCrMoV has a wider distribution than Base and BaseMoV, however the shape does not change significantly between 2 and 16 hours.

After 2 hours tempering there is a similar distribution of lath widths for the three steels, see [Figure 95](#), indicating that the steels tempering stages have not yet differed. The average size of the laths in three steels appears to double from water quenched to 2 hours temper. There is expected to be no difference in lath size on quenching, however, BaseSiCrMoV is 0.3µm larger than the other two steels, this has been ascribed as the experimental error, and applied to all results. During tempering, annihilation of dislocations is expected, as cementite carbides form at dislocation sites (section 2.6.1). These carbides provide ineffective interference with the coarsening of the laths, this could be due to a combination of a large size and small number density, therefore as cementite carbides form and dislocations decrease there is more chance for the lath size to increase, providing an explanation of the increased lath size (Hou et al., 2018). The changes in lath size are the same; therefore, the

contribution to hardness will be the same, for the three steels.

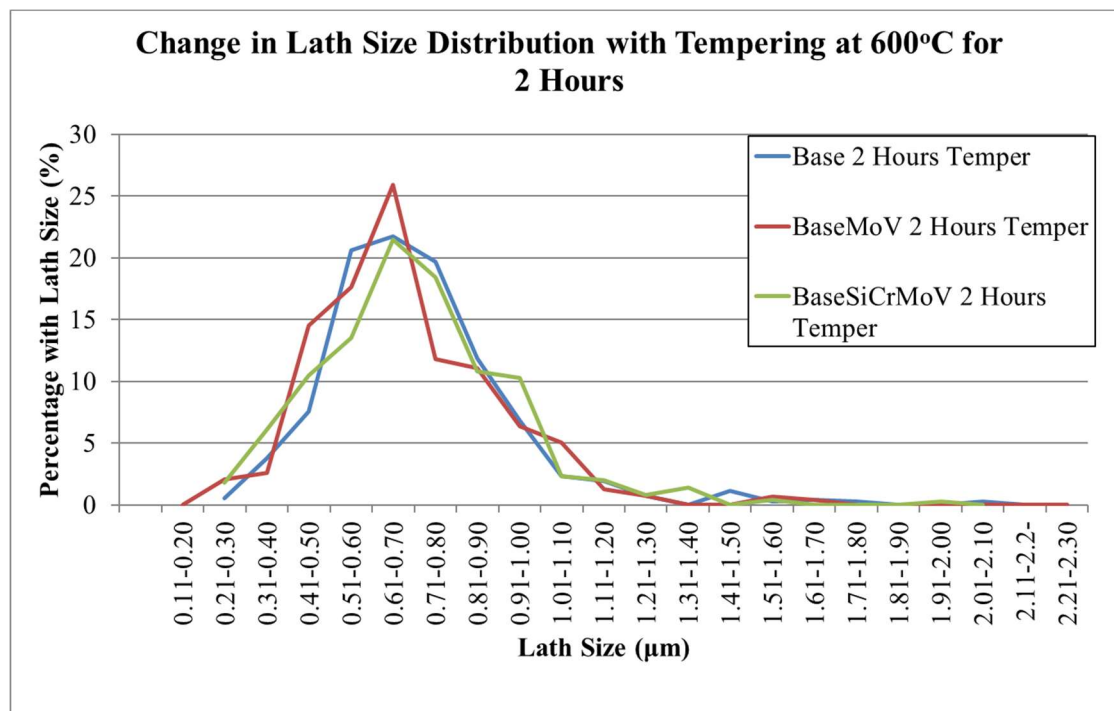


Figure 95 Changes in Lath Size Distribution with Tempering at 600 °C – For 2 Hours

There is no deviation between BaseMoV and BaseSiCrMoV on tempering from 0 hours to 2 hours. There is a slight increase for Base between 2 hours and 16 hours (0.1µm), however this not as significant as the 0.3µm increase from 0 hours to 2 hours and it is only 1 bin size increase, it not deemed to be a real increase in size. There is a wider distribution of lath size for Base at 16 hours compared to the other two compositions, indicating that the lath sizes are becoming larger quicker. It has been commented the difference in distribution may be an indication of insufficient data collection, however the data size is in excess of 1,000 lath measurements across the sample.

For the range of widths found in this work from 0 – 16 hours (Min: Base 0 hours 0.31 – 0.40µm; Max: Base 16 hours 0.71 – 0.80µm), they are calculated to have a contribution to hardness of 75 HV and 25 HV respectively. Using the data from [Figure 46](#) there is predicted

a difference in hardness of around 50 HV from lath size contribution. This does not take into consideration other strengthening methods, and changes in the contribution on tempering. Furthermore, it is important to consider the error associated with lath size measurements ($\pm 0.3\mu\text{m}$), which provides an explanation of the predicted 50 HV increase in hardness between the steels, which is not shown experimentally.

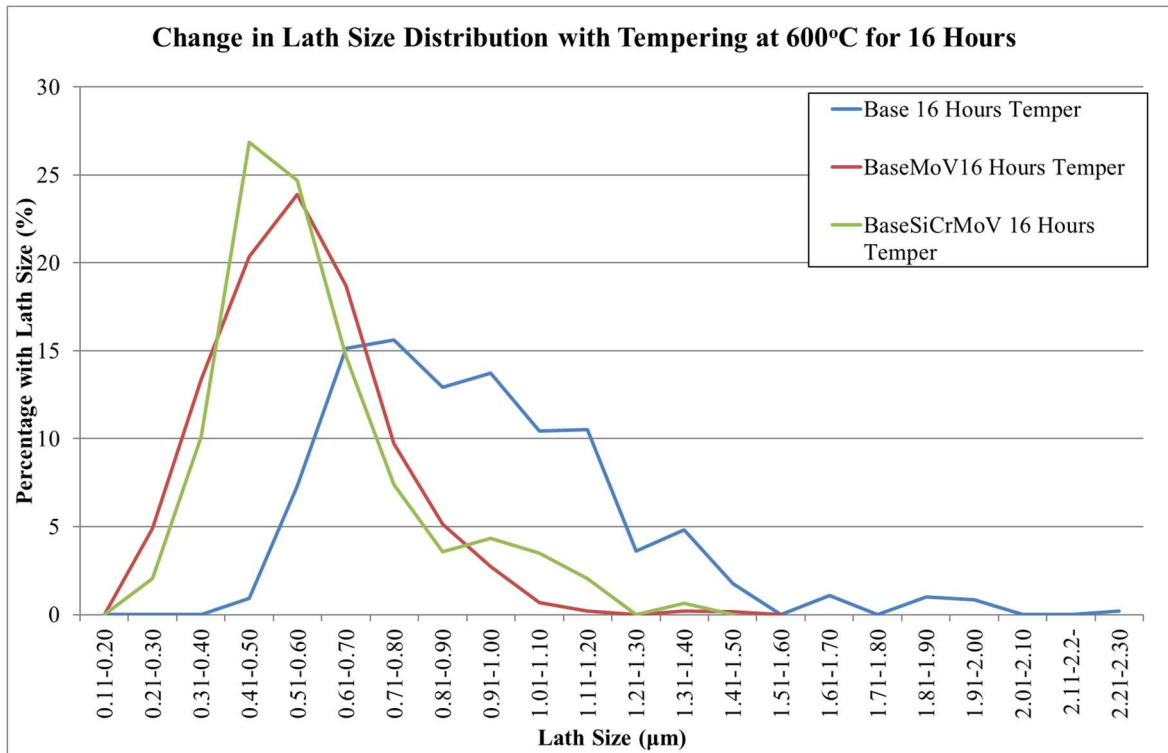


Figure 96 Changes in Lath Size Distribution with Tempering at 600 °C – 16 hours temper

5.2.3: Lattice Parameter

Lattice parameter data, [Table 31](#), indicate that there is less carbon in the matrix after 2 hours tempering in the Base steel, (0.11 → 0.04 wt. %) than in the as-quenched condition. 2 hours was chosen as this matches TEM results which found only cementite present. This indicates that there is less carbon to add additional strength to the matrix. Lattice parameters have not been calculated for BaseMoV and BaseSiCrMoV on tempering.

Using Thermo-Calc the predicted carbon content of the Base steel is 0.0273, after 2 hours (allowing only BCC and cementite) tempering the lattice parameter indicates that carbon has not fully come out of solid solution. The carbon content predicted by Thermo-Calc and the carbon determined experimentally by the lattice parameter is different. The XRD data have been found to have a resolution of 0.026°, this is thought to be a true representation of the BCC structure, as four peaks associated with the BCC lattice were analysed, (001)_α, (002)_α, (211)_α, and (022)_α. As carbide volume fraction is predicted to be 2.5% and under, any carbide interaction would be difficult to detect with XRD. Another difficulty with using lattice parameters, derived by XRD to give carbon content is that any dislocations in the structure could have a higher density of carbon. Any effect of this may result in differences in predicted carbon content. However, when the lattice parameter error is included in analysis there is little deviation between the two values reported.

Table 31 Lattice parameter and predicted carbon content

Sample	Lattice Parameter (±0.001 Å – Based on experimental repeatability)	Predicted Carbon Content
Base	2.870	0.11
Base – 2hours at 600 °C	2.867	0.04

5.2.4: Hardness

The strengthening contributions are given in Table 32, the as-quenched strengthening and summary of expected change on tempering is given.

Table 32 Summary of change in strengthening mechanism on tempering

	As – Quenched	Tempering – Expected Changes
Solid Solution Strengthening (Alloying Elements)	Present for alloyed steel	Effect to remain stable once carbides have fully precipitated (2 hours +)
Solid Solution Strengthening (Carbon)	Present for all	Carbon is expected to be removed from SSS
Precipitation Strengthening	Present for all.	Expected to decrease as carbides become larger and further apart – assuming no secondary hardening. BaseSiCrMoV carbides are still small and numerous.
Precipitation Strengthening (Fine Carbides)	-	BaseMoV and BaseSiCrMoV exhibit fine carbides
Dislocation Density	Present – Not measurable	Expected decrease as more carbon comes out of solid solution – Not measurable
Phase Balance	Fully Martensitic Microstructure	No change – Microstructure is still fully martensitic
Grain Size – Lath Size	Slight indication BaseSiCrMoV had wider distribution	All composition showed a slight increase to 2 hours. No significant change after. Hardness contribution will be the same for the three.

After tempering there is a significant drop in hardness for the three steels after 30 minutes tempering see Figure 97, the large decrease in hardness for Base (100 HV) more than BaseMoV and BaseSiCrMoV; this is thought to be more of the carbon coming out of solid solution. However, there is no evidence in terms of data to back this up as 2 hours and 16 hours were more extensively researched. After 30 minutes tempering there is a significant difference in hardness (100 HV) between Base and BaseMoV/BaseSiCrMoV, Figure 97.

SEM images have not been included in analysis, as TEM from Ju, 2018 was carried out from

2 hours backing up complete transformation from epsilon to cementite carbide. There appears to be a plateau in hardness from 30 minutes to 2 hours for all three steels (which again suggests that secondary hardening is not the cause as the plateau is also shown for the Base steel that does not contain any secondary hardening elements). The plateau is within the scatter in hardness values so may not be related to any metallurgical phenomena, however it may be due to spheroidisation of cementite, as there is literature evidence indicating that there is no epsilon carbide present after 400 °C for 5 minutes seconds in a Fe-0.55C-2.2Si wt. % (B.-N. Kim et al., 2012). However, data from Ju, 2018 shows that the complete change from mixed epsilon/cementite to fully cementite at 2 hours spans the plateau time.

The three steels follow the same tempering gradient between 30 minutes and 16 hours tempering. This trend then continues during tempering to 16 hours, with BaseMoV and BaseSiCrMoV having a very similar hardness, 321.2 and 320.0 HV respectively. There is no evidence of alloying elements producing a secondary hardening effect (which has been reported for tempering of martensite containing Mo as a plateau or increase in HV after approximately one hour for tempering at 600°C, discussed in section 2.7.3 of the literature review). The absence in secondary hardening is believed to be due to the amounts of alloying elements present being less than the literature values quoted for an effect to be shown, Cr-1; Mo-0.90-4 V-0.05-0.2 wt. % ((Grange et al., 1977; Irani, 1965; Irvine & Pickering, 1960; Tekin; & Kelly, 1965). This is compared to the maximum Cr-0.8; Mo-0.5; V-0.05 wt. % for the three steels. Results from Ju, 2018 do indicate that there are alloy carbides on tempering. Ju, 2018 reports the presence of needle-shaped carbides in BaseMoV/BaseSiCrMoV between 2 and 16 hours tempering, however as the carbides are so fine little difference could be determined between the two compositions, carbides are reported to be less than 100 nm and not visible using SEM (Ju, 2018). This results in similar hardness values for BaseMoV and BaseSiCrMoV, which are consistently 100 HV higher than Base, for 30 minutes temper – 16

hours at 600 °C. The presence of the needle-shaped carbides would suggest these carbides are providing additional strength to BaseMoV and BaseSiCrMoV compared to the Base, the finer carbides are discussed fully in section 5.2.1. After 16 hours tempering there is still a 100 HV difference in hardness between the Base and alloyed steels.

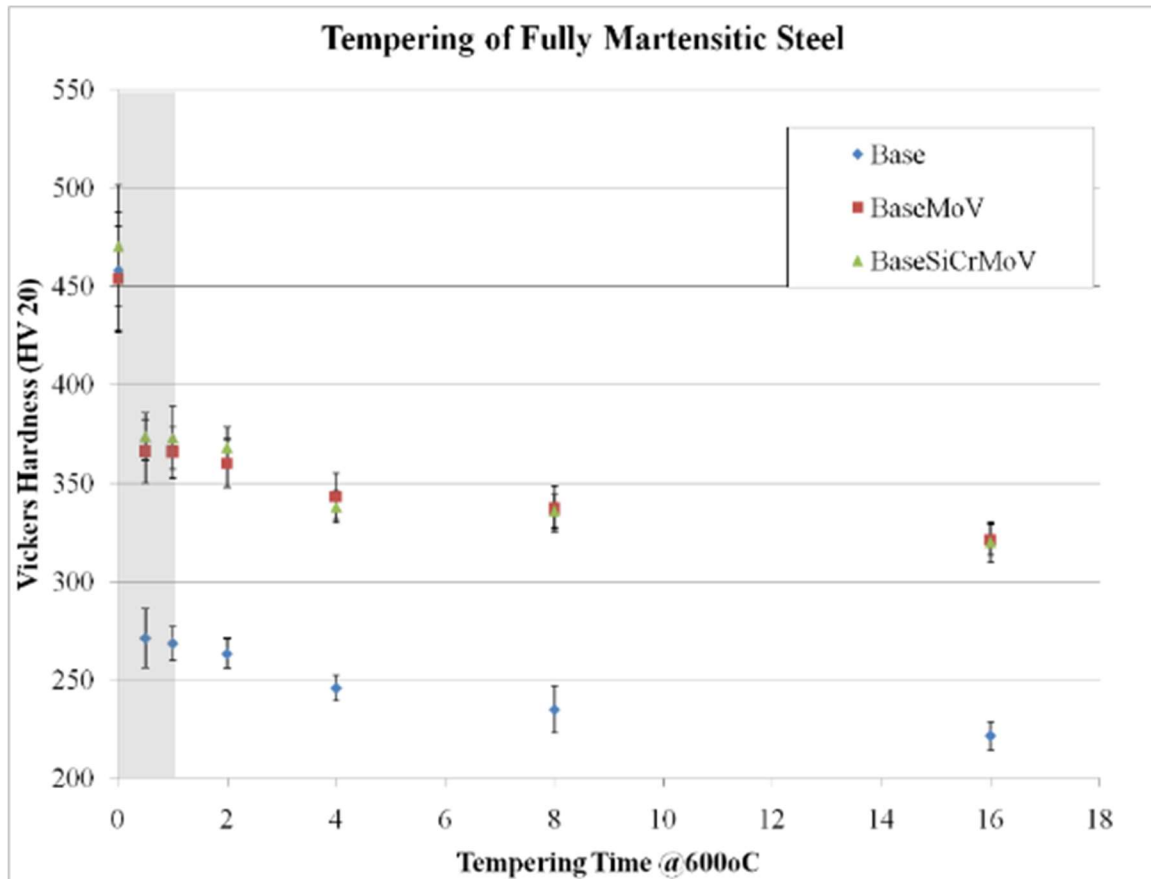


Figure 97 Change in hardness on tempering up to 16 hours (Base-BaseMoV-BaseSiCrMoV) – Grey region indicates the expected secondary hardening region based on literature reports (Baker & Nutting, 1959; Fujita, 2000; Grange et al., 1977; Kwon et al., 1997; Won Jong Nam et al., 2003; Tekin; & Kelly, 1965) Compositions C wt. % Min -0.15, Max – 0.19. Mo wt. % Min – 0.00, Max – 3.07. Cr wt. % Min – 0.00, Max – 2.25, V wt. % Min – 0.00, Max – 0.2. See section 2.7 for more details.

5.3: 100 Hours Temper

Tempering of the three compositions was carried out up to 100 hours. This was initially to see if hardness could be predicted for longer tempering times, based on the tempering response from 30 minutes to 16 hours.

5.3.1: Hardness

The experimental hardness values can be seen in [Figure 98](#), where the Base and BaseMoV have a similar hardness (185 and 190 HV respectively).

BaseSiCrMoV has a significantly higher hardness of 263 HV, which is lower than predicted but shows that the strengthening mechanisms which are present now have greater combined hardness contributions compared with Base and BaseMoV steels.

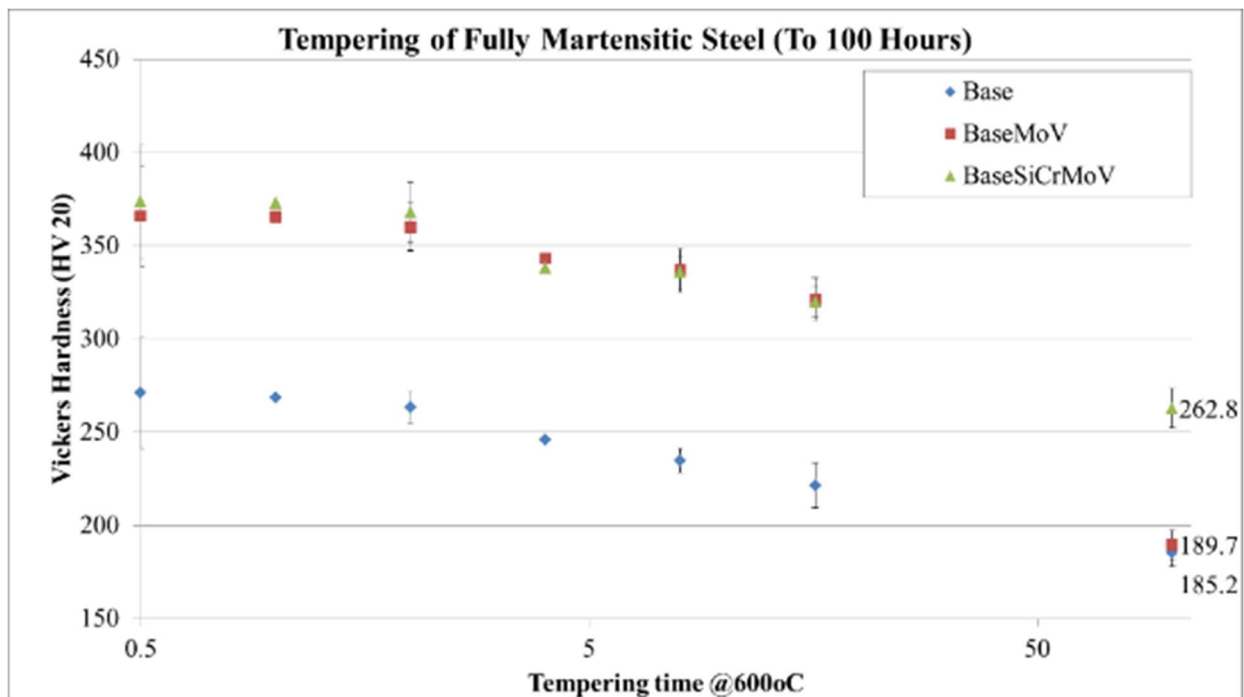


Figure 98 Hardness values after 100 hours tempering for Base, BaseMoV and BaseSiCrMoV martensitic steels

5.3.2: SEM Images

Figure 99, Figure 100 and Figure 101 show the differences between the microstructures of the three steels after tempering for 100 hours.

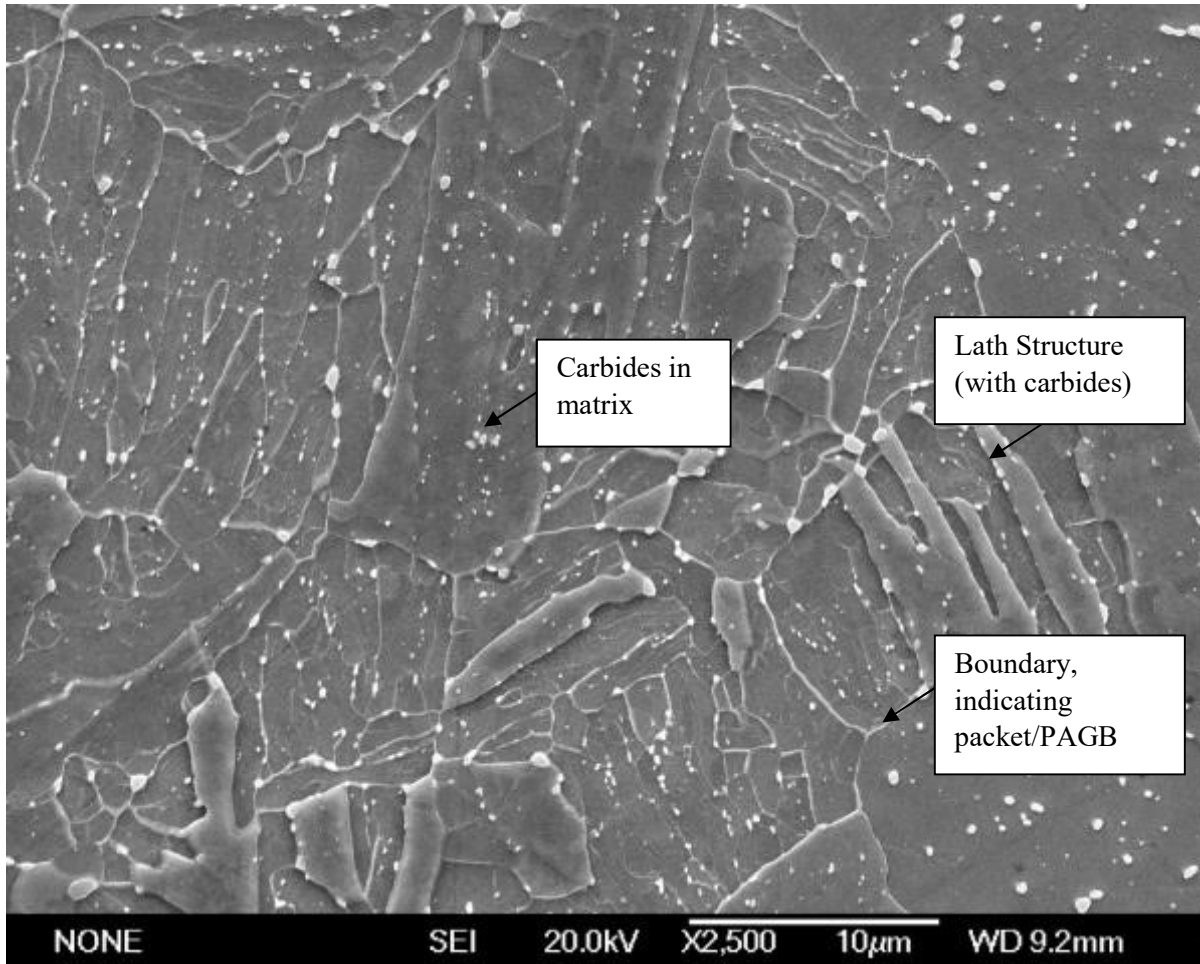


Figure 99 Base after 100 hours tempering (185.2 ± 14.5 HV)

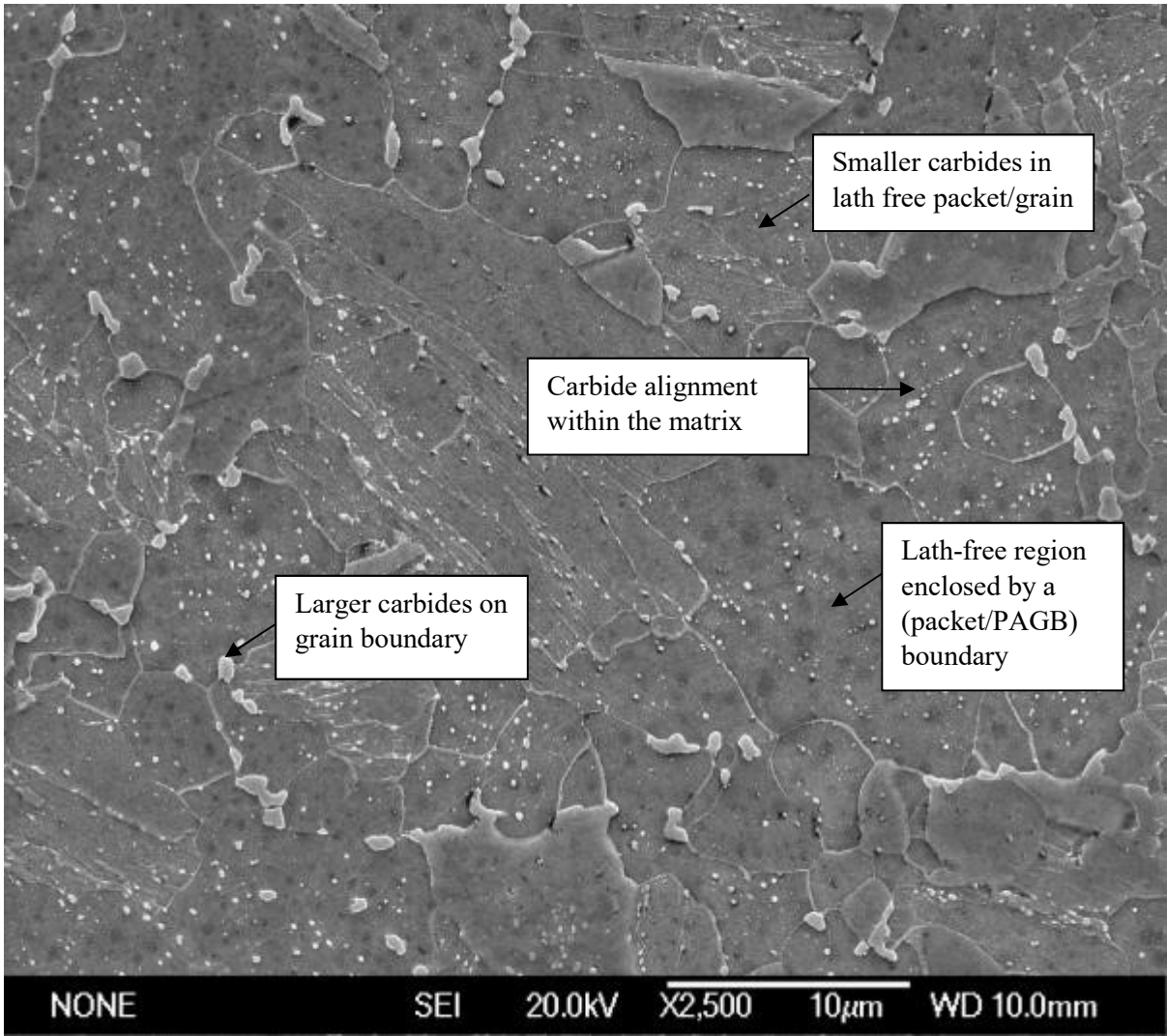


Figure 100 BaseMoV after 100 hours tempering (189.7 ± 7.3 HV)

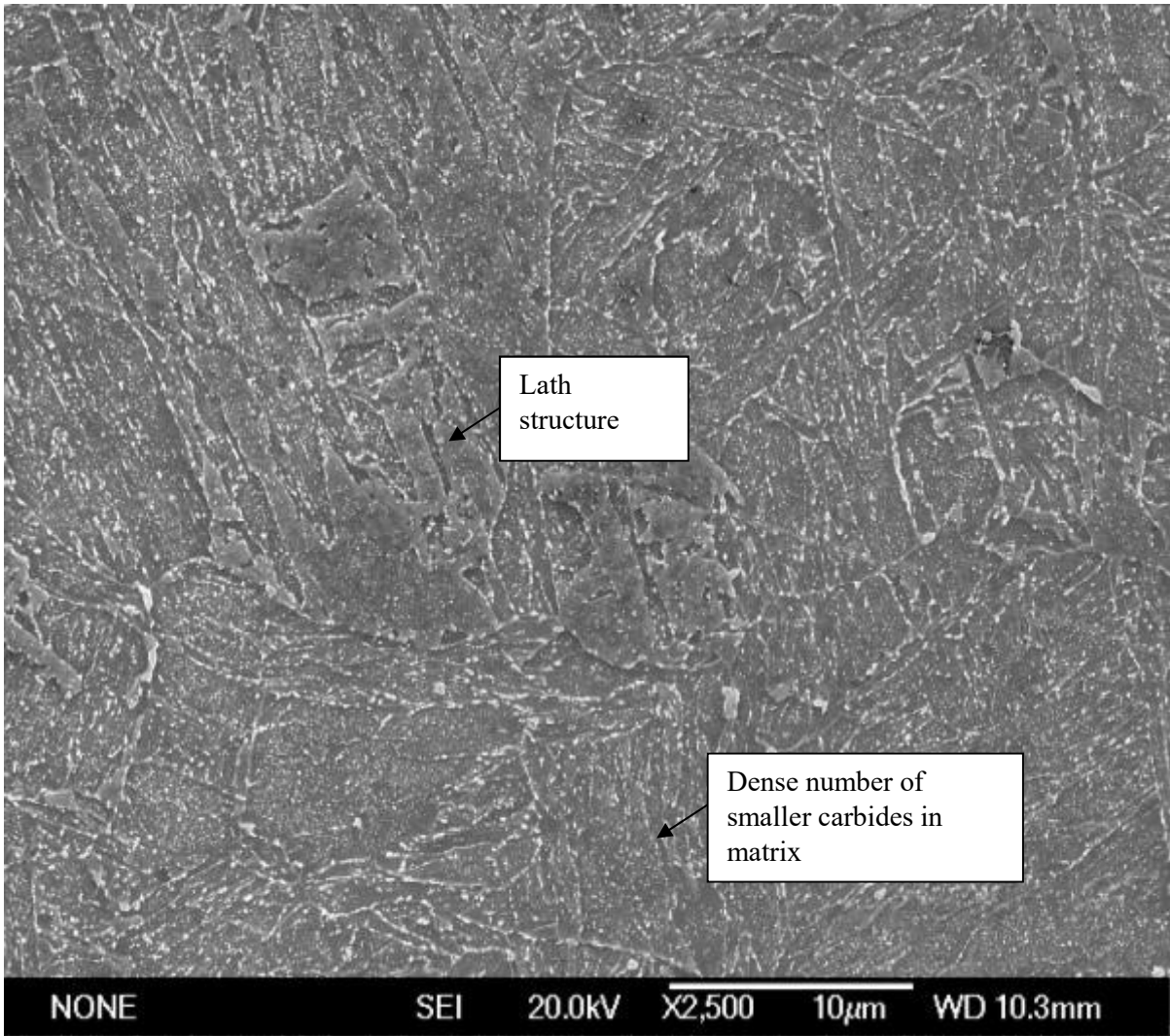


Figure 101 BaseSiCrMoV after 100 hours tempering (262.8 ± 7.3 HV)

BaseMoV shows the remnants of a lath-like structure within the packets /PAGBs, there are carbides present in the matrix of these features. The carbides in the matrix are still aligned but evidence of lath boundaries is absent implying that these (and their contribution to strength) have been lost. The carbide size distribution in the BaseMoV steel appears bimodal with coarse ($> 1 \mu\text{m}$) on the PAG boundaries and finer ($< 1 \mu\text{m}$) carbides in the grains with some evidence of remnants of a lath structure, this is based on appearance.

5.3.3: Carbides

Base does not show a bimodal split in carbide size and the PAGBs are not as delineated as shown for the BaseMoV steel, this is only based on appearance. BaseSiCrMoV has retained a much higher number density of finer carbides, and has retained a lath structure, fully detailed in [Table 33](#).

Due to time limitations the carbide sizes were not fully analysed for Base and BaseSiCrMoV. Carbide sizes were not accurately measured (due to time constraints), an approximation of carbide sizes was carried out using ImageJ, determining average carbide size and area percent of image. This method has its limitations, as it is not quantitative; however, it gives a starting basis for qualitative analysis. BaseMoV was analysed from the 100 hours mixed microstructure, but for comparison purposes it was analysed in the same manner as Base and BaseSiCrMoV in this section. [Table 33](#) may give results which are not representative of the real data values, due to inadequate numbers of size measurements; however, the area percent estimations can still be used qualitatively (as representative images are used) to identify trends to be investigated further in future work.

Using Thermo-Calc, BaseMoV is predicted to have cementite, M_7C_3 and MC carbides present at equilibrium. Data from Ju, 2018 indicates that there are smaller carbides which form on tempering (Ju, 2018). This suggests that there are alloy carbides forming independently of cementite. Kroupa, 1998 predicts $M_7C_3+M_3C / M_7C_3+MC$ for slightly longer tempering in a similar steel with 0.1 wt. % C, 0.32 wt. %V, 0.70wt. % Mo after 100 hours at 600 °C (Kroupa et al., 1998), with the longer tempering times having a similar result to Thermo-Calc for BaseMoV. This also indicates that there may be intermediate phases which Thermo-Calc has not identified, such as M_3C present in Kroupa's data but not predicted for BaseMoV at equilibrium. Visual analysis (from ImageJ) has found 20/30% of the grain boundary is covered by $1\mu\text{m}+$ carbides. In BaseMoV there is around 30 – 40% of the matrix area which is

covered by carbides, visually observed from [Figure 100](#).

BaseSiCrMoV is predicted to have four forms of alloy carbides at equilibrium (M_7C_3 , M_6C , MC , and $M_{23}C_6$), no cementite is predicted at equilibrium. Looking at [Figure 101](#) there is found to be a denser coverage from carbides in the matrix, with 80 – 90% of the total area covered and sparse boundary coverage.

As BaseSiCrMoV has more matrix area covered in carbides this indicates that there is better resistance to tempering than the other two compositions. Section 2.6.1.5 discusses that with longer tempering times there is a loss in lath structure and no carbides within laths, which results in a reduction in strengthening mechanisms.

5.3.4: Hardness

BaseMoV and BaseSiCrMoV have a difference in hardness of around 70 HV at 100 hours, whilst at 16 hours there was no significant difference. The higher number density of smaller carbides for BaseSiCrMoV compared to BaseMoV provides a reason as to why BaseSiCrMoV has a higher hardness value. This could also be a contribution from the finer laths in BaseSiCrMoV helping retain smaller carbides.

Differences in the cementite and secondary carbide compositions (Thermo-Calc shows a difference in predicted carbides) are likely to drive precipitation at the grain boundaries, resulting in larger carbides on the boundaries compared to the matrix. Data from Nam, 1999, shows that in a 0.45%C – 0.22%Si – 0.62%Mn – 0.004%P – 0.0038%S steel, tempered up to 50 hours at 700 °C, that the carbides on the boundaries were larger and remained at longer tempering times, while the particles within laths were dissolved, illustrating the difference of carbide growth at boundaries and within laths (W. J. Nam, 1999).

BaseSiCrMoV has the most alloying elements, with silicon noted in the literature to slow down the tempering of martensite; as there is no cementite predicted, it is likely to be reducing the rate at which alloy carbides form. There is predicted to be a similar volume fraction of carbides compared to Base (60-70%) and BaseMoV (30-40%) for 0.2 – 0.6 µm carbides; however, the BaseSiCrMoV carbides appear smaller and to cover a larger area (80-90% for 0.5µm and under), suggesting that preferential formation of alloy carbides, which do not coarsen, is occurring. This is based on visual examination along with Thermo-Calc predictions of the equilibrium carbides and assumes that equilibrium has been reached. Up until 16 hours there is no evidence of the additions having any more effect than that exhibited by BaseMoV. However, in [Figure 101](#) it is evident that there is a prominent lath-like structure, with small numerous carbides within the matrix.

This suggests that Si has the effect reported in the literature at the longer tempering times.

Using visual comparison, it is evident the BaseSiCrMoV carbides are smaller than those found in Base and BaseMoV and have a lower area fraction, shown in Table 33.

Table 33 Summary of carbide for 100 hours temper

Composition	Grain Boundary Carbides	In matrix
Base	Up to 1 μm carbides on boundary, with 5% being 1 μm +. Less than 10% Coverage.	Range: 0.2 -0.6 μm = 60-70% Coverage. Few carbides between 0.61 – 1 μm range (<5%).
BaseMoV	Carbide size is 1 μm +. Covering 20/30%.	Range: 0.2-0.6 μm = 30-40% Coverage. Few carbides between 0.6 1– 1 μm range (<5%)
BaseSiCrMoV	Carbide size of 1 μm + has sparse converge with 0-5% of particles	Carbide size is 0.5 μm and under. Dense coverage (80-90%).

5.4: Summary of martensitic tempering

On tempering there is a significant drop in hardness from water quenching to 30 minutes temper.

The effect of carbides on hardness is found to be the same for BaseMoV and BaseSiCrMoV, due to small numerous carbides and the presence of needle-shaped carbides, which are too small to resolve. Both BaseMoV and BaseSiCrMoV are found to be 100 HV higher than Base in the tempered condition (up until 16 hours) although they have similar hardness in the as-quenched condition, the changes in number density of smaller carbides can be used to predict this change.

Grain size is the same for the three steels. Lath size contribution is found to be the same for all compositions after 2 and 16 hours, indicating that the change in lath size occurs at the early stages of tempering. There is evidence that the Base lath size is increasing, with an increasing lath size distribution, this suggests that at 16 hours there is a difference in tempering response between the steels, however there is not a rapid decrease in hardness compared to the other two compositions, suggesting this is not significant.

It is predicted that the carbon in solid solution is at equilibrium from 2 hours onwards, meaning it will not change or have significant differences in its effect (in solution) on hardness or mechanical properties.

The changes in hardness on tempering between 30 minutes and 16 hours are determined to be from changes in dislocation density (not quantified) and changes in carbide contribution to strength, which is expected to be the main reason the alloyed steels are harder than Base.

Martensitic tempering up to 100 hours found that Base and BaseMoV have a similar hardness, while BaseSiCrMoV was found to benefit from alloying elements at longer times, with smaller more numerous carbides resulting in a higher hardness.

BaseMoV was found to have a larger coverage of large ($1\mu\text{m}+$) carbides on the grain boundaries compared to the other two steels, resulting in a loss of lath structure and ultimately strength. In comparison BaseSiCrMoV has smaller more numerous carbides, where laths are visually present.

5.5: Summary for Martensitic Microstructure

The martensite in all three steels was found to be lath-martensite, with the potential for a small percentage of lower bainite. It was referred to as lath martensite. On quenching the main difference between the compositions was the hardness, resulting from the different additions in alloying elements.

On tempering the response of Base is similar to what is documented in the literature, the hardness values decrease on tempering and carbides get larger with a larger carbide separation. Base carbides are mostly on the lath boundaries at longer tempering times, as expected. There is no noticeable difference in lath size average; however, Base has a larger lath distribution compared to BaseMoV and BaseSiCrMoV.

Between 30 minutes to 16 hours Base is 100 HV lower when compared to BaseMoV and BaseSiCrMoV who have a similar hardness. Any changes in tempering response are not noticeable from the hardness values. However, after 100 hours tempering it is found that BaseMoV has a significant drop in hardness compared to BaseSiCrMoV, which makes the hardness of BaseMoV comparable to Base. This indicates that there is a difference in tempering response during longer tempering times depending on which alloying additions are present, however the effect on hardness can only be seen at longer tempering times.

Chapter 6: Bainite

Chapter 6 examines the formation of a fully bainitic microstructure and tempering of this microstructure. To produce bainite a method was developed after testing different experimental techniques, detailed in Chapter 4. Sample sizes can also be found in Chapter 4.

6.1: Bainite Production

6.1.1: Desired Microstructure

To study a mixture of martensitic and bainitic microstructures, a fully lower bainitic microstructure needed to be produced. [Figure 2](#) demonstrates that bainite is a microstructure produced by a slower cooling rate than what is needed to produce a martensitic structure; such as a steel core cooling slower in comparison to the surface. However, the cooling needs to be fast enough to avoid the formation of undesirable microstructures such as ferrite and pearlite.

A lower bainitic microstructure was chosen instead of upper bainitic microstructure as carbon partitioning from upper bainite to the surrounding austenite would stabilise the austenite and may cause issues when later producing mixed microstructures. For example, if greater amounts of upper bainite were formed, this would result in carbon partitioning into the remaining austenite, the carbon contents of the austenite would increase and bainitic carbide precipitation would not occur before martensitic formation. That martensite would have higher carbon content and different characteristics (such as hardness and morphology), changing with the proportion of bainite this is discussed in section 2.14 of the literature review.

6.1.2: TTT Diagram

The TTT diagrams below were predicted using Bhadeshia and Babu software, [Figure 102](#), [Figure 103](#) and [Figure 104](#). The TTT diagrams each show that a fully bainitic microstructure is theoretically possible. Therefore, it was considered plausible to produce different fractions of bainite and martensite, by cooling through the bainitic region and into the martensitic region. Green lines indicate a possible cooling path to a fully bainitic microstructure with 6, 8, 11 seconds for Base, BaseMoV and BaseSiCrMoV respectively. The paths avoid the ferritic nose and avoid martensitic transformation.

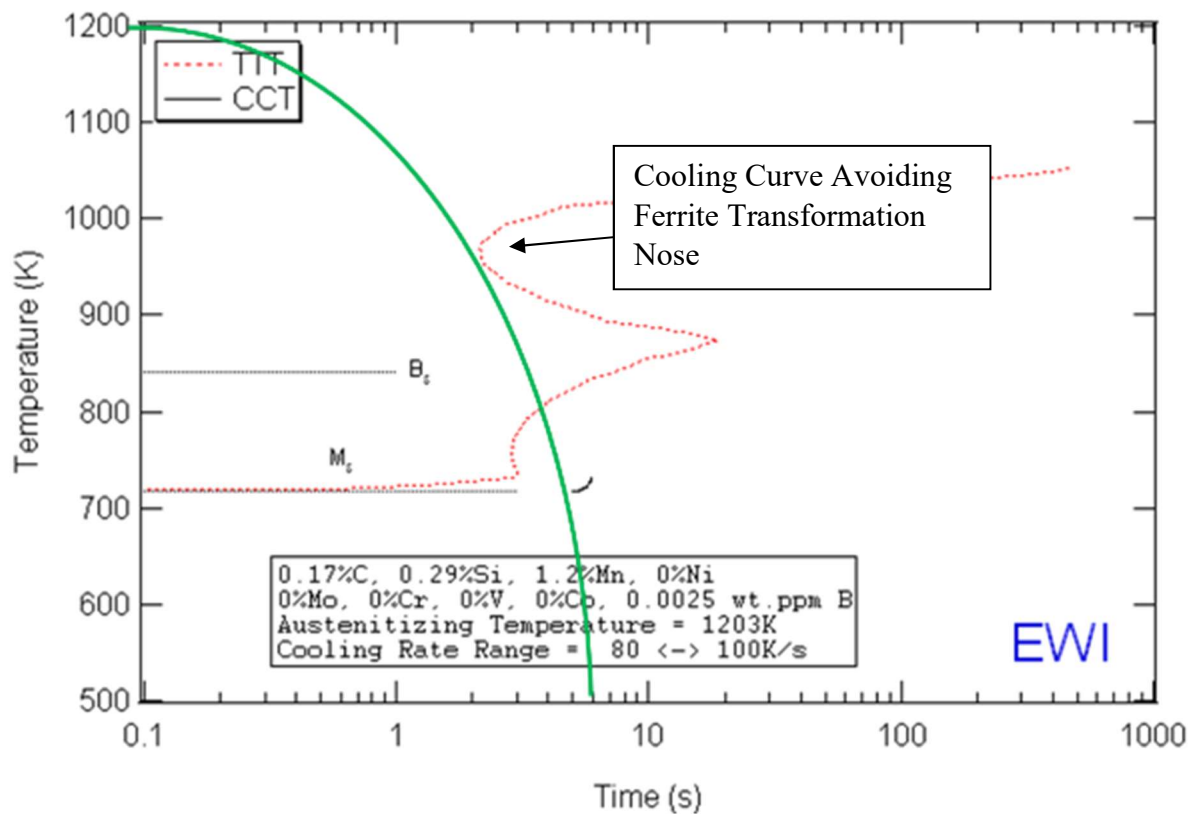


Figure 102 TTT curve predicted using Bhadeshia and Babu program for Base (H. K. D. H. Bhadeshia & Babu, 2015)

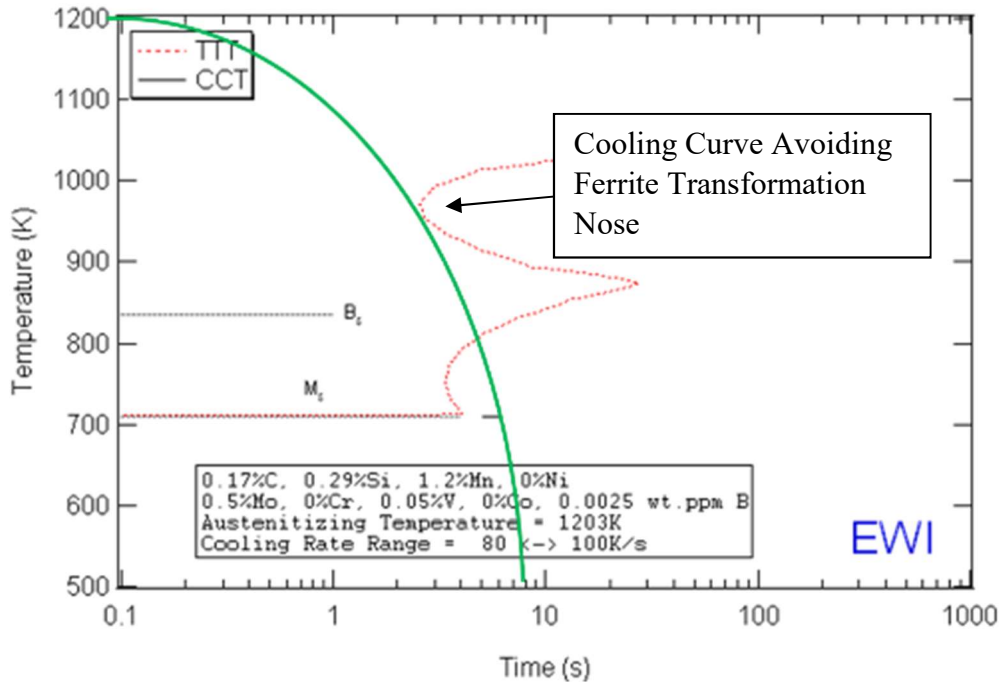


Figure 103 TTT curve predicted using Bhadeshia and Babu program for BaseMoV (H. K. D. H. Bhadeshia & Babu, 2015)

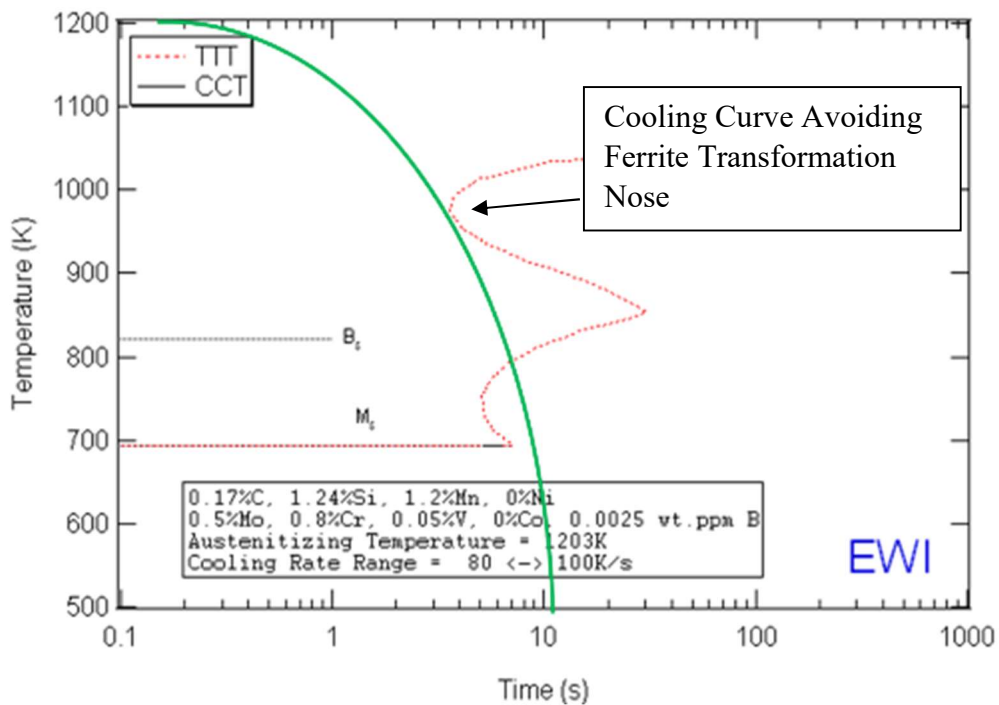


Figure 104 TTT/CCT curve predicted using Bhadeshia and Babu program for Base SiCrMoV (H. K. D. H. Bhadeshia & Babu, 2015)

6.2: Microstructural Production

The following section details the different trials in cooling used in getting a fully lower bainitic microstructure. Once satisfied that a fully bainitic microstructure could be produced then the mixtures of martensite and bainite would be produced in subsequent work.

6.2.1: Oil Quenching

Oil quenching is slower than the water quenching which gave a fully martensitic microstructure, discussed in section 5.1.

To produce a bainitic microstructure the cooling rate needed to be slower than the water quenching, therefore oil cooling was trialed to produce a bainitic microstructure. Results can be seen in [Figure 105](#).

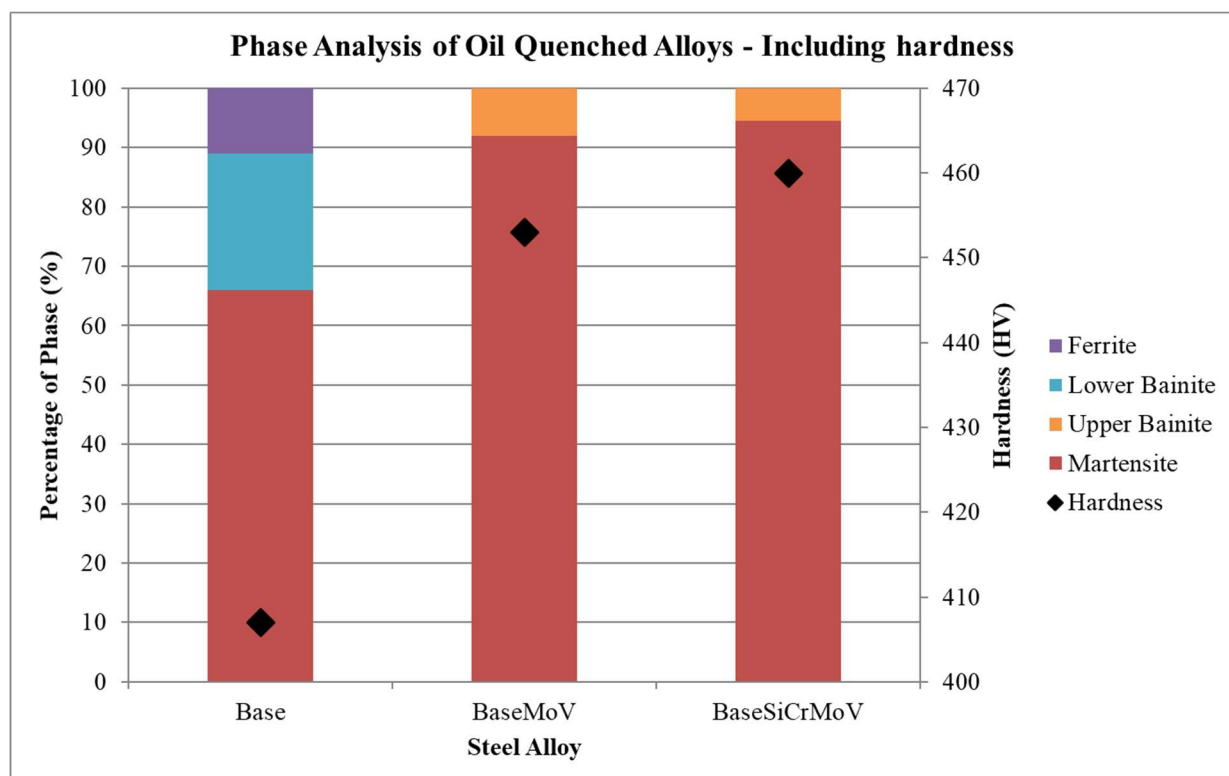


Figure 105 Phase analysis of oil quenched alloys - including hardness

Base: The oil-quenched Base sample had a hardness which was lower than that in the fully martensitic condition, 407 HV compared to 457 HV. This indicates that the slower cooling is

effective enough to change the properties of the steel, however when the microstructure was analysed there were large sections of martensite (40%), see [Figure 106](#). Bainite was present (23%), helping prove that bainite could be produced; however, a 100% lower bainite was the aim of this experimental work. There was also 11% ferrite found. When the TTT in [Figure 102](#) is observed, the cooling time needed to get a bainitic microstructure is around 6 seconds.

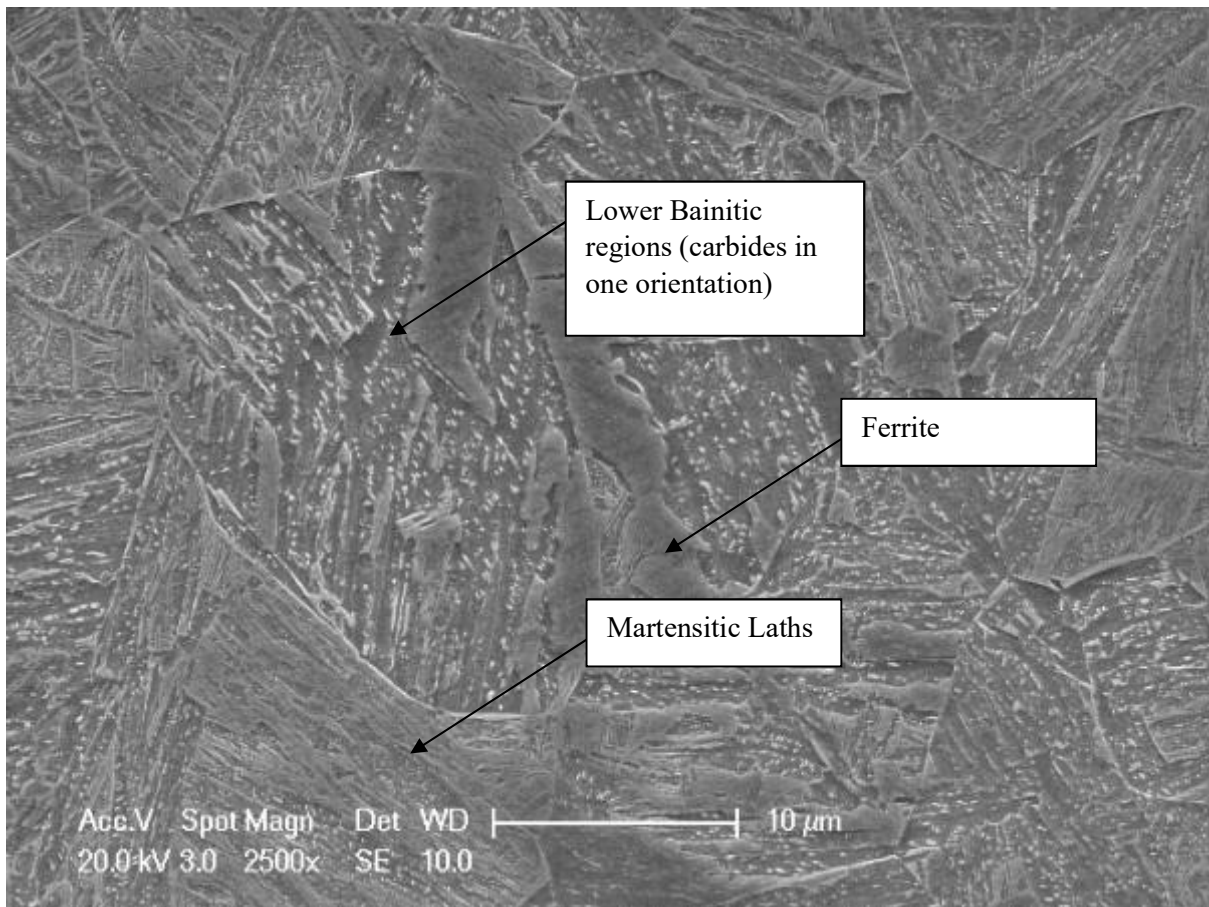


Figure 106 Base Oil Quenched (407.4 ± 32.5 HV)

BaseMoV –The hardness of BaseMoV after oil quenching was the same as after water quenching, 453 HV. BaseMoV has a higher hardenability than the comparable Base steel which means that slower cooling may still result in martensite formation. It is therefore expected that the BaseMoV would have higher amounts of martensite than the comparable Base. It was found as 90% of the microstructure comprises of martensite and 10% bainite, see

Figure 107. The identical hardness can be contributed to experimental scatter in hardness testing along with comparable microstructures.

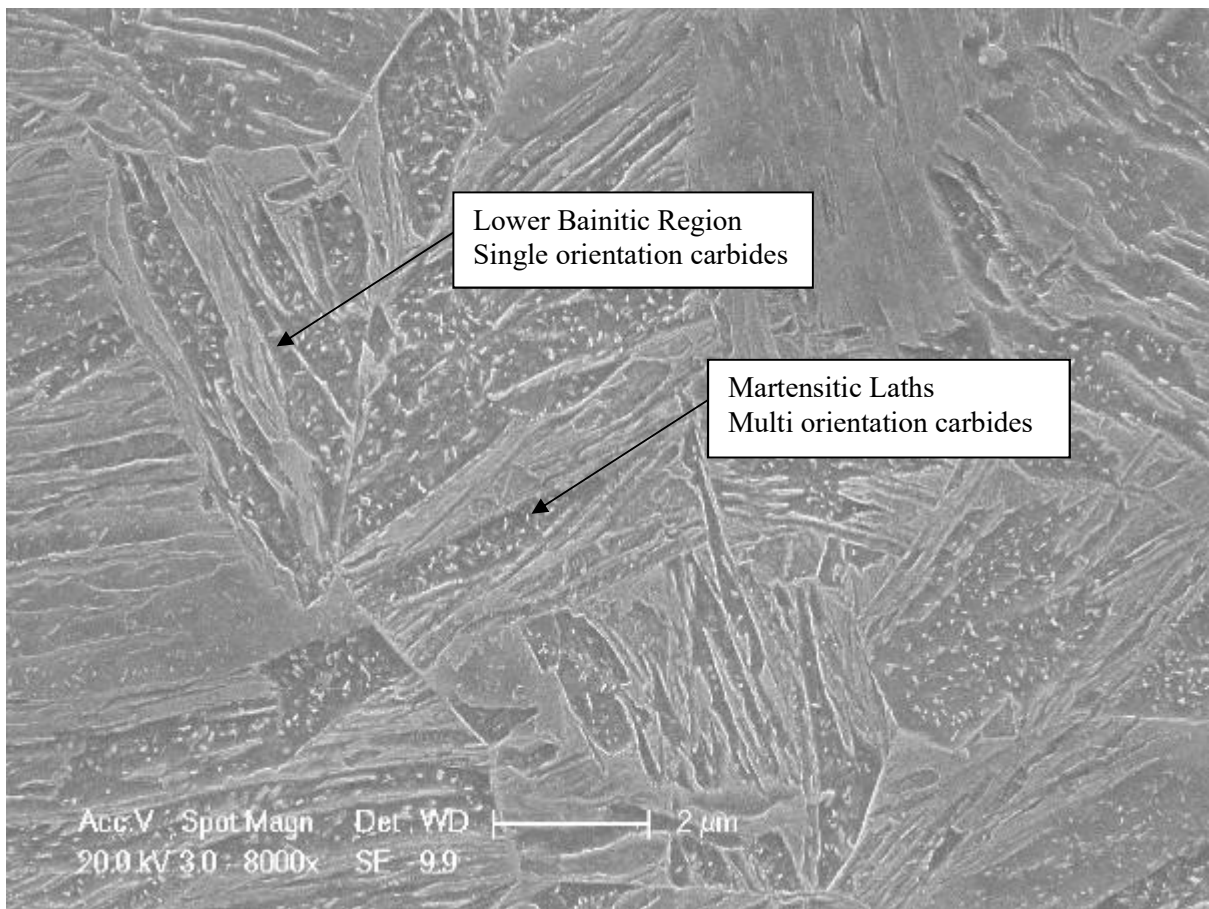


Figure 107 BaseMoV Oil quenched (453.5 ± 16.4 HV)

BaseSiCrMoV– BaseSiCrMoV had more martensite than BaseMoV, as expected, with 95% martensite and 5% bainite, see Figure 108. The hardness was 459 HV, comparable to the water quenched condition, 470 HV. Any difference in hardness can be contributed to experimental scatter and the slower cooling may produce a more auto-tempered microstructure, resulting in less strength from solid solution strengthening. This has not been investigated as the aim of this experimental work was to produce a fully bainitic microstructure, initial hardness and microstructural analysis revealed that this had not been achieved so further work was deemed not to be appropriate.

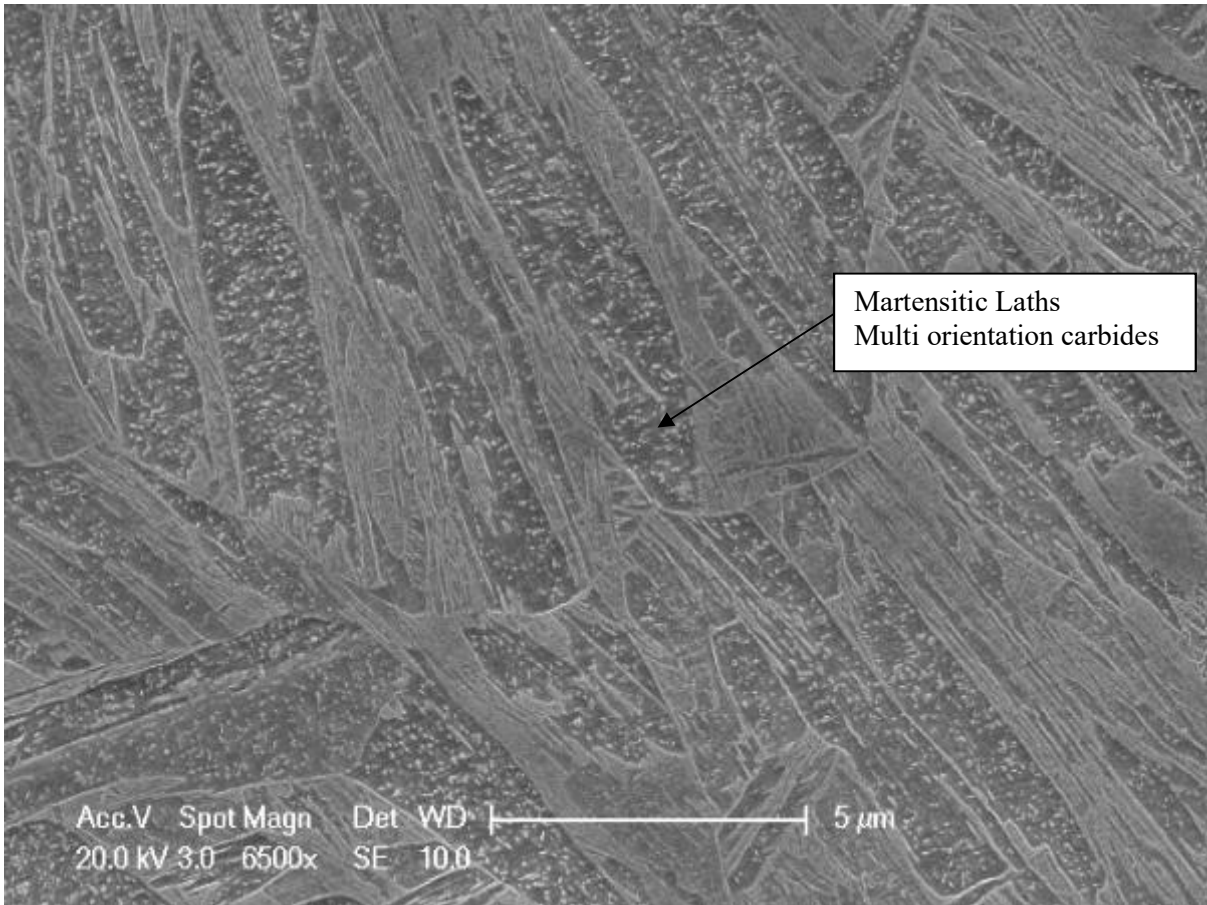


Figure 108 BaseSiCrMoV oil quenched (459.9 ± 16.0 HV)

Oil Quenching Summary –The use of oil quenching did not produce the bainitic microstructure desired for Base/BaseMoV/BaseSiCrMoV as the cooling rate was too fast and large quantities of martensite were present. Therefore, a slower cooling rate was needed to reliably produce bainite.

6.2.2: Furnace Cool

BaseSiCrMoV - has the highest hardenability therefore a trial was carried out to determine if furnace cooling could produce a bainitic microstructure and decide if this would be a suitable method for Base and BaseMoV for producing bainite.

The results are shown in [Figure 109](#); there is 60% ferrite produced, with an example of the microstructure shown in [Figure 110](#). Regions can be seen where ferrite and pearlite are at the grain boundaries and in the matrix. This method was too slow to produce bainite and therefore efforts were not focused in trialling Base and BaseMoV with furnace cooling, as they have a lower hardenability and would produce more ferrite.

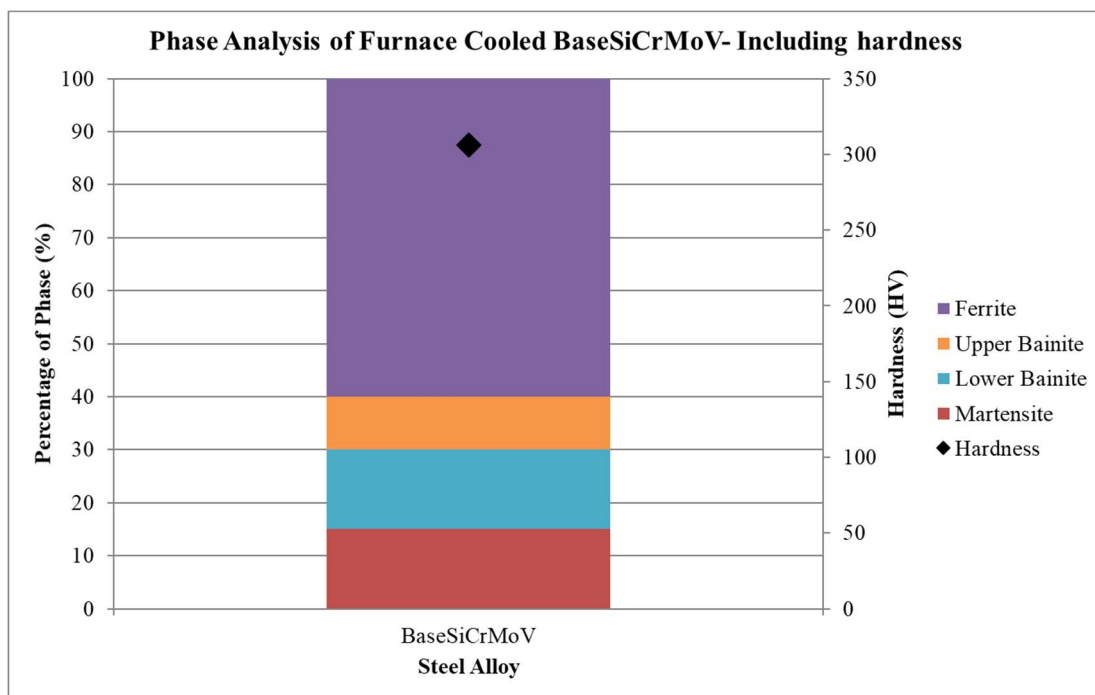


Figure 109 Phase Analysis of furnace cooled BaseSiCrMoV- including hardness

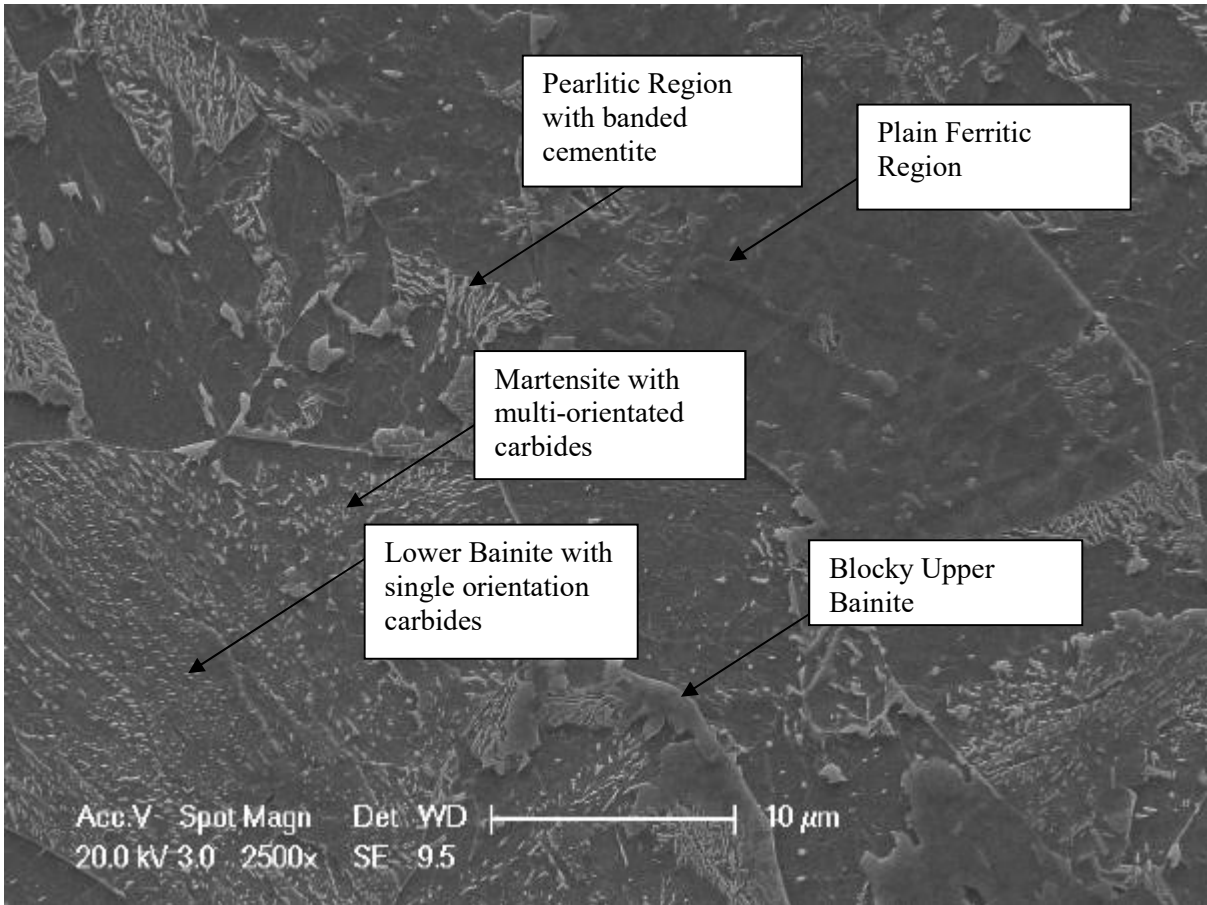


Figure 110 BaseSiCrMoV Furnace Cooled (306.3 ± 16.1 HV)

6.2.3: Air Cooling

Air cooling was the next trialled method, with samples removed from the furnace and left to cool at room temperature, microstructure analysis and hardness values can be seen in [Figure 111](#).

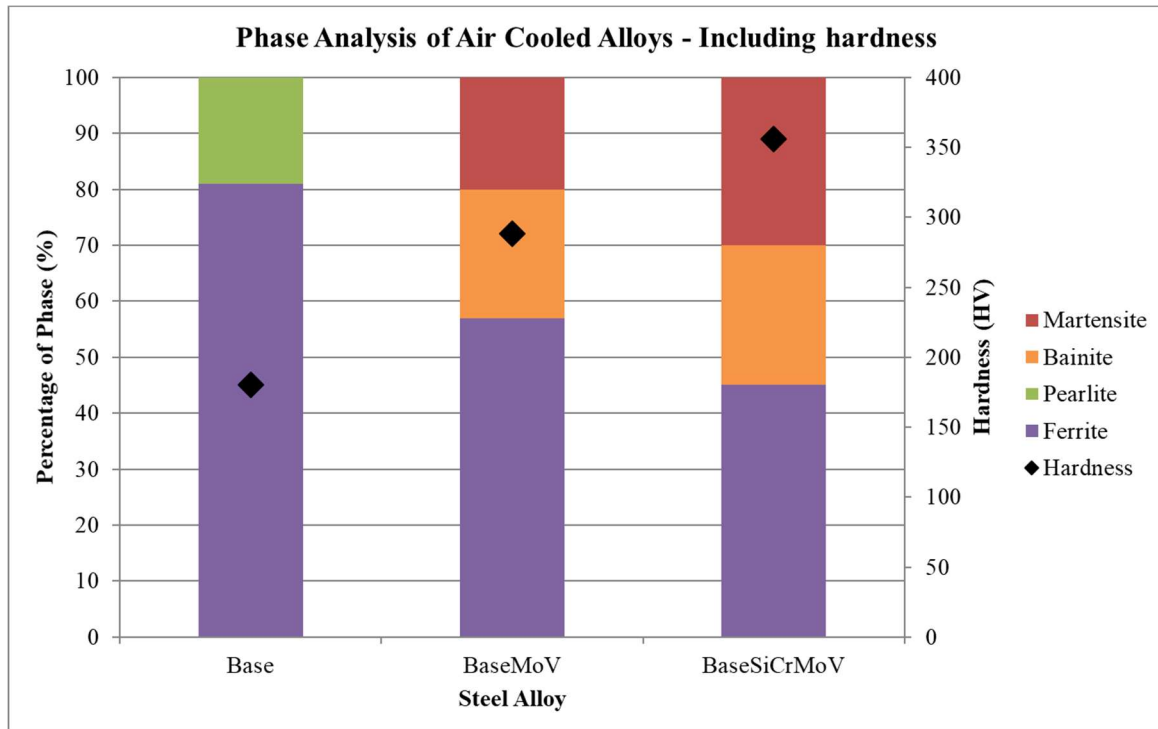


Figure 111 Phase Analysis of Air Cooled Alloys - Including Hardness

Base - The Base had a hardness of 180 HV and a fully ferritic/pearlitic microstructure, this cooling rate was too slow to produce bainite. [Figure 112](#) shows the pearlite and ferritic microstructure.

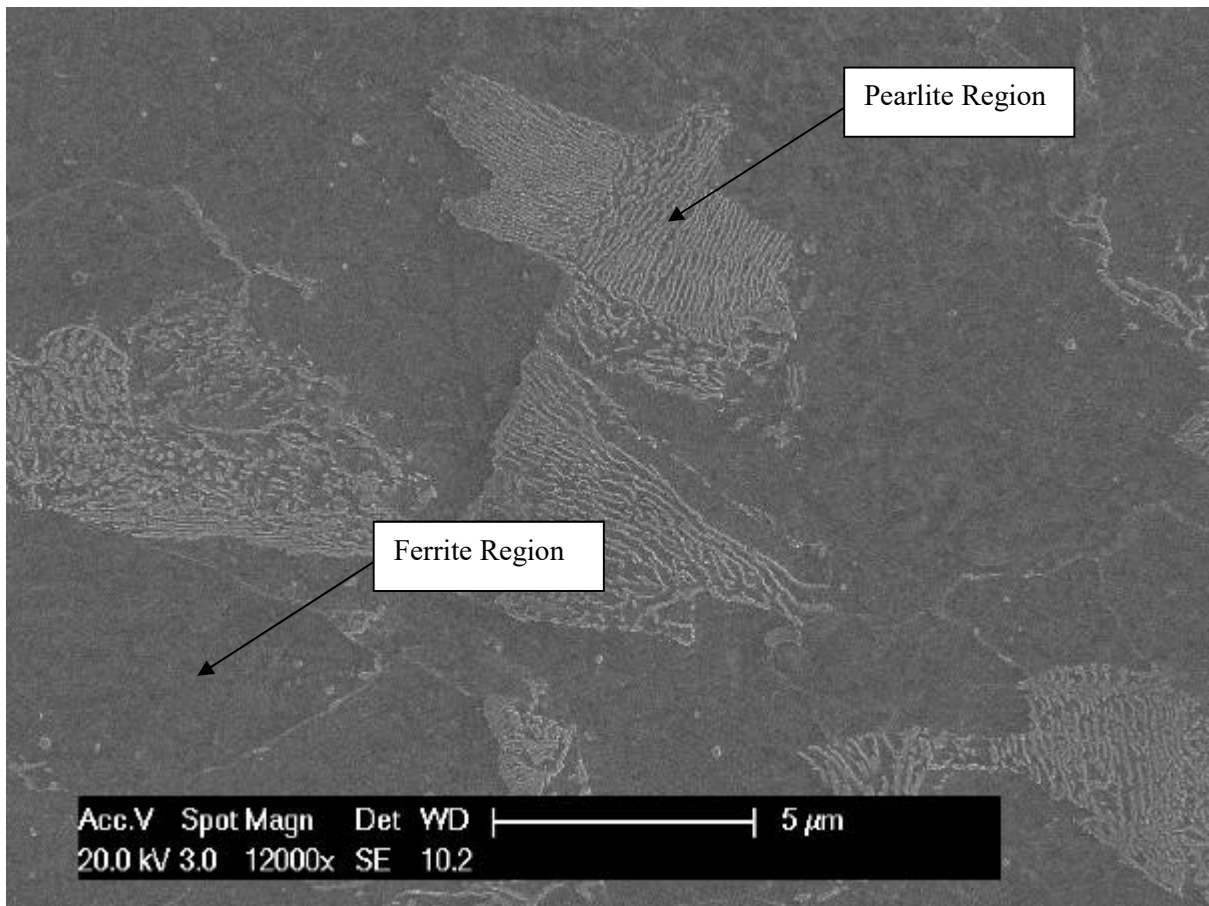


Figure 112 Base Air Cooled (180.2 ± 4.2 HV)

BaseMoV - BaseMoV had a hardness of 288 HV, higher than the Base composition, but still significantly lower than the BaseMoV after water quenching to produce martensite. The microstructural analysis shows 80% ferrite/pearlite and 20% bainite/martensite. This cooling rate is again too slow to produce the desired microstructure; this again demonstrates that there is a higher hardenability than Base.

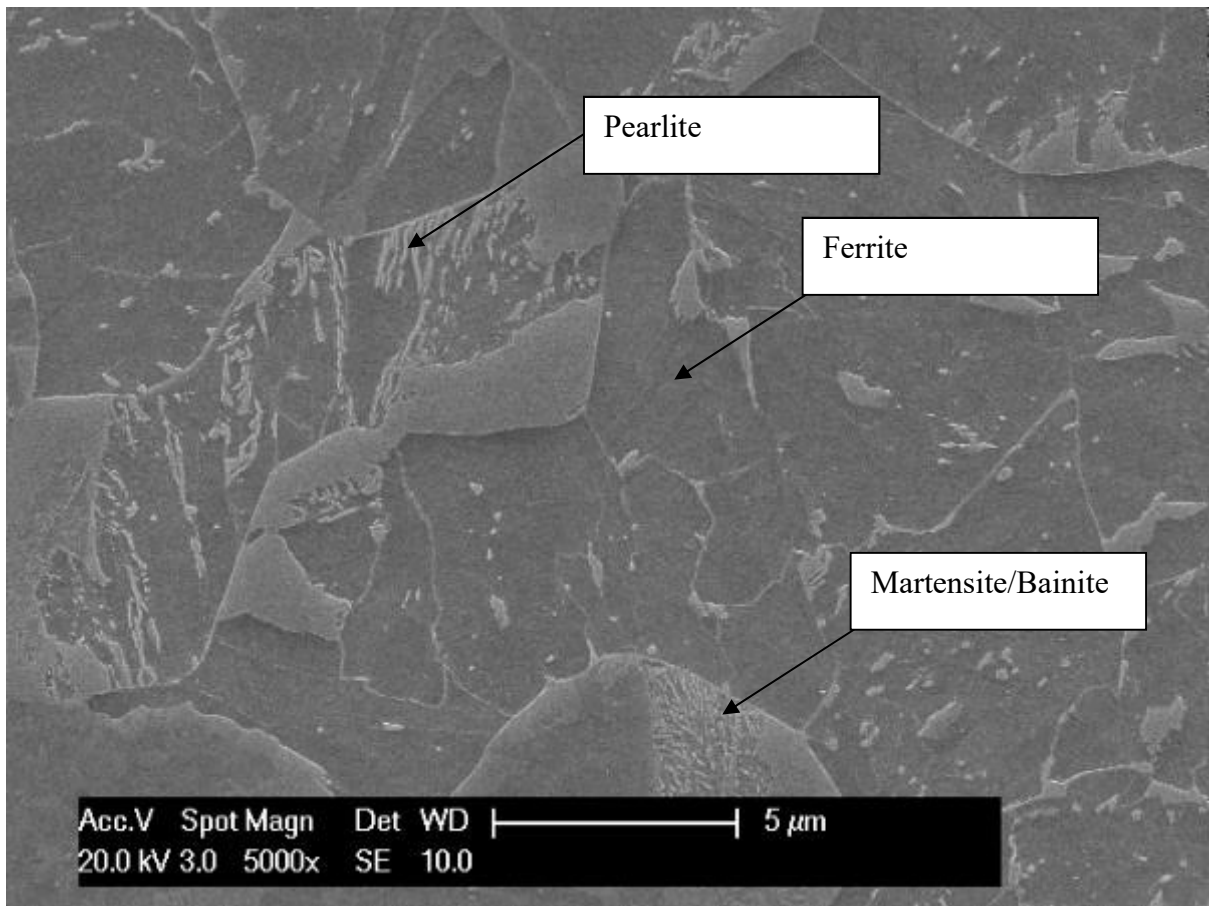


Figure 113 BaseMoV Air Cooled (288.1 ± 11.6 HV)

BaseSiCrMoV - As the sample with the highest level of alloying elements increasing hardenability, BaseSiCrMoV would be expected to have the greatest chance of having more bainite if Base and BaseMoV did not produce a satisfactory result. There was 25% bainite produced and 30% martensite; however, there was also 45% ferrite. Again, this shows the rate of cooling was too slow to produce the desired microstructure of 100% bainite. [Figure 114](#) shows that the upper bainite is growing from the grain boundaries but is interrupted by martensite/bainite formation. In this figure ferrite has been identified as having no carbides and no internal structure, while upper bainite is identified as having large lath boundaries and carbides which are aligned.

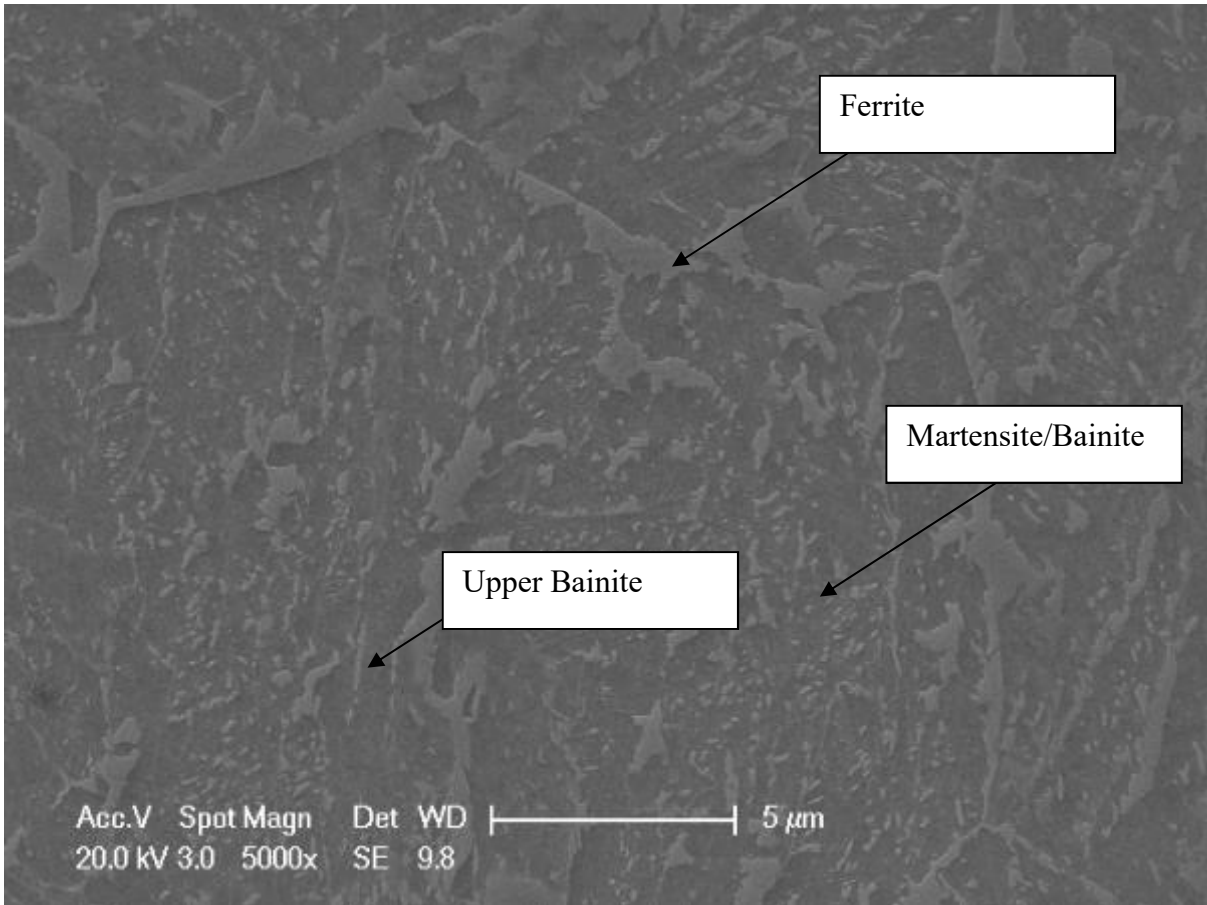


Figure 114 BaseSiCrMoV Air Cool (359.1 ± 15.2 HV)

6.2.4: Isothermal Holds

Isothermal holds were carried out, where the sample was taken from the furnace after normalisation and immediately placed in a cooler furnace, with the aim of isothermally producing bainite. The hardness results are shown in [Table 34](#).

Table 34 Hardness of Base/BaseMoV/BaseSiCrMoV after normalisation for 1 hour at 925 °C, then moved to a 500 °C furnace for 5 minutes finished with a water quench

Alloy	Hardness (HV)
Base	175
BaseMoV	461
BaseSiCrMoV	496

Placing the samples in a 500 °C furnace did not result in instant cooling as the 925 °C sample

released heat into the furnace, this increased the temperature. The cooling to 500 °C did not occur during the 5-minute hold.

Base - The Base had hardness comparable to the air cooled sample (175 and 180 HV respectively), which was mostly ferritic, image analysis was not carried out as it was unlikely to be bainitic, due to bainite being harder than ferrite. The ferritic hardness was thought to be due to the sample having a low hardenability and forming ferrite on the slow cool to 500 °C within the furnace.

BaseMoV - The BaseMoV had a hardness of 460 HV; this is similar to the water quenched martensitic steel and indicates that a bainitic microstructure was not produced. As BaseMoV has a higher hardenability than Base it is able to produce martensite with a slower cooling rate. When [Figure 102](#) and [Figure 103](#) are compared it is evident that BaseMoV can cool slower than Base without entering the ferrite nose, this means that ferrite transformation does not occur and when the sample is quenched after 5 minutes hold then there is martensite formation.

BaseSiCrMoV - BaseSiCrMoV was expected to produce the same results as BaseMoV, in terms of having hardness indicative of martensite. This did occur; however, the hardness was 496 HV, which was higher than in the water quenched martensite which had a hardness of 453 HV. The mechanism which was thought to result in this was a lower level of auto-tempering than the water quenched condition. Section 2.6.1 predicts the hardness of an as-quenched martensite with an unalloyed carbon content of 0.18 wt. % C to be ~500. BaseSiCrMoV has additionally alloying strength of 38 HV (discussed in section 5.16.1), and 0.17 wt. % C. The as-quenched condition (453 HV) exhibited auto-tempering, which would reduce the hardness. It is therefore realistic that a 0.17 wt. % C steel with alloying strengthening and no auto-tempering may exhibit a hardness of 496 HV. However, the aim of

this experimental work was to produce a bainitic microstructure, the hardness was not indicative of bainite and therefore this was not examined further.

6.3: Isothermal Holds

6.3.1: Dilatometry Isothermal Holds

After cooling trials were carried out it became evident that a fully bainitic microstructure could not be produced with conventional cooling. Therefore, isothermal holds produced by specialist instruments would be utilised. Base was not considered due to its low hardenability needing too high a cooling rate.

6.3.1.1: BaseMoV

Results from dilatometric isothermal holding, indicated that there was a completed transformation after 1 minute at 430 °C. Transformation was deemed to be complete once no further length change in the sample was detected, see [Figure 64](#). Section 2.9 discusses how the bainitic transformation is accompanied by a volume change; once the volume remains stable no more bainite is forming.

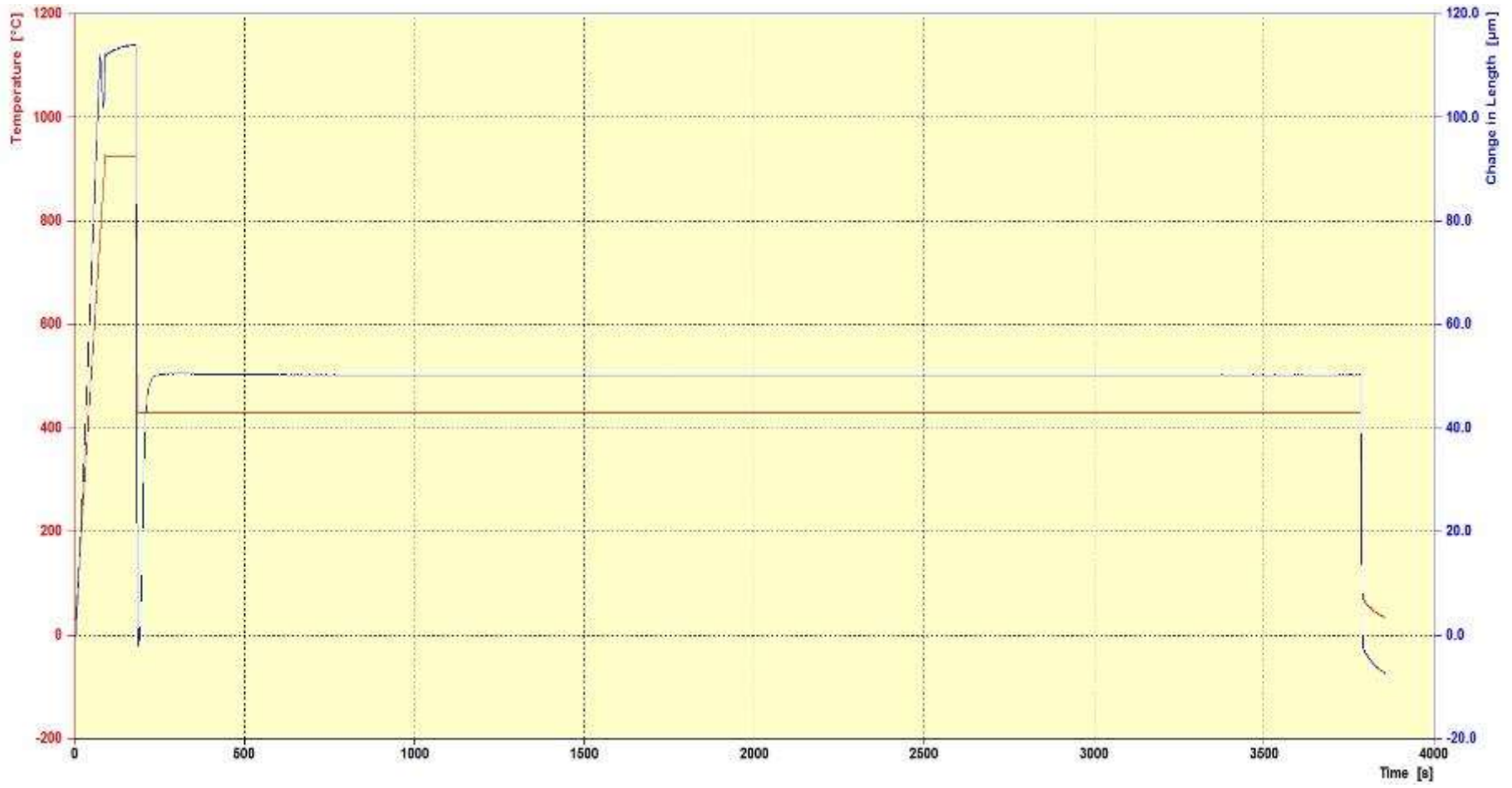


Figure 115 Dilatometry transformation of BaseMoV, with isothermal hold at 430 °C for 1 hour.

6.3.1.1.1: Gleeble Isothermal Holds

Gleeble tests were carried out at 430 °C for 5 minutes to ensure that complete transformation to lower bainite had occurred. Metallographic images were analysed and found to have 96% lower bainite and 4% of another phase, which is formed of blocky, carbide free regions Figure 116 (352 HV). This is a strong indication that the correct temperature and holding time are used for creating lower bainite. On cooling from the normalising temperature (925 °C) to the isothermal hold temperature, the cooling rate was 50 °C/s; sufficiently quick enough to avoid the formation of ferrite, which is evidenced in Figure 116, where no ferrite is detectable. Another indication that a fully bainitic microstructure is formed can be seen in Figure 117, after the isothermal hold at 425 °C the specimen is cooled rapidly to room temperature. A martensitic transformation would be evidenced by a kink in the cooling curve at the martensitic start temperature (423 °C), as it is an exothermic reaction and would slow down cooling. There is no kink evident near the martensitic start temperature, which indicates that there is no martensitic formation.

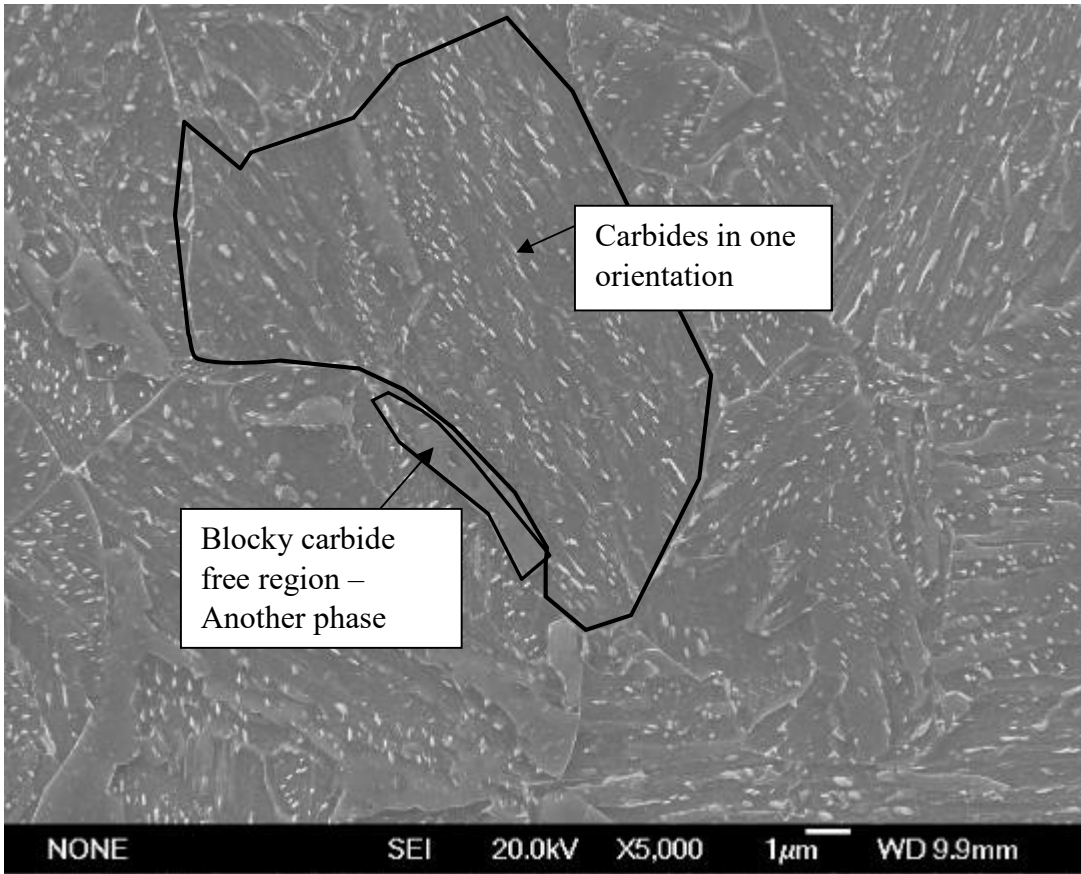


Figure 116 BaseMoV held at 430 °C for 5 minutes (351.5 ± 4.0 HV)

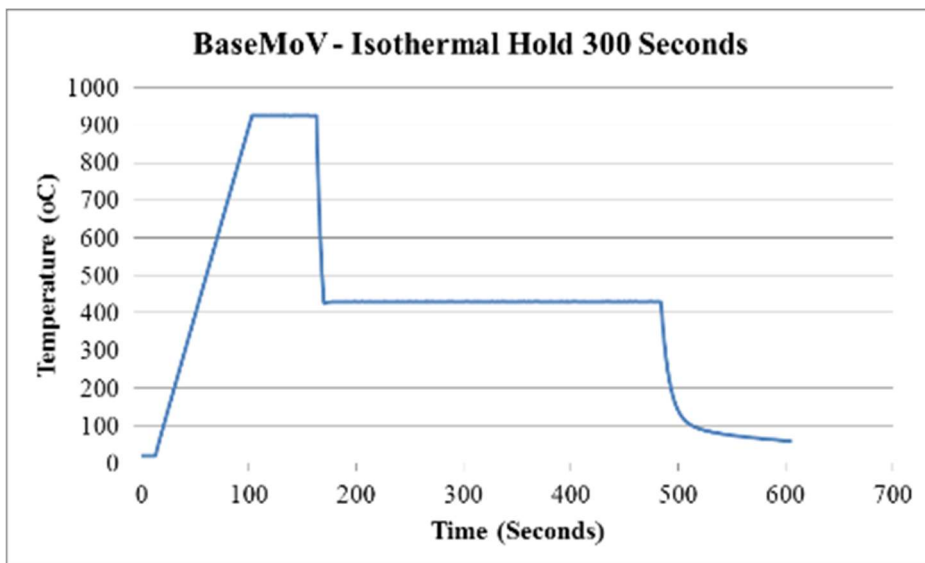


Figure 117 300 (5 minute) second isothermal hold of BaseMoV at 430 °C

6.3.1.1.2: XRD

XRD was carried out to determine if there were any FCC phases present which were not identified in the microstructural analysis. This would identify if complete FCC to BCC transformation occurred and confirm no retained austenite was present.

Retained austenite has an FCC structure and therefore would produce peaks overlapping the BCC structure. The most intense peak would be expected at the (111) peak, which has a peak 1-2 angles before the ferrite (110) peak. In this instance it would mean that there would be a small peak present just before the peak at the 49 angles. An example of a FCC peak is shown in [Figure 118](#) for a 0.35 wt. % C low alloy bainitic steel (Talebi et al., 2018). BCC peaks are shown in [Figure 119](#) and [Figure 120](#). There are no peak at the 49-theta position and therefore the amount of retained austenite is not significant. It is noted that the lack of FCC phase could be a result of crystallographic orientation and texture (Pashangeh, et al., 2019).

XRD was carried out to determine what the other phase present may be. There was no evidence of retained austenite and therefore the other phase was determined to not be significant and the microstructure produced from the isothermal hold was referred to as lower bainite.

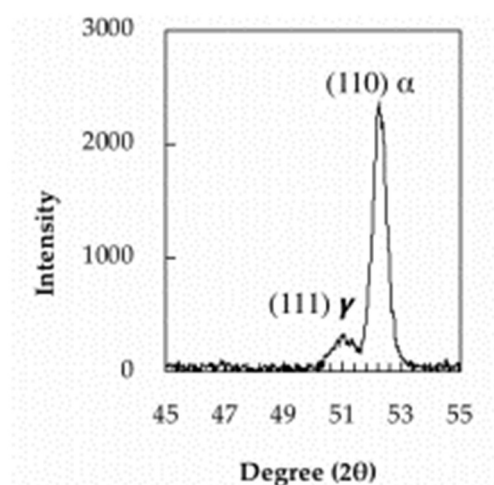


Figure 118 (111) – FCC peak and (110) – BCC peak in a 0.35 wt. % C low alloy bainitic steel (Talebi, Jahazi et al. 2018)

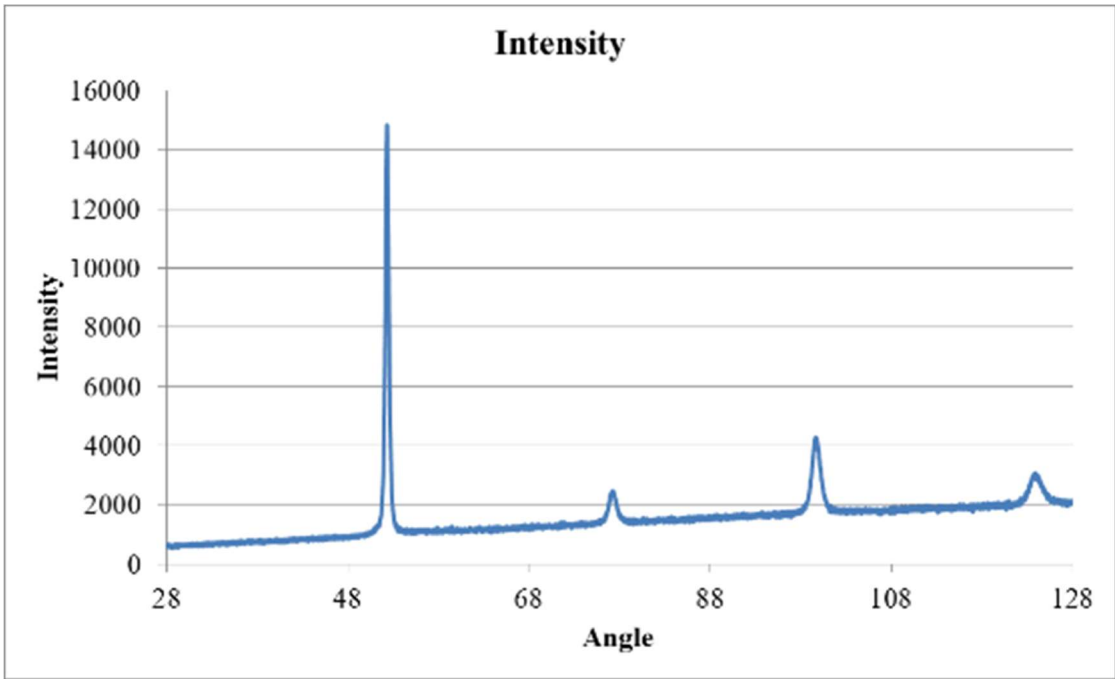


Figure 119 XRD pattern of BaseMoV held for 430 °C for 5 minutes

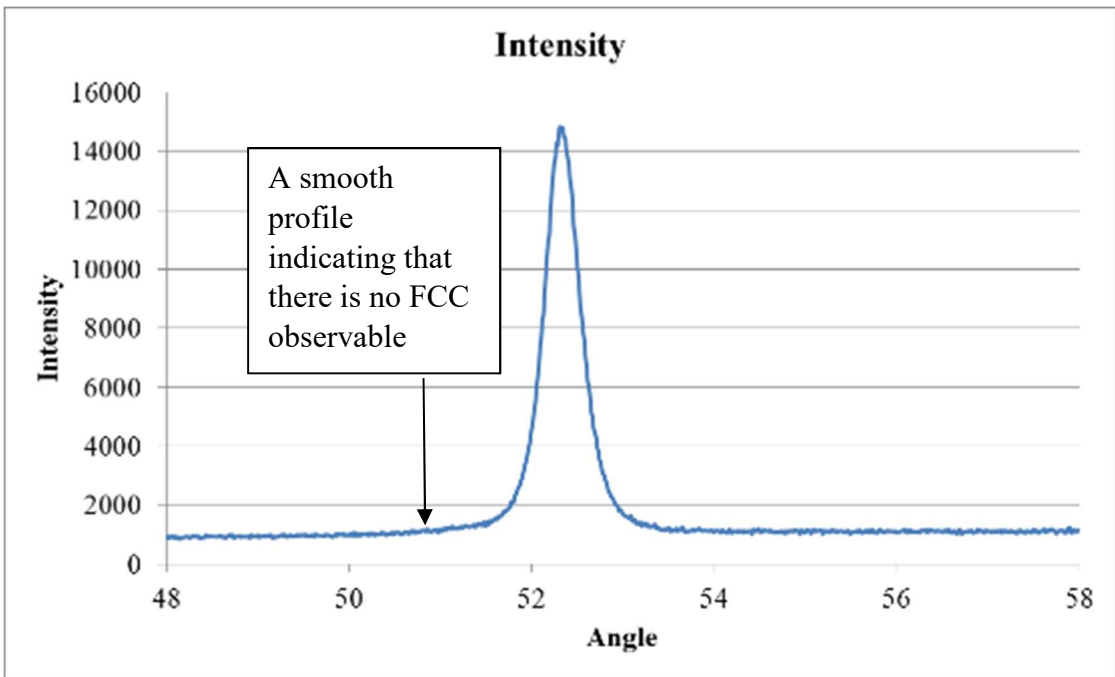


Figure 120 XRD pattern of BaseMoV held for 430 °C for 5 minutes

6.3.2: Dilatometry Isothermal Holds

6.3.2.1: BaseSiCrMoV

To produce a fully bainitic microstructure an isothermal holding temperature was determined using the predicted Ms Temperature (423 °C), and the sample was held above this temperature to avoid any inaccuracies from the equation, which may result in unwanted martensitic transformation. Using the Steven and Haynes equation (Chapter 2.9, equation 2.5), the Bs temperature was found to be 574 °C, so an isothermal hold temperature of 441° C was found to be within a region expected to form lower bainite. It is also important to note that a rapid cooling rate after normalisation is needed to avoid ferrite formation. Bainite isothermal holds can then be carried out, without another microstructural phase present.

6.3.2.1.1: Gleeble

BaseSiCrMoV was held at 441 °C for 15 minutes and subsequent phase analysis found 59% lower bainite/41% of another phase, thought to be retained austenite/ferrite, see example in Figure 121. The hardness results of 268 HV was lower than the bainite produce for BaseMoV (352 HV), highlighting issues in producing a completely transformed bainitic microstructure in BaseSiCrMoV.

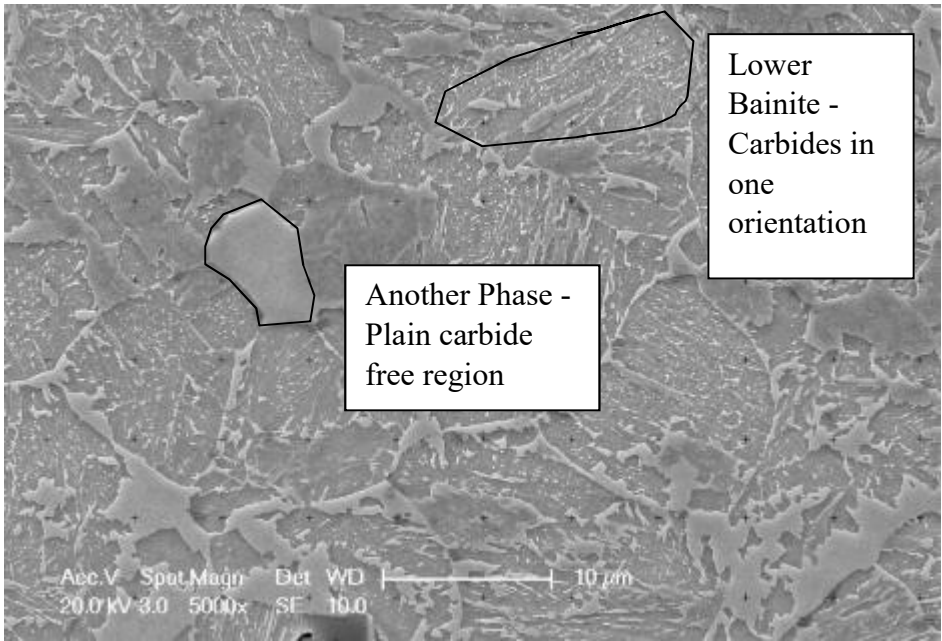


Figure 121 BaseSiCrMoV held at 441 °C for 15 minutes (268.0 ± 9.0 HV)

Another isothermal hold was carried out at 441 °C for 60 minutes, producing 43% lower bainite/57% of another phase, see [Figure 122](#) (368 HV). The difference in microstructure analysis shows a variety of microstructures formed but the higher hardness value indicates that there is a harder phase present.

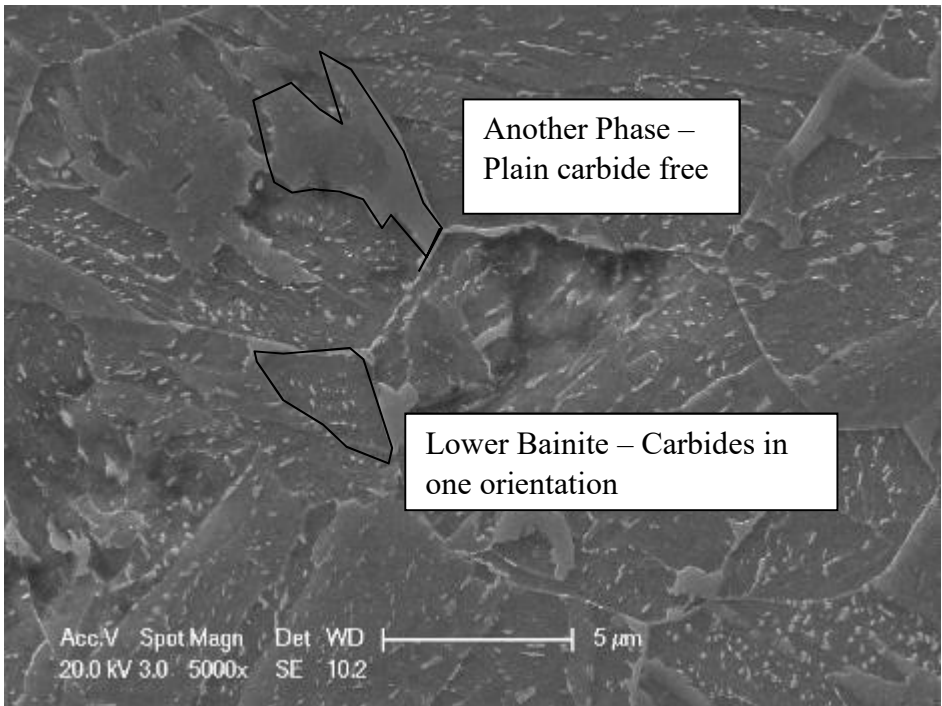


Figure 122 BaseSiCrMoV held at 441 °C for 60 minutes (368.4 ± 16.0 HV)

6.3.2.1.2: XRD

It was thought that there was a considerable amount of retained austenite in the 15 minutes hold, due to the lower hardness; this was tested for using XRD, see [Figure 123](#) and [Figure 124](#). The results of this did not find conclusive proof of retained austenite; however, there is an indication around 51° that there may be small quantities of an FCC structure, indicative of retained austenite. The intensity of the peak is not significantly higher than the baseline. Liquid nitrogen quench was also used to further investigate if there is any retained austenite, discussed next.

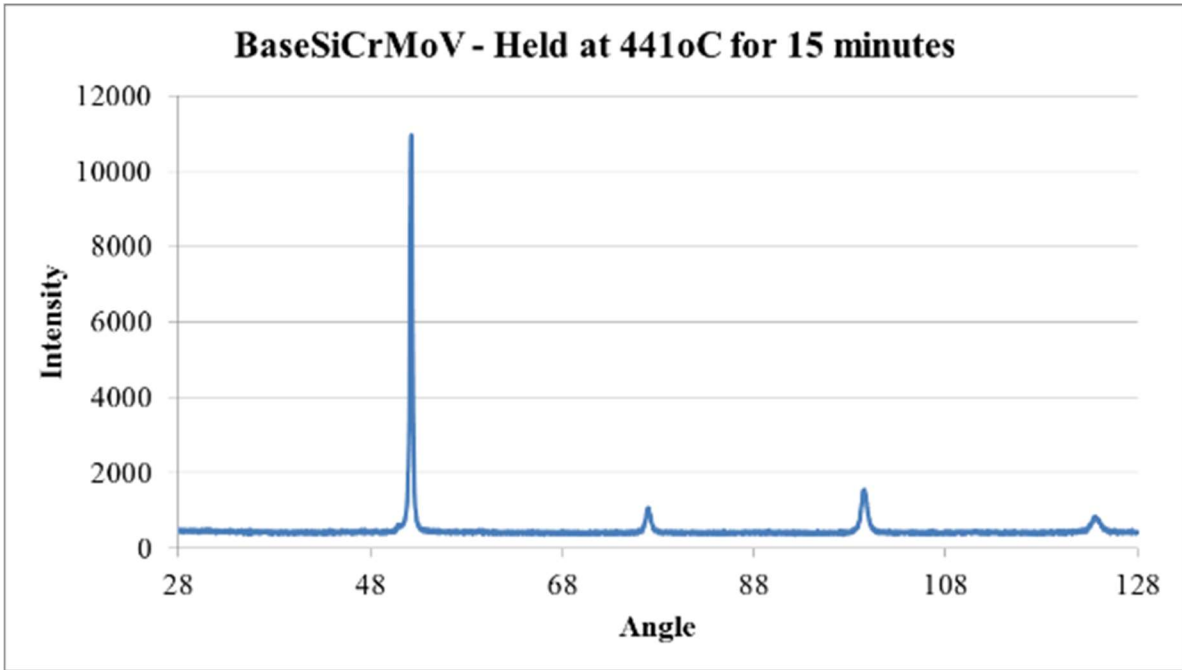


Figure 123 XRD pattern of BaseSiCrMoV held at 441 °C for 15 minutes (Angle 28-128)

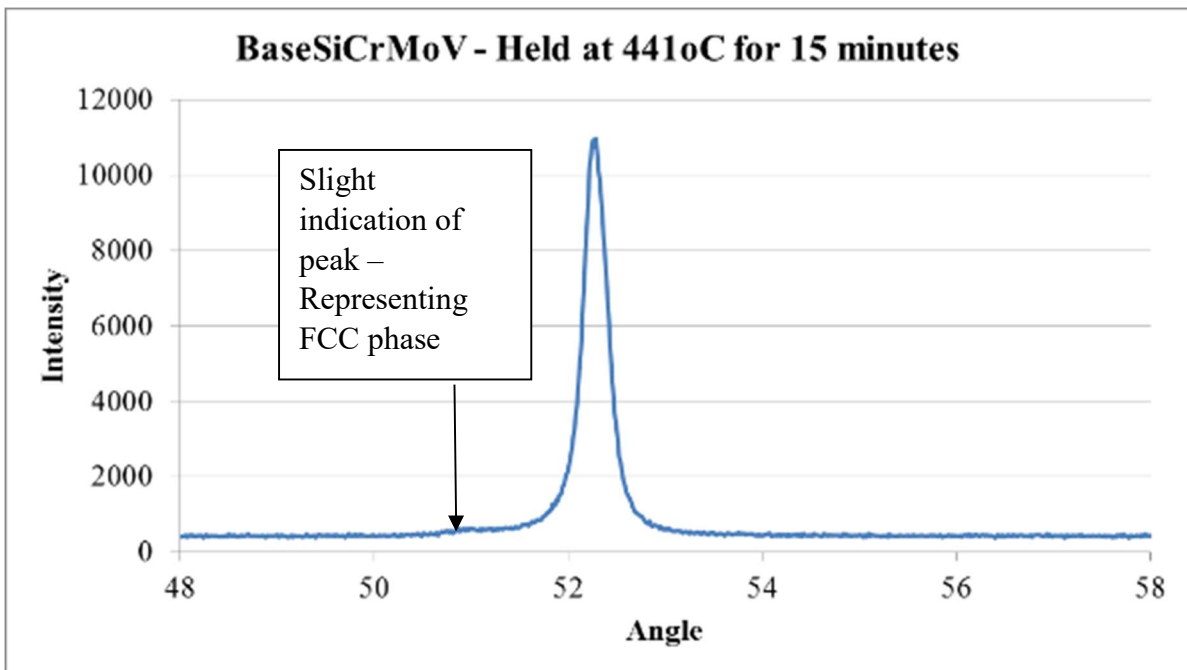
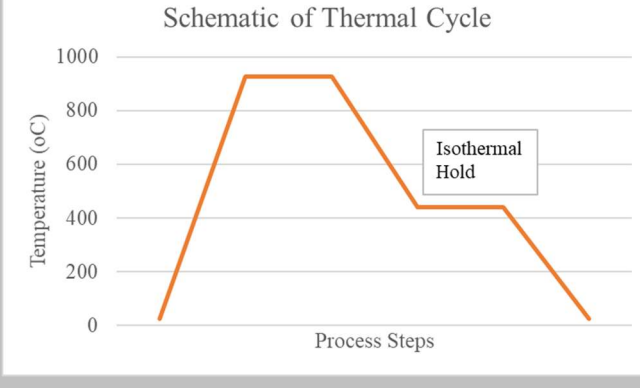
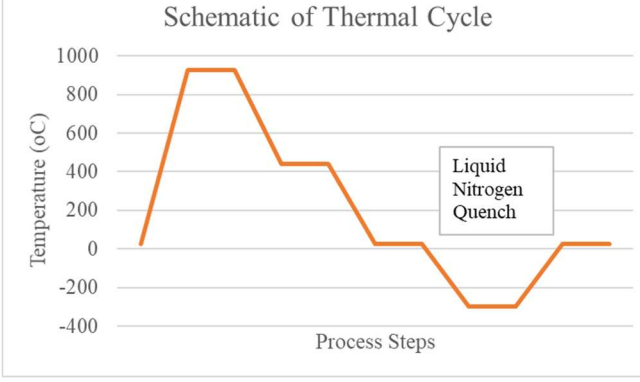


Figure 124 XRD pattern of BaseSiCrMoV held at 441 °C for 15 minutes (Angle 48-58)

6.3.2.1.3: Liquid Nitrogen Quench

The 15 minutes at 441 °C samples were quenched into liquid nitrogen; this reduced the temperature below the M_f temperature and produced a fully transformed microstructure. The evidence that the microstructure had fully transformed was that the hardness increased by ~110 HV, indicating a hard martensitic phase, see [Table 35](#). The introduction of the liquid nitrogen quench significantly increased the room temperature hardness of the steel; this can only occur from phase transformation in this case it would be austenite to martensite. This means that the microstructure has a mixture of upper bainite and austenite; transformation from austenite is not complete.

Table 35 Comparison between BaseSiCrMoV – 15 minutes at 441 °C followed by air cool and air cooled with subsequent liquid nitrogen quench

Sample / Condition	Hardness (HV)	Schematic of Thermal Cycle
BaseSiCrMoV – 15 minutes at 441 °C followed by air cool	268 ± 9	
BaseSiCrMoV – 15 minutes at 441 °C followed by air cool, and subsequent liquid nitrogen quench	382 ± 17	

6.3.2.1.4: XRD discussion

The 1-hour hold was not tested with XRD as the holding time was not practical for the number of repeated samples needed for this project. The long holds are demanding on the Gleeble and there is an increased chance of thermocouples decoupling, resulting in data which cannot be used and wasted material. Neither the 1 hour hold, nor the 15 minute hold produced a fully lower bainitic microstructure. The areas of blocky, carbide-free microstructure were determined to be from the addition of Si to the composition. It was found in the literature that it can retard the formation of cementite, which would result in the plain carbide-free microstructure, as discussed in section 2.8.3.

6.4: Production of lower bainite - Summary

Base was determined not to be a viable composition for the reliable and repeatable production of bainite. Base was able to form mixtures of different microstructures, but its low hardenability means that cooling rapidly enough to a bainitic isothermal hold temperature is challenging. It would be desirable to produce a fully bainitic Base microstructure and determine the different affects the alloying elements have compared to the Base martensitic structure, but this was not possible.

BaseMoV was a suitable alloy combination to produce a fully lower bainitic microstructure; this was achieved using isothermal holds. The Gleeble was the equipment which was most readily available, so this was used to produce future bainitic samples and subsequent martensitic/bainitic mixtures.

BaseSiCrMoV was not able to form a fully bainitic sample using a Gleeble isothermal transformation. The bainite produced was upper bainite, however there was retained austenite present, due to the Si addition retarding the formation of the cementite carbides within the matrix. This means that varying the volume fraction of bainite would alter the nature of subsequent martensite in mixtures.

6.4.1: CCT Diagram

A CCT diagram was produced for the BaseMoV. The CCT diagram in [Figure 67](#) shows that a cooling rate quicker than 21 °C per second would produce a martensitic microstructure. The CCT diagram also provides further confirmation that lower bainite was produced from the isothermal hold temperatures, as holding at 430 °C would produce a microstructure within the bainitic region.

6.5: Analysis of lower bainitic microstructure

6.5.1: Bainitic Carbide Size

Bainitic carbide sizes are shown in [Figure 125](#); these are for equivalent circle diameter (ECD), as they have been calculated using the carbide area. [Figure 126](#) shows the carbides are lenticular and in the same orientation within laths and is a further indication that lower bainite has been obtained. The ECD average of the carbides is 401 - 450 nm, this is larger than the carbides in the martensitic microstructure after quenching (section 5.1.1).

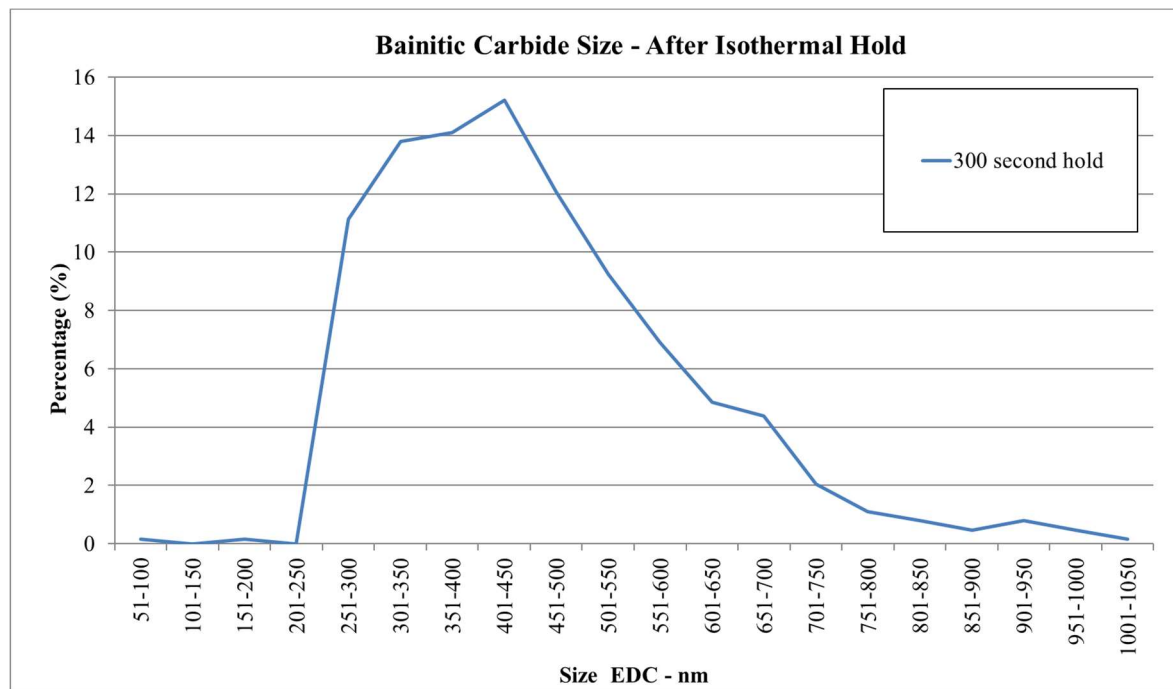


Figure 125 Bainitic Carbide Size - After Isothermal Hold

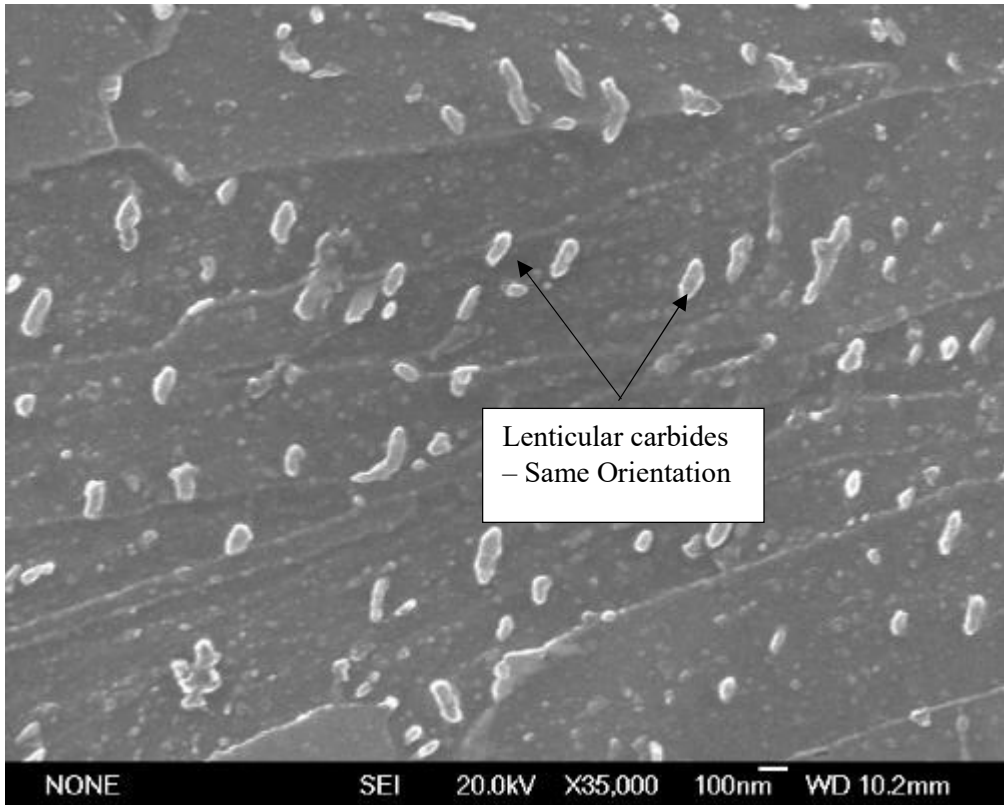


Figure 126 BaseMoV isothermal hold for 5 minutes, showing carbide size and orientation

6.5.2: Bainitic Lath Size

The lath size of the 5 minute isothermal hold BaseMoV was investigated and compared to that in the water quenched martensitic sample. The two microstructures have the same mode of 0.31 – 0.40 μm , however the isothermally held sample has a distribution towards a wider lath size when compared with the martensite which was water quenched.

Lath size is determined by factors such as carbon content, chemical driving force, interfacial and strain energy. When [Figure 46](#) in section 2.13, is observed it is expected that the difference in lath size is 50 nm between 0.15 and 0.2 wt. % C. As BaseMoV has a C composition of 0.17 wt. % C and lath size bins have an associated error of $\pm 0.3 \mu\text{m}$ then it would not be possible to estimate sizes as accurately for different carbon contents.

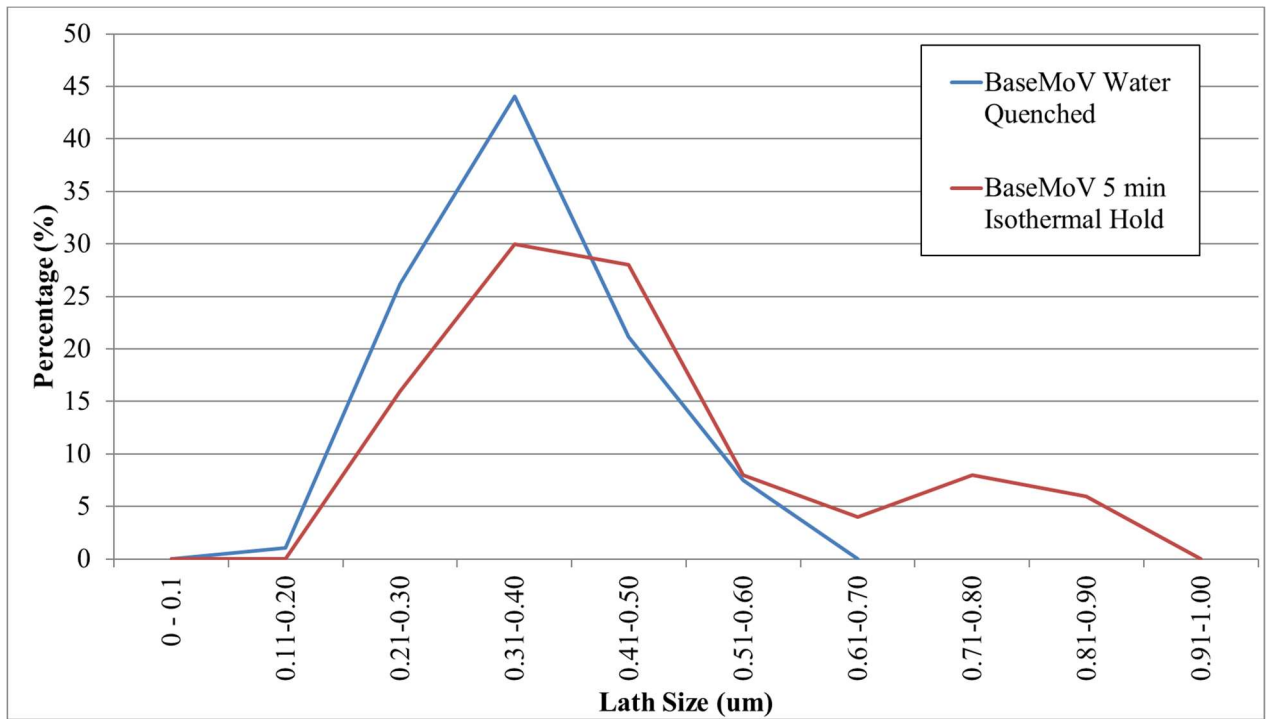


Figure 127 Comparison between the lath size of as-quenched martensite and bainite with an isothermal hold of 5 minutes

6.6: Tempering

6.6.1: Microstructure

The bainite was tempered between 30 minutes and 16 hours at 600 °C; below are the SEM images from 2 and 16 hours ([Figure 128](#) and [Figure 129](#) respectively). Both figures show that there are bainitic laths and single orientation carbides; this is expected from a lower bainitic microstructure. There are no areas of martensite, which would be present if there was significant retained austenite which would form martensite on quenching (as discussed in section 2.10.2).

There is no noticeable difference in microstructures from 2 to 16 hours, this indicates that the bainite is stable and there are no significant changes in morphology occurring.

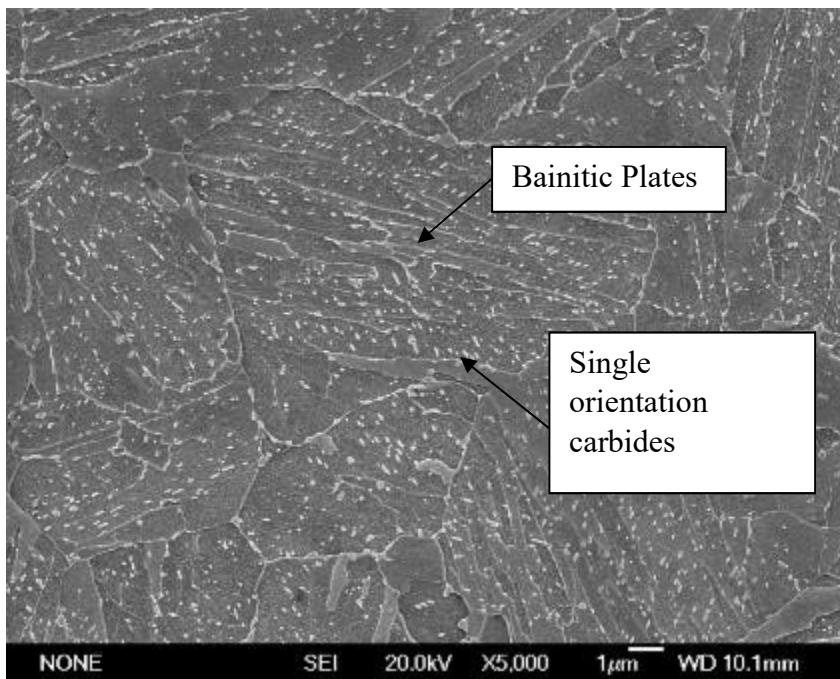


Figure 128 BaseMoV Bainite - 2 hours at 600 °C (312.6 ± 10.0 HV)

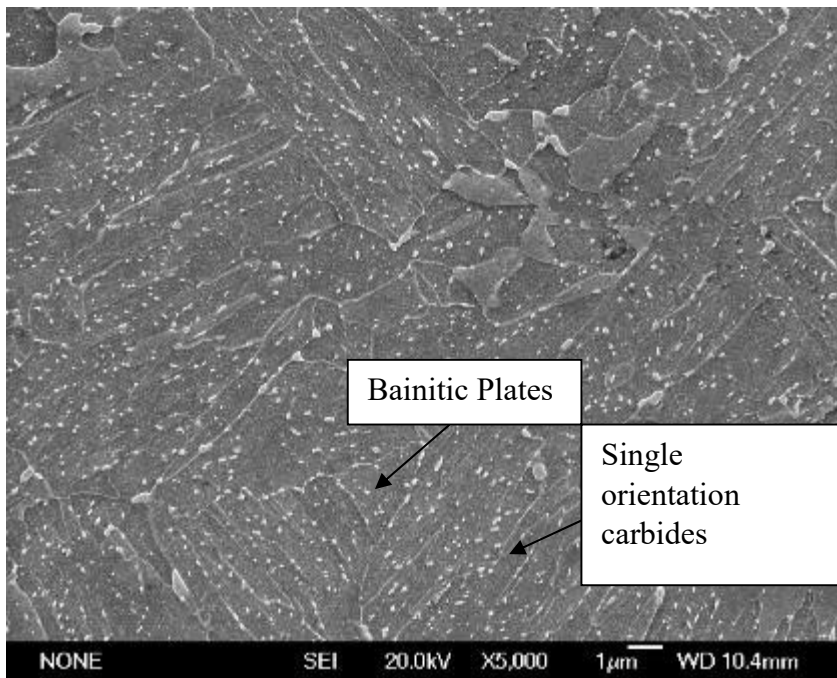


Figure 129 BaseMoV Bainite - 16 hours at 600 °C (292.7 ± 10.0 HV)

6.6.2: Hardness

The tempering of bainite, in comparison to martensite is shown in [Figure 130](#). The bainite starts at a lower hardness (352 HV) than martensite (451 HV) and has a smaller drop in hardness after the first 30 minutes temper (Martensite: - 87 HV, Bainite: -29 HV). This is consistent with literature which indicates that bainite is less responsive than martensite to tempering in terms of drop in hardness (section 2.10). Bainite forms at a higher temperature than martensite and martensite has more carbon in solid solution, which forms carbides on tempering. Bainite already has stable cementite carbides on transformation, and there is no driving force for more carbon to come out of solid solution, meaning that there is not as rapid a response during tempering. The tempering timeline of bainite (discussed in the literature review), indicates that, after carbides have precipitated, the next stage of tempering is gross recovery of the transformation dislocation substructure; this is associated with the reduction in hardness from 0 to 30 minutes tempering.

SEM analysis has found that both martensite and bainite have carbides on tempering, [Figure](#)

85 and [Figure 129](#) respectively; however, the martensitic carbides have not fully transformed to cementite and lower bainite has larger, more stable carbides.

After quenching and during tempering at 600 °C, bainite is consistently lower in hardness than martensite and appears to give a hardness variation with time that is parallel to that for martensite between 30 minutes and 16 hours. This partially matches with the literature which reports martensite to be harder than bainite when first formed and during the initial temper, for 1,000 seconds (16 minutes) at 700 °C, in a 0.45 wt. % C. After this time the bainite was harder than the martensite and the tempering profiles are not parallel. This is discussed in section 2.10. The 3 compositions (Base/BaseMoV/BaseSiCrMoV) with a martensitic microstructure found to temper at the same rate, which was down to changes other than carbide sizes (section 2.6). This may result in the reduction of hardness in martensite and bainite being the same as different strengthening mechanisms reduce in potency, for example increased lath size, and reduced solid solution strengthening.

The lower bainitic steel shows an increase in hardness from 2 to 4 hours tempering (2 HV). 2 HV is less than the resolvable hardness measurements and therefore this may be an effect of scatter and not a metallurgical effect. The comparable martensite does not show this effect, if there is a genuine increase in hardness. However, the martensite does show a plateau in hardness from 30 minutes to 1 hour, this may be due to transformation from epsilon carbide to cementite; another suggestion is that it is secondary hardening. As bainite has cementite which is fully formed before tempering there is no transformation associated.

The lower bainite samples may be exhibiting secondary hardening at 4 hours; however, this effect is diminished at 8 hours. When microstructures and carbide analysis are also investigated it is not evident that there are new smaller carbides indicative of secondary hardening between 2 and 16 hours; indication that this is not a genuine effect and that the

hardness increase is due experimental scatter from the hardness measurements.

Nam, 1999 finds that the hardness of bainite becomes larger than martensite with longer tempering times. This is reported to be because bainitic carbides are less sensitive to tempering, due to higher thermal stability of cementite in bainite compared to martensite, smaller amounts of carbon in solution and a lower driving force for solute diffusion, due to the more uniform distribution of cementite in bainite compared to martensite.

The higher stability of bainitic cementite compared to martensitic cementite results in a strength remaining for longer tempering times; however, this is not seen for tempering up to 16 hours. The difference in hardness between martensite and bainite at 2 hours is 11% and at 16 hours is 8%, this does show a very subtle softening of martensite compared to the bainite, which may be from the subtle differences in furnace temperatures.

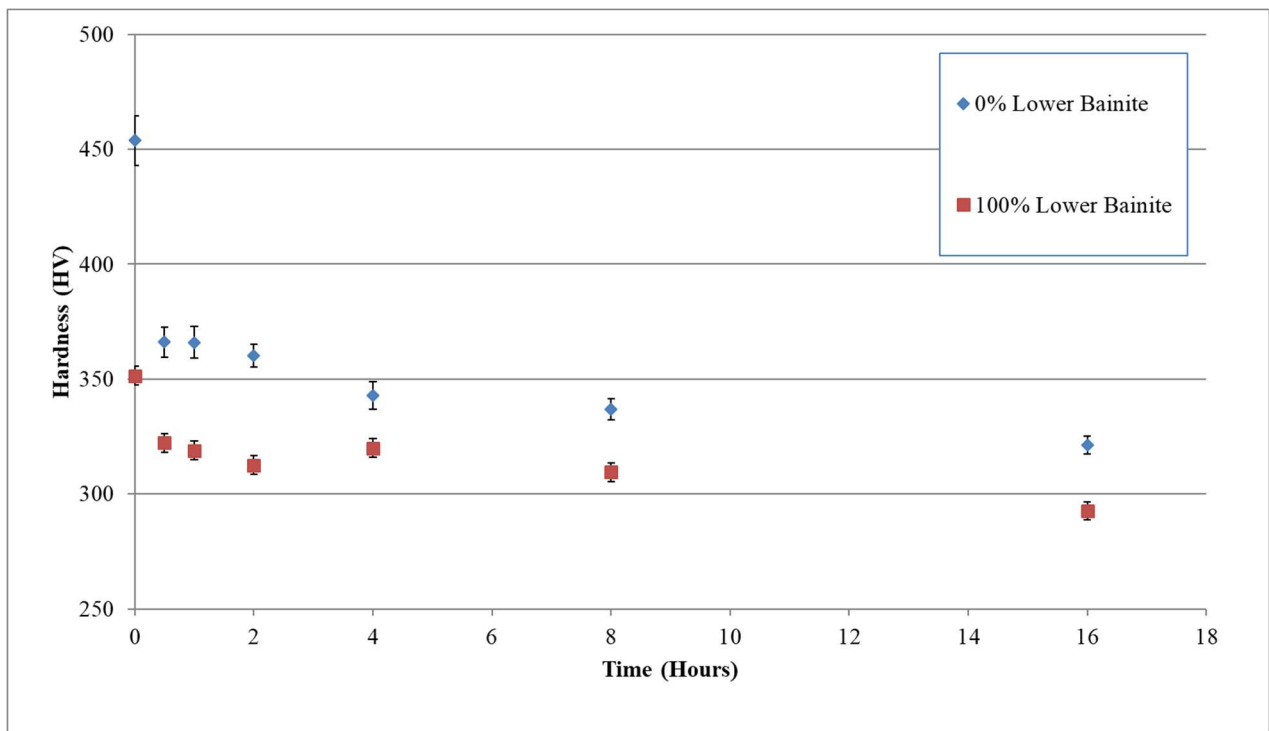


Figure 130 Tempering of martensite and bainite

6.6.3: Carbide Sizes on tempering

The variation in size of carbides in the 100% bainite samples tempered from 2 hours to 16 hours is shown in [Figure 131](#). The minimum carbide size has the same mode for the 2 and 16 hours temper at 600 °C, 50 - 59 nm. This indicates that there is little change in size.

The maximum carbide size shows a difference in mode on tempering from 2 to 16 hours (75 - 99 nm → 100 - 124 nm), however this is not a noticeable increase in size as the histograms are overlapping. The mode aspect ratio does not change during tempering, remaining stable at 0.56 - 0.60 nm. This indicates that although coarsening/spheroidisation is occurring it is not significant between 2 and 16 hours temper in the lower bainitic microstructure. Section 2.10.1 reviewed reports on the coarsening of bainitic carbides and indicated that tempering from 2 hours (7200 seconds) to 16 hours (57,600 seconds) at 700 °C increased the carbide size by less than 1 micron. The tempering temperature is higher than the 600 °C used in this study; however, that study does report that lower bainitic carbides are relatively stable on tempering, which is also shown here.

The results show no noticeable difference in shape and size when the bainite is tempered from 2 to 16 hours. The bainitic carbides are stable on tempering.

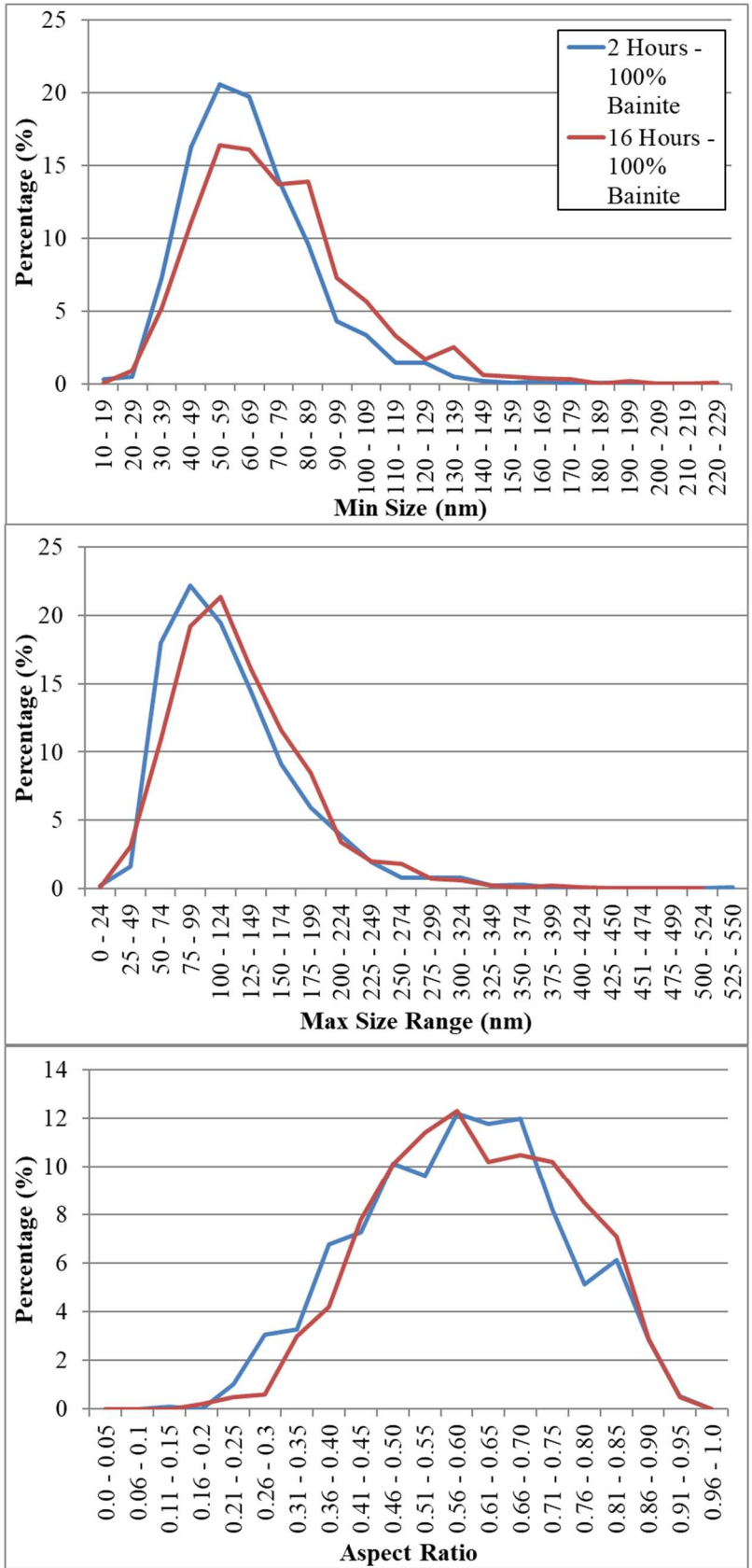


Figure 131 Bainite - 2 hours vs. 16 hours

6.6.4: Lath Size

6.6.4.1: Bainite

The lath size of bainite appears to be stable on tempering, see [Figure 132](#). The mode for the lower bainite lath size is 0.31 - 0.40 μm after the isothermal hold, and for the 2 and 16 hours temper there is a mode of 0.41 - 0.50 μm . As previously discussed (section 5.2.2) there is an error of $\pm 0.3 \mu\text{m}$, which would indicate that the increase in lath size from isothermal hold to 2 hours is not significant. The distribution of lath sizes indicates little difference between 2 hours and 16 hours. With increasing lath width, i.e. 0.51 - 0.6 μm to 0.61 - 0.7 μm , the bainite condition (isothermal hold, 2 hours temper or 16 hours temper) with largest percentage in each bin alters, an indication that any difference in distribution can be accounted for by experimental scatter, confirming that the bainitic lath sizes are stable on tempering.

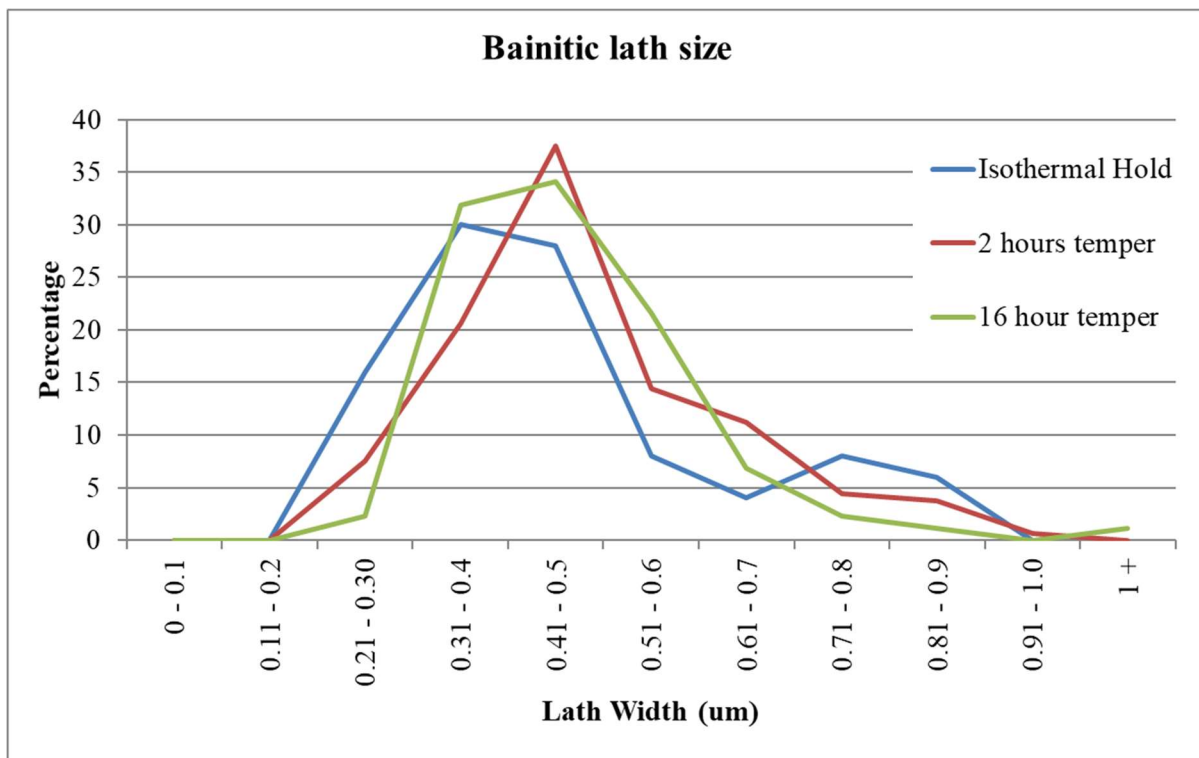


Figure 132 Bainitic lath size

6.6.4.2: Comparison to Martensite

Bainitic and martensitic laths are compared after 2 hours tempering. Bainite has a mode of $0.41 - 0.50 \mu\text{m}$ (38% of the data) and martensite has a mode of $0.61 - 0.70 \mu\text{m}$ (26% of the data). There is a difference in distribution ranges, with martensite having a wider distribution than bainite, indicating coarsening of the martensitic laths. The percentage of data at the mode value also indicates that bainite has a stronger tendency towards smaller lath sizes when compared to martensite. These data indicate that bainite has a smaller lath size than martensite at 2 hours tempering. Bainite is expected to have a more stable microstructure so the bainite coarsening at a slower rate than martensite is logical and expected.

When the 16 hours data are examined the mode of bainite is $0.41 - 0.50 \mu\text{m}$ (34% of the data) and martensite has a mode of $0.51 - 0.61 \mu\text{m}$ (24% of the data). This would indicate that the martensitic laths have decreased in size on tempering, this is unlikely based on literature results (section 2.6.3.3), however when errors are considered the difference in mode can be explained by experimental scatter. The distribution of the martensitic laths indicates that the laths are still larger in the martensite than in the bainite after 16 hours tempering. This is in line with Nam, 1999 which states bainite to be a more stable than martensite on tempering (W. J. Nam, 1999).

Literature report of the contribution of lath to mechanical properties were summarise in Section 2.13.1. Equation 2.9 was used to predict the hardness contribution from laths in the martensite and bainite for the BaseMoV steel. A lath size between $0.41 - 0.50 \mu\text{m}$ is expected to have a contribution to hardness of around 50 and 62 HV, whilst a lath size of $0.61 - 0.70 \mu\text{m}$ is expected to have a contribution of between 42 and 36 HV. These lath sizes cover the smallest and largest laths on tempering, when the experimental error is considered to be $\pm 0.3 \mu\text{m}$, then it is difficult to ascribe changes in the mechanical properties to variations shown in the lath data. When the distribution of the laths is considered bainite has a smaller lath size

than martensite. Martensite shows a larger distribution at 16 hours than bainite, see [Figure 133](#). As there is an associated error of $\pm 0.3 \mu\text{m}$, then there is no discernible difference in mode, however there is a clear difference in distribution, with lower bainite being skewed to the left when compared to martensite, indicating smaller lath sizes. There are no reasons why martensitic laths would reduce in size during tempering. One suggestion would be that the laths are reducing due to the carbide precipitation on the lath boundaries. BaseSiCrMoV exhibits a reduction in lath sizes, but this is the most stable of the three compositions with the least carbide precipitation on the laths, which means that the reduction in lath size is likely to be due to experimental error.

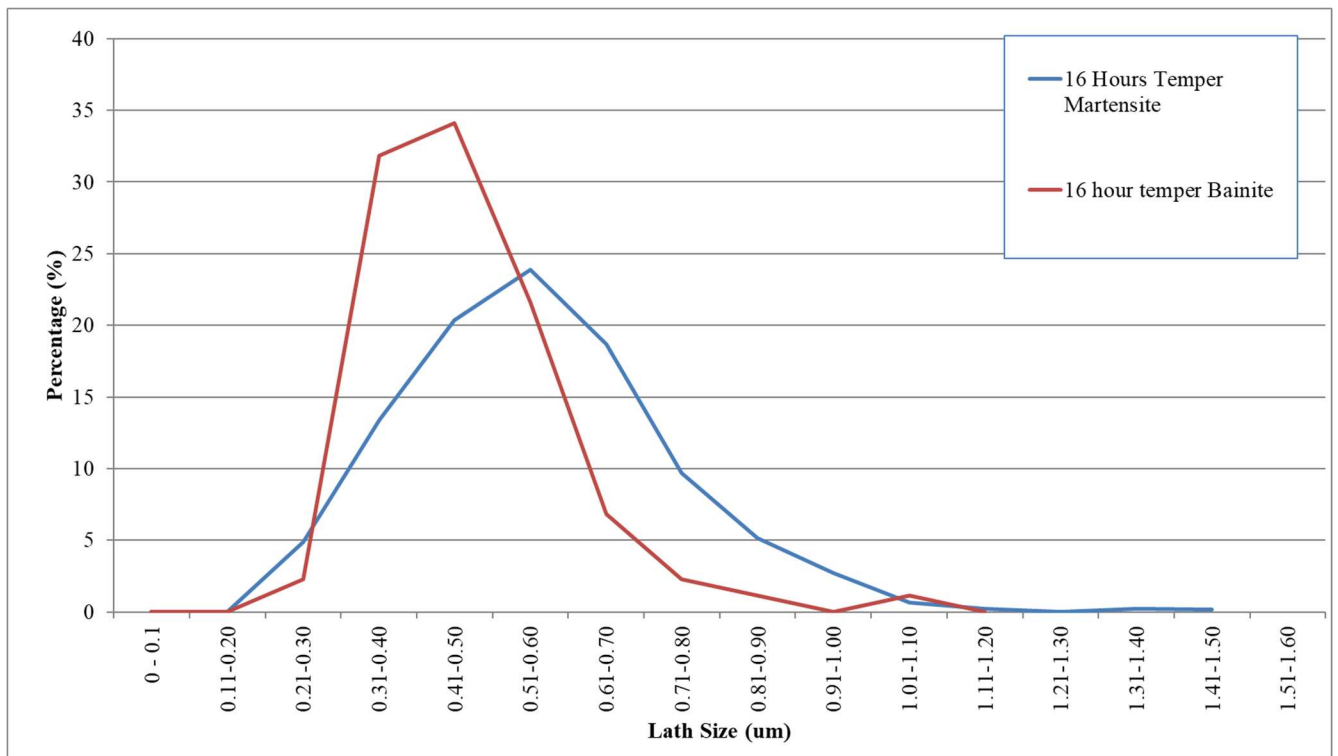


Figure 133 Comparison of martensitic and bainitic lath sizes at 16 hours temper

6.7: Summary

6.7.1: Bainite Production

This chapter has looked at the production of a bainitic microstructure. Image analysis, hardness, XRD and isothermal hold results have been used to confirm the conditions under which a fully lower bainitic structure has been produced. Results indicate that ~4% of another phase is present, which could not be identified by XRD. The lower bainite produced by the Gleeble method is deemed most appropriate for this work.

6.7.2: Tempering

The tempering of lower bainite shows that bainitic carbides and laths are stable on tempering. When compared to martensite, bainite has a smaller lath size after 2 and 16 hours. This is expected as the literature reports that bainite has a more stable microstructure than martensite.

Chapter 7: Mixed Microstructure Results

Chapter 7 looks at the production and tempering of mixed microstructures, methods detailed in Chapter 4. Gleeble samples $10 \times 10 \times 77$ mm were used for these tests.

7.1: As-quenched

As discussed in section 4.9, different isothermal holds were used to produce different mixtures of martensite and lower bainite; these are shown in [Table 14](#) and reproduced in [Table 36](#). The ideal mixtures are also shown; however, these could not be produced exactly. The microstructures produced are deemed appropriate as there is a condition with more lower bainite, another condition with more martensite, and a third condition with an almost balanced mixture of the two phases.

Table 36 Details of holding times and microstructures obtained

Isothermal Hold Time (Seconds)	Martensite (%)	Lower Bainite (%)	Sample Identifier	Ideal Microstructure
8	70	30	70% Martensite: 30% Bainite	75% Martensite: 25% Bainite
13	56	44	56% Martensite: 44% Bainite	50% Martensite: 50% Bainite
20	30	70	30% Martensite: 70: Lower Bainite	25% Martensite: 75% Bainite

7.1.1: Microstructure

The as-quenched microstructures are shown in [Figure 134](#) - [Figure 136](#). The longer the holding time the greater the amount of lower bainite which is visible (the method of distinction discussed in section 4.5.1), as expected (Matas, 1961; Pinto da Silva et al., 2014). The presence of lath martensite shows martensite does form after the isothermal holds of 8, 13 and 20 seconds, supporting stroke data from the Gleeble, discussed in section 7.1.2.

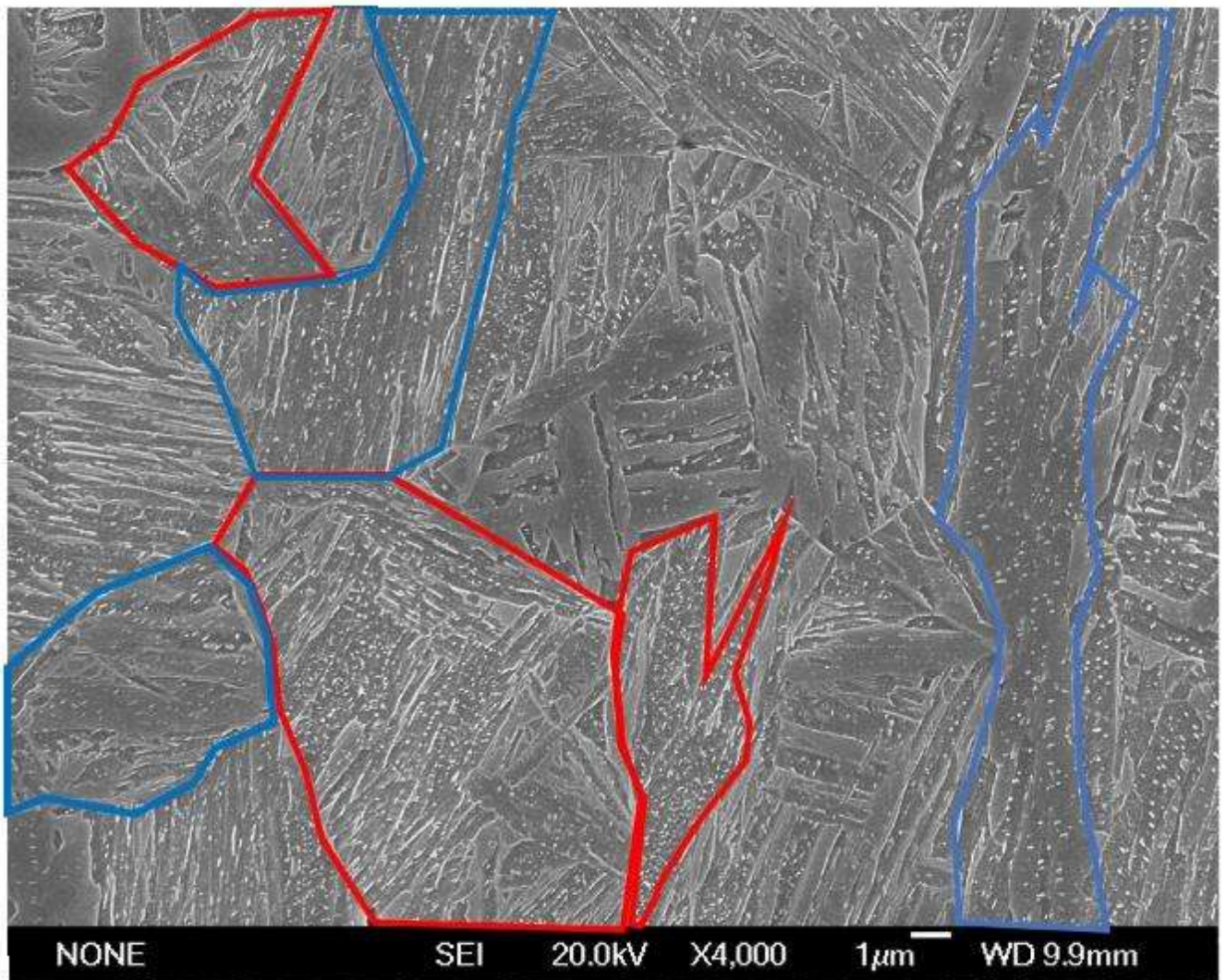


Figure 134 BaseMoV 8 Second Isothermal Hold (Blue – Lower Bainite, Red – Martensite) (425.1 ± 4.0 HV)

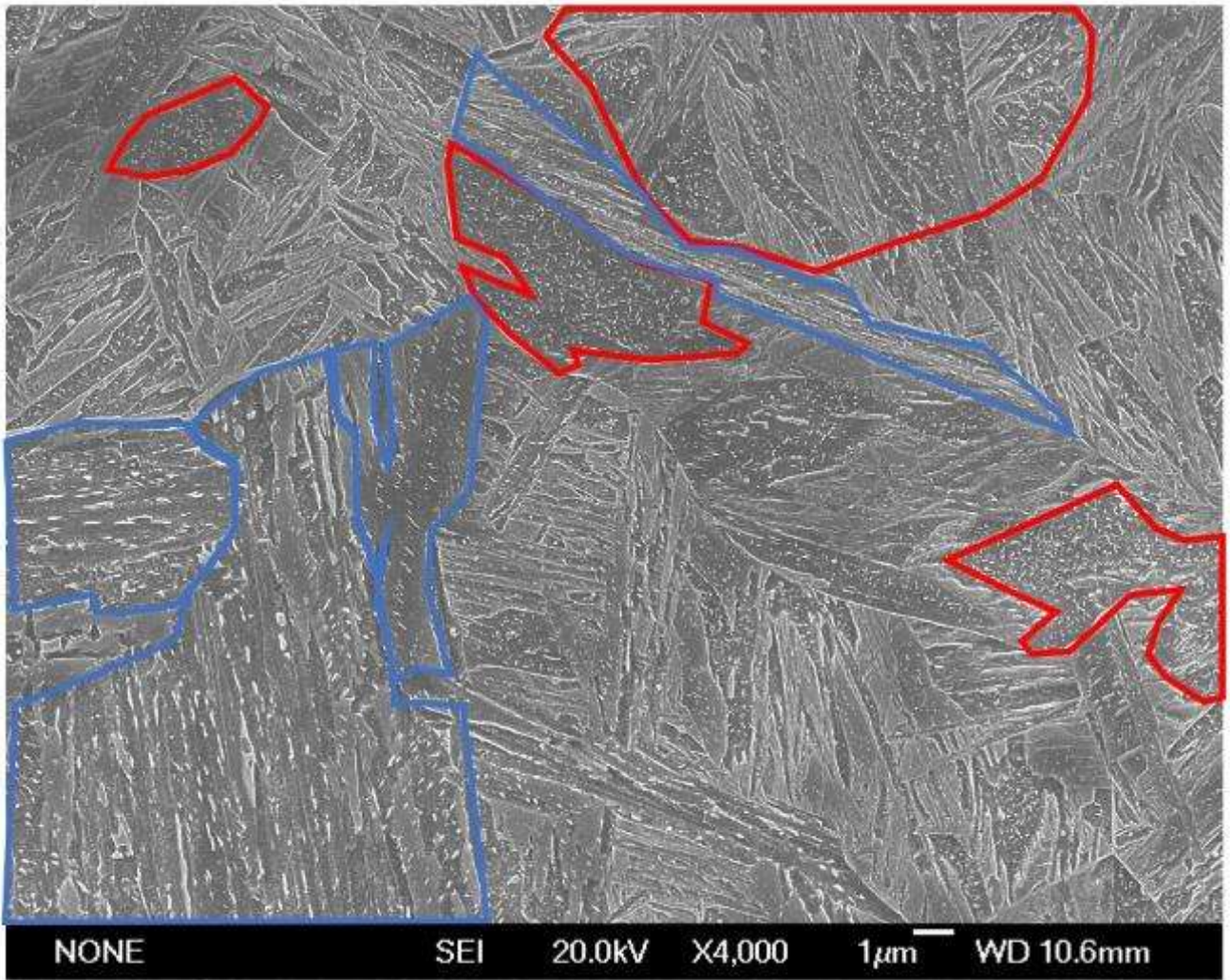


Figure 135 BaseMoV 13 second isothermal hold (Blue – Lower Bainite, Red – Martensite) (411.6 ± 6.2 HV)

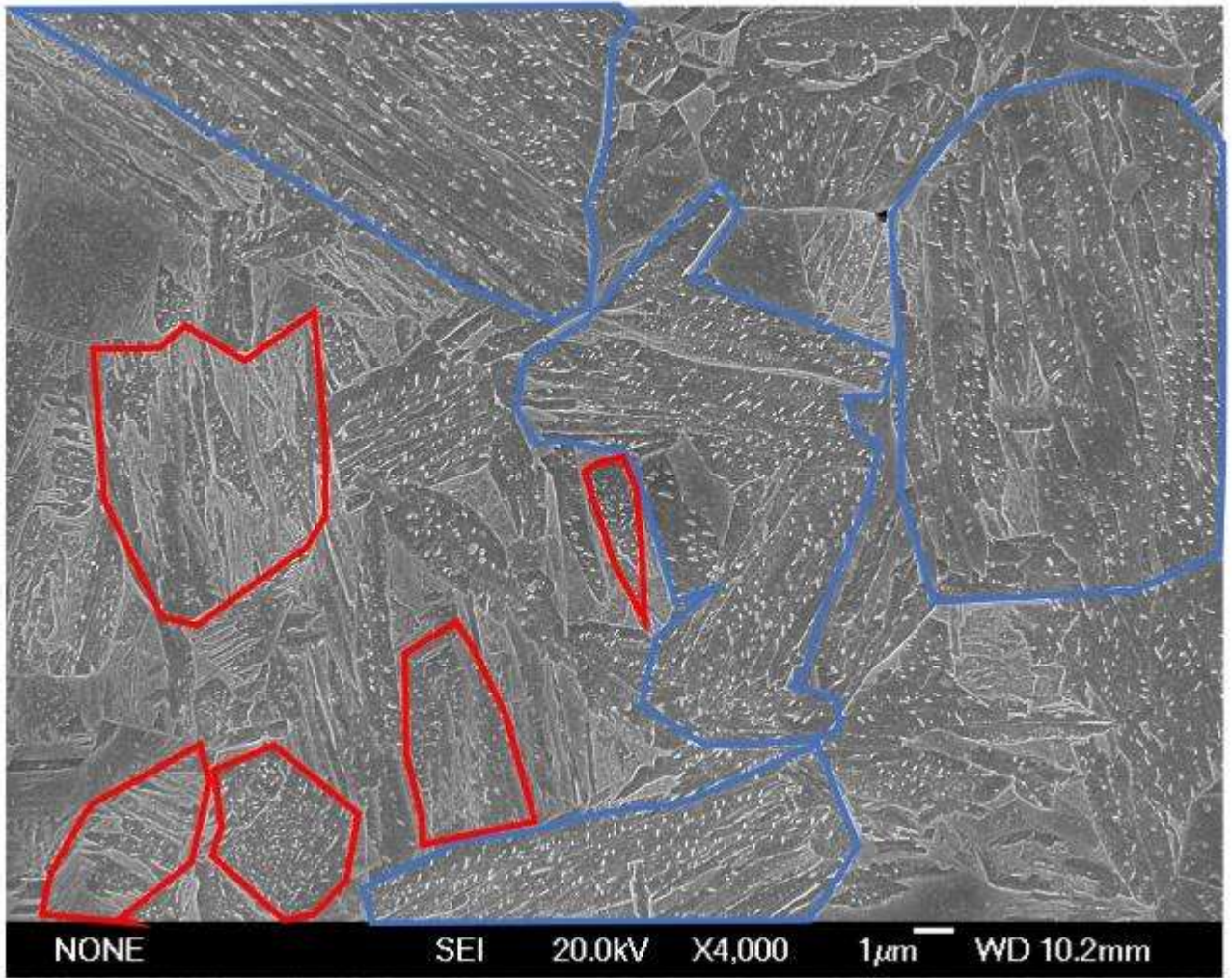


Figure 136 BaseMoV 20 second hold (Blue – Lower Bainite, Red – Martensite) (380.7 ± 4.2 HV)

7.1.2: Gleeble Stroke

Figure 137 shows the change in Gleeble stroke during isothermal hold at 430 °C. The stroke represents the change in length in the material used and is associated with bainitic transformation. It can be observed that the longer the isothermal hold the larger the difference in stroke, indicating that more bainite has formed. With the assumption that the 300 second hold produces 100% lower bainite, then the 8 second hold has 40% of the full transformation, 13 seconds has 56% and 20 seconds has 78%. These results are compared in Table 37, which shows that microstructural analysis and the change in stroke The holds at 8 and 20 seconds have a difference in stroke which would be indicative of a bainitic microstructure percentage produced being greater than the actual results, as the amount predicted by the stroke is higher than the microstructural point count analysis. However, there is a difference of less than 10% of the predicted value. This is thought to be due to differences accurately using the stroke data to see changes smaller than millimetres. Dilatometry attachments were not used, as there is not enough room for the copper grips and air quench, as mentioned in the methods sections. The hardness results discussed in section 7.1.5 also verify that the microstructural analysis is accurate for the different conditions.

There is a difference in starting positions of the stroke as this is associated with sample size, and exact free-span distance between the copper grips (see Figure 63 in section 4.7). The Gleeble stroke is not completely accurate and there are two main issues with using the Gleeble stroke to indicate a change in size;

- i). The rapid cooling from 925 °C to 430 °C results rapid contraction of the sample and the Gleeble copper grips need to account for this minute difference with large equipment, this may result in over/under estimations of the stroke as the equipment stabilise.
- ii). As the sample is held at 430 °C the Gleeble stabilises, the grips heat and expand, resulting in an artificially high increase in stroke.

The increase in stroke indicates that there is progressively more bainite formed, however the change in stroke does not match with measurements from the micrograph. However, more accurate hardness results show a correlation between hardness and microstructural analysis, using the rule of mixtures, as there are difficulties in using the stroke this gives a more accurate indication of the microstructures present.

Figure 66 can also be used to analyse the difference in isothermal hold. The boxed region shows where there is a disruption in cooling; this is martensitic transformation. The shorter the holding time, the larger the interruption, as more of the material can form martensite and hence the latent heat involved in martensitic formation increases.

Table 37 Isothermal hold time comparing microstructural analysis and percentage change in stroke

Isothermal Hold Time (Seconds)	Martensite (%)	Lower Bainite (%)	Stroke Change in Length – Compared with 300 second hold being 100% - Indicating amount of bainitic transformation that is complete	Ideal Microstructure
8	70	30	40%	75% Martensite: 25% Bainite
13	56	44	56%	50% Martensite: 50% Bainite
20	30	70	78%	25% Martensite: 75% Bainite

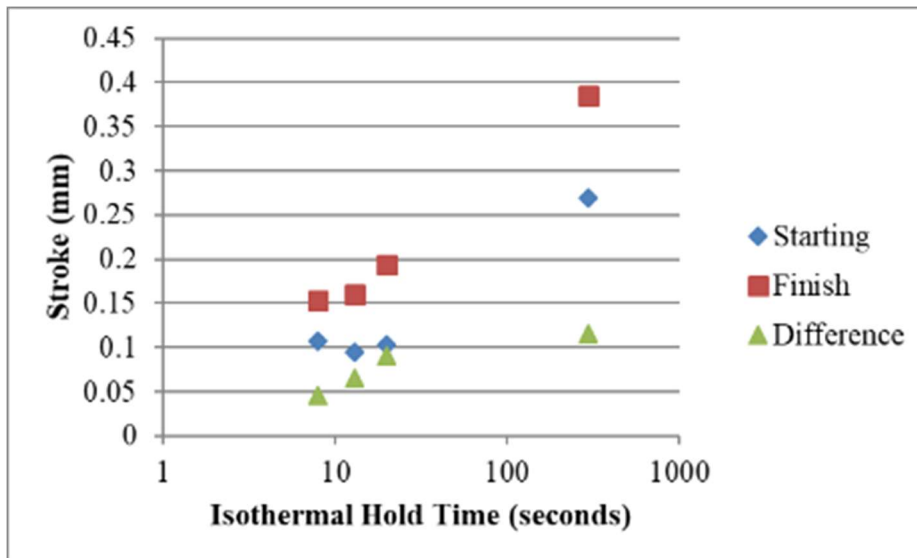


Figure 137 Change in Gleeble stroke measurement during isothermal hold at 430 °C between 0 and 300 seconds

7.1.3: Lath Size

There is discussion in the literature (section 2.14.6) that the mechanism of the bainitic transformation can partition the martensitic grains, in turn making the martensitic packets and laths finer, which would increase the strength of the martensite. Work by Tomita looks at mixtures of bainite and martensite. There was found to be a 100 MPa increase in strength from 0% bainite to 20% bainite due to refinement of the martensitic substructures along with a “brazing effect” in a 0.4 wt. % C; this is however not seen with a 0.2 wt. % C (Y. Tomita, 1991). This indicates that this effect is dependent on carbon content. As this work focuses on 0.17% C then grain size refinement is unlikely to be occurring. Effects of alloying elements Mo and V on PAG size would be the same for both martensite and bainite. As prior austenite grains tend to transform to bainite or martensite fully rather than all grains transforming partially the formation of differing amounts of bainite would not alter the size of martensite that subsequently forms.

Figure 138 compares the distribution of the martensitic lath widths in a 56% Martensite:44% Lower Bainite mixture (looking at laths in the martensitic regions only) to that of a fully martensitic sample. The distributions do not differ for the two lath conditions; if partitioning

of carbon has occurred then a finer lath would be expected in the mixed microstructure, as the carbon would alter the M_s temperature. If the martensite has the same carbon content, then the same transformation temperatures are expected, the coarsening of laths is dependent on time and temperature, therefore no differences are expected. There is no indication carbon is partitioning during the formation of lower bainite, based on lath size measurements and M_s temperatures remaining stable for all the mixed conditions; this means that the martensite/laths in the singular and mixed microstructures are expected to form at the same temperature, and under similar mechanical constraint from the prior formed lower bainite, resulting in comparable sizes. This is further evidenced by similar M_s temperature for the three mixed microstructures, discussed in section 4.8. If lower bainite is causing the remaining austenite to partition, this would constrain the martensitic formation, even if carbon enrichment is not present. This would result in an alteration of the M_f temperature. Gleeble results show changes to M_f temperature to be insignificant.

The bainitic lath sizes were not investigated after isothermal holding. The bainite forms at the same temperature for the mixtures and singular phase. As bainite is a time-dependent transformation, with formation progressing more with increased isothermal hold time, it is expected that bainite in the 8, 13, 20 and 300 second hold will be like-for-like and have the same lath size distributions. To add to this the transformation of martensite occurs in the areas of austenite which have not had enough time to transform to bainite; therefore, not affecting the characteristics of bainite already present.

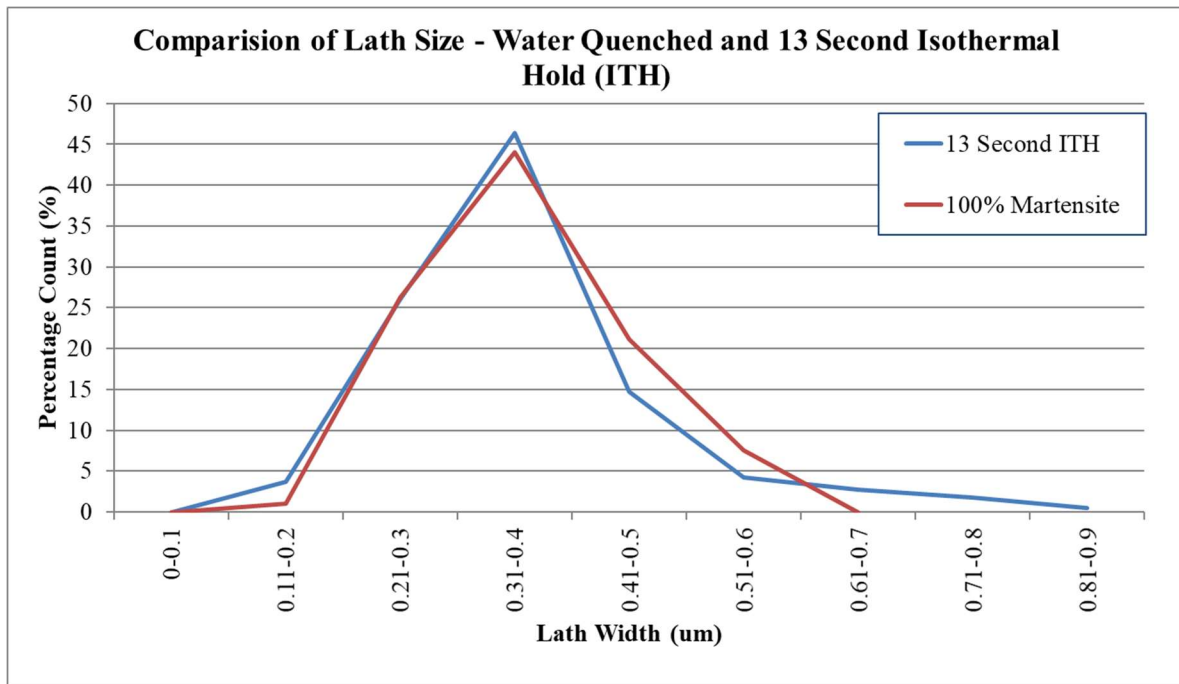


Figure 138 Comparison of lath Size of Water Quenched Martensite and 13 second ITH Martensite

7.1.4: Carbide Size

The size of the bainitic carbides after isothermal holding were analysed and found to be comparable to those in the mixed microstructure when only considering the bainitic regions (which have carbides facing in one orientation), see [Figure 141](#). For ease of comparison the area of the carbides (nm^2) were used to produce the ECD (equivalent circle diameter) sizes. This would not take into consideration the aspect ratio of the carbides, which may show some conditions to have more elongation. However, SEM images have been examined (examples [Figure 139](#) and [Figure 140](#)), showing similar elongated bainitic carbides for all conditions, and it is therefore determined to be a suitable method to compare the starting conditions.

It is determined to be a suitable method for comparing starting conditions as carbides of comparable size, size range and morphology are present.

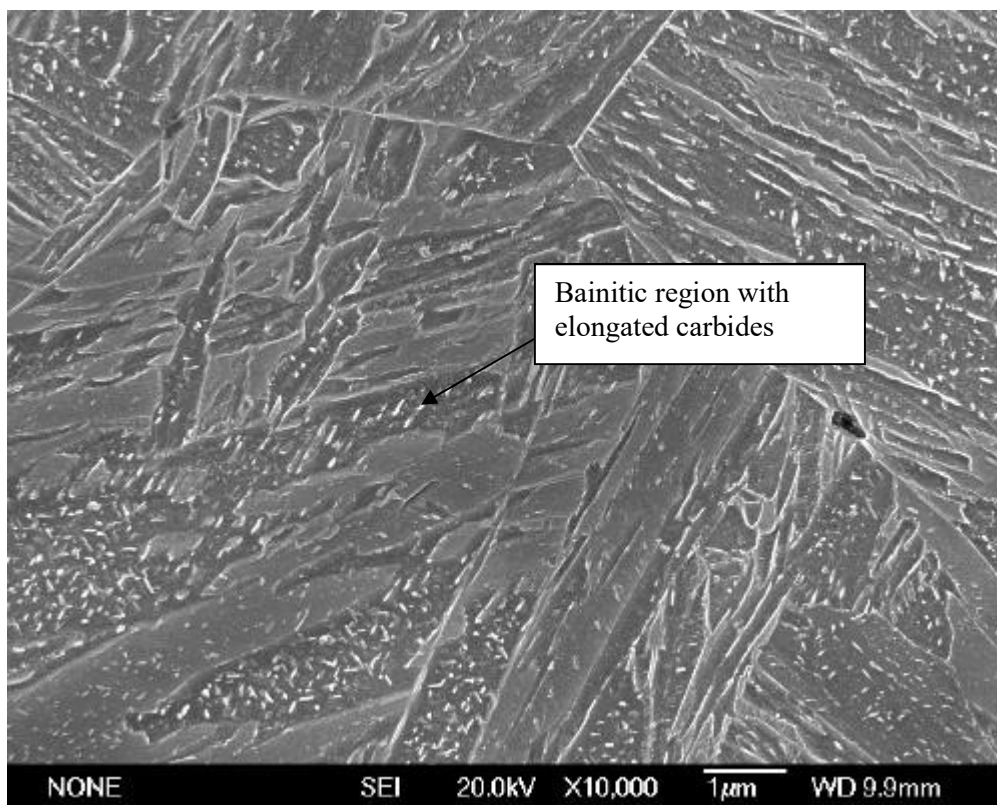


Figure 139 BaseMoV Isothermal Hold at 430 °C for 8 seconds showing elongation in bainitic carbides

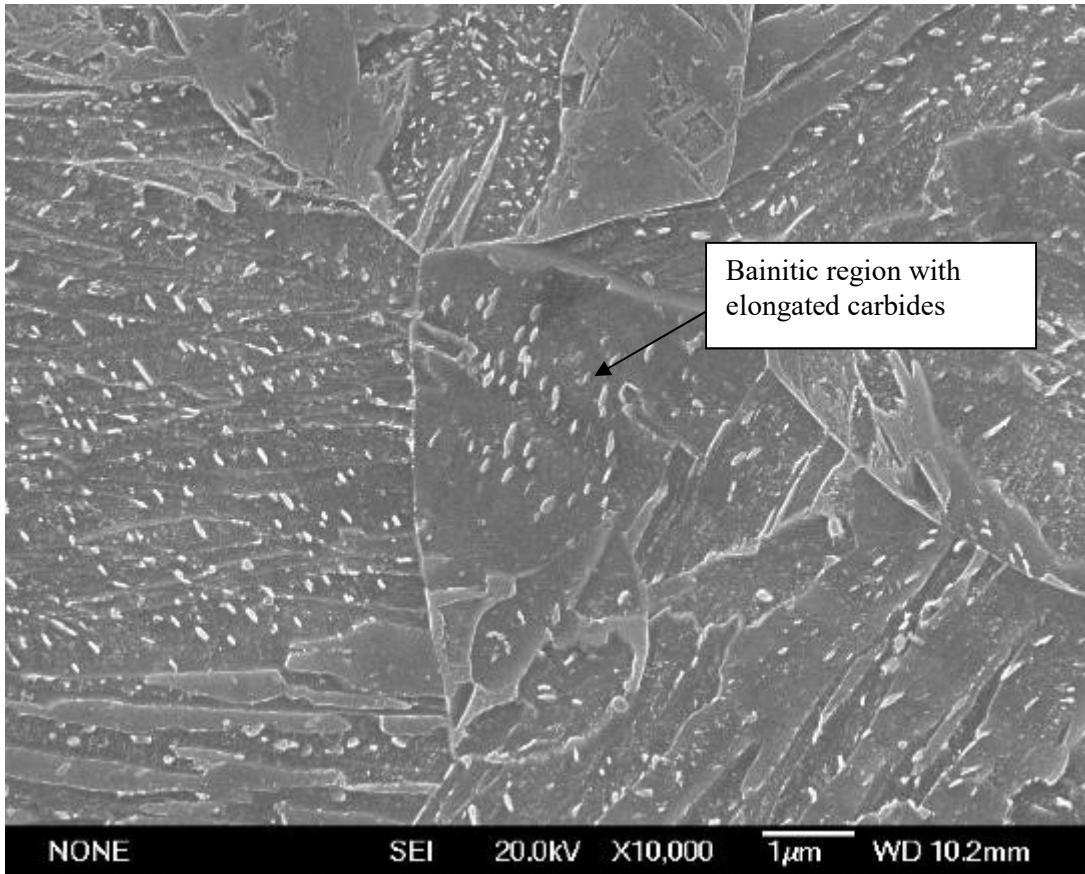


Figure 140 BaseMoV Isothermal Hold at 430 °C for 20 seconds showing elongation in bainitic carbides

The mode of ECD carbide size distribution of the 8, 13 and 20 second hold specimen was 351 - 400 nm, while the 300 second hold had a mean size of 401 – 450 nm. This is only one bin higher than the rest of the mode sizes; which means any increase would not be significant.

The histogram distribution of 13, 20 and 300 seconds is similar, in terms of shape, mode and range, indicating similarity in carbide population. The carbide size distribution for the 8 second hold shows a skew which is slightly to the left in comparison to the other isothermal hold times. This would indicate that the carbides are smaller, however as the mode values are the same this can be accounted for by experimental error as the carbides cannot be resolved under 30 nm this would mean that an error of ± 30 nm can be expected and would show no difference in contribution to mechanical properties. As bainitic carbides form during formation for which the conditions are the same, there is no expectation that the bainitic

carbides should not be equivalent (section 2.8). However, Nam 1999, studied the carbide diameter of bainite carbides (inside and on boundaries) and these are found to be between 150 – 200 nm after 3 minutes at 700 °C, increasing with longer holding times, up to 50 hours. This indicates that the carbides held at longer times may have had the opportunity to coarsen. The study by Nam is at a higher temperature, but it indicates that there is the potential for the held carbides to start coarsening. These are smaller than the carbides found in this study and have a different carbon content. Within this work the carbide size similarity indicates that the bainite carbides in the mixed microstructures and singular phase bainite are like-for-like.

The martensitic carbides were not investigated as the BaseMoV composition is the same in both the mixed and martensitic condition. Also, the lath size and Ms temperature are comparable for the martensite and mixed conditions, it is therefore thought that the martensitic carbides would also be comparable. The cooling after Ms is the same for the mixed steels. When compared to the fully martensitic steels, which is expected to have a cooling rate of 60 °C per second between 800 – 500 °C (based on work by J. Driscoll and backed by [Figure 67](#), in section 4.11 showing a BaseMoV CCT diagram), the mixed microstructure samples have a cooling rate of between 17 and 20 °C per second between 400 – 200 °C. Carbide size is based on cooling after Ms temperature, the bainitic steel is cooled more slowly than martensite at the lower temperature, however as the cooling of steel follows a Newtonian cooling curve, it is expected that the cooling will be comparable between the martensite and bainite containing steels within the martensitic region. This is also verified by the cooling rates being quick enough to produce martensite, as show in [Figure 67](#) of section 4.11. Comparable cooling rates are further backed up in later sections where the martensitic carbides in the fully martensite and mixed conditions are comparable at 2 hours; also, hardness values follow the Rule of Mixtures, suggesting that the martensite in the fully martensitic condition and mixed condition contribute the same to the overall strength.

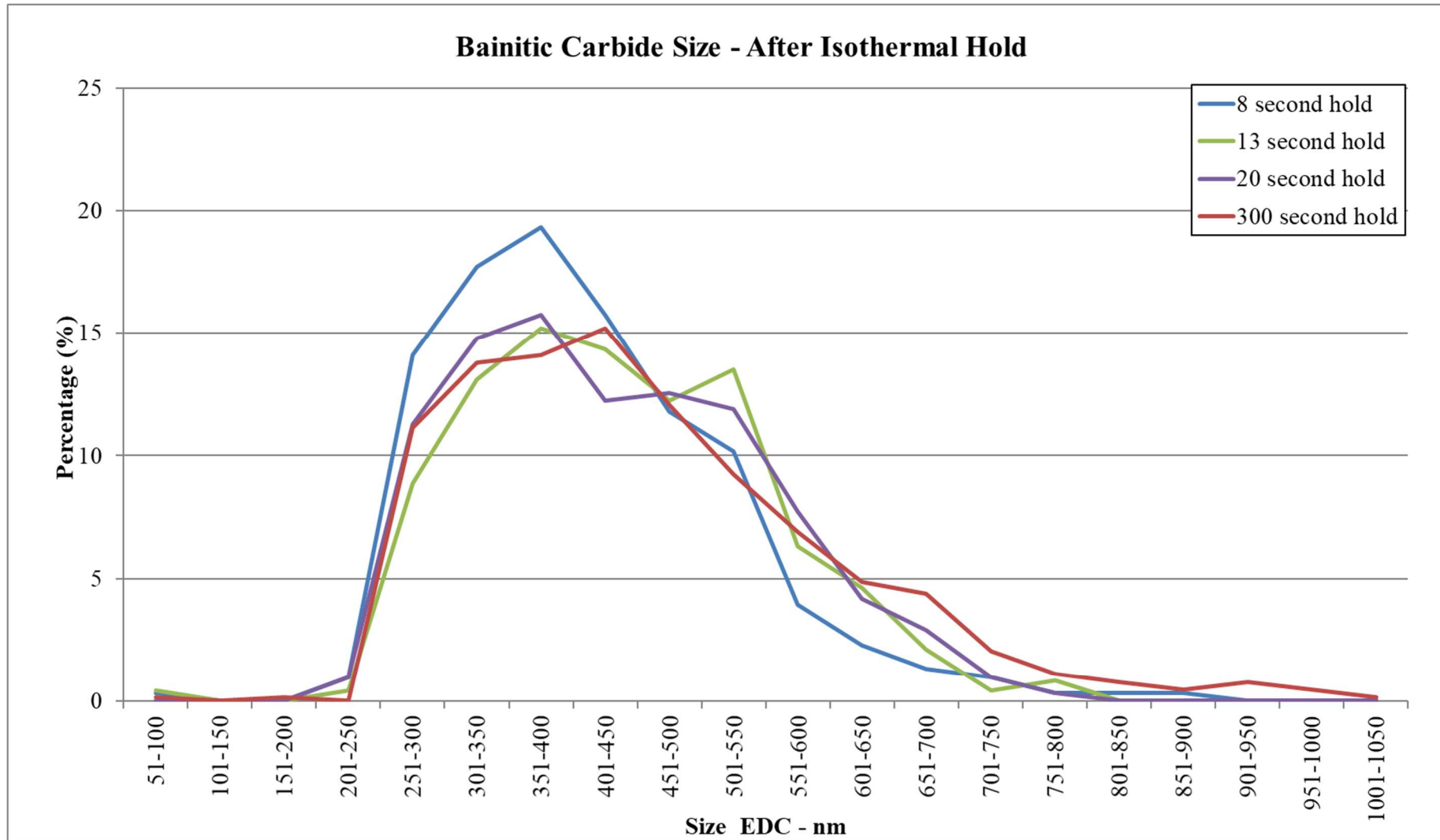


Figure 141 Bainitic Carbide Size in nm (Equivalent Circle Diameter) after Isothermal Hold

7.1.5: Hardness

The hardness of the martensite, bainite, and martensite + bainite mixtures are shown in [Figure 142](#). The Rule of Mixtures (RoM) variation between hardness and bainite fraction agrees with all the experimental data points, indicating that the two phases are acting independently with regards to hardness. The majority of literature focuses on higher carbon steels, where the difference in hardness between martensite and bainite produces a brazing effect at around 20% lower bainite (Barranco, 1992; Park & Kwon, 2001; Y. Tomita, 1991), see section 2.14.5. Although the lowest mixed percentage of lower bainite is 70% martensite: 30% lower bainite, there is no indication of a brazing effect. This effect would not be expected as the carbon level (0.17 wt. %) is not high enough to produce a hardness in the martensite which causes the brazing effect.

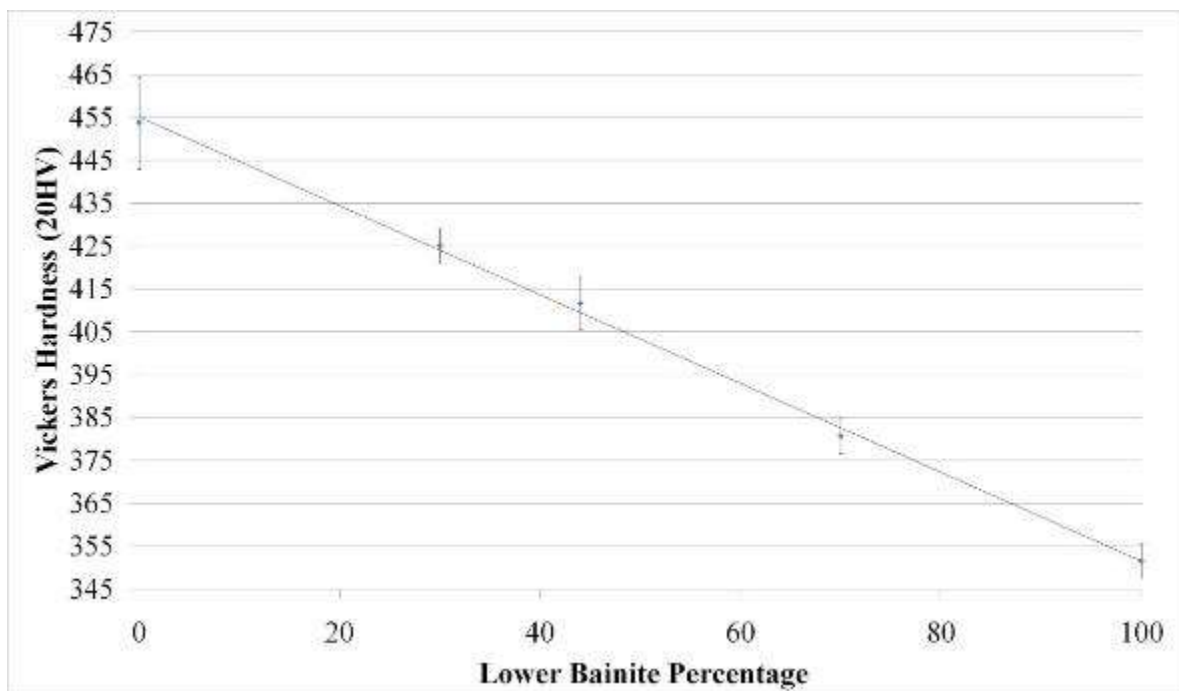


Figure 142 Vickers Hardness after isothermal hold (bainite/mixtures) and water quenching (martensite)

7.2: Tempering 30 minutes to 16 hours

7.2.1: Vickers Hardness vs. Percentage of Lower Bainite

On tempering there is general agreement with the Rule of Mixtures from 30 minutes to 2 hours, indicating that the components in the mixed microstructure are tempering at the same rate as in the singular microstructures, see [Figure 143](#). The trendlines connect the martensite and lower bainite as these microstructures have the least associated error after identification (i.e. the micrographs show an almost fully martensitic or bainitic microstructure).

After 2 hours the trendlines deviate away from the Rule of Mixtures, which can be accounted for by experimental error associated with the hardness measurements (due to equipment errors of ± 4 HV) and temperature discrepancies (when the furnace door was at 613 °C 10/15/20 cm from the back of the furnace read 597/610/613 °C respectively). This is exhibited more at larger tempering times where there is more opportunity to deviate from the desired tempering.

The 70% martensite: 30 % lower bainite and 30% martensite: 70% lower bainite show excellent agreement with the Rule of Mixtures but the 56% martensite: 44% lower bainite shows deviation. The 56% martensite: 44% lower bainite is consistently below the trendline on tempering, this is again thought to be because of temperature discrepancies, and linked to the fact that the microstructure was produced in a similar time-period. The mixtures of microstructure did not show deviation biased to one side of the rule of mixture possibly due to them being closer in actual temperature to the desired temperature.

The sample was placed in the furnace near the K type thermocouple but could not be touching due to experimental limitations. The furnace temperature was set depending on the readout given by the reading for the K type thermocouple placed in the furnace, then the readout on the furnace controller was altered so that the thermometer which reading the thermocouple placed within the furnace by the sample was at 600 °C. Throughout the

experimental work the readout on the furnace controller for the mixed microstructures during tempering was between 615 °C and 618 °C, this was over the period of 06/12/2015 and 18/09/2017. The furnaces can lose their stability over time, as the elements inside become more used and degraded.

The influence that differences in temperatures and the hot zone size have on the furnace is that the samples tempered at '600 °C' based on the K type thermocouples reading may experience a different tempering than predicted. This means that two samples with identical microstructure and composition, tempered on different dates for the same amount of time may exhibit different tempering responses, due to actual temperatures within the furnace being different. Samples which have the same microstructural composition were tempered within the same time-period, as they were produced within a similar timeframe. This means that the 56% martensite: 44% bainite tempered for 2 hours and 16 hours would be tempered in a furnace with similar conditions of degradation and trends in hardness could be discerned.

At 8 and 16 hours temper there is greater discrepancy of data around the trendline which is associated with time at temperature. As tempering time increases the discrepancies between the mixed conditions has the potential to increase as the time at temperature changes; with the result that the 8 and 16 hours tempers are more likely to show greater scatter around the trendline, i.e. as samples spend longer at the incorrect temperature, the more it may result in different tempering responses. As samples heat treated in a given time-period had the same microstructure it stands to reason the values would be on one side of the RoM line. This is backed up by [Figure 143](#) which shows that for each microstructural condition, for example 30% martensite, 70% lower bainite, there is consistent deviation above or below the RoM line from 8 hours onwards. This is consistent from 30 minutes onwards for the 56% martensite: 44% bainite and the 30% martensite: 70% lower bainite. The 70% martensite: 30% lower bainite is not consistently either above or below the trendlines, however when

error bars are considered it places the range of readings consistently below the RoM on tempering.

A sample tempered for 16 hours at 600 °C has a Larson Miller Parameter (LMP) of 18.02, while 16 hours at 590 °C has an LMP of 17.87. This would result in under/over tempering (depending on the temperature) and therefore the resulting steel will be softer/harder than steel tempered using the desired process. This has been summarised in Table 38, which shows that an under tempering temperatures for 16 hours and an over tempering temperature for 8 hours may result in the 16 hour sample having less tempering than the 8 hours hold.

Table 38 Larson Miller Tempering Parameters

Time	Parameter +/- 10		
	590 °C	600 °C	610 °C
0.5	16.57	16.76	16.96
2	17.09	17.29	17.49
8	17.61	17.81	18.02
16	17.87	18.08	18.28

It is also important to note that when the hardness is plotted against time then the mixtures of microstructure show similar tempering curves, shown in Figure 144.

There is not a complete convergence of hardness at 16 hours temper; however, all the microstructures have exhibited a reduction in hardness and there is general agreement with the Rule of Mixtures.

There is no systematic increase in hardness for the lowest percentage of lower bainite (70% martensite: 30% lower bainite), which, coupled with the blocky microstructure shown in Figure 134 further indicates that the ‘brazing effect’ is not acting in these samples.

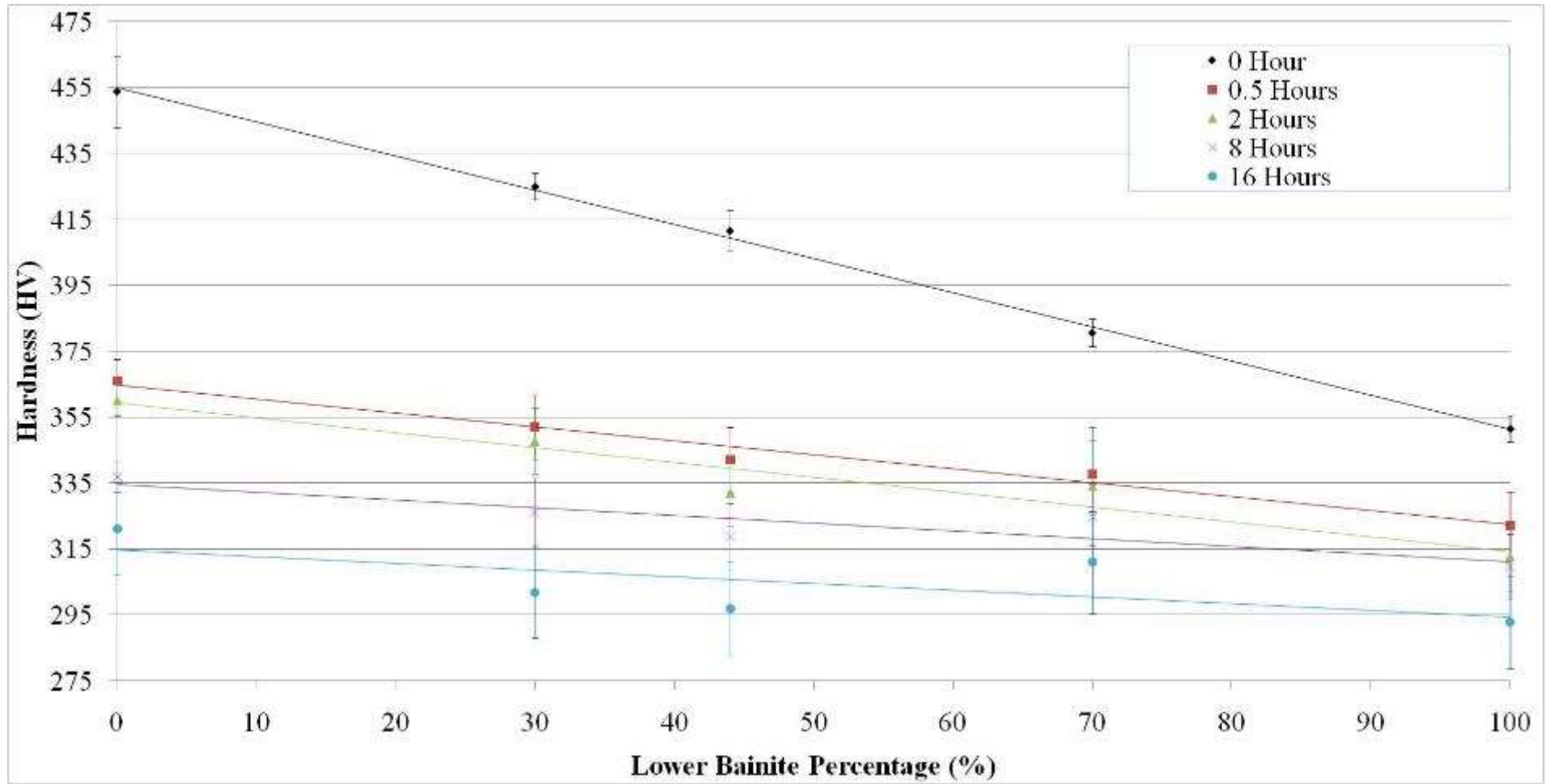


Figure 143 Comparison between Vickers Hardness and Predicted Lower Bainite Percentage

Hardness trends match with the literature (section 2.15); in which Barranco investigated a Cr 1.02 – Mo 0.48 – V 0.10 wt. % steel (predicted wt. % C between 0.3-0.4 and predicted twinned martensite). The microstructures studied included 100% martensite, 100% bainite, mixtures of martensite with 66% bainite and martensite with 22% bainite. The work found that with increased tempering temperatures for 1 hour there was reduction in hardness for all conditions, but not a complete convergence, however, the work of Barranco does not have tempering of mixtures for prolonged periods.

In this work, in order to observe whether the trends of the mixed microstructures obey the RoM based on the softening rates for fully martensitic and bainitic samples, the hardness was measured as a function of tempering time (Figure 144). Martensite shows the greater drop in hardness, and bainite shows the smaller drop (Discussed previously in section 6.6.2). On tempering, the mixed phases show a systematic drop in hardness, the mixture with the most martensite remains the hardest between 30 minutes and 2 hours. The increase at 4 hours is discussed in greater detail in section 6.6.2. However, the hardness deviation is not thought to be secondary hardening, therefore revised error bars have been added to Figure 143 and Figure 144.

At 8 and 16 hours there is a shift in hardness rankings, summarised in Table 39. During tempering the 70% bainite: 30% martensite goes from being the softest of the 3 mixtures, to the hardest. However, when error bars are also considered, it is likely this is due to the temperature discrepancies and hardness measurement scatter. All the microstructures show a similar trendline, with a rapid drop in hardness after 30 minutes, followed by a gradual drop in hardness with subsequent tempering.

Table 39 Ranking the mixed microstructure hardness on tempering

Hardness Ranking (1: Hardest, 3: Softest)	Tempering Time (Hours)				
	0	0.5	2	8	16
30% Bainite	1	1	1	1	2
56% Bainite	2	2	3	3	3
70% Bainite	3	3	2	2	1

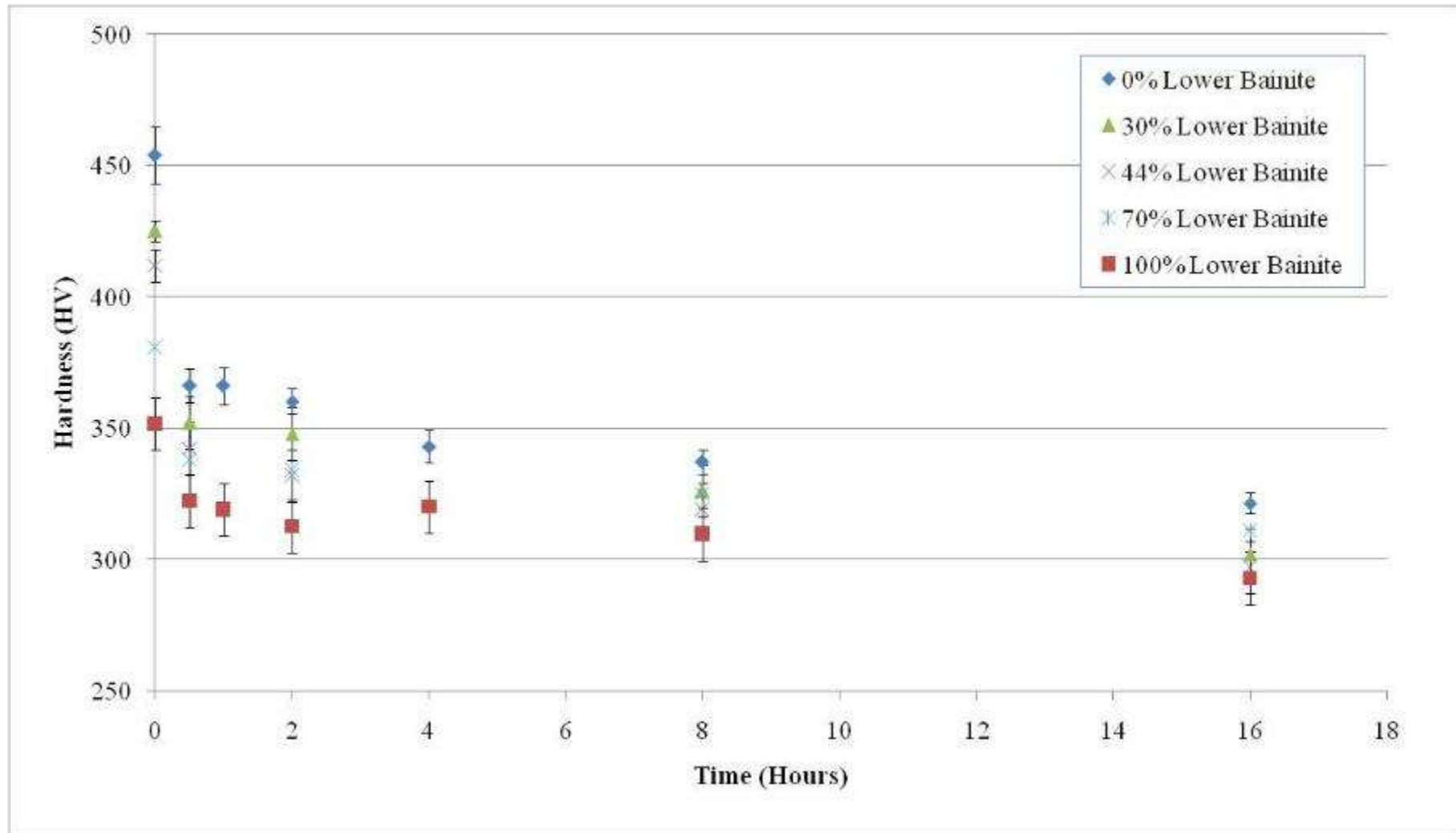


Figure 144 Comparison between Vickers Hardness and Tempering Time at 600 °C

7.2.3: Tempering Carbide Analysis

Carbide sizes have been measured at 2 hours and 16 hours, for both the single-phase martensite, single-phase lower bainite and the mixed 56% martensite:44% bainite structures. Carbide measurements were carried out using SEM measurements and an average of all the carbides in an image was taken for each condition; not distinguishing between carbides within the laths and those on lath boundaries. This method may have resulted in a skewing of data towards smaller more numerous carbides, with a higher density of smaller carbides in the laths compared to larger less numerous carbides on the lath boundaries. However, a sufficient number of carbides per set of histograms (1000+) were analysed to give a representative distribution.

Mode relates to the value which is shown the most often. Min refers to the smallest size of the carbide and the max is the largest, shown in [Figure 145](#).

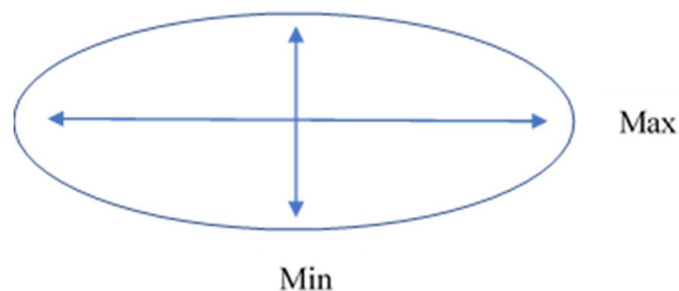


Figure 145 Schematic representing the maximum and minimum dimensions of the carbides

Table 40 Mode Min, Max and Aspect Ratio of the carbides in martensite and bainite microstructures, along with carbide density

	Mode Min Value (nm)	Mode Max Value (nm)	Mode Aspect Ratio	Carbide Density/ μm^2
2 Hours – 100% Martensite	40 – 49	50 – 74	0.56 – 0.60	8.94
2 Hours – 56% Martensite	40 – 49	50 – 74	0.66 – 0.70	7.67
16 Hours – 100% Martensite	40 – 49	50 – 74	0.51 – 0.55	7.72
16 Hours – 56% Martensite	50 – 59	100 – 124	0.66 – 0.70	5.64
2 Hours – 100% Bainite	50 – 59	75 – 99	0.56 – 0.60	5.74
2 Hours – 44% Bainite	50 – 59	75 – 99	0.56 – 0.60 / 0.61 – 0.65	6.61
16 Hours – 100% Bainite	50 – 59	100 – 124	0.56 – 0.60	4.61
16 Hours – 44% Bainite	50 – 59	100 – 124	0.46 – 0.50	4.79

7.2.3.1: 2 Hours Temper – Martensite and Martensite in Mixed Condition

Figure 146 presents a comparison between the tempering for 2 hours of 100% martensite and the martensite in the mixed microstructure, considering only the martensitic carbides. The minimum carbide size shows little difference between the two populations, with the same mode (40 – 49 nm) and a similar distribution. There is a minimal indication of the martensitic carbide population in the mixed microstructure having a wider distribution than the carbide population in the fully martensitic microstructure. The lack of significance was determined as the martensite for 2 hours has 0.3% of data larger than 130nm and the 56% martensite 2 hours microstructure has 1.4% of data larger than 130nm. The maximum size shows the two carbide populations to have the same mode (50 - 74 nm), however the 56% martensite

microstructure has a higher percentage of carbides within the 50-74 nm bin, almost 10% more. The two carbide populations have a similar maximum size distribution, which indicates that even if there are differences with the percentage of carbides in each bin then the overall trends are similar. The two populations of carbides have a similar distribution for aspect ratio, although these are not completely smooth so that the central part of the distribution for the martensite in the mixed microstructure is shifted slightly to the right so that the mode of the two is not the same (56% martensite 0.66 – 0.70 and 100% martensite: 0.56 - 0.60). The difference in aspect ratio would suggest that the carbides are more spherical for the 56% martensite carbide. This would be reasonable as it would suggest that the 56% martensite is tempering at a quicker rate in the mixed microstructure than in the 100% martensite.

It is important to note that although there is significant after 100 hours when compared to carbide growth after 16 hours. This is in contradiction to the overall hardness reduction.

7.2.3.2: 16 Hours Temper – Martensite and Martensite in Mixed Condition

Figure 147 shows the martensitic carbides which have been examined after 16 hours

tempering. The minimum carbide size has a mode of 40 - 49 nm for the 100% martensite and 50 – 59 nm for the 56% martensite; however, the distribution shape is similar. The max size shows the same similarities with distribution shape; however, the max size modes are different (100% martensite: 50 - 74 nm and 56% martensite: 100 - 124 nm). This would indicate that the 56% martensite is becoming more lenticular than the 100% martensite. The aspect ratio shows a similar distribution for the two carbide conditions with mode values of the following, 56% martensite: 0.66 – 0.70 and 100% martensite: 0.51 – 0.55 nm. This is a similar discrepancy found for the 2-hour temper. This change is not expected as it indicates the aspect ratio of martensite has decreased the opposite of what is expected in literature as martensitic carbides become more spherical on tempering (section 2.6.1.4). This shows that the difference is associated with scatter in the data.

7.2.3.3: 2 Hours Temper – Bainite and Bainite in Mixed Condition

Figure 148 shows the carbides in the bainite. After 2 hours of tempering the 100% bainite and the 44% bainite have a similar minimum size, in terms of distribution and mode (50-59 nm). The maximum size shows this trend with a similar distribution and mode (75-99 nm). The aspect ratio of 44% bainite has a mode across two bins 0.56-0.60 nm and 0.61-0.65 nm. The 100% bainite has an aspect ratio mode of 0.56 – 0.60. Both carbide types have a similar distribution of aspect ratio. This indicates that the two bainitic carbide types are like-for-like.

7.2.3.4: 16 Hours Temper – Bainite and Bainite in Mixed Condition

After 16 hours of tempering the minimum sizes of the carbides show little difference, with a mode of 50-59 nm for both the 100% bainite and 44% bainite; there is also a similar shape of carbide distribution, see Figure 149. The maximum carbide size shows the same trend, with a mode of 100-124 nm for both carbide conditions. A difference in aspect ratio was found with 0.46 – 0.50 for the 44% bainite and 0.56 – 0.60 for the 100% bainite. This is a similar discrepancy which is found in the martensitic carbides and is from experimental error, as the minimum and maximum carbide size shows that there is little difference between the carbides.

Any deviations are considered not to be significant and the overall distribution of the histograms is similar. The carbides in the mixed microstructure show no deviation on tempering from those in the singular phase. This is important as it means that the carbides in the bainite are tempering at the same rate and contributions to hardness in the mixed microstructure are the same.

7.2.3.5: From 2 to 16 hours – All Conditions

In the mixed microstructure the martensitic minimum mode increases one bin, on tempering from 2 to 16 hours. The max mode almost doubles, this suggests elongation. The fully martensitic microstructure carbides have a stable minimum mode, and stable maximum mode, suggesting spheroidisation. The difference in behaviour between the carbides is an indication of different growth mechanisms; spheroidisation and elongation. The 100% martensite has a reduction in aspect ratio, while 56% martensite has an increase in aspect ratio. Work by Nam did find that there is a difference in coarsening rates for carbides on boundaries and within boundaries.

Based on the literature the presence of bainite should not affect the way the martensitic carbides in the mixed microstructure are affected by tempering, compared to the fully martensitic carbides. The martensite and bainite are in two distinct regions and therefore the availability of carbon in for carbide in the martensitic region is similar to the fully martensitic microstructure, they should coarsen at the same rate. Therefore, this difference can be accounted for in the experimental scatter.

From the hardness results, it shows that the mixed microstructure hardness is appearing to be getting closer to the bainitic sample, this therefore may be a real effect.

For bainite it shows that the minimum mode remains the same and the maximum increases by one bin. This is for carbides in the fully bainitic condition and the bainitic carbides in the mixed condition; indicating similarity in behaviour. The mixed martensitic carbides have the same min and max mode as the bainitic samples; indicating that they are how similar. The mixed martensite has a higher number density than the bainitic conditions and is more spherical, which indicates that it is not bainitic carbides which have been sampled and that there is a genuine effect of the mixed martensitic carbides coarsening to be similar to the bainitic carbides.

7.2.3.6: Carbide Density 2 Hours – All Conditions

The carbides per μm^2 are presented in Table 40. Results show that the martensite in singular and mixed conditions at 2 hours, are 8.94 and 7.67 carbides per μm^2 respectively, a difference of 1.27 carbides per μm^2 . The bainite in the singular and mixed conditions at 2 hours, are 5.74 and 6.61 carbides per μm^2 respectively, a difference of 0.87 carbides per μm^2 . At this stage there is little difference between the like-for-like for both microstructures, and martensite has more carbides per μm^2 than the bainite, which may suggest smaller carbides.

7.2.3.7: Carbide Density 16 Hours – All Conditions

All carbide sets exhibit a decrease in carbide number density from 2 to 16 hours tempering, this indicates that the carbides are further apart, and size data also shows that the carbides are increasing in size, Table 40. At 16 hours temper there is a carbide density of 7.72 per μm^2 for the 100% martensite and 5.64 per μm^2 for the 56% martensite, a difference in 2.08 carbides per μm^2 . There is a carbide density of 4.61 per μm^2 and 4.79 per μm^2 for the 100% bainite and 44% bainite respectively; a difference in 0.18 carbides per μm^2 . This indicates that carbide density with bainite is largely similar after tempering. The martensite in the mixed condition is 1.03 carbides per μm^2 different from the fully bainitic condition. The number density values indicate that the martensite in the mixed condition is showing tendency towards the bainitic carbides in terms of number density.

The 100% martensite is showing a smaller max value than other carbide conditions at 16 hours, this indicates that it is not significantly increasing in size. However, in Figure 147 (focusing on the max carbide size for 100% martensite), apart from the skewing to the left there is a similar shape in distribution which indicates that there are still carbides which are increasing in size.

7.2.3.8: Carbide Summary

Bainitic carbides are like-for-like in the mixed and singular phases from 2 to 16 hours temper.

The min mode value is remaining stable and the mode max value is slightly increasing in size and the number density is decreasing.

Martensitic carbides are not like-for-like in the mixed and singular phases from 2 to 16 hours temper. The carbides in the mixed condition are increasing in size at a faster rate than in the fully martensitic condition; resulting in carbides with the same size as bainitic carbides.

Overall it appears that the martensitic carbides in the mixed microstructure are coarsening in a manner closer to bainite than the martensite.

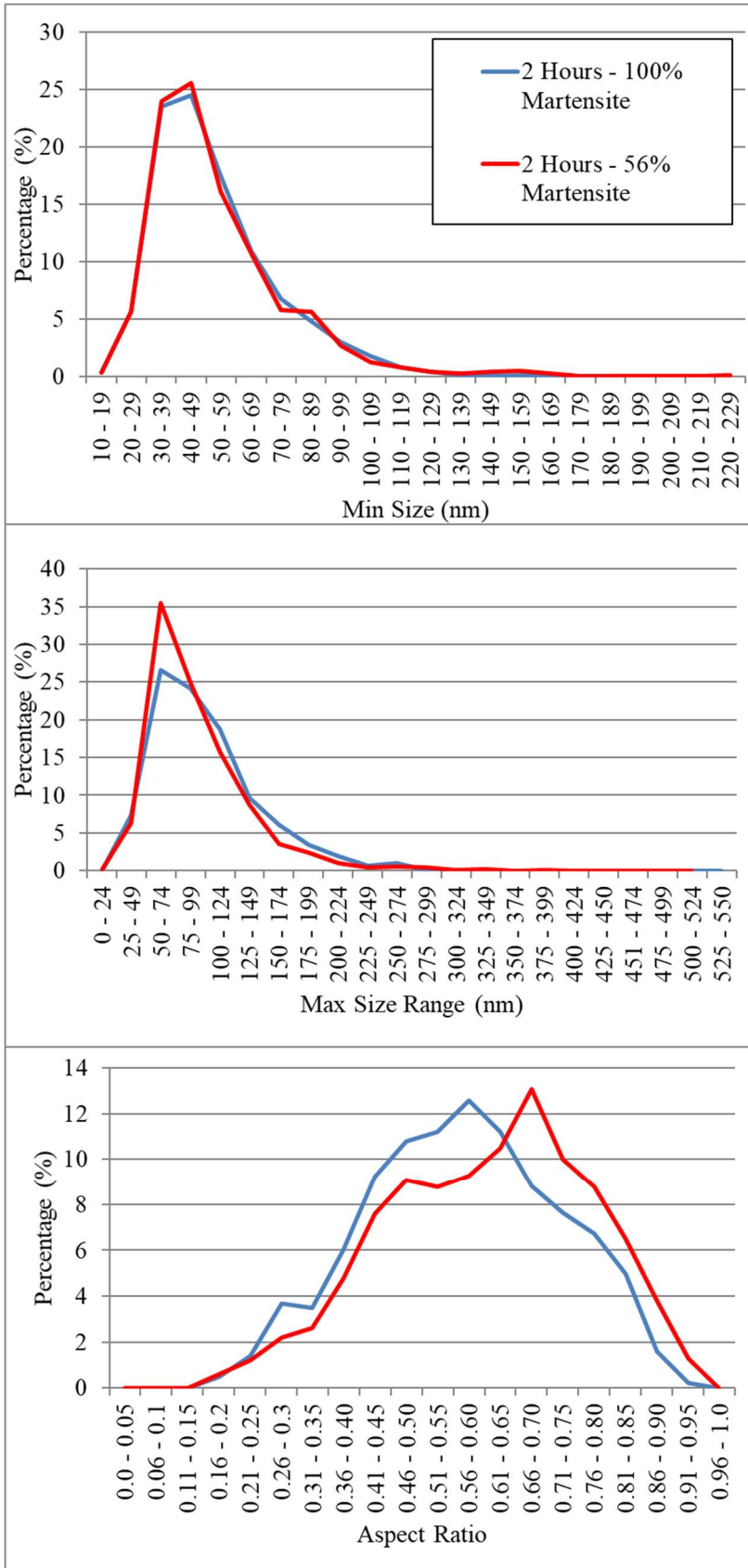


Figure 146 2 hours - 100% Martensite vs. 56 % Martensite (Min Size/Max Size/Aspect Ratio)

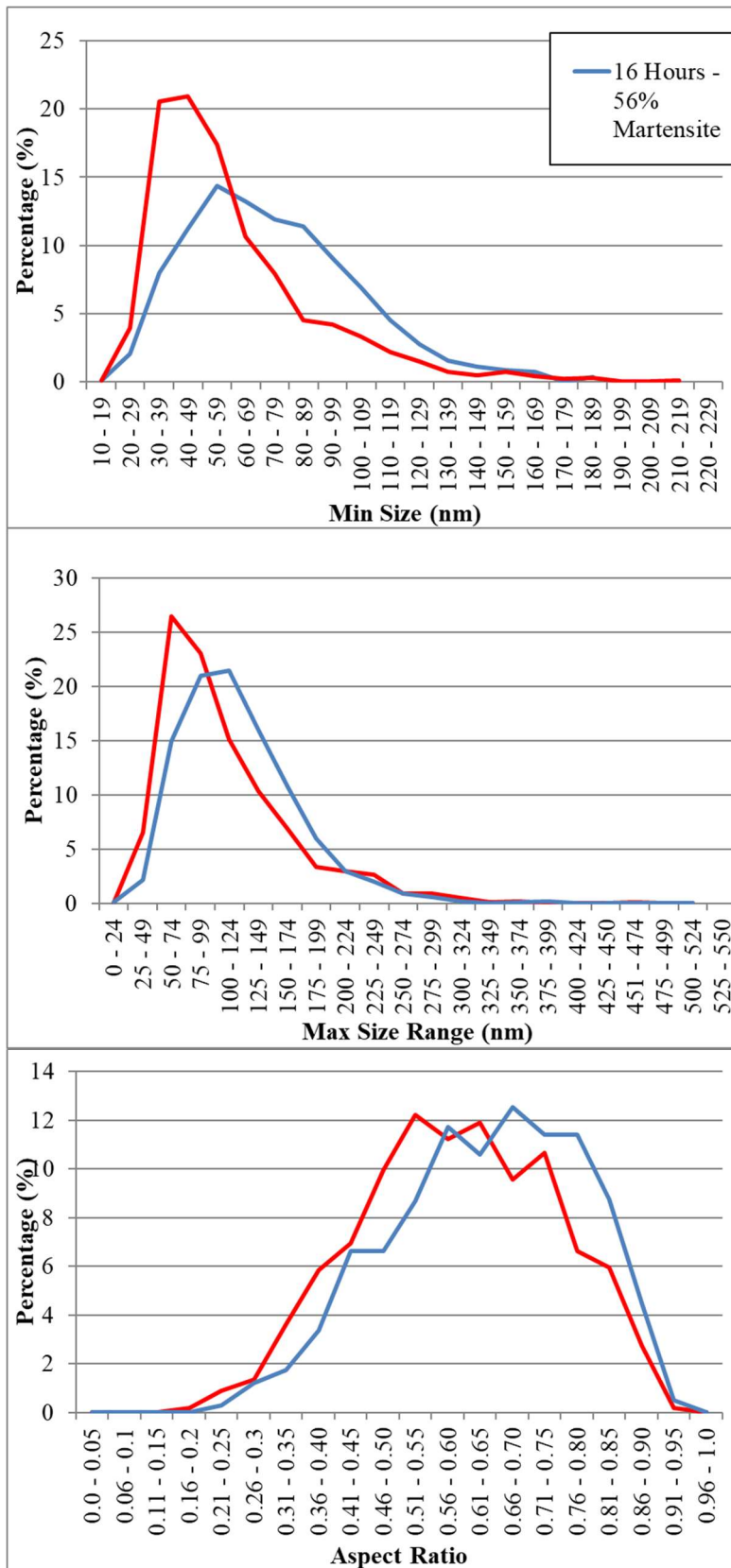


Figure 147 16 Hours - 100% Martensite vs. 56 % Martensite (Min Size/Max Size/Aspect Ratio)

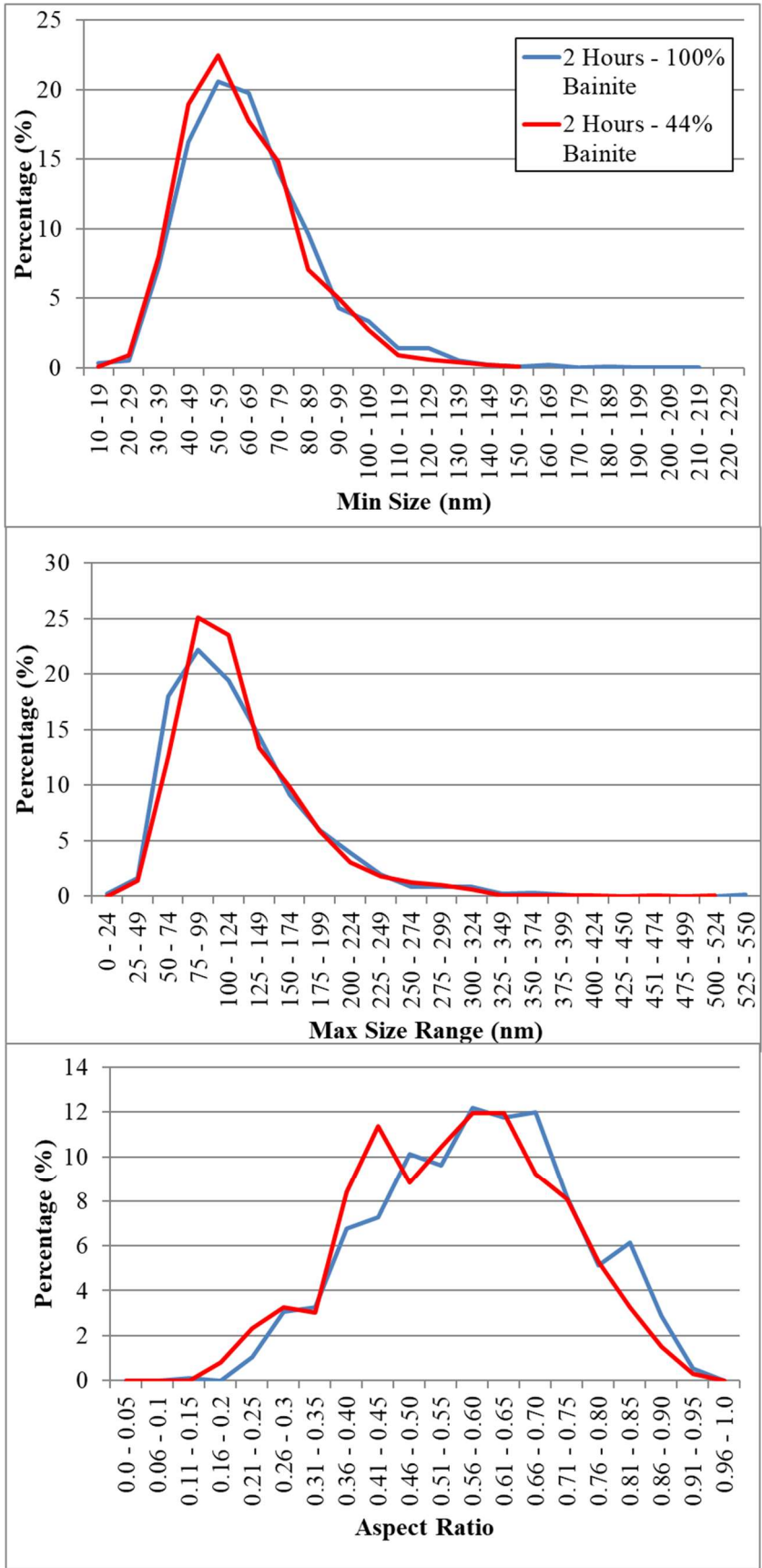


Figure 148 2 Hours 100% Bainite vs. 44% Bainite (Min Size/Max Size/Aspect Ratio)

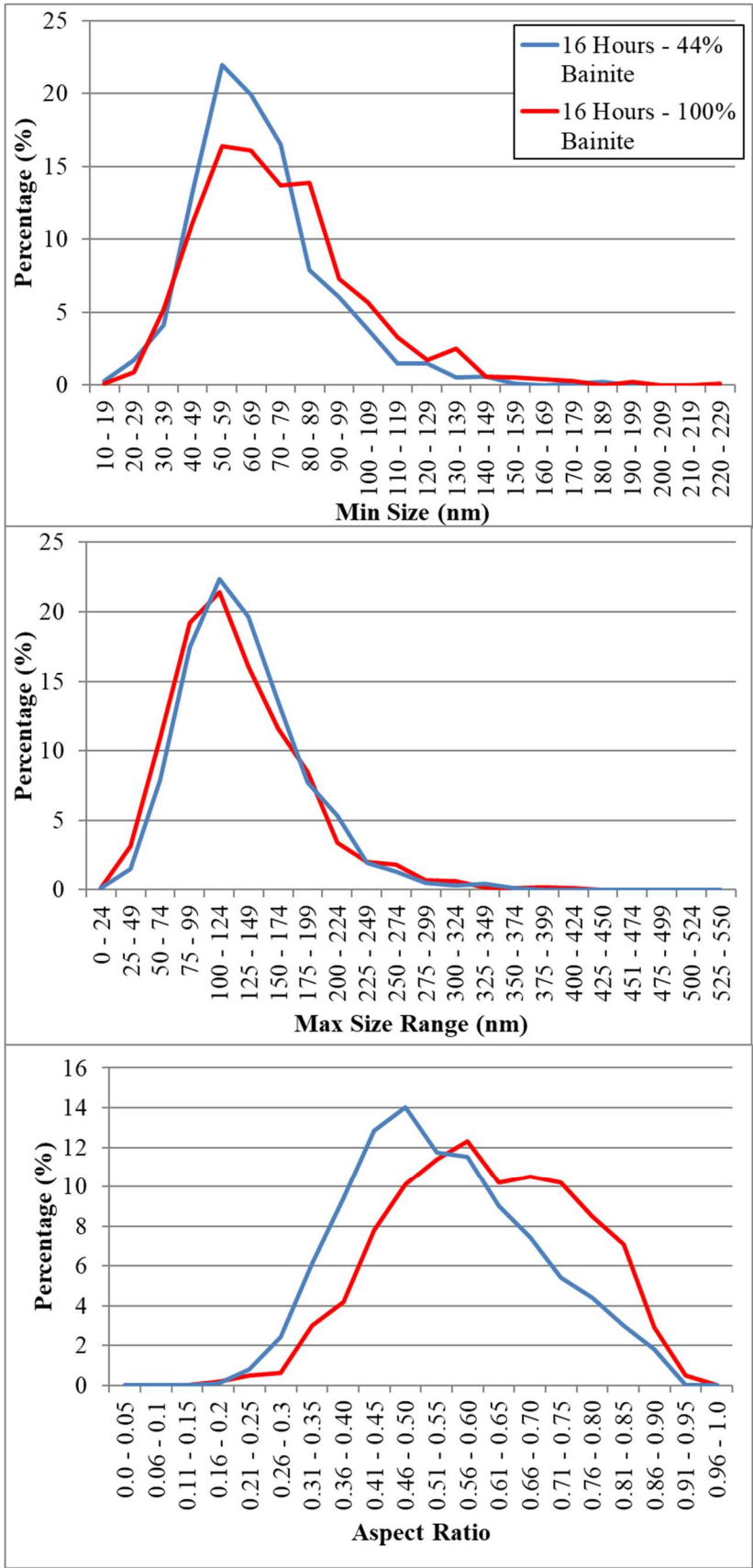


Figure 149 16 Hours 44% Bainite vs. 100% Bainite (Min Size/Max Size/Aspect Ratio)

7.2.4: Summary Tempering to 16 hours

Mixtures of martensite and lower bainite were successfully produced, all with similar martensitic start temperatures, indicating that the martensite phase in the mixed and singular microstructures is comparable. These follow a Rule of Mixtures, in terms of hardness in the as-quenched condition. The lath sizes of the martensite in the mixed condition and singular phase were found to be comparable, a further indication that like-for-like microstructures were produced.

The carbide sizes (equivalent circle diameter in nm) of the bainite after the isothermal holds were analysed. The four sets of carbides have a similar distribution and the mode values are comparable, demonstrating that the starting condition for the bainitic carbides are comparable in the singular and mixed conditions.

On tempering the samples appear to follow a Rule of Mixtures for hardness. After 8 and 16 hours temper there is more experimental scatter due to the furnaces, but the distribution of data points either side of the Rule of Mixture trend line indicates this is scatter. However, there is suggestion of deviation from the Rule of Mixtures, based on carbide and hardness data in the mixed condition (44% lower bainite: 56% martensite).

The bainite in the mixed microstructures temper in the same manner as the singular phase when looking at the carbide size and distribution. The martensite in the mixed microstructure is not tempering in the same way as the martensite; this is evidenced by changes in the carbide sizes, as the mixed martensitic carbides tempering a manner similar to bainite.

Overall this shows that there was successful production of martensite and lower bainite mixtures, from the hardness, lath, carbide size and micrographs. On tempering the Rule of Mixtures appears to be followed initially, however after 2 hours tempering there is indication that this starts to deviate based on hardness and carbide size (for 16 hours).

7.3: Tempering 100 hours

Martensite, bainite and a 44% lower bainite: 56% martensite mixed sample were tempered for 100 hours at 600 °C; they were placed in the furnace simultaneously, therefore tempering times are directly comparable and any discernible differences in hardness are not due to scatter. This was carried out to determine if the differences in tempering at 16 hours were experimental or real effects.

7.3.1: Hardness

7.3.1.2: Experimental HV Values

Figure 150 shows the actual hardness of the 100% bainite, 44% lower bainite:56% martensite and 100% martensite. The martensite has a lower hardness than expected, while the bainite follows the expected trend. The martensite has a hardness of 190 HV after 100 hours tempering; it was expected to have a value of 300 HV. Although there is expected to be experimental variation the actual value is over 100 HV different from that expected and shows a significant drop in hardness. Bainite has a hardness of 264 HV, which is around 26 HV different from the expected hardness of 290 HV. This is below what is expected, however the method used for determining the predicted hardness is extrapolated for 84 hours after the last data point, therefore a 26 HV difference does not show significant deviation from the trendline.

Due to the long tempering times, the 3 samples were placed in the furnace at the same time, so should have identical tempering in terms of the holding time and temperature.

Another observation is that the bainite is now the hardest microstructure after 100 hours tempering, and the martensite is the softest. This shows that the rate of change in strengthening contributions has altered markedly for the martensite and bainite between 16 and 100 hours of tempering. Figure 150 shows that the difference in hardness between the two microstructures is reducing, therefore it may be suggested that a difference is starting at

16 hours; the data at 100 hours support this and show that the martensite has a more rapid softening of hardness compared to bainite.

The 56% martensite: 44% bainite has a hardness of 204 HV, this is also lower than expected and shows hardness which appears to be closer to that of the martensite, not following the Rule of Mixtures, further shown in Figure 151.

The next sections discuss the response to tempering for the different microstructural constituents, to determine why there is such a large difference in tempering response of the martensite and bainite, and why the mixed microstructure is closer in hardness to martensite.

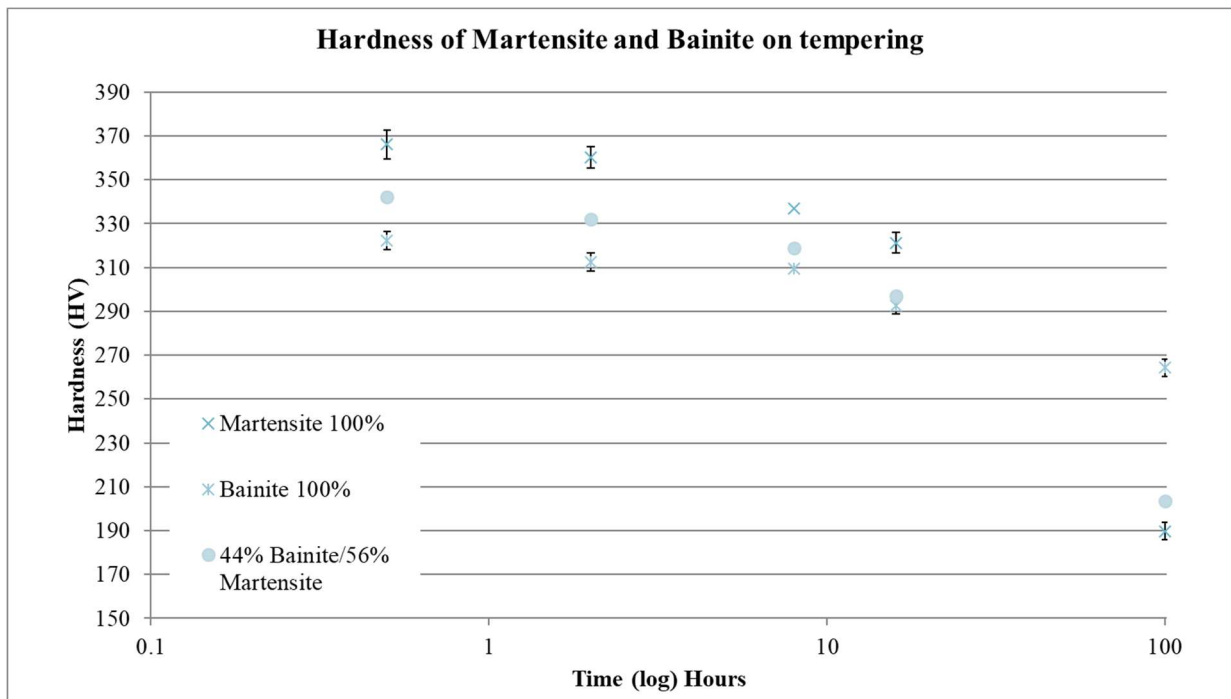


Figure 150 Hardness on tempering up to 100 hours (Hardness (HV) vs. Time (log) Hours)

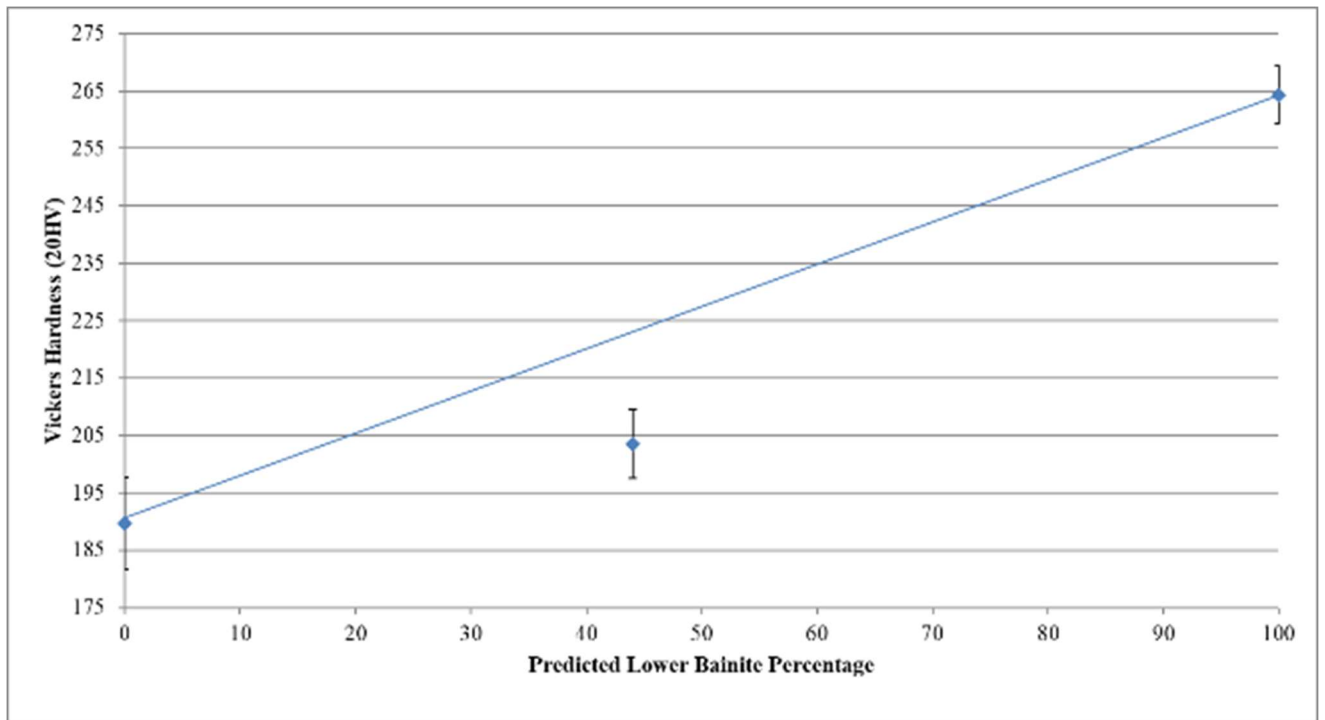


Figure 151 Tempering up to 100 Hours (Hardness vs. Percentage of Lower Bainite)

7.3.2: Micrographs

When looking at the change in microstructure from 16 hours to 100 hours there are several differences, both in terms of morphology, i.e. laths, and carbide characteristics. These are summarised in [Table 41](#) and discussed fully below.

7.3.2.1: Martensite

Martensite has a lath structure visible at 16 hours; there are also small multi-oriented carbides throughout, [Figure 152](#). At 100 hours ([Figure 153](#) and [Figure 154](#)) there is a large loss of lath structure, with large carbides ($1\ \mu\text{m}^+$) on PAGB and smaller carbides in the matrix.

Martensite 100 Hour Images

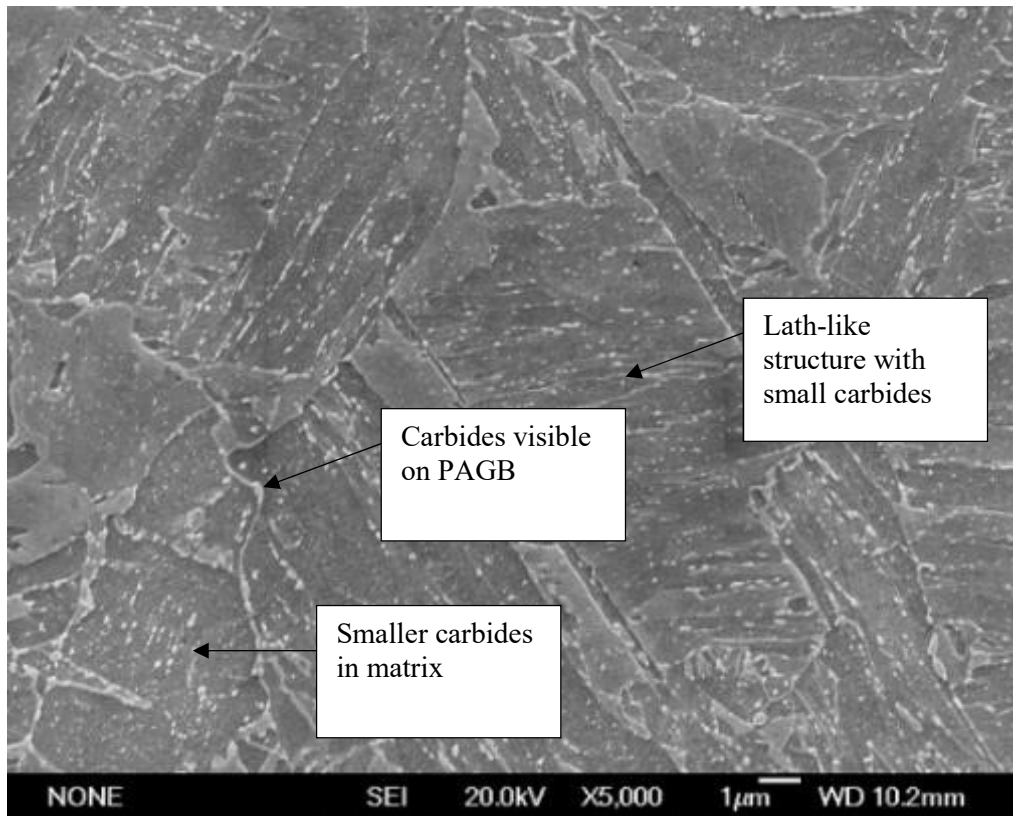


**Figure 152 Martensite- Comparison between 16 and 100 Hours Temper (16 Hours) –
×5,000 Magnification (321.3 ± 4.0 HV)**

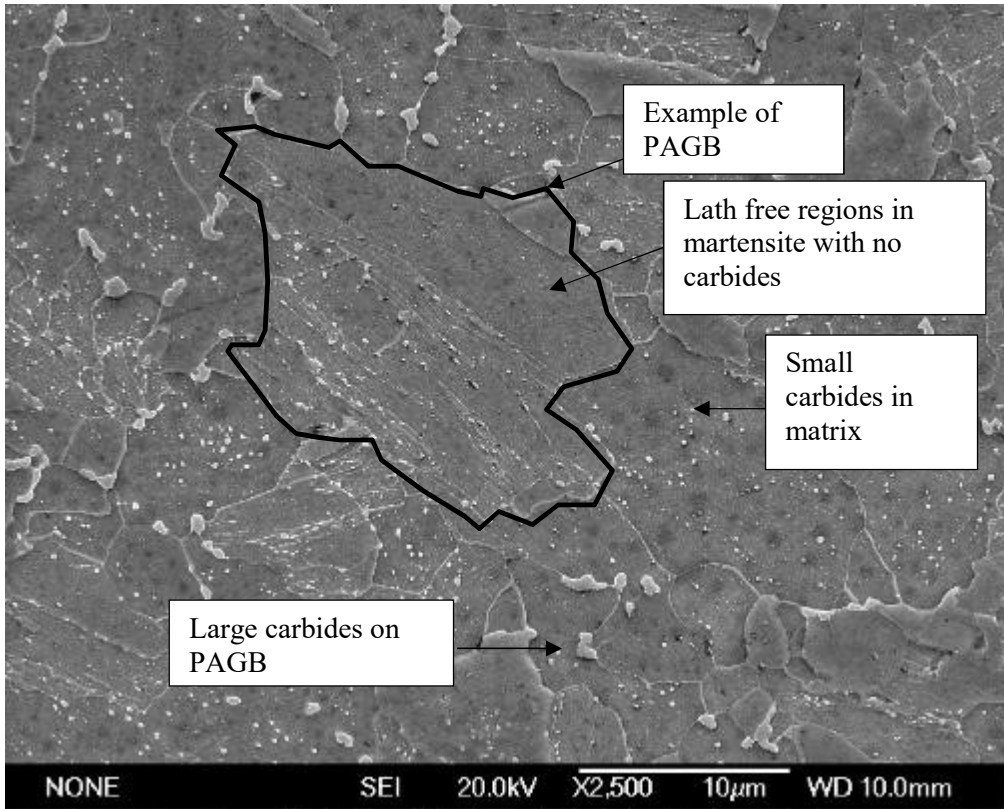


Figure 153 BaseMoV - Martensite - 100 Hours $\times 2,500$ Magnification (189.7 ± 6.0 HV)

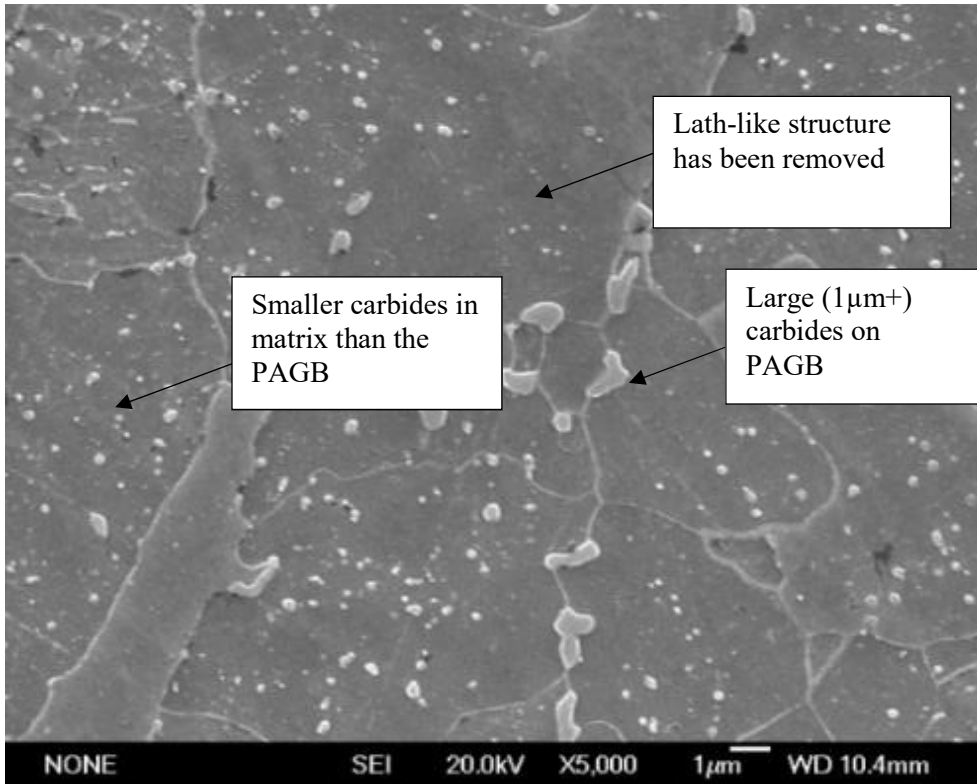


Figure 154 Martensite- Comparison between 16 and 100 Hours Temper (100 Hours) $\times 5,000$ Magnification (189.7 ± 6.0 HV)

7.3.2.2: Bainite

Bainite has a lath structure at 16 hours, with carbides visible throughout. At 100 hours there are regions free from carbides and laths. There are significantly larger carbides present, in the matrix and on the PAGB, as well as regions of smaller carbides within the matrix (Figure 155 and Figure 156).

Bainite

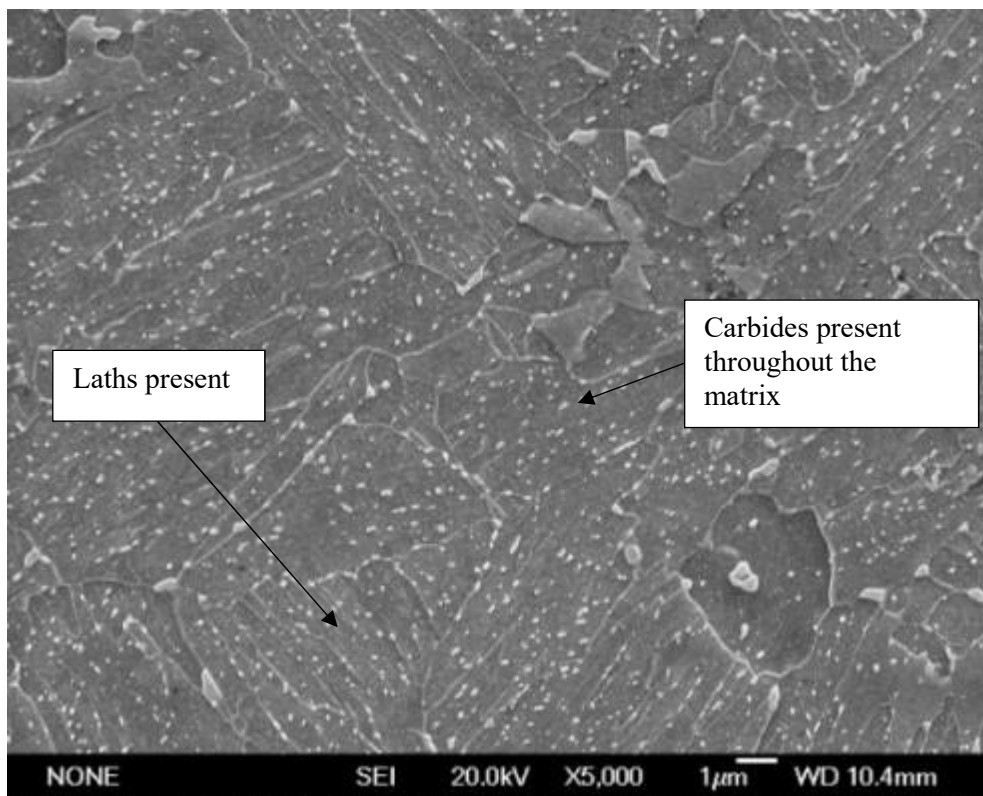


Figure 155 Bainite - Comparison Between 16 and 100 Hours Temper (16 hours) ×5,000 Magnification (292.7 ± 10.0 HV)

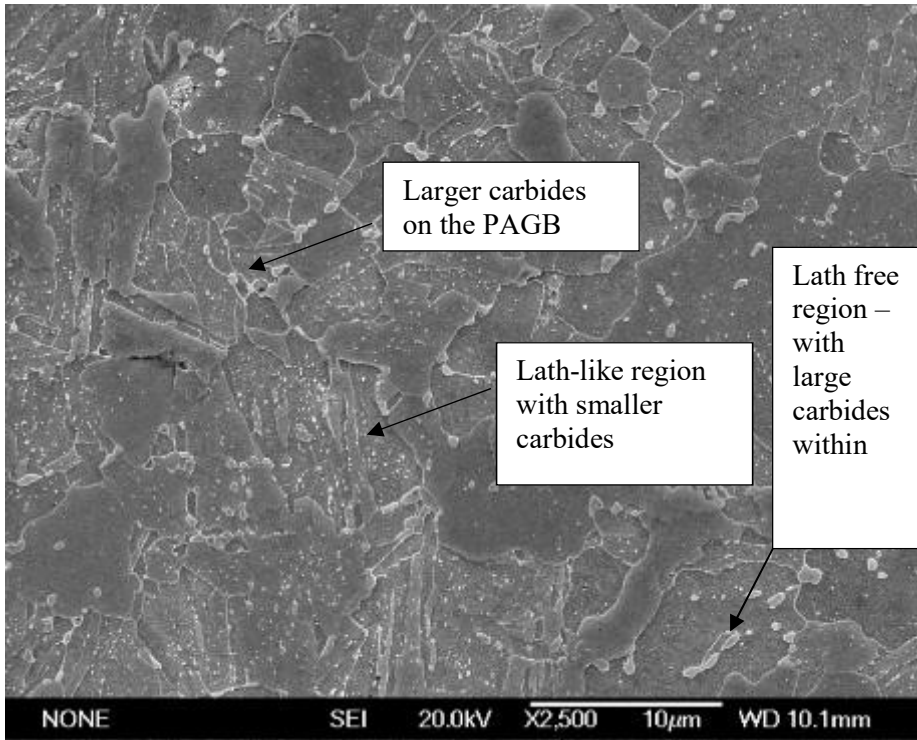


Figure 156 BaseMoV - Bainite - 100 hours $\times 2,500$ Magnification (264.3 ± 10.0 HV)

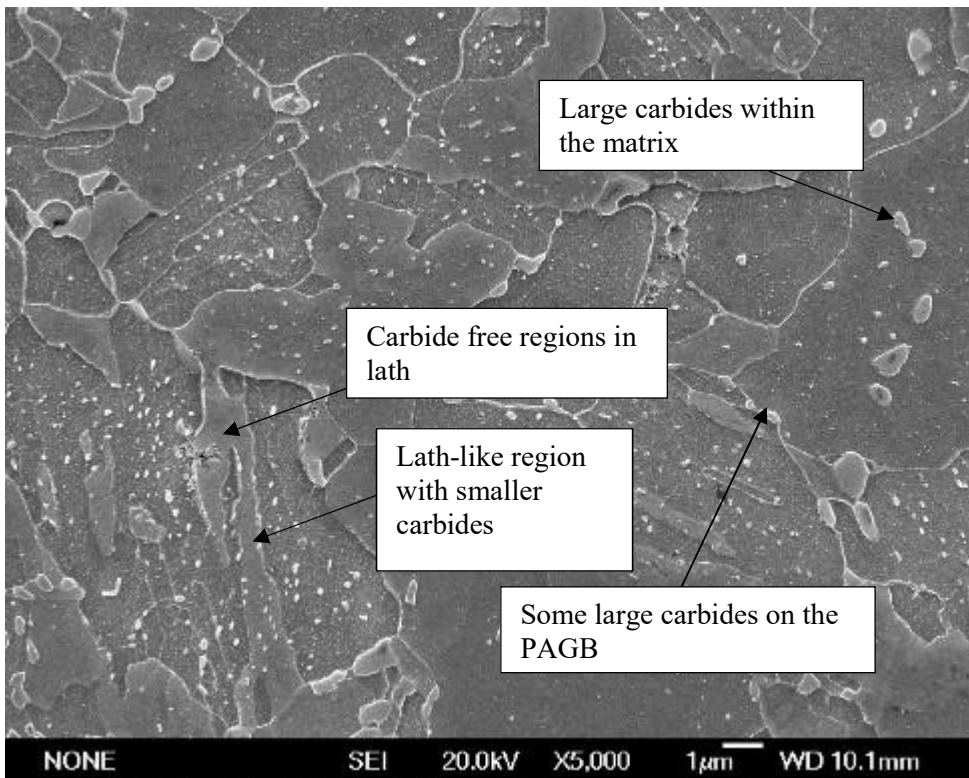


Figure 157 Bainite - Comparison Between 16 and 100 Hours Temper (100 hours) $\times 5,000$ Magnification (264.3 ± 10.0 HV)

7.3.2.3: Singular Phase Comparison

The fully martensitic sample exhibits an absence of most lath structures after tempering for 100 hours, shown in [Figure 153](#) and [Figure 154](#). There are very few laths and fewer numbers of smaller carbides in the matrix compared to the bainite regions and there are larger carbides on the PAGB. The bainitic condition retains laths and has numerous carbides, shown in [Figure 155](#) and [Figure 156](#).

[Figure 157](#) shows the bainite tempered for 100 hours. It can be observed that there are lath-free regions, the same as in for martensite, however in the bainite these regions of lath-free areas are less frequent and regions which do have laths have small numerous carbides. The bainite also has globular carbides in the matrix where laths are not present; this is not shown in the martensitic condition. Visual estimations have found that the bainite is 30% lath-free and the martensite is around 70% lath-free.

7.3.2.4 Mixed Microstructure

The mixed microstructure has bainite and martensite present at 16 hours, with regions of multi-oriented carbides and single oriented carbides distinguishable, both exhibiting laths. At 100 hours there are lath-containing/ lath-free areas, along with carbide-free and carbide-containing areas. The mixed microstructure has the larger carbides on the PAGB and within the matrix, than when compared to the 16 hours micrograph. This shows that features of both microstructures, bainite and martensite, are present at 100 hours.

It is reported in the literature that some types of steels do not follow the Rule of Mixtures, such as ferrite and martensite dual phase steel, with inhomogeneous plastic deformation making the steel closer in strength to ferrite, the softer phase (Bergstrom, 2010).

The microstructure is now comparable to dual phase (DP) steel, which contains ferrite and martensite. The 100 hour tempered martensite is similar to the ferrite in the DP due to its loss in strengthening components. The martensite is now largely lath and carbide free, and any

carbides present are larger with a wider spacing, reducing the strength of the martensite.

The bainite present acts like the martensite in the DP steel. There are laths present still and carbides within the laths. There is a difference in hardness like the ferrite and martensite in the DP steel, like the martensite and bainite at 100 hours temper. This explains the mixed microstructure having a hardness more comparable to the softer martensite, and why it doesn't follow the Rule of Mixtures.

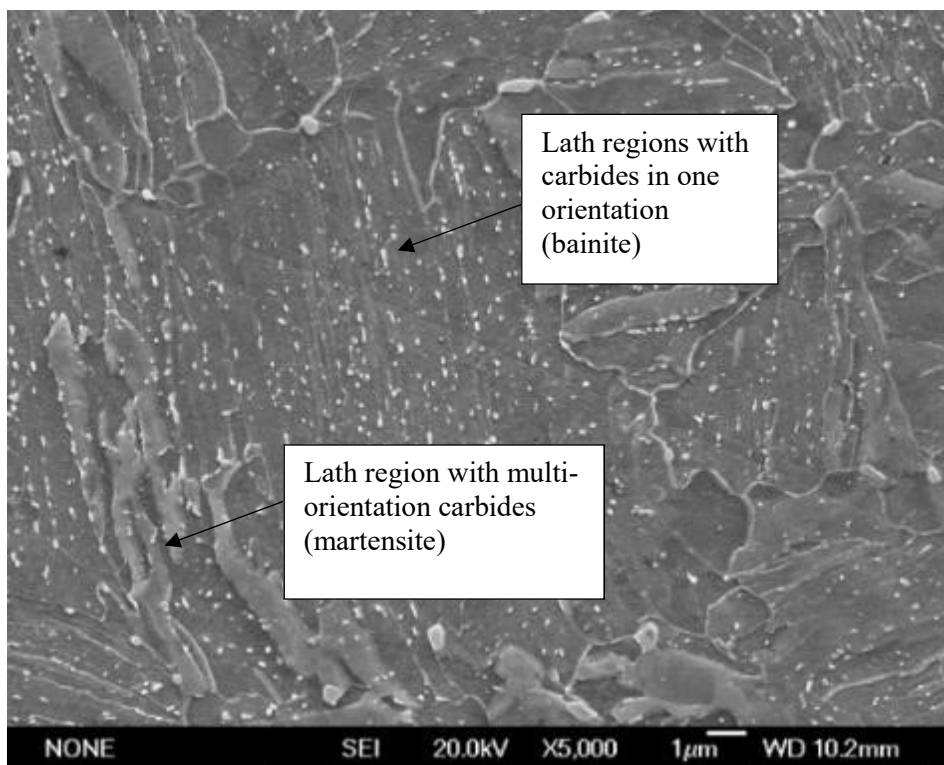


Figure 158 Mixed Microstructure - Comparison Between 16 and 100 Hours Temper (16 hours) ×5,000 Magnification (297.0 ± 10.0 HV)

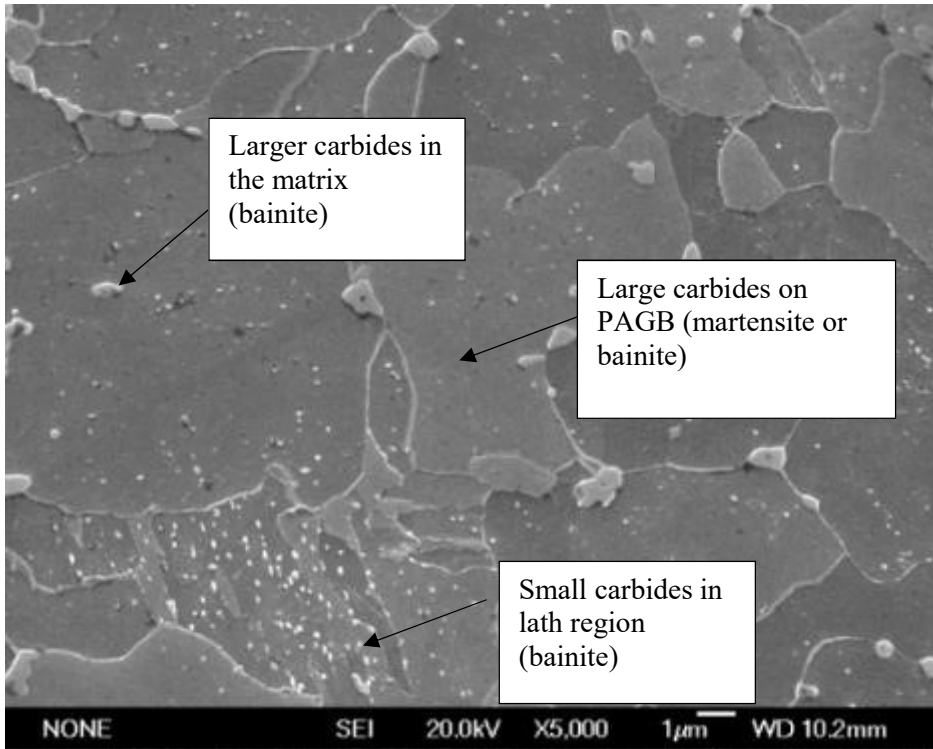


Figure 159 Mixed Microstructure - Comparison Between 16 and 100 Hours Temper (100 hours) ×5,000 Magnification (203.5 ± 10.0 HV)

100 hours Mixed

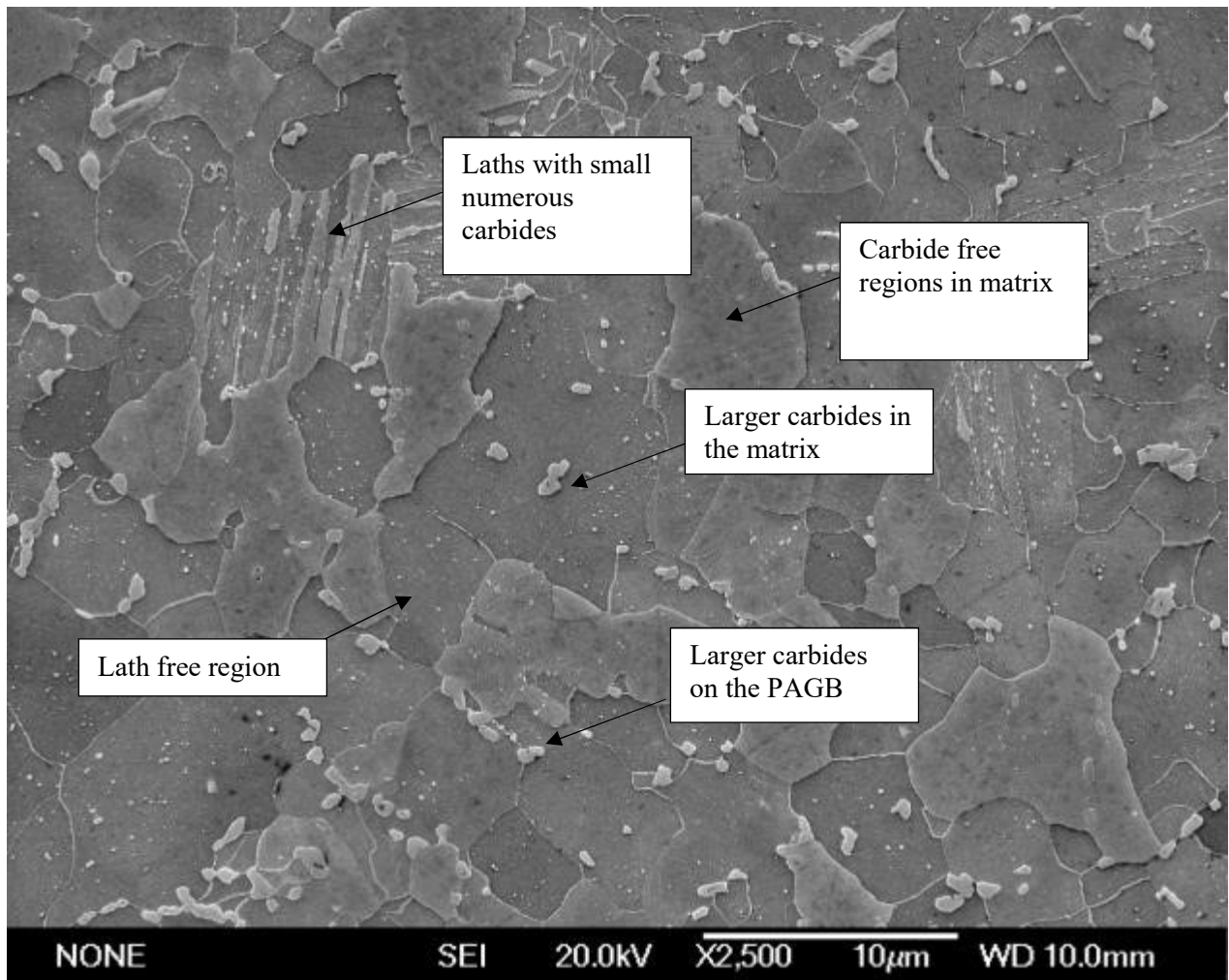


Figure 160 BaseMoV - Mixed Microstructure - 100 Hours $\times 2,500$ Magnification (203.5 ± 10.0 HV)

7.3.2.5 Mixed Microstructure Compared to Singular Microstructures

The mixed microstructure shown in [Figure 159](#) is like the fully bainitic samples, except there are fewer regions which have laths retained; this reflects the mixed microstructure, as martensite has fewer laths retained than bainite. As martensite has not lost of the lath regions it is not expected that the mixtures of laths verse non-laths would mimic the parent microstructures at 54:46. In the bainite there is an estimated 30% of the regions not containing laths, and in the martensite, there is 70% of regions not contained laths. When linear interpolation is used it is expected to be around 50% lath free in the mixed microstructure. However, the actual value of lath free regions is closer to the martensite with 70% being lath free.

Distinction of martensite and bainite in the mixed conditioned at 100 hours temper is difficult due to lack of distinction between features. There are laths present in martensite, typical of the bainitic condition and carbide free regions in the bainite, typical of the martensitic condition [Figure 158](#) and [Figure 160](#). Therefore, when looking at features within the mixed microstructure a representative number of measurements were taken, and values compared to the singular martensite and bainite microstructures.

Table 41 Comparison of microstructural features at 100 hours temper

	Martensite	Mixed Microstructure	Bainite	Comment
16 Hour Features	Lath structure with small multi-orientated carbides	Laths present with small multi-orientated carbides in martensitic regions and single orientated carbides in bainitic regions	Laths present with small single orientated carbides present throughout	Martensite and bainite can be distinguished easily.
100 hours laths	Large loss of lath structure (70%). Martensite has the largest amount of lath loss	Areas of lath structure lost. Closer to 70%.	Regions free of laths (30%)	Following RoM the mixed microstructure should have 50% lath loss
Carbides in matrix	Reduced number of small carbides present in matrix – compared to 16 hours. Large regions where no carbides are present	Large carbides within the matrix. Regions which match both martensite and bainite are found – but cannot be distinguished.	Carbides in lath free regions are larger. Globular carbides in lath-free matrix. Lath-like regions have smaller carbides	Martensite has fewer smaller carbides in the matrix compared to bainite.
Carbides on PAGB	1 $\mu\text{m}+$ carbides are present	Large carbides on PAGB	Large carbides on PAGB	
Boundary coverage by carbides	~20/30% Most coverage	~10% (Expected to be 15-20% using RoM)	~5%	
Overall	Loss in lath structure and reduced number of carbides in matrix and increased number on the PAGB.	Has features of both martensite and bainite	Some lath free regions with larger globular carbides within. A few carbides on the PAGB.	

7.3.3: Lath Size

The 100% martensite (as mentioned previously) in the results section shows there is a vast loss of laths and formation of larger carbides in the matrix. Visual estimations have found that the bainite is 30% lath-free and the martensite is around 70% lath-free. This is looking at 100% microstructures.

The hardness results of the mixed microstructure could indicate that there is a deviation from the Rule of Mixtures, so that the lath size of the bainite and the bainite in the mixed phases were compared. The results, [Figure 161](#), show the same shape of distribution between the two conditions. Previous results have indicated that there is an error of $\pm 0.3 \mu\text{m}$ in lath width measurements; this means there is no discernible difference in the average lath width. In terms of lath size this indicates that the bainite in the singular and mixed condition are tempering at the same rate and are comparable. [Figure 46](#) in the literature review summarised the strengthening contribution from lath sizes; this shows that the larger the lath size the less prominent the difference in strengthening contribution. The difference between a lath size of $0.6 \mu\text{m}$ and $0.7 \mu\text{m}$ would be a difference in 10 HV. With experimental error included this is not seen as a significant difference.

As there are significant areas which do not have laths present, only the regions which have laths could be examined; the lath spacing may indicate the original lath spacing between lath boundary carbides which have not yet dissolved, where the lath can remain stable. Lath-free regions may be in grains where the carbides have dissolved allowing lath boundary movement.

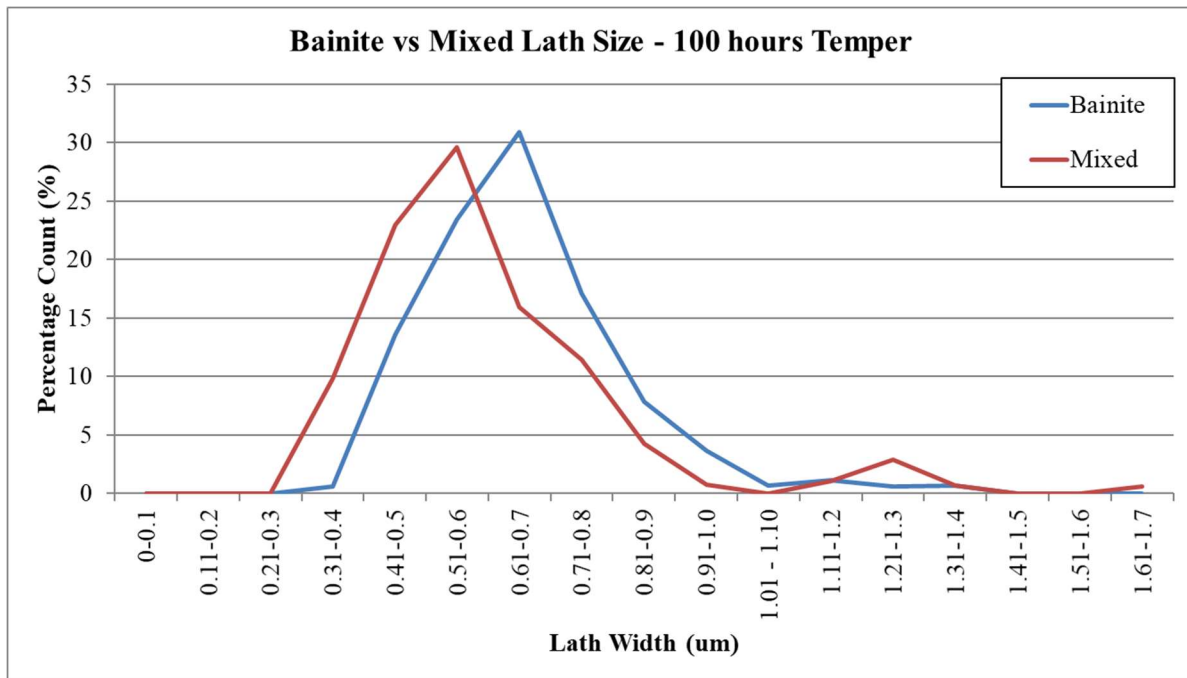


Figure 161 Bainite vs. Mixed Microstructure Lath Size - 100 Hours Temper

7.3.4: Carbide Size at 100 hours tempering

The modal carbide size (min/max/aspect ratio) and compositions were examined in the 3 samples, [Figure 164](#), [Figure 165](#) and [Figure 166](#) and summarised in [Table 42](#). The change in carbide size is also shown in [Figure 162](#) and [Figure 163](#), this is to give a different visual representation of the change in carbide size across the tempering range, 30 minutes to 100 hours. In the mixed microstructure it is difficult to discern which carbide belongs to which phase, so carbides were taken from all regions. From visual examination of the micrographs it appeared that martensite and bainite had different carbide sizes, with martensite thought to have larger carbides than the bainitic microstructure. The mixed microstructures were expected to have a carbide distribution which overlapped the martensitic and bainitic carbides. This was found not to be the case, as there was no clear distinction between martensitic and bainitic carbides in the mixed microstructure samples, when examining the histograms. The mixed microstructure histogram did cover the full range of carbides for

martensite and bainite, which indicated a representative range of carbides were measured in terms of distribution.

Table 42 Mode Min, Max, Aspect Ratio of carbides in martensitic, bainitic and mixed microstructure at 100 hours tempering, including carbide density

	Mode Min Value (nm)	Mode Max Value (nm)	Mode Aspect Ratio	Carbide Density /μm^2
Martensite	50 – 59	75 – 99	0.71 – 0.75	4.0
Mixed	60 – 79	75 – 99	0.71 – 0.75	4.3
Bainite	70 – 79	100 – 124	0.66 – 0.70	4.1

7.3.4.1 Minimum Carbide Size

The minimum carbide size is shown in [Figure 164](#) and found to be 50-59, 60-69 and 70-79 nm for martensite, mixed and bainite microstructures respectively. The three carbide types have similar histogram distributions; however, the martensite shows a larger skew of carbides to the right, indicating that there are more carbides of a larger size.

7.3.4.2 Maximum Carbide Size

The maximum carbide size is shown in [Figure 165](#) and found to be 75-99, 75-99 and 100-124 nm for martensite, mixed and bainite respectively. Again, martensite shows a larger histogram distribution to the right, indicating more carbides of a larger size. The mode size of the larger carbides is within 1 bin size for all of the microstructures, showing little difference.

There was an indication that the randomly sampled mixed microstructure carbides were similar in size to bainitic carbides, this may be due to bainite having smaller carbides, with a higher number density, and would also back up results that martensite is starting to have larger carbides with a lower number density. This is show in [Figure 164](#) and [Figure 165](#)

where the martensitic carbides have a larger number of carbides at a higher percentage count compared to the mixed and bainitic carbide sizes.

7.3.4.3 Aspect Ratio

To determine if there is any difference in carbide shape the aspect ratio were measured and presented in Figure 166. Aspect ratio of 0.71 - 0.75, 0.71 – 0.75 and 0.66 – 0.70 were found for martensite, mixed and bainite respectively. The distribution of bainite indicates more elongated carbides, while martensite is found to have more spherical carbides. The mixed microstructure has a distribution between the two conditions. Martensite is found to have a ‘hump’ in the aspect ratio distribution, which indicates two regions of carbide sizes. From examination of the images, this would be consistent with the larger carbides on grain boundaries and the smaller carbides within the matrix.

7.3.4.4: Change in Carbide Size (30 minutes to 100 hours)

Carbides sizes have been compared on tempering for the mixed, martensitic and bainitic microstructure. As stated, early carbide sizes in the mixed microstructure cannot be distinguished, so they have been given the same values for both martensitic and bainitic carbides sizes. This means that the values at 100 hours may be larger or smaller than the actual values. Figure 162 shows that martensite in the mixed microstructure has an increase in minimum size when tempered from 30 minutes to 100 hours, this is more rapid than the martensite in the mixed condition. The bainite shows little increase in size until the later tempering times. The bainite in the mixed condition shows the same trend as the bainite.

Figure 163 shows that the maximum size of the martensite appears to increase, then decrease with increased tempering times. The trend does show an overall increase in size and becomes more spherical, when the minimum size is considered. Both bainite and the mixed microstructure carbides show an increase in size. Martensite in the mixed condition has a slower increase in size, while the bainitic maximum carbide size is stable at 16 hours.

From the data it would indicate that both martensite and bainite are over-tempering, but some bainitic regions are resistant to over-tempering, retaining finer carbides (further evidenced by micrographs). In some regions the tempering has led to lath-free regions in the martensite and the bainite, where larger carbides are found.

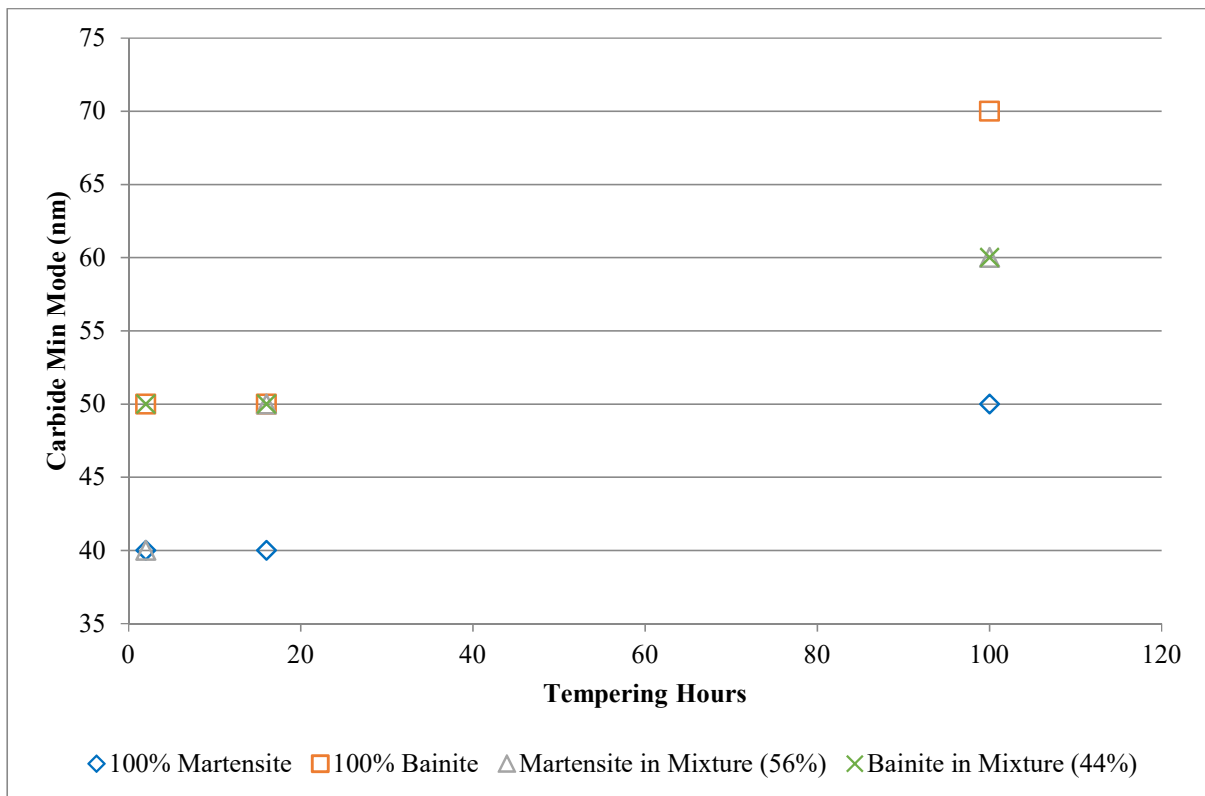


Figure 162 Min Mode of Carbides on tempering at 2, 16 and 100 hours

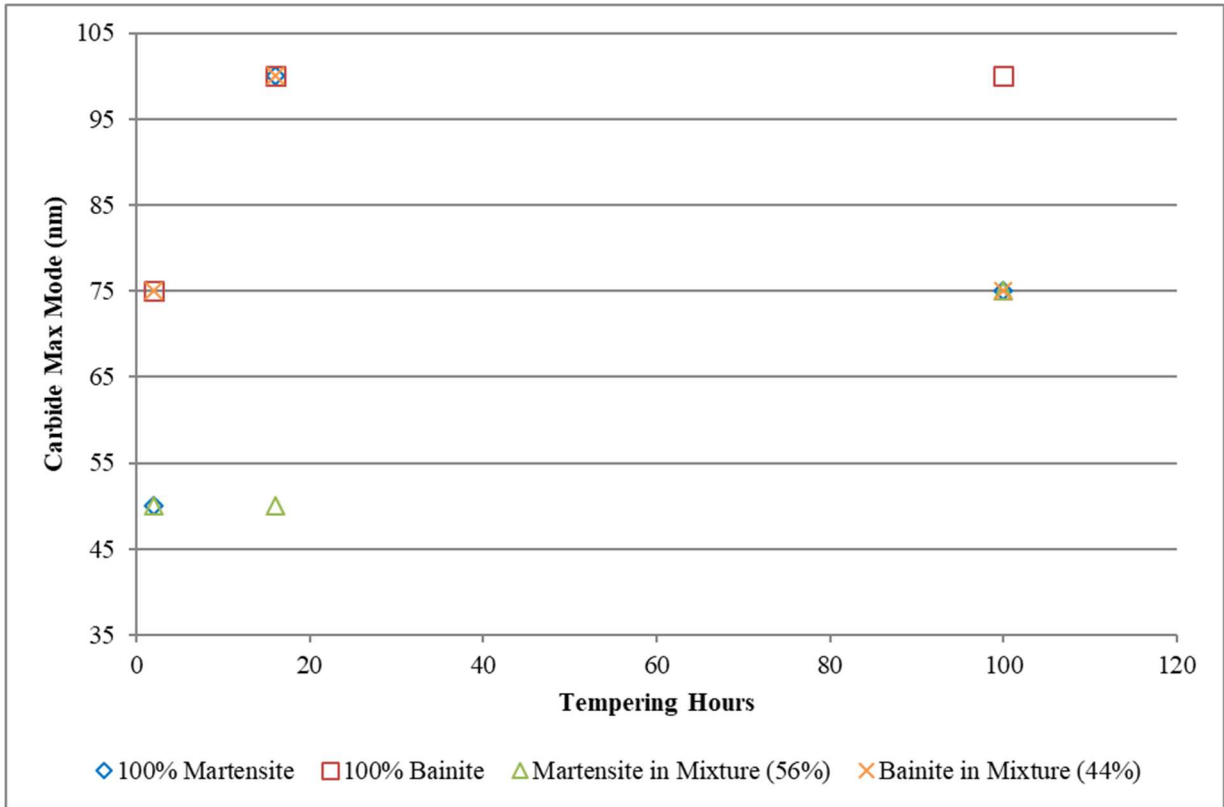


Figure 163 Max Mode of Carbides on tempering at 2, 16 and 100 hours

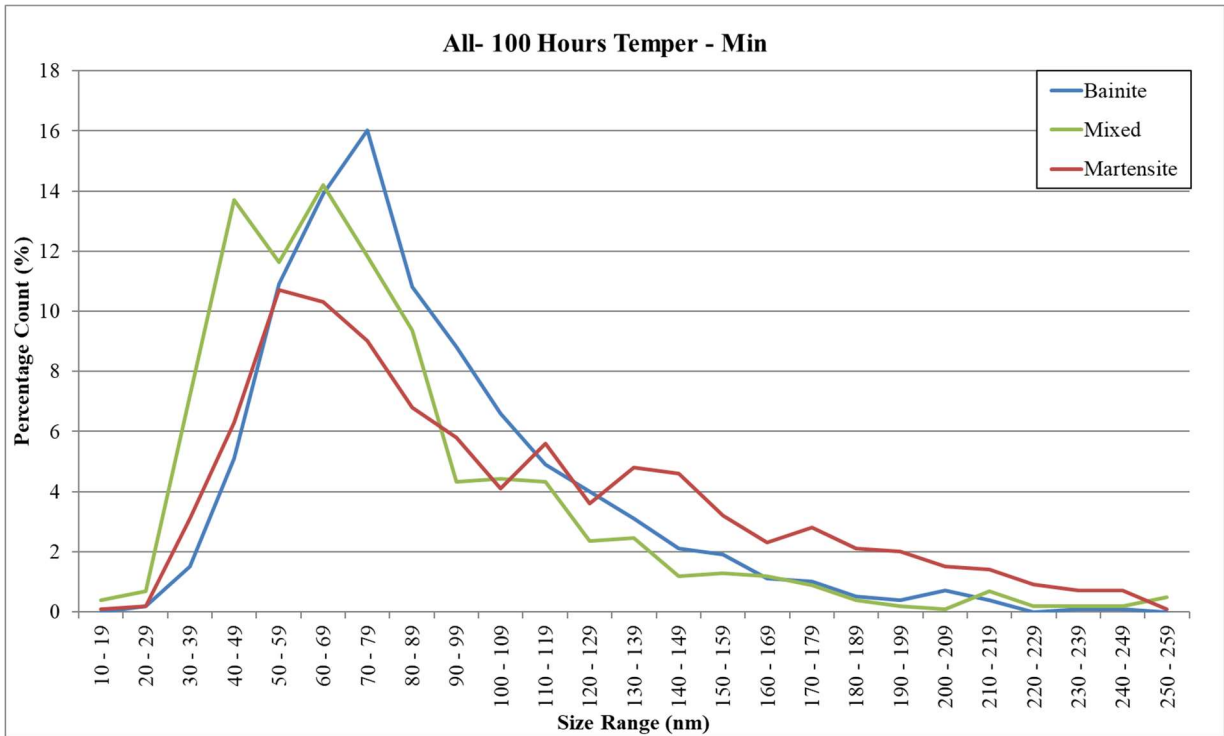


Figure 164 Carbide Size for 100 hours temper (Min - Width)

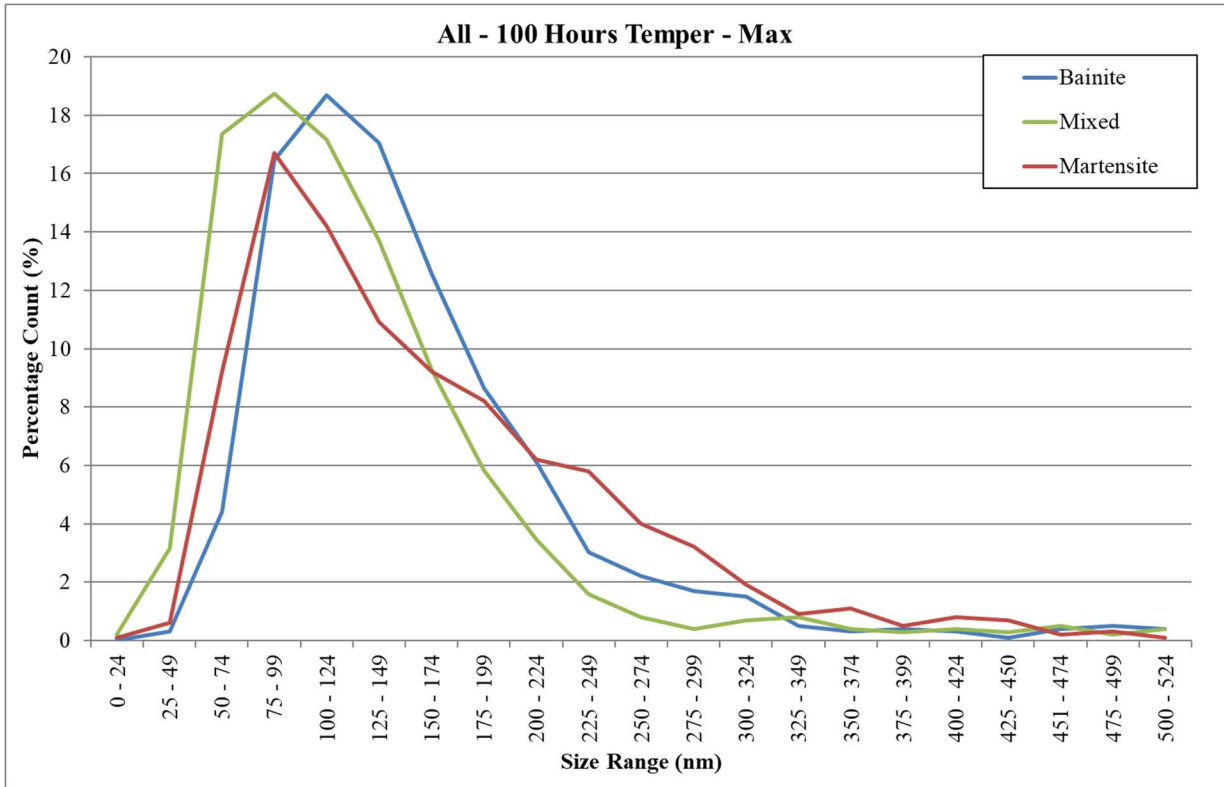


Figure 165 Carbide Size for 100 Hours Temper (Max - Length)

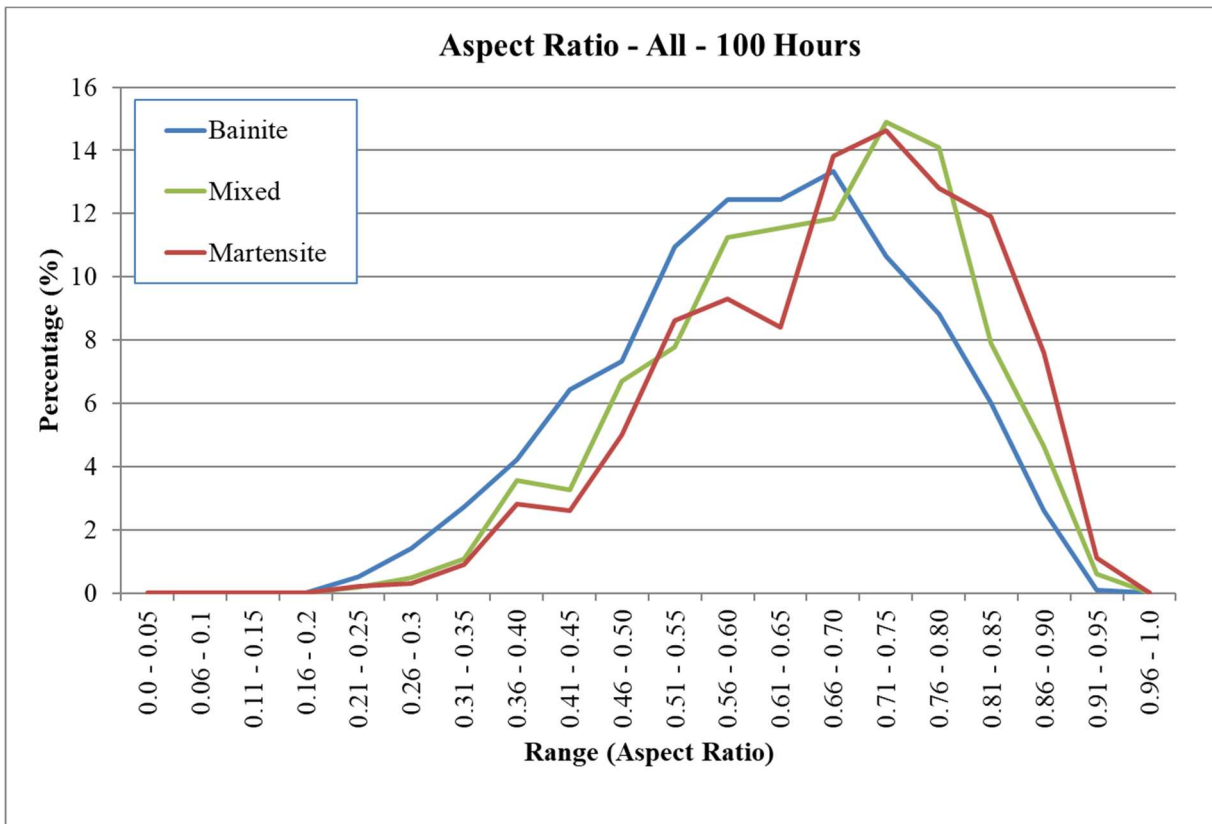


Figure 166 Carbide Size for 100 Hours Temper (Aspect Ratio)

7.3.5: Compositions

The compositions of the carbides after 100 hours tempering was investigated, using EDX. It is estimated that carbides with a size of 1 μm and smaller are not suitable for analysis with EDX, as the interaction area of the EDX beam would sample the carbides and the surrounding matrix giving an inaccurate analysis of the carbide composition. Table 43 shows the composition of alloy-containing carbides.

The ratio of alloying element to Fe has been determined using the following equation

$$\text{Ratio} = \text{Alloying Element \%} / (\text{Fe\%} + \text{Alloying Element \%})$$

Equation 7.1

Table 43 Alloying containing carbides of bainite, martensite and mixed microstructure

Elements – Alloy containing Carbides	Bainite 100 hours (Carbides within grain and on grain boundaries)	Mixed 100 hours (carbides within grain and on grain boundaries)	Martensite 100 hours (Typically on grain boundary)	16 Hours (Ju, 2018)	Pseudo-Equilibrium (Ju, 2018)
Mn	0.04	0.10	0.40	0.089	0.169
Mo	0.01	0.10	0.20	0.015	0.001
Other	0.01	-	0.01	-	-

7.3.5.1 Comparison of Singular Phases

Martensite was found to have molybdenum-enriched carbides (ratio of 0.20 for Fe, mostly at the PAGBs, as these carbides were large enough to be analysed. Coarser bainitic carbides (1 μm +) had a lower enrichment of molybdenum with a ratio of 0.01 to Fe. This indicates that the martensitic carbides are becoming enriched with Mo, but the bainitic carbides are not having the same level of enrichment for carbides of similar size. The carbon data have not been included in the analysis, as there are often issues with C quantification; the C

equilibrium is predicted at 0.0027 wt. % C using Thermo-Calc data.

The substitutional alloying element contents for Mn and Mo have been analysed as these are the main alloying elements present in the carbides investigated using EDX. The Mn element content in martensitic carbides after tempering for 16 hours was determined by Ju 2018, with a ratio of 0.089; this is lower than the pseudo-equilibrium amount of 0.169. After tempering for 100 hours the Mn ratio in martensitic carbides was 0.40, which indicates that there has been enrichment. This is higher than the predicted amount but confirms that the amount is increasing in concentration. Another explanation which has not been investigated is that Mn-rich alloying carbides are appearing, section 5.2 discusses how BaseMoV is predicted at equilibrium to have cementite and M_7C_3 with Mn present. MC carbides are predicted but Mn is not predicted to be present. The martensitic carbides are more enriched in Mo compared to the bainitic and mixed microstructure carbides. The lack of carbides in the matrix means that those on the PAGB are stable, growing at the expense of the smaller carbides within the matrix. BaseMoV is predicted to have 2.2×10^{-2} volume fraction of carbides, with the following stable carbides (volume fractions included), cementite (1.3×10^{-2}), M_7C_3 (6.3×10^{-3}) and MC (2.7×10^{-3}); these carbides are predicted to have Mo alloying addition further backing up the thought that they are stable carbides on the PAGB. It is also worth noting that the Mo carbide ratio, in the fully martensitic condition, was 0.015 increasing to 0.20 at 100 hours. This is becoming further away from pseudo-equilibrium cementite, indicating enrichment of carbides. Bainite has a value which is closer to pseudo-equilibrium which indicates that it is enriching slower than the martensitic carbides.

The carbides in the bainite do not appear to follow the same trend as the martensitic carbides, with carbides within the matrix remaining stable, whilst in martensite these have mostly disappeared at 100 hours tempering or are of a small size. As there is such severe tempering (100 hours) it would be expected that the bainite and martensite would show similar

tempering responses, due to two microstructures having the same base BaseMoV compositions.

Bainite and martensite do not appear to have the same composition-modified when examining those over 1 μm . There is no robust evidence that these are secondary carbides as there is no apparent appearance of new carbides. One suggestion for this occurrence is that the lower bainitic cementite carbides do not form via a para-equilibrium mechanism (discussed in section 2.8.4.1). From the data analysis of Caballero and Miller, it was found that the lower bainitic carbides formed via partial-para-equilibrium, with the Cr being enriched in the cementite, compared to the surrounding ferrite matrix. This would mean that there is a higher amount of alloying element in the carbide, which would bring it closer to the equilibrium condition on formation.

Martensitic carbide para-equilibrium is discussed in section 2.2.2, where cementite formed from the martensite transformation is not enriched with alloying elements, and the ferrite and cementite have the same alloying composition on transformation. This would be in line with what is expected from the martensite and why there is a carbide evolution as an equilibrium stage is reached.

Differences in carbide transformation driving force would support the hypothesis that the bainitic carbides are being enriched with alloying elements on formation. A difference in starting conditions would provide a difference in driving force for transformation to the predicted equilibrium carbides, with lower bainitic carbides starting off closer to equilibrium compared to the martensitic carbides. This would help to stabilise the carbides within the matrix of the bainite and reduce the number of larger carbides found on the PAGBs. The difference in the two mechanisms can explain why the martensite has more carbides on the PAGBs compared to the bainite and explains why there are more stable carbides present in

the bainite. These carbides also contribute to the stabilisation of laths, explaining why the bainite has more stable laths compared to martensite, subsequently resulting in the higher hardness.

Further evidence that bainitic carbides are formed by a partial-para-equilibrium can be obtained using TEM or atom probe tomography; however, this is out of the scope of this project.

7.3.5.2 Comparison of Singular Phases to Mixed Condition

The mixed microstructure was found to have molybdenum-enriched carbides, (ratio of 0.10 to Fe) on the PAGBs, similar to the fully martensitic sample after tempering for 100 hours. The carbides were not as enriched as the martensitic carbides, indicating that less molybdenum was present in the carbides. As the alloying elements are determined as a ratio this adds to the robustness of these results and means that like-for-like comparisons can be made about the data.

The carbides in the mixed microstructure has a Mn composition closer to bainite; there are two explanations why bainitic carbides have a lower amount of Mn compared to martensitic carbides, indicating that carbides are less Mn-rich. Firstly, the carbides analysed may have been taken from more bainitic regions than martensitic regions, skewing results. Or this is a genuine effect and the mixed martensitic carbides are enriching more slowly than when compared to martensite. This would back up results found from the hardness values and the carbide sizes.

7.3.5.3 Carbide Summary

Martensitic carbides are becoming enriched with Mo, this amount is higher than predicted.

The martensitic carbides are more enriched than bainite and mixed microstructures; the mixed microstructure has enrichment similar to bainite, but this may be due to the sampling in the mixed microstructure being skewed towards larger bainitic carbides. The bainitic and martensitic carbides are not following the same enrichment trend, this is something which could be investigated in further work.

7.3.6: Summary – 100 Hours

There is a difference between the tempering response of the martensite and bainite at 100 hours compared to 16 hours. Martensite and bainite are both shown to be over-tempering, with loss of lath-like regions, however bainite is shown to retain a significant number of laths when compared to martensite.

The mixed microstructure starts to deviate from the Rule of Mixtures at 16 hours, but there is indication it is tempering in a manner more like that of bainite. The Rule of Mixtures is not followed at 100 hours tempering, thought to be due to the lack of laths/carbides resulting in a similar strengthening mechanism as dual-phase steel, where the mixed microstructure has hardness closer to the softer phase, martensite.

There is evidence to suggest that Mo-rich carbides are forming on the PAGBs where diffusion is easier. In the bainitic condition there are smaller carbides within the matrix, which suggests there is not as much of a driving force for carbide coarsening within the matrix of cementite particles, as compared to martensite. One reason for this may be there is no driving force for the coarsening / enrichment of cementite, perhaps due to lower bainitic carbides transforming via a partial-para-equilibrium mechanism.

Chapter 8: Simulation of Heating and Cooling using COMSOL

8.1: Comparison to Experimental Data

TATA Steel produced data on the cooling of 3 steel plates (20 mm, 50 mm and 75 mm thick), shown in [Figure 167](#).

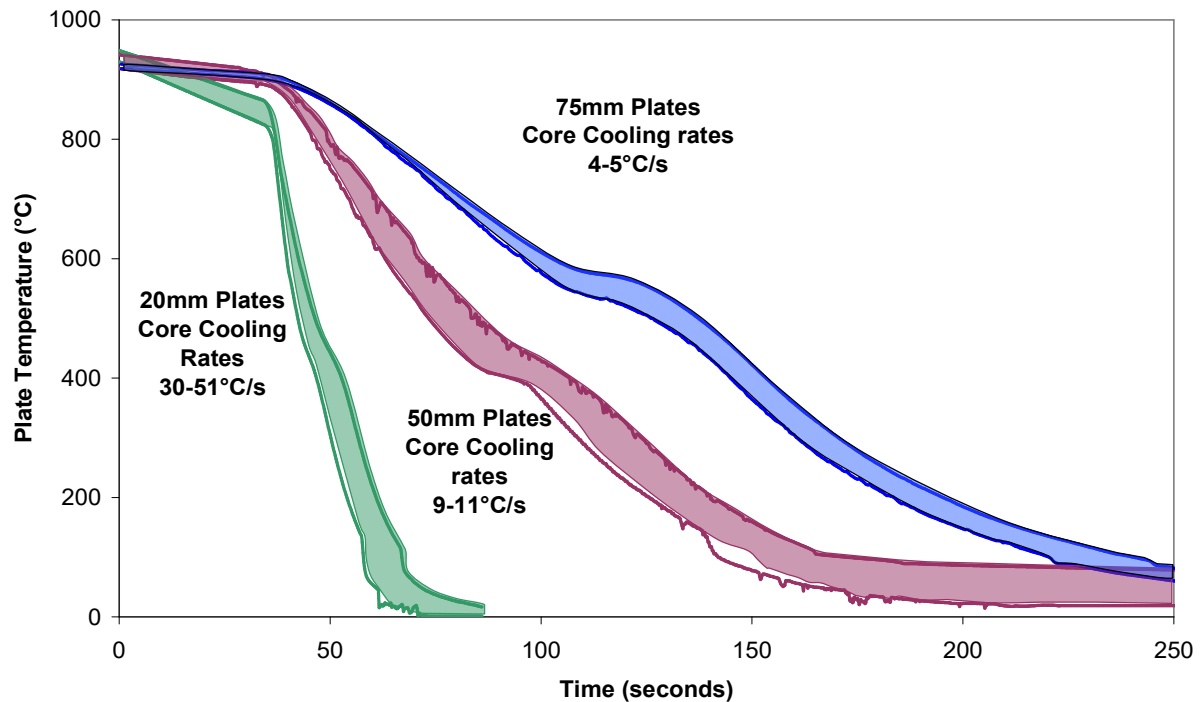


Figure 167 Cooling of steel plates, figure provided by TATA Steel, looking at core cooling rates

There is a transformation happening in the 75 mm thick plate just below 600 °C. The transformation is expected to be an exothermic transformation, as there is a kink in the cooling curve, as heat is released. The transformation is likely to be a ferritic/pearlitic transformation based on the high temperatures, but as the steel is not provided this cannot be known for definite. To avoid any transformation within the COMSOL model then the cooling temperature range was taken between 800 – 600 °C. The data given from TATA steel is a fixed point in the process and cannot be altered, therefore the data from COMSOL shall be fitted to the experimental data.

8.2: Cooling Curve

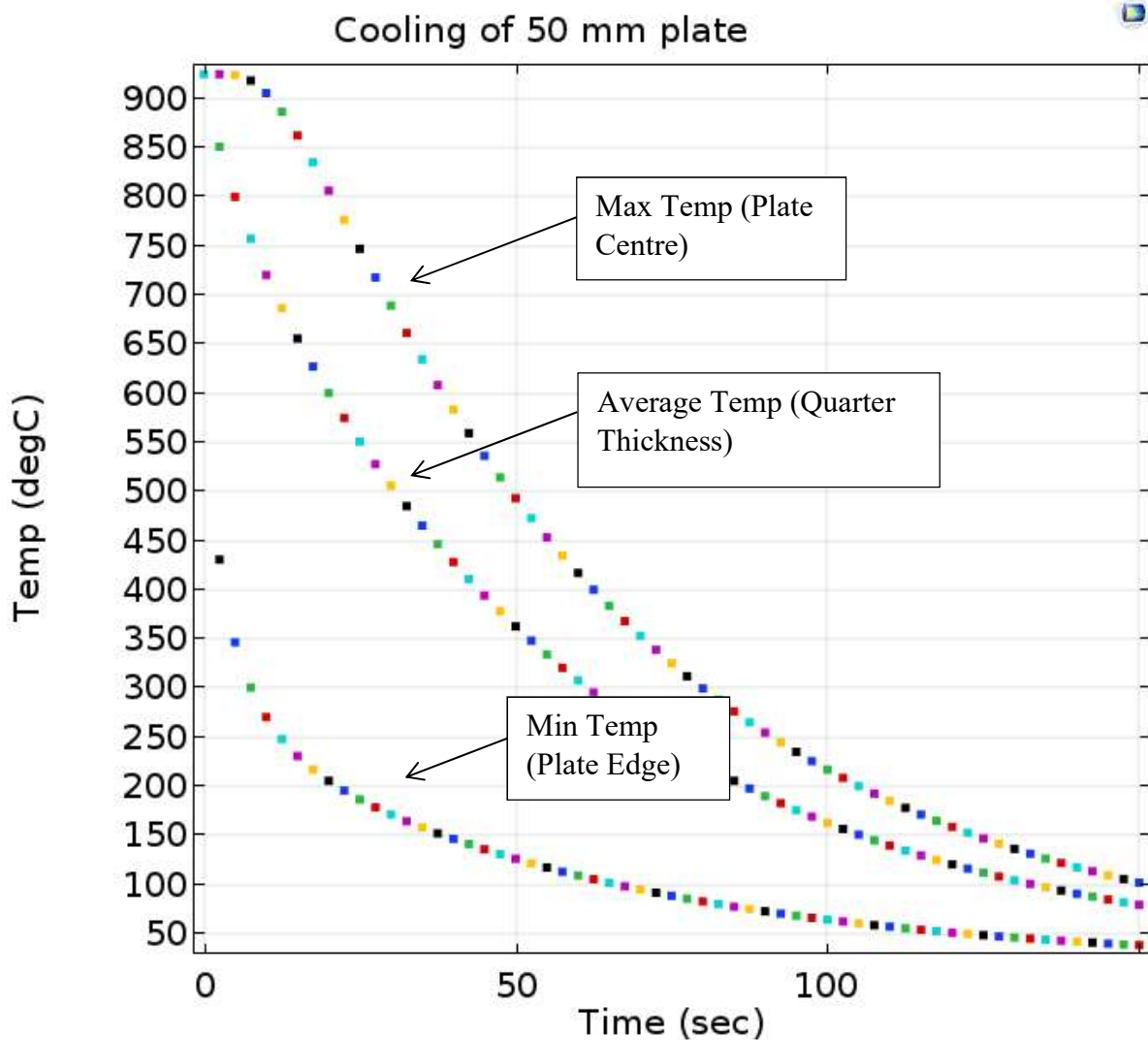


Figure 168 Cooling Curve from COMSOL, using parameters in Table 16

There is agreement with the TATA cooling rate and the COMSOL model, the COMSOL data are for the maximum temperature, which would represent the core cooling rate, in line with what was carried out by TATA steel. The 50 mm thick plate will be used in the following study, looking at heating times.

Table 44 shows the comparison between the provided data and COMSOL predictions. As the data from TATA steel is over a range it is difficult to plot the TATA steel data against the COMSOL data, so the times taken to cool are considered. The shape of the real-time data

(See [Figure 167](#)) shows that there is an almost linear drop in temperature between 800 – 600 °C. Plotting the COMSOL and real-time data may be considered in the future if there were problems with the predicted cooling time matching real-time data.

Table 44 Comparison between experimental data and COMSOL cooling rates from 800-600 °C

Plate Thickness (mm)	Cooling rate (°C/sec)- TATA	Cooling Rate (°C/sec) – COMSOL
20	50 – 32.3	49
50	11.2 – 9.0	11
75	5.6 – 4.7	5

8.3: Comparison of Parameters

A limitation of COMSOL is that material properties are fixed and cannot be altered as the temperature of the material changes. This means that the properties chosen need to be adequate as the materials cools, and that properties which are temperature dependent should be investigated to ensure that there is not a dramatic effect on the predicted cooling rates if the parameters value for the maximum temperature is chosen instead of for the minimum temperature. From the COMSOL values which can be programmed Heat Capacity, Thermal Conductivity and Density have been examined further to ensure the validity of the cooling model.

8.3.1: Heat Capacity

Heat capacity was shown to have an effect on the cooling curve of the steel, shown in [Figure 169](#). The initial value of 500kg.K is similar to what is expected in the literature (Metals, 1985) however when this was compared to the TATA data there was an ill fit. Values were chosen in increments to determine the best fit, such as 1 kg. K, 1000 kg. K and 1500 kg.K. 1000 kg. K was found to have the closest fit to the three values and further refinement was carried out to choose the best fit. This was found to be 925 kg.K, so was chosen to fit the

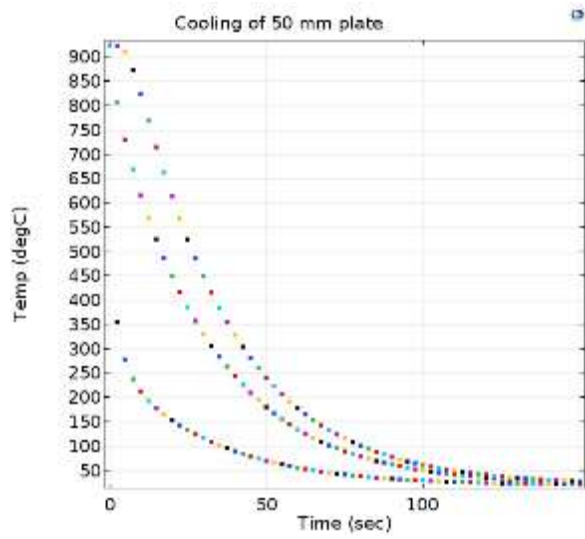
COMSOL data to experimental data provided by TATA Steel in [Figure 167](#), and quantified in [Table 44](#).

8.3.2: Thermal Conductivity

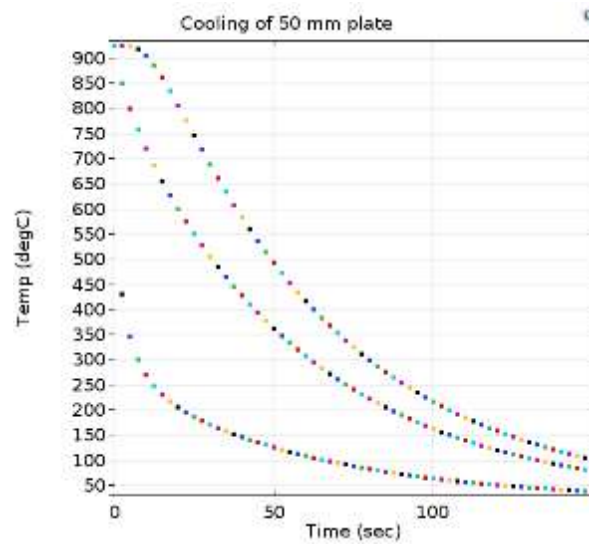
Thermal Conductivity changes with temperature the value of 43 W/(m.K) for 600-800 °C, as it was in line with the literature range used to determine what values should be chosen and matched TATA's experimental results in terms of cooling time, so that the model fitted with the experimental data provided (Metals, 1985). Comparisons of the three potential values of thermal conductivity can be seen in [Figure 170](#).

8.3.3: Density

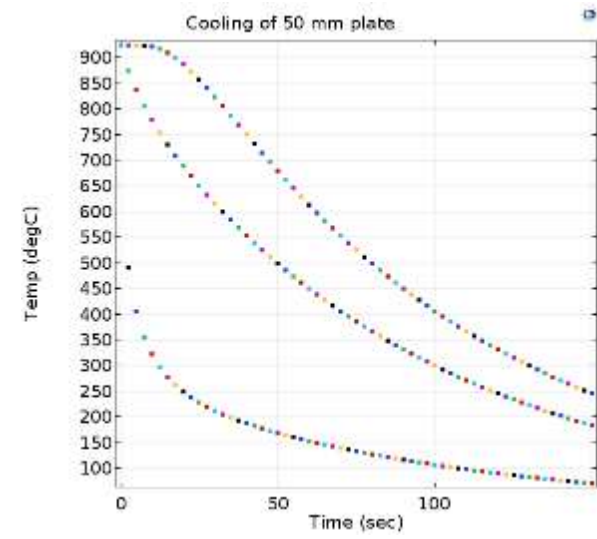
Thermo-Calc was carried out to determine the density of BaseMoV and found to be between 7625 – 7825 (kg/m³), between 925 °C and room temperature. This agrees with literature values given for steel (Metals, 1985). A value of 7750 (kg/m³) was chosen to be representative of the cooling process. The range was calculated using COMSOL and it was found that there is no noticeable effect of changing the minimum and maximum values shown in [Figure 171](#). The fact that the cooling curves do not change with the different densities mean that any of the values could reasonably be used and gives a good indication that the density values used are valid.



500 kg. K

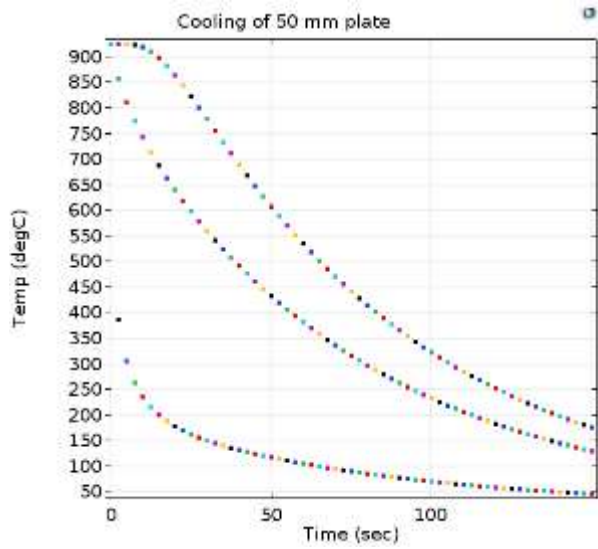


925 kg. K

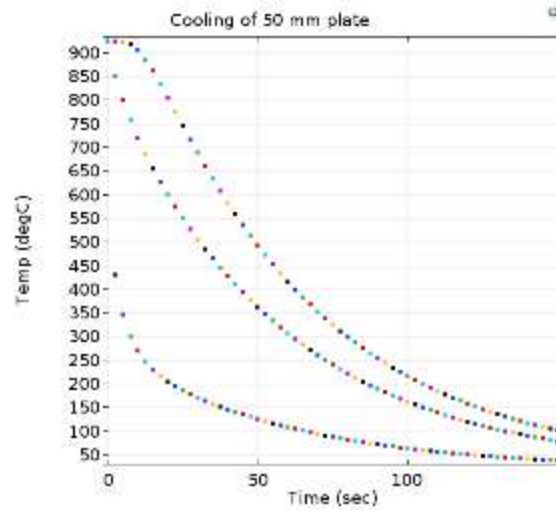


150kg. K

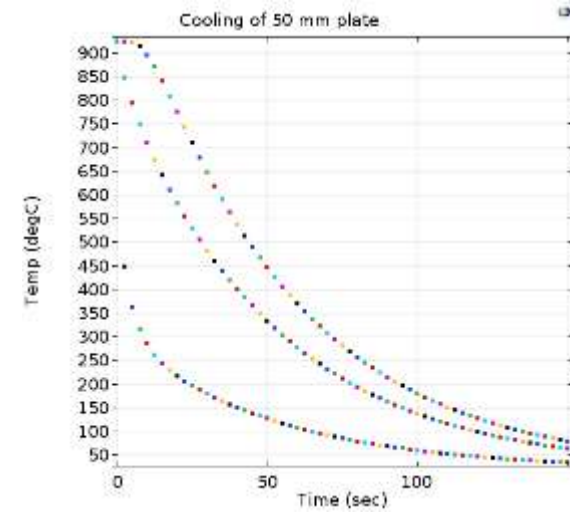
Figure 169 Heat Capacity comparison



30W/ (m.K)

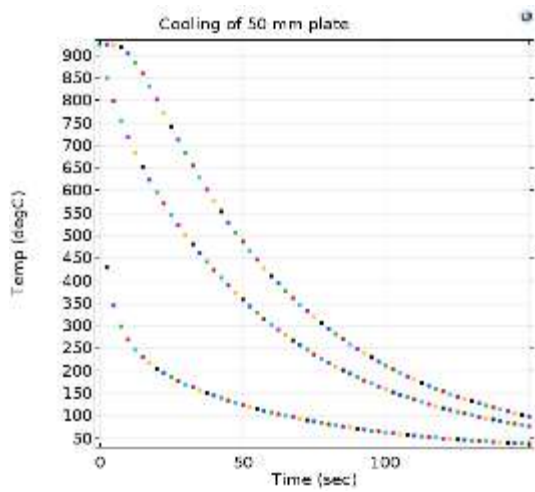


43W/ (m.K)

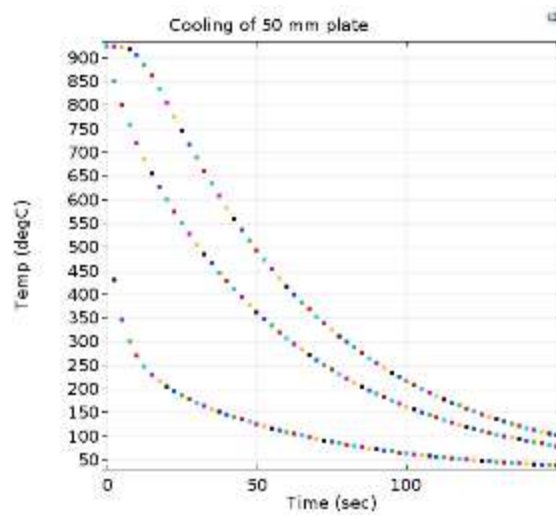


50W/ (m.K)

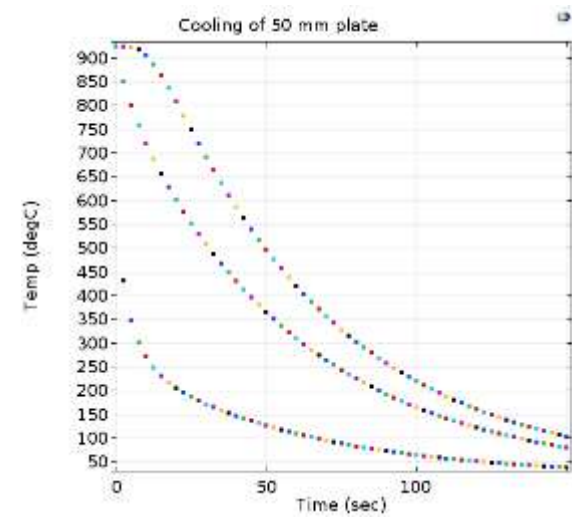
Figure 170 Thermal Conductivity Comparisons



7625 (kg/m³)



7750 (kg/m³)



7825 (kg/m³)

Figure 171 Density Data Comparison

8.4: CCT Diagram

A CCT diagram was produced for BaseMoV, see [Figure 67](#). A cooling rate of 21 °C/sec and slower was found to produce a mixed (bainite + martensite) microstructure. The COMSOL model was used to determine which plate thickness would produce a cooling rate of 21 °C/sec; this was found to be 33 mm thick. Any plates which are thicker than 33 mm would cool slower than 21 °C/sec and have a mixed microstructure.

Further evidence of the robustness this statement comes from the plates which were originally provided by TATA Steel, which was air cooled from 925 °C. The CCT diagram also shows that anything which slows cooler than 3.3 °C/second between 800-500 °C produce a mixture of ferrite and bainite. As the BaseMoV plate has a thickness of 36 mm and a martensite and bainite mixture this indicates that it cools quicker than 3.3 °C/second.

Another determining factor is that the 75 mm steel showed a transformation around 600 °C, thought to be a ferrite + pearlite transformation. This would limit the thicknesses that the study is applicable for i.e. thicknesses that cool slowly enough to form ferrite and pearlite (3.3 °C/s between 800 – 500 °C) may not be applicable to the cooling/heating model, and further verification would need carried out.

8.5: Heating of steel from room temperature to 600 °C

COMSOL was used to predict the heating time of the plate. COMSOL parameters were changed where appropriate such as a heat transfer coefficient, which was modified to fit with the experimental data, shown in [Figure 172](#).

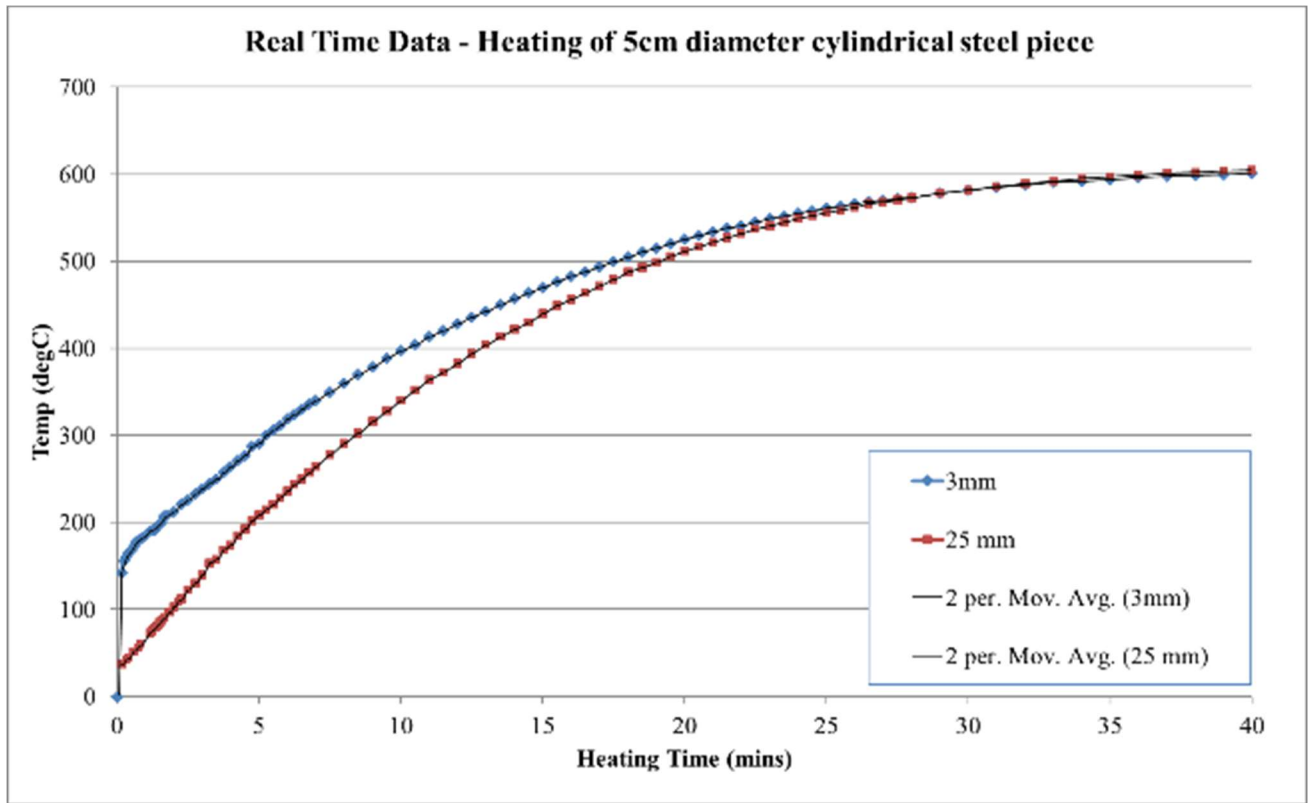


Figure 172 Real Time Data - Heating of 5 cm diameter cylindrical steel piece

8.6: Comparison of Parameters

8.6.1: Comparison to Data

To ensure that the model was accurate experimental data were needed for comparison.

A 50 mm diameter cylindrical section of steel was used. K type Thermocouples were used to determine the difference in surface and central temperature of the cylinder. A 25 mm deep hole was drilled into the centre of the steel, for the central temperature and a 3 mm deep hole was drilled for the surface temperature (to ensure the thermocouple did not move). The sample was 70 mm in length to ensure that radial heat flow dominated the heating rate.

Heating times are shown in [Figure 173](#), approximately 40 minutes was needed for the steel cylinder to reach temperature. There was a difference around 100 °C in the first ten minutes of heating, after 20 minutes there is much smaller difference in temperature. Therefore, simulation does not have the same shape as the experimental heating curves, with the simulation showing a much more rapid heating than what occurs in practice. Possible reasons for this are that the simulation does not consider any chill effect as the sample was placed in the furnace. The results of this is that the sample takes more time to heat, while the simulation does not consider this, resulting in a quicker time for the simulation. Further improvements may be introducing a lag into the simulation to replicate experimental data. Limitations also include lack of heating knowledge. The rate at which thermal energy would affect the material heating rate. This means that the modelling would need to be repeated for different furnaces. However, it shows that an accurate fit can be produced.

The results of this indicate that 50 mm section will reach the tempering temperature about 40 minutes after being placed in the heating unit.

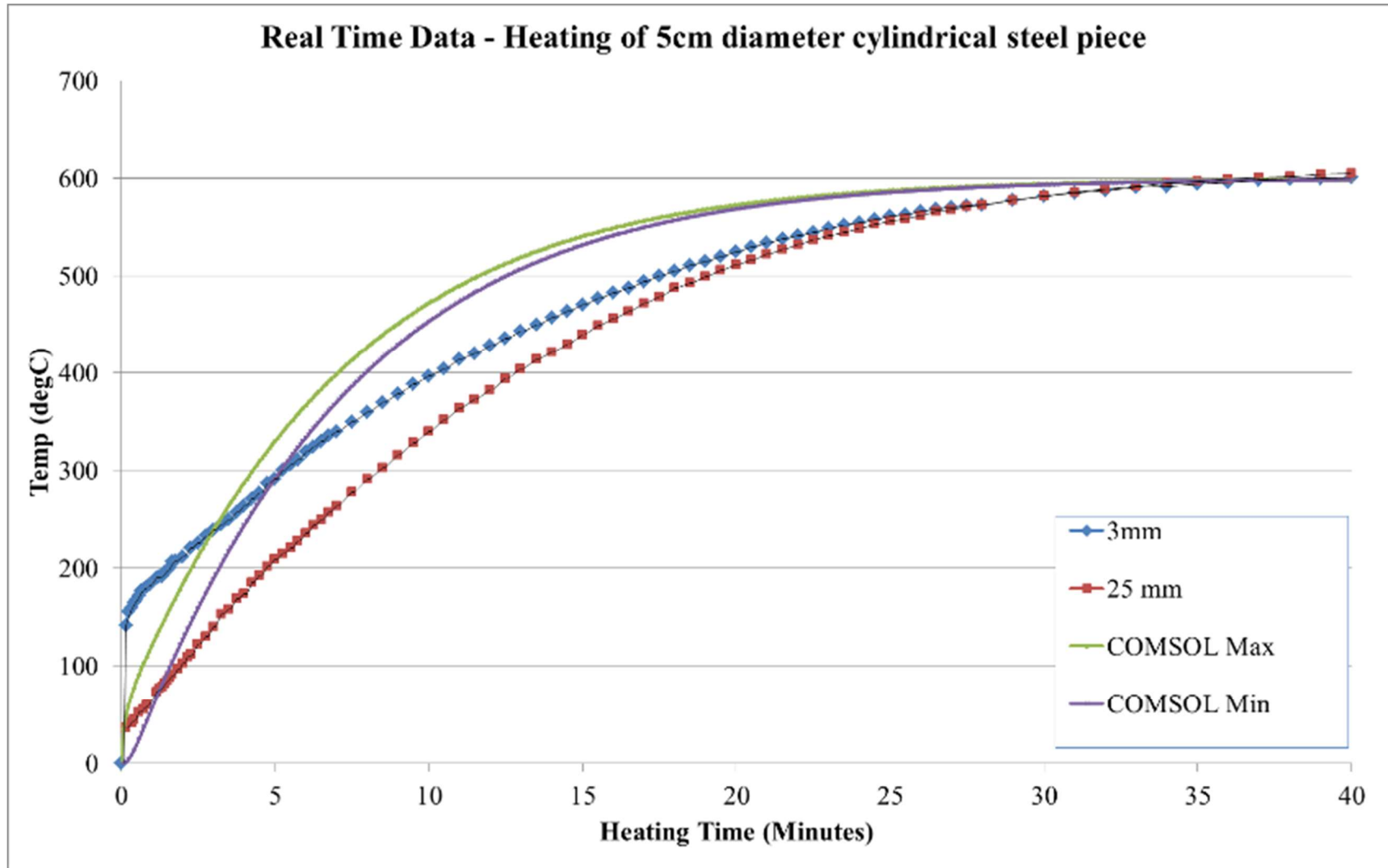


Figure 173 Comparison between COMSOL and heating data

8.6.2: Surface Emissivity

Surface emissivity of the sample on heating was thought to be different from the cooling, as water quenching could remove any scale present, changing the surface and therefore the surface emissivity. [Figure 174](#) shows emissivity from the range of 0 -1, including the value used for the sample cooling, 0.79. The full range of surface emissivity was chosen as it was known that the sample may have scale on it, giving a darker surface, closer to the value 1. If this scale is dislodged then a shiny surface may be revealed, with a value closer to 0.

There is little difference on the heating response simulation with different values, therefore the same surface emissivity of 0.79 was used, the same as what was chosen for cooling.

8.6.3: Heat Transfer Coefficient

The heat transfer coefficient of the sample was found to be a determining factor on cooling, therefore the value was investigated for heating simulations. The heat transfer coefficient used for heating was $400\text{W}/(\text{m}^2 \cdot \text{K})$; however, $100\text{W}/(\text{m}^2 \cdot \text{K})$ and $1000\text{W}/(\text{m}^2 \cdot \text{K})$ were also used to see how much this influences the simulation results, shown in [Figure 175](#). During cooling this value was chosen as to fit the experimental data, the same approach was chosen here. $100\text{W}/(\text{m}^2 \cdot \text{K})$ to $1000\text{W}/(\text{m}^2 \cdot \text{K})$ were the extreme limits. The value of $400\text{W}/(\text{m}^2 \cdot \text{K})$ was chosen after numerous runs of COMSOL when a similar heating time and curve was produced to that of the real heating time data ([Figure 172](#)). This was not chosen from the literature but chosen to help match the COMSOL and experimental data, shown in [Figure 175](#).

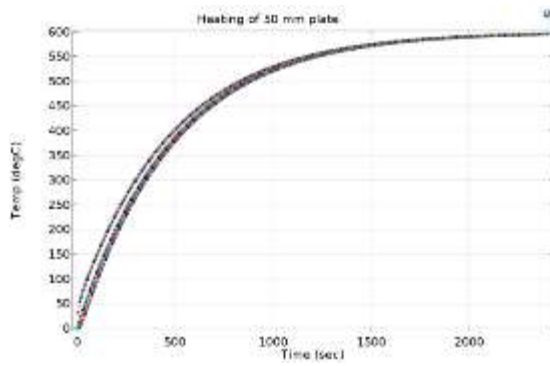
There was a vast difference for the different heat transfer coefficient for the 3 values used, which shows that the value used is important. The value of $1,000 \text{ W/m}^2 \cdot \text{K}$ heats too quickly, reaching $600 \text{ }^\circ\text{C}$ after ~ 1000 seconds. $100 \text{ W/m}^2 \cdot \text{K}$ and $400 \text{ W/m}^2 \cdot \text{K}$ show differences in shape, however they both reach $600 \text{ }^\circ\text{C}$ at similar times, comparable to the real-time data, which takes around 40 minutes or 2400 seconds (See [Figure 172](#)).

The temperature after 1000 seconds, approx. 16 minutes, was chosen for comparison so that the curves shape could be compared. The real-time data showed heating to $475 \text{ }^\circ\text{C}$ after this time and the $100 \text{ W/m}^2 \cdot \text{K}$ and $400 \text{ W/m}^2 \cdot \text{K}$ showed heating to $350 \text{ }^\circ\text{C}$ and $550 \text{ }^\circ\text{C}$ respectively (See [Figure 172](#)). Neither values fit with experimental data completely, however $400 \text{ W/m}^2 \cdot \text{K}$ gives a heating which is around $75 \text{ }^\circ\text{C}$ away from the real data, so this parameter was chosen. Further work was not carried out to get an exact value as the time given to heat the sample was within the time given by real-time data.

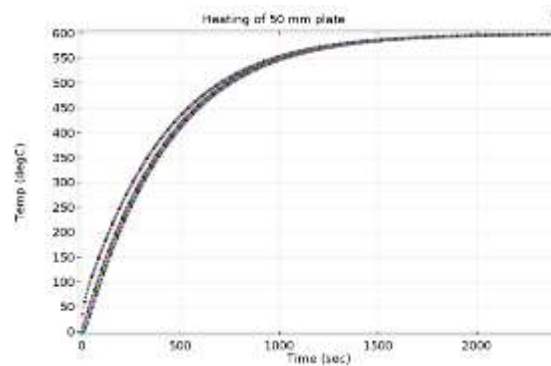
As the coefficient value of $400 \text{ W/m}^2 \cdot \text{K}$ reaches $600 \text{ }^\circ\text{C}$ at the same time as the real-time data and the heating curve is a similar shape as the real-time data (within $75 \text{ }^\circ\text{C}$) it was decided $400 \text{ W/m}^2 \cdot \text{K}$ was a suitable value.

8.6.4: Heat Capacity at Constant Pressure

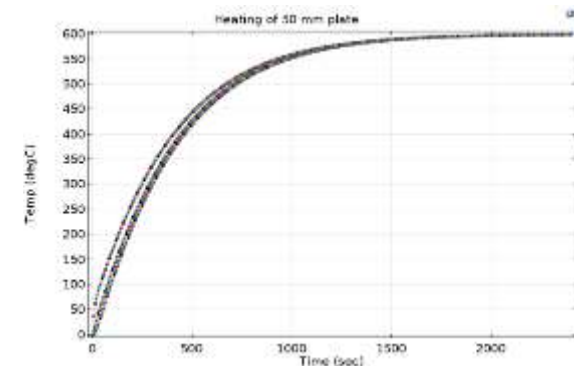
As the COMSOL data was fitting experimental results the heat capacity at constant pressure was not investigated further.



0

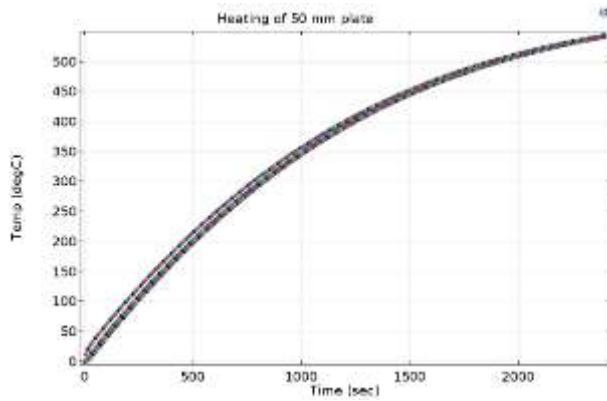


0.79

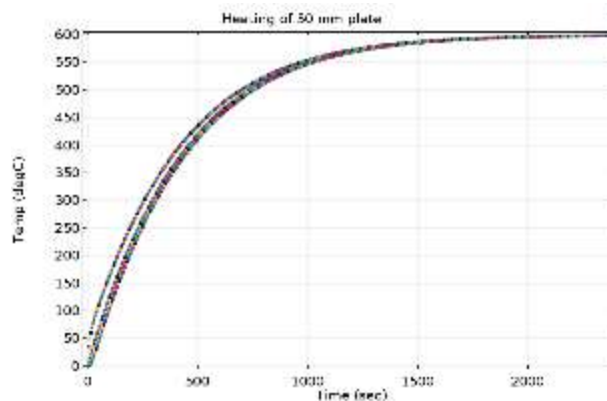


1

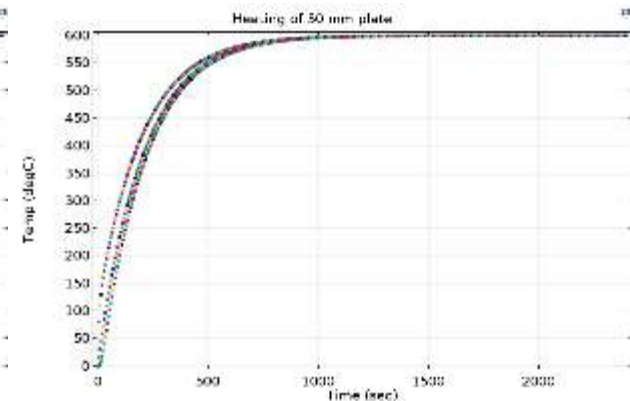
Figure 174 Surface emissivity on heating (Range 0 - 1)



100W/ (m². K)



400W/ (m². K)



1000W/ (m². K)

Figure 175 Heat Transfer Coefficient Comparison

Chapter 9: Summary

9.1: Summary of Discussion

The tempering response of martensite, lower bainite and mixed microstructures of the two phases at 600 °C has been examined for a low carbon alloyed steel grade that is used commercially in the quenched and tempered (Q&T) condition. The microstructures represent those that can be found in thick plates due to the differences in cooling rate that can occur, and times of 0.5 to 16 hours. 100 hours tempering have been considered as this represents the range shown for thick plates where there are variations in heating rate through thickness. 100 hours temper was investigated to determine if effects at 16 hours were experimental or real effects. A model alloy (termed Base), which is similar to the commercial S690 grade, has been investigated along with two other steels that contain higher alloying additions (BaseMoV and BaseSiCrMoV) to examine the effect of Si, Cr, Mo and V additions to the tempering response.

9.2: Conclusions

The main conclusions are as follows:

1. The as-quenched martensite was found to be auto-tempered lath martensite for all three steels and the as-quenched hardnesses were 457, 453 and 470 HV, for Base, BaseMoV and BaseSiCrMoV respectively.
2. The three steels show a similar tempering response to what is expected in the literature, i.e. initial significant reduction in hardness after 0.5 hours tempering (of 187, 88 and 97 HV for Base, BaseMoV and BaseSiCrMoV steel) due to remaining carbon in solution in as-quenched martensite forming carbides.
3. For tempering up to 16 hours, the alloying additions in BaseSiCrMoV compared to BaseMoV steel result in little difference in hardness, although both have a higher

hardness compared to the Base steel; however, when tempering is extended to 100 hours then the BaseSiCrMoV shows less decrease in hardness (after 100 hours it has a hardness of ~260 HV compared to ~185-190 HV for Base and BaseMoV steels). Therefore, alloying additions of 1.24 wt. % Si and 0.8 wt. % Cr do not appear to affect the tempering response or mechanical properties (hardness) for tempering to 16 hours, however at longer times differences in the equilibrium carbide type, sizes and number density result in higher hardness for the BaseSiCrMoV steel. BaseSiCrMoV is predicted to have M_7C_3 , M_6C , MC, $M_{23}C_6$ carbides present, with no cementite, where Base and BaseMoV are still predicted to have cementite present. There is more carbide coverage within the BaseSiCrMoV matrix, 80-90%, compared to Base and BaseMoV, with coverages of 60-75% and 30-45% respectively. BaseSiCrMoV does not contain any carbides larger than 1 μm in the matrix, but Base and BaseMoV do. Along with less carbide coverage on the grain boundary (0-5%), compared to (<10%) and (20-30%) for Base and BaseMoV respectively.

4. No secondary hardening peak, or reduction in softening, was observed for the Mo-containing steels in the tempering time range of 4 - 16 hours (time reported in other Cr-Mo-containing steels for secondary hardening), which may reflect the relatively low levels of Cr and Mo in these steels.
5. The hardness and tempering response of a fully lower bainitic sample, produced in the BaseMoV material, was evaluated. The lower bainite microstructure had a hardness of 351 HV and showed a lower tempering response than when compared to a fully martensite microstructure. After 100 hours tempering it was found that the bainite was harder than the martensite (264 HV compared to 190 HV), which has been related to differences in lath structure, carbide size and number density. It is hypothesised that the differences in initial cementite carbide distribution in lower bainite compared to

martensite affect the tempering process with the lath structure being retained for longer in lower bainite. It has been found that the bainitic carbides are larger than martensite carbides after initial microstructure formation and that bainitic lath sizes are skewed towards larger lath widths.

6. When the heat treatment is used to generate a mixture of the two microstructures (martensite and lower bainite) there is excellent agreement between the measured hardness and that predicted with the Rule of Mixtures using the individual phase hardness values as input: this indicates that the strength can be predicted from a known microstructure or the microstructure mix needed for a particular starting hardness estimated.
7. During tempering to 16 hours there is a general agreement between the measured and predicted (with the Rule of Mixtures using the relevant single phase tempered hardness data) hardness values, considering experimental scatter. This is important as it means that the softening during tempering in the mixed microstructure can be approximately predicted, and therefore times needed to give a desired hardness can be calculated if the initial microstructure is known. No brazing effect (reported in the literature for mixed microstructures of martensite and bainite where the bainite fraction is approximately 20%) was observed; it is suggested that this is because of the relatively low (0.17 wt. %) C content in this steel.
8. Longer tempering times of 100 hours were investigated (for fully bainitic, fully martensitic and a 44% lower bainite: 56% martensite mix), and it was determined that the mixed phase hardness deviated from the Rule of Mixtures prediction, with a hardness 20 HV lower than predicted. This was thought to be due to the martensite and the bainite in the mixed microstructure tempering at different rates, such that the microstructure

behaved in a similar fashion to a dual phase steel, where the resulting strength of the two phases is closer to the softer phase, in this case martensite. The martensite is now largely lath- and carbide-free, and any carbides present are larger with a wider spacing, reducing the strength of the martensite (acting like ferrite). The bainite present acts like the martensite in the DP steel as there are significant areas containing laths present still and carbides within the laths, adding to strength. There are large carbides within the bainite matrix, it is unknown if these are remnants of lath coarsening.

9. A simple COMSOL model was developed to predict the through thickness thermal profile during cooling for thick plate. The resulting cooling rate at a given material thickness can be used with the relevant CCT curve to determine what phases will be present. The thermal model can also be used to determine the heating rate and hence dwell time at temperature during tempering allowing the tempering conditions to achieve a desired hardness to be defined.
10. In the 100 hours investigation the martensitic carbides are more enriched with Mo than bainite and mixed microstructures; the mixed microstructure has carbide enrichment similar to that in bainite, but this may be due to the sampling. In the single phased microstructures, the bainitic and martensitic carbides are not following the same enrichment trend; this is something which could be investigated in further work and may indicate the bainitic carbides are transforming via a partial-para-equilibrium mechanism. Also, after 100 hours tempering both martensite and bainite are over-tempering, but some bainitic regions are resistant to over-tempering, retaining finer carbides. Martensite has a bimodal distribution of carbides, thought to be larger carbides on the grain boundary and smaller carbides within the matrix.

The outcome of this project means that good mechanical properties can be produced

industrially with fewer alloying additions (BaseMoV instead of BaseSiCrMoV) in an energy efficient manner by using the known tempering response and thermal model to design appropriate heat treatment schedules.

Chapter 10 Further Work

The mixed microstructure trials show that there is general agreement between the measured and predicted (with the Rule of Mixtures) hardness values for tempering below 16 hours.

This can be investigated further, with a larger array of times studied. Currently there are no data between 16 hours and 100 hours, and therefore the point at which deviation between good and poor predictability using the Rule of Mixture occurs is not known. In addition, more in-depth study is required to understand the changes in the microstructures occurring at 100 hours, for example if the larger carbides in the bainite matrix are remnants of the lath coarsening, and if this also occurred in the martensite.

The bainitic carbides can be analysed after formation with TEM or atom probe tomography; this will give an indication if partial-para-equilibrium is occurring. This would be important work as it is a phenomenon which is not reported in the literature and would apply to steels used for elevated temperature service e.g. power generation grades. Other factors which can be investigated are how widespread the effect is i.e. is it every carbide or a select few based on size / local composition. If successful, carbides during tempering can be studied to find how this influences the carbide evolution during tempering to 100 hours; determining the mechanism of carbide stability.

Advanced characterisation facilities such as synchrotron x-rays could be utilised and methods developed for accurate determination of the microstructures present.

There is room to improve the microstructural characterisation of the 100 hours tempered microstructure. The carbide size and distribution can be fully analysed in a qualitative manner and the martensite, bainite and mixed samples compared.

Bibliography:

- Alibeyki, M., Mirzadeh, H., Najafi, M., & Kalhor, A. (2017). Modification of Rule of Mixtures for Estimation of the Mechanical Properties of Dual-Phase Steels. *Journal of Materials Engineering and Performance*, 26(6), 2683-2688. doi:10.1007/s11665-017-2687-6
- Andrews, K. W. (1965). Empirical formulae for the calculation of some transformation temperatures. *J.I.S.I.*, 203, 721-729.
- Argon, A., & J. Bickerman, J. (1971). *The Physics of Strength and Plasticity* (Vol. 24).
- Baker, R. G., & Nutting, J. (1959). The Tempering of 2.25%Cr-1%Mo Steel for Quenching and Normalizing. *J. Iron Steel Inst.*, 192, 257-268.
- Bakhsheshi-Rad, H. R., Monshi, A., Monajatizadeh, H., Idris, M. H., Abdul Kadir, M. R., & Jafari, H. (2011). Effect of Multi-Step Tempering on Retained Austenite and Mechanical Properties of Low Alloy Steel. *Journal of Iron and Steel Research, International*, 18(12), 49-56. doi:[http://dx.doi.org/10.1016/S1006-706X\(12\)60009-0](http://dx.doi.org/10.1016/S1006-706X(12)60009-0)
- Barranco, J. M. C., P.J; Kapp, J.A. (1992). *Tempering effects for lower bainite, martensite, and mixed microstructures on impact, fracture and related mechanical properties of ASTM A723 Steel (AD-A254 617)*. Retrieved from <https://apps.dtic.mil/dtic/tr/fulltext/u2/a254617.pdf>
- Barton, C. J. (1969). The tempering of a low-carbon internally twinned martensite. *Acta Metallurgica*, 17(8), 1085-1093. doi:[http://dx.doi.org/10.1016/0001-6160\(69\)90053-4](http://dx.doi.org/10.1016/0001-6160(69)90053-4)
- Bergstrom, Y. G., Y. Sterkenburg, D. (2010). A Dislocation-Based Theory for the Deformation Hardening Behaviour of DP Steels. *Journal of Metallurgy*, 2010, 16.
- Bhadeshia, H. (1997). Martensite and Bainite in Steels : Transformation Mechanism & Mechanical Properties. *Journal de Physique IV Colloque*, 7.
- Bhadeshia, H. K. D. H. (2001). *Bainite in Steels: Transformations, Microstructure and Properties*: IOM Communications.
- Bhadeshia, H. K. D. H. (2018). Solution to the Bagaryatskii and Isaichev ferrite–cementite orientation relationship problem. *Materials Science and Technology*, 34(14), 1666-1668. doi:10.1080/02670836.2018.1470746
- Bhadeshia, H. K. D. H., & Babu, S. S. (2015). Get TTT and CCT Diagram with Steel Composition. Retrieved from <http://calculations.ewi.org/vjp/secure/TTTCCTPlots.asp>
- Bhadeshia, H. K. D. H., David, S. A., Vitek, J. M., & Reed, R. W. (1991). Stress induced transformation to bainite in Fe–Cr–Mo–C pressure vessel steel. *Materials Science and Technology*, 7(8), 686-698. doi:10.1179/mst.1991.7.8.686
- Bhadeshia, H. K. D. H., & Edmonds, D. V. (1979). The bainite transformation in a silicon steel. *Metallurgical Transactions A*, 10(7), 895-907. doi:10.1007/bf02658309
- Bhadeshia, H. K. D. H., & Honeycombe, R. W. K. (2007). *Steels: Microstructure and Properties* (Third Ed.). Great Britain: Elsevier.
- Bhadeshia, H. K. D. H., & Honeycombe, S. R. (2006). 8 - The Heat Treatment of Steels: Hardenability. In H. K. D. H. B. R. Honeycombe (Ed.), *Steels (Third Edition)* (pp. 167-181). Oxford: Butterworth-Heinemann.
- Bjerregaard, L., Geels, K., Ottesen, B., & Ruckert, M. (2000). *Struers: Metalog Guide* (3rd Ed.). Denmark: Struers.
- Bradshaw, F. J., Hoyle, G., & Speight, K. (1953). Diffusion of Silicon in Ferrite. *Nature*, 171, 488. doi:10.1038/171488a0
- Bureau, N. (1955). *X-ray Powder Data File (cric 539 4 3) card for alpha-iron*.
- Caballero, F. G., Miller, M. K., Babu, S. S., & Garcia-Mateo, C. (2007). Atomic scale observations of bainite transformation in a high carbon high silicon steel. *Acta Materialia*, 55(1), 381-390. doi:<http://dx.doi.org/10.1016/j.actamat.2006.08.033>
- Caballero, F. G., Miller, M. K., & Garcia-Mateo, C. (2014). Influence of transformation temperature on carbide precipitation sequence during lower bainite formation. *Materials Chemistry and Physics*, 146(1), 50-57. doi:<https://doi.org/10.1016/j.matchemphys.2014.02.041>
- Campbell, F. C. (2008). *Elements of Metallurgy and Engineering Alloys*: ASM International.
- Canale, L. C. F., Yao, X., Gu, J., & Totten, G. E. (2008). A historical overview of steel tempering parameters. *International Journal of Microstructure and Materials Properties*, 3(4-5), 474-525. doi:10.1504/ijmmp.2008.022033
- Capdevila, C., Caballero, F., & García de Andrés, C. (2002). *Determination of Ms Temperature in Steels: A Bayesian Neural Network Model* (Vol. 42).
- Caron, R. N., & Krauss, G. (1972). The tempering of Fe-C lath martensite. *Metallurgical Transactions*, 3(9), 2381-2389. doi:10.1007/bf02647041
- Chang, K. (1984). THE SILICON EFFECT IN THE TEMPERING OF MARTENSITE IN STEELS. *JOURNAL DE PHYSIQUE*, 45(C9), 397-401.
- Delagnes, D., Lamesle, P., Mathon, M. H., Mebarki, N., & Levaillant, C. (2005). Influence of silicon content on the precipitation of secondary carbides and fatigue properties of a 5%Cr tempered martensitic steel. *Materials Science and Engineering: A*, 394(1–2), 435-444. doi:<http://dx.doi.org/10.1016/j.msea.2004.11.050>
- Deng, X. T., Fu, T. L., Wang, Z. D., Misra, R. D. K., & Wang, G. D. (2016). Epsilon carbide precipitation and wear

- behaviour of low alloy wear resistant steels. *Materials Science and Technology*, 32(4), 320-327. doi:10.1080/02670836.2015.1137410
- Dieter, G. E., & Bacon, D. (1988). *Mechanical Metallurgy*: McGraw-Hill.
- Driscoll, J. (2014). *Investigation into the Microstructure and Precipitation Characteristics of Reheated Quenched and Tempered 701 Steel (RQT701) Quenched from 925 °C in Austenite to an Autotempered Martensitic Microstructure, and Tempered at 580 °C, 600 °C and 620 °C for Between 1 and 100 Hours*. (Masters Thesis), The University of Birmingham, Under Examination.
- Edmonds, D. V., & Cochrane, R. C. (1990). Structure-property relationships in bainitic steels. *Metallurgical Transactions A*, 21(6), 1527-1540. doi:10.1007/bf02672567
- Fereiduni, E., & Ghasemi Banadkouki, S. S. (2013). Reliability/unreliability of mixture rule in a low alloy ferrite–martensite dual phase steel. *Journal of Alloys and Compounds*, 577, 351-359. doi:<https://doi.org/10.1016/j.jallcom.2013.05.209>
- Fujita, N. (2000). *Modelling Carbide Precipitation in alloy steels*. (Doctor of Philosophy), University of Cambridge.
- Furillo, F. T., Purushothaman, S., & Tien, J. K. (1977). Understanding the Larson-Miller parameter. *Scripta Metallurgica*, 11(6), 493-496. doi:[http://dx.doi.org/10.1016/0036-9748\(77\)90164-8](http://dx.doi.org/10.1016/0036-9748(77)90164-8)
- Galindo-Nava, E. I., & Rivera-Díaz-del-Castillo, P. E. J. (2015). A model for the microstructure behaviour and strength evolution in lath martensite. *Acta Materialia*, 98, 81-93. doi:<http://dx.doi.org/10.1016/j.actamat.2015.07.018>
- Gau, J. S. (1981). *Microstructure and Properties of Dual Phase Steels Containing Fine Precipitates*. Retrieved from University of California:
- Ghassemi-Armaki, H., Chen, R. P., Maruyama, K., Yoshizawa, M., & Igarashi, M. (2009). Static recovery of tempered lath martensite microstructures during long-term aging in 9–12% Cr heat resistant steels. *Materials Letters*, 63(28), 2423-2425. doi:<https://doi.org/10.1016/j.matlet.2009.08.024>
- Ghosh, G., & Olson, G. B. (2002). Precipitation of paraequilibrium cementite: Experiments, and thermodynamic and kinetic modeling. *Acta Materialia*, 50(8), 2099-2119. doi:[http://dx.doi.org/10.1016/S1359-6454\(02\)00054-X](http://dx.doi.org/10.1016/S1359-6454(02)00054-X)
- Gingell, A. D. B., Bhadeshia, H. K. D. H., Jones, D. G., & Mawella, K. J. A. (1997). Carbide precipitation in some secondary hardened steels. *Journal of Materials Science*, 32(18), 4815-4820. doi:10.1023/A:1018695317549
- Gojic, M., Kosec, L., & Matkovic, P. (1998). The effect of tempering temperature on mechanical properties and microstructure of low alloy Cr and CrMo steel. *Journal of Materials Science*, 33(2), 395-403. doi:10.1023/a:1004375914591
- Gottstein, G. (2004). *Physical Foundations of Materials Science*.
- Grange, R. A., & Baughman, R. W. (1956). Hardness of tempered martensite in carbon and low alloy steels. *Transactions of American Society of Metals, XL VIII*, 165-197.
- Grange, R. A., Hribal, C. R., & Porter, L. F. (1977). Hardness of Tempered Martensite in Carbon and Low-Alloy Steel. *Metallurgical Transactions A*, 8A, 1775-1785.
- K. Han, T.D. Mottishaw, G.D.W. Smith, D.V. Edmonds, A.G. Stacey. (1995). Effects of vanadium additions on microstructure and hardness of hypereutectoid pearlitic steels. *Materials Science and Engineering*. 190 (A), 207-214.
- Hehemann, R. F., Kinsman, K. R., & Aaronson, H. I. (1972). A debate on the bainite reaction. *Metallurgical Transactions*, 3(5), 1077-1094. doi:10.1007/bf02642439
- Hou, Z., Babu, R. P., Hedström, P., & Odqvist, J. (2018). Microstructure evolution during tempering of martensitic Fe–C–Cr alloys at 700 °C. *Journal of Materials Science*, 53(9), 6939-6950. doi:10.1007/s10853-018-2036-7
- Hussein, A.-H. A., Abdu, M. T., El-Banna, E.-S. M., Soliman, S. E., & Tash, M. M. (2016). Interrelation of Steel Composition, Hardening Route, and Tempering Response of Medium Carbon Low-Alloy Steels. *Journal of Materials Engineering and Performance*, 25(4), 1463-1473. doi:10.1007/s11665-016-1957-z
- Hutchinson, B., Hagström, J., Karlsson, O., Lindell, D., Tornberg, M., Lindberg, F., & Thuvander, M. (2011). *Microstructures and hardness of as-quenched martensites (0.1–0.5%C)* (Vol. 59).
- International, A. (2016). Standard Test Method for Determining Volume Fraction by Systematic Manual Point Count E562-11 (pp. 7).
- Irani, J. J. H., R.W.K. (1965). Clustering and precipitation in iron-molybdenum-carbon alloys. *Journal of the Iron and Steel Institute*, 203(August), 826-833.
- Irvine, K. J., & Pickering, F. B. (1960). The tempering characteristics of low-carbon low-alloy steels. *Journal of the Iron and Steel Institute*, 194, 137-153.
- Irvine, K. J., Pickering, F. B., Heselwood, W. C., & Atkins, M. (1957). The Physical Metallurgy of low-carbon, low-alloy steels containing boron. *Journal of the Iron and Steel Institute, May*, 54-57.
- Jang, J. H., Kim, I. G., & Bhadeshia, H. K. D. H. (2010). ϵ -Carbide in alloy steels: First-principles assessment. *Scripta Materialia*, 63(1), 121-123. doi:<https://doi.org/10.1016/j.scriptamat.2010.03.026>
- Janovec, J., Svoboda, M., Výrostková, A., & Kroupa, A. (2005). Time–temperature–precipitation diagrams of carbide evolution in low alloy steels. *Materials Science and Engineering: A*, 402(1–2), 288-293. doi:<http://dx.doi.org/10.1016/j.msea.2005.04.048>
- Ju, Y. (2018). *Characterisation and modelling of precipitation during short term tempering of low carbon alloyed steels*. (PhD), University of Birmingham.
- Kaneko, K., Matsumura, S., Sadakata, A., Fujita, K., Moon, W. J., Ozaki, S., . . . Tomokiyo, Y. (2004).

- Characterization of carbides at different boundaries of 9Cr-steel. *Materials Science and Engineering: A*, 374(1), 82-89. doi:<https://doi.org/10.1016/j.msea.2003.12.065>
- Khan, S. A., & Bhadeshia, H. K. D. (1990). Kinetics of Martensitic transformation in partially bainitic 300M steel. *Materials Science and Engineering: A*, 129(2), 257-272. doi:[https://doi.org/10.1016/0921-5093\(90\)90273-6](https://doi.org/10.1016/0921-5093(90)90273-6)
- Kiattisaksri, P. M., S; Poncelow, J; Madeni, J.C; Hellner, R.L; Coleman, S; Liu, B; Mishra, B; Olson, D.L. (2011). *ASSESSMENT OF MICROSTRUCTURE IN GRADE T22 Cr-Mo STEEL BY NONDESTRUCTIVE TOOLS*. Paper presented at the AIP Conference
- Kim, B.-N., San Martín, D., Chao, J., & Rivera-Díaz-del-Castillo, P. (2012). *The Effect of Silicon on the $\varepsilon \rightarrow \theta$ Transformation in Ultra-Strong Spring Steels* (Vol. 2).
- Kim, B., Boucard, E., Sourmail, T., San Martín, D., Gey, N., & Rivera-Díaz-del-Castillo, P. E. J. (2014). The influence of silicon in tempered martensite: Understanding the microstructure-properties relationship in 0.5–0.6% C steels. *Acta Materialia*, 68(0), 169-178. doi:<http://dx.doi.org/10.1016/j.actamat.2014.01.039>
- Korablev, V. A., Obukhov, V. D., & Ustinovshchikov, Y. I. (1975). Effect of chromium on the rate of carbide formation processes during tempering. *Metal Science and Heat Treatment*, 17(12), 1052-1055. doi:10.1007/bf00664213
- Kozeschnik, E., & Bhadeshia, H. K. D. H. (2008). Influence of silicon on cementite precipitation in steels. *Materials Science and Technology*, 24(3), 343-347. doi:10.1179/174328408X275973
- Krauss, G. (1978). Hardenability concepts with applications to steel: proceedings of a symposium held at the Sheraton-Chicago Hotel, October 24-26, 1977 (pp. vii, 626 p.). [New York]: Metallurgical Society of AIME.
- Krauss, G. (2012). Tempering of martensite in carbon steels. In E. Pereloma & D. V. Edmonds (Eds.), *Phase Transformations in Steels* (Vol. 2, pp. 126-150): Woodhead Publishing.
- Krauss, G., & Marder, A. R. (1971). The morphology of martensite in iron alloys. *Metallurgical Transactions*, 2(9), 2343. doi:10.1007/bf02814873
- Krauss, G., & Thompson, S. W. (1995). Ferritic Microstructures in Continuously Cooled Low- and Ultralow-carbon Steels. *ISIJ International*, 35(8), 937-945. doi:10.2355/isijinternational.35.937
- Kroupa, A., Výrostková, A., Svoboda, M., & Janovec, J. (1998). Carbide reactions and phase equilibria in low-alloy Cr–Mo–V steels tempered at 773–993 K. Part II: Theoretical calculations. *Acta Materialia*, 46(1), 39-49. doi:[https://doi.org/10.1016/S1359-6454\(97\)00239-5](https://doi.org/10.1016/S1359-6454(97)00239-5)
- Kwon, H., Lee, K. B., Yang, H. R., Lee, J. B., & Kim, Y. S. (1997). Secondary hardening and fracture behavior in alloy steels containing Mo, W, and Cr. *Metallurgical and Materials Transactions A*, 28(13), 775-784. doi:10.1007/s11661-997-1005-6
- Lindsley, B. M., A. (1998). The morphology and coarsening kinetics of spheroidized FeC binary alloys. *Acta Materialia*, 46(1), 341-351. doi:[http://dx.doi.org/10.1016/S1359-6454\(97\)00165-1](http://dx.doi.org/10.1016/S1359-6454(97)00165-1)
- Liu, J., Strangwood, M., L, D., & C, P., Jonathan. (2014). Non-destructive characterisation of N/Al level in P91 steels using electromagnetic sensors. *31*, 1743284714Y.1743284000. doi:10.1179/1743284714Y.0000000642
- Liu, S., Madeni, J. C., Olson, D. L., Hellner, R., Petr, V., & Coleman, K. (2009). Evolution of carbide precipitates in 2½Cr–1Mo steels in power industry: morphology and stability, and characterisation techniques. *Energy Materials*, 4(2), 51-60. doi:10.1179/174892310X12811032099955
- Llewellyn, D. T. (2013). *Steels: Metallurgy and Applications*: Elsevier Science.
- Maalekian, M. (2007). *The Effects of Alloying Elements on Steels (I)*. Retrieved from Technische Universität Graz:
- Man, T. H., Liu, T. W., Ping, D. H., & Ohmura, T. (2018). TEM investigations on lath martensite substructure in quenched Fe-0.2C alloys. *Materials Characterization*, 135, 175-182. doi:<https://doi.org/10.1016/j.matchar.2017.11.039>
- Maropoulos, S., & Ridley, N. (2005). The dependence of mechanical properties on structure in low alloy steel forgings. *Journal of Materials Science*, 40(18), 4753-4759. doi:10.1007/s10853-005-0780-y
- Martin, J. W., & Doherty, R. D. (1976). *Stability of Microstructure in Metallic Systems*: Cambridge University Press.
- Matas, S. J. H., R.F. (1961). The structure of bainite in hypoeutectoid steels. *Transactions of the Metallurgical Society of AIME*, 221, 179-185.
- McFarlane, B. (2018). RQT 701 Quenched and Tempered Steel Plate. Retrieved from www.brownmac.com/products/quenched-and-tempered-steel-plate/rqt-701
- Mesquita, R. A., Barbosa, C. A., Morales, E. V., & Kestenbach, H. J. (2011). Effect of Silicon on Carbide Precipitation after Tempering of H11 Hot Work Steels. *Metallurgical and Materials Transactions A*, 42(2), 461-472. doi:10.1007/s11661-010-0430-0
- Mesquita, R. A., & Kestenbach, H.-J. (2012). Influence of silicon on secondary hardening of 5wt% Cr steels. *Materials Science and Engineering: A*, 556(0), 970-973. doi:<http://dx.doi.org/10.1016/j.msea.2012.06.060>
- Metals, A. S. f. (1985). *Metals Handbook Desk Edition*. Metals Park, Ohio.
- Miyamoto, G., Oh, J. C., Hono, K., Furuhashi, T., & Maki, T. (2007). Effect of partitioning of Mn and Si on the growth kinetics of cementite in tempered Fe–0.6 mass% C martensite. *Acta Materialia*, 55(15), 5027-5038. doi:<http://dx.doi.org/10.1016/j.actamat.2007.05.023>
- Mohrbacher, H. (2010). *Principal effects of Mo in HSLA steels and cross effects with microalloying elements*. Paper presented at the International Seminar in Applications of Mo in Steels, Beijing, China.
- Molkeri, A., Pahlevani, F., Emmanuelawati, I., & Sahajwalla, V. (2016). Thermal and mechanical stability of retained

- austenite in high carbon steel: An in-situ investigation. *Materials Letters*, 163, 209-213.
doi:<http://dx.doi.org/10.1016/j.matlet.2015.10.083>
- Morito, S., Huang, X., Furuhashi, T., Maki, T., & Hansen, N. (2006). The morphology and crystallography of lath martensite in alloy steels. *Acta Materialia*, 54(19), 5323-5331.
doi:<http://dx.doi.org/10.1016/j.actamat.2006.07.009>
- Morito, S., Yoshida, H., Maki, T., & Huang, X. (2006). Effect of block size on the strength of lath martensite in low carbon steels. *Materials Science and Engineering: A*, 438-440, 237-240.
doi:<http://dx.doi.org/10.1016/j.msea.2005.12.048>
- Nam, W. J. (1999). Effect of Initial Microstructure on the Coarsening Behavior of Cementite Particles. *ISIJ International*, 39, 1181-1187.
- Nam, W. J., Kim, D. S., & Ahn, S. T. (2003). Effects of alloying elements on microstructural evolution and mechanical properties of induction quenched-and-tempered steels. *Journal of Materials Science*, 38(17), 3611-3617. doi:10.1023/a:1025625330442
- Ohmori, Y., Ohtani, H., & Kunitake, T. (1971). *The Bainite in Low Carbon Low Alloy High Strength Steels* (Vol. 57).
- Ohmori, Y., Ohtani, H., & Kunitake, T. (1974). Tempering of the Bainite and the Bainite/Martensite Duplex Structure in a Low-Carbon Low-Alloy Steel. *Metal Science*, 8(1), 357-366. doi:10.1179/msc.1974.8.1.357
- Ohmura, T., Minor, A. M., Stach, E. A., & Morris, J. W. (2004). Dislocation-grain boundary interactions in martensitic steel observed through in situ nanoindentation in a transmission electron microscope. *Journal of Materials Research*, 19(12), 3626-3632. doi:10.1557/JMR.2004.0474
- Ollilainen, V., Kasprzak, W., & Holappa, L. (2003). The effect of silicon, vanadium and nitrogen on the microstructure and hardness of air cooled medium carbon low alloy steels. *Journal of Materials Processing Technology*, 134(3), 405-412. doi:[http://dx.doi.org/10.1016/S0924-0136\(02\)01131-7](http://dx.doi.org/10.1016/S0924-0136(02)01131-7)
- Ooi, S. W., Cho, Y. R., Oh, J. K., & Bhadeshia, H. K. D. H. (2013). Carbon Enrichment in Residual Austenite during Martensitic Transformation. *International Conference on Martensitic Transformations (ICOMAT)* (pp. 179-185): John Wiley & Sons, Inc.
- Padmanabhan, R., & Wood, W. E. (1984). Precipitation of ϵ carbide in martensite. *Materials Science and Engineering*, 65(2), 289-297. doi:[http://dx.doi.org/10.1016/0025-5416\(84\)90090-9](http://dx.doi.org/10.1016/0025-5416(84)90090-9)
- Park, K.-T., & Kwon, H.-J. (2001). Interpretation of the strengthening of steel with lower bainite and martensite mixed microstructure. *Metals and Materials International*, 7(2), 95-99. doi:10.1007/bf03026946
- Pavlina, E. J., Van Tyne, C. J., & Speer, J. G. (2015). Effects of combined silicon and molybdenum alloying on the size and evolution of microalloy precipitates in HSLA steels containing niobium and titanium. *Materials Characterization*, 102, 35-46. doi:10.1016/j.matchar.2015.02.013
- Peet, M. J., Babu, S. S., Miller, M. K., & Bhadeshia, H. K. D. H. (2017). Tempering of Low-Temperature Bainite. *Metallurgical and Materials Transactions A*, 1-9. doi:10.1007/s11661-017-4086-x
- Peet, M. J., Hasan, H. S., & Bhadeshia, H. K. D. H. (2011). Prediction of thermal conductivity of steel. *International Journal of Heat and Mass Transfer*, 54(11), 2602-2608.
doi:<https://doi.org/10.1016/j.ijheatmasstransfer.2011.01.025>
- Peng, F., Xu, Y., Gu, X., Wang, Y., Liu, X., & Li, J. (2018). The relationships of microstructure-mechanical properties in quenching and partitioning (Q&P) steel accompanied with microalloyed carbide precipitation. *Materials Science and Engineering: A*, 723, 247-258. doi:<https://doi.org/10.1016/j.msea.2018.03.061>
- Petty, E. R. (1970). *Martensite: Fundamentals and Technology*: Longman.
- Pham, A. H., Ohba, T., Morito, S., & Hayashi, T. (2013). Energetic stability of boundary between variants in lath martensite. *Journal of Alloys and Compounds*, 577, Supplement 1, S583-S586.
doi:<http://dx.doi.org/10.1016/j.jallcom.2012.02.008>
- Pinto da Silva, E., Xu, W., Föjler, C., Houbaert, Y., Sietsma, J., & Petrov, R. H. (2014). Phase transformations during the decomposition of austenite below Ms in a low-carbon steel. *Materials Characterization*, 95, 85-93.
doi:<http://dx.doi.org/10.1016/j.matchar.2014.06.003>
- Podder, A. (2011). *Tempering of a mixture of Bainite and Retained Austenite*. (Doctor of Philosophy PhD), University of Cambridge.
- Saeidi, N., & Ekrami, A. (2009). Comparison of mechanical properties of martensite/ferrite and bainite/ferrite dual phase 4340 steels. *Materials Science and Engineering: A*, 523(1), 125-129.
doi:<https://doi.org/10.1016/j.msea.2009.06.057>
- Samuel, F. H., & Hussein, A. A. (1982). Tempering of medium- and high-carbon martensites. *Metallography*, 15(4), 391-408. doi:[http://dx.doi.org/10.1016/0026-0800\(82\)90030-1](http://dx.doi.org/10.1016/0026-0800(82)90030-1)
- Samuel, F. H., & Hussein, A. A. (1983). A comparative study of tempering in steel. *Materials Science and Engineering*, 58(1), 113-120. doi:[http://dx.doi.org/10.1016/0025-5416\(83\)90142-8](http://dx.doi.org/10.1016/0025-5416(83)90142-8)
- Shima Pashangeh, Hamid Reza Karimi Zarchi, Seyyed Sadegh Ghasemi Banadkouki and Mahesh C. Somani. (2019). Detection and Estimation of Retained Austenite in a High Strength Si-Bearing Bainite-Martensite- Retained Austenite Micro-Composite Steel after Quenching and Bainitic Holding (Q&B). *Metals*. 9 (492), 21.
- Shorowordi, K. M., & Ali Bepari, M. M. (2002). Effects of molybdenum additions on the structure, depth, and austenite grain size of the case of carburized 0.13% carbon steels. *Journal of Materials Engineering and Performance*, 11(6), 625-630. doi:10.1361/105994902770343610
- Smith, E., & Nutting, J. (1957). The tempering of low-alloy creep-resistant steels containing chromium, molybdenum,

- and vanadium. *Journal of the Iron and Steel Institute*, 187, 314-330.
- Speich, G. R. (1969). Tempering of plain carbon martensite. *Transactions of the Metallurgical Society of AIME*, 245.
- Speich, G. R., & Leslie, W. C. (1972). Tempering of steel. *Metallurgical Transactions*, 3(5), 1043-1054.
doi:10.1007/BF02642436
- Steven, W. H., A.G. (1959). The temperature formation of martensite and bainite in low-alloy steels, some effects of chemical composition. *The Journal of the Iron and Steel Institute*, 183, 10.
- Talebi, H., Jahazi, M., & Melkonyan, H. (2018). *Retained Austenite Decomposition and Carbide Precipitation during Isothermal Tempering of a Medium-Carbon Low-Alloy Bainitic Steel* (Vol. 11).
- Tekin, E., & Kelly, P. M. (1965). Secondary hardening of vanadium steels. *JISI*, 203, 715-720.
- Thomson, R. C., & Bhadeshia, H. K. D. H. (1994a). Changes in chemical composition of carbides in 2·25Cr–1Mo power plant steel - Part 1 Bainitic Microstructure. *Materials Science and Technology*, 10(3), 193-204.
doi:10.1179/mst.1994.10.3.193
- Thomson, R. C., & Bhadeshia, H. K. D. H. (1994b). Changes in chemical composition of carbides in 2·25Cr–1Mo power plant steel -Part 2 Mixed Microstructures. *Materials Science and Technology*, 10(3), 205-208.
doi:10.1179/mst.1994.10.3.205
- Thomson, R. C., & Miller, M. K. (1996). An atom probe study of cementite precipitation in autotempered martensite in an Fe□Mn□C alloy. *Applied Surface Science*, 94–95(0), 313-319. doi:[http://dx.doi.org/10.1016/0169-4332\(95\)00392-4](http://dx.doi.org/10.1016/0169-4332(95)00392-4)
- Thomson, R. C., & Miller, M. K. (1998). Carbide precipitation in martensite during the early stages of tempering Cr- and Mo-containing low alloy steels. *Acta Materialia*, 46(6), 2203-2213. doi:[http://dx.doi.org/10.1016/S1359-6454\(97\)00420-5](http://dx.doi.org/10.1016/S1359-6454(97)00420-5)
- Tomita, Y. (1991). Effect of martensite morphology on mechanical properties of low alloy steels having mixed structure of martensite and lower bainite. *Materials Science and Technology*, 7(4), 299-306.
doi:10.1179/mst.1991.7.4.299
- Tomita, Y., & Okabayashi, K. (1985). Mechanical properties of 0.40 pct C-Ni-Cr-Mo high strength steel having a mixed structure of martensite and bainite. *Metallurgical Transactions A*, 16(1), 73-82.
doi:10.1007/bf02656714
- ToolBox, T. E. (2003). Emissivity Coefficients of some common Materials. Retrieved from https://www.engineeringtoolbox.com/emissivity-coefficients-d_447.html
- Totten, G. E., & Howes, M. A. H. (1997). *Steel Heat Treatment Handbook*: Taylor & Francis.
- Tu, M.-Y., Hsu, C.-A., Wang, W.-H., & Hsu, Y.-F. (2008). Comparison of microstructure and mechanical behavior of lower bainite and tempered martensite in JIS SK5 steel. *Materials Chemistry and Physics*, 107(2–3), 418-425. doi:<http://dx.doi.org/10.1016/j.matchemphys.2007.08.017>
- Van Bohemen, S. M. C. (2012). *Bainite and martensite start temperature calculated with exponential carbon dependence* (Vol. 28).
- Vieira, I. D. M., Emmanuel. (2017). *Tempering response of bainitic and martensitic microstructures*. Paper presented at the 3rd Pan American Materials Congress.
- Wadhwa, A. S., & Dhaliwal, E. H. S. (2008). *A Textbook of Engineering Material and Metallurgy*: University Science Press.
- Y. Koo, J., J. Young, M., & Graule, T. (1980). *Law of mixtures in dual-phase steels. [Ferritemartensite]* (Vol. 11).
- Yang, Z.-G., & Fang, H.-S. (2005). An overview on bainite formation in steels. *Current Opinion in Solid State and Materials Science*, 9(6), 277-286. doi:<http://dx.doi.org/10.1016/j.cossms.2006.06.005>
- H. L. Yi, K.Y.Lee, H. K. D. H. Bhadeshia. (2011). Mechanical Stabilisation of Retained Austenite in δ–TRIP Steel. *Materials Science and Engineering*. 528 (A), p5900-5903.
- Young, c. H., & Bhadeshia, H. K. D. H. (1994). Strength of mixtures of bainite and martensite. *Materials Science and Technology*, 10(3), 209-214. doi:10.1179/mst.1994.10.3.209
- Zhu, K., Bouaziz, O., Oberbillig, C., & Huang, M. (2010). An approach to define the effective lath size controlling yield strength of bainite. *Materials Science and Engineering: A*, 527(24–25), 6614-6619.
doi:<http://dx.doi.org/10.1016/j.msea.2010.06.061>